A RHEOLOGICAL STUDY OF THREE

LINEAR LOW DENSITY POLYETHYLENE FILM RESINS

by

© Tony Samurkas

Submitted to the Faculty of Graduate Studies and Research

of McGill University

in Partial Fulfillment

of the Requirements for the

Degree of Master of Engineering

Department of Chemical Engineering

McGill University

Montreal, Canada

September 1985

FOR MY PARENTS

ABSTRACT

The recent, rapid growth in the use of linear low density polyethylene (LLDPE) for plastic film production by the blown film process has resulted in a great deal of interest in the rheological properties of this material, as these properties govern processing behavior. In particular, knowledge of rheological properties is necessary for the design of processing equipment.

The main objectives of this work were to investigate and compare the rheological properties of three, superficially similar LLDPE film blowing resins with those of a conventional, branched LDPE film resin. The rheological properties of these resins were measured over a wide range of strain rates at three temperatures. The properties measured were shear viscosity, first normal stress difference, complex modulus, entrance pressure drop, extrudate swell and extrudate distortion characteristics.

The apparently similar LLDPE resins showed dramatic differences in zero-shear viscosity, extrudate swell, entrance pressure drop and susceptibility to extrudate distortion in shear flow, the differences in the other

measured properties being less pronounced. The LDPE resin tended to be more elastic than the linear resins while the LLDPE resins were more viscous than the LDPE resin at processing shear rates.

The entrance pressure loss data were used to estimate the extensional flow behavior of these materials although the method used [142] is thought to yield only qualitativley meaningful results.

Résumé

Au cours des dernières années, l'utilisation de plus en plus grande du polyéthylène basse densité linéaire (PBDL) pour la production de film soufflé est responsable de l'intérêt accru pour les propriétés rhéologiques de ce matériau, et ce surtout pour la conception de l'équipement du procédé.

Le principal objectif de ce travail est d'étudier et de comparer les propriétés rhéologiques de trois résines de PBDL (en apparence identiques) avec celles d'une résine conventionnelle de polyéthylène basse densité (PBD). Les propriétés rhéologiques de ces résines ont été évaluées à trois températures différentes, pour une grande variété de vitesses de déformation. Les propriétés mesurées sont la viscosité en cisaillement simple, les contraintes normales, le module complexe, la perte de charge d'entrée, le gonflement à la filière ainsi que la rupture d'extrudat.

Malgré leurs caractéristiques similaires, les résines de PBDL ont démontré des différences marquées au niveau de la viscosité Newtonienne, du gonflement à la filière, de la perte decharge d'entrée et de l'état de surface de l'extrudat

en cisaillement simple, les autre propriétés ne présentant pas de différence appréciable. La résine de PBD a démontré des propriétés élastiques plus prononcées que les résines de PBDL; par contre, les résines de PBDL se sont avérées plus visqueuses que celle de PBD aux taux de cisaillement retrouvés lors de procédé.

La perte de charge d'entrée dûe a l'écoulement du polymère dans le convergent, a servi au calcul des propriétés élongationnelles de ces matériaux, même si la méthode utilisée [142] ne fournit que des informations qualitatives.

ACKNOWLEDGEMENTS

Firstly, I would like to extend my sincere thanks to my research supervisor, Professor J.M. Dealy, for his encouragement, guidance and patience throughout the course of this work.

In addition, I would like to thank the following:

-Messrs. Giacomin, Mutel and Pangalos for the many useful discussions that we have shared.

-Messrs. Kallos and Huang and Ms. Fusey for their assistance with the biaxial extensiometer interface circuit.

-The Natural Sciences and Engineering Research Council (NSERC) for financial assistance in the form of a scholarship from 1982 to 1984.

-The Department of Chemical Engineering for teaching assistantships granted to me during the course of my studies.

I would also like to thank all of my colleagues within the department for having helped create a stimulating social and professional environment in which to work. Special

thanks must go to Lorraine whose friendship and support have made my stay at McGill a particularly happy one.

TABLE OF CONTENTS

FIGURES

LIST OF TABLES

NOMENCLATURE

A or a	Acierno model adjustable parameter
a_i	Extensional flow coefficient
B	Extrudate swell ratio
C^{-1}	Finger strain tensor
d	Capillary diameter
D	Extrudate diameter
e	Bagley entrance correction
F	Total normal force in cone and plate flow
G	Modulus of elasticity
G'	Storage modulus
G''	Loss modulus
H	Spectrum strength of relaxation spectrum
k	Power law constant
L	Length
M	Torque or molecular weight
M_c	Critical molecular weight
M_n	Number average molecular weight
M_w	Weight average molecular weight
M_z	Z-average molecular weight
M_{z+1}	(Z+1)- average molecular weight
n	Power law constant
N_1	First normal stress difference

N_2	Second normal stress difference
P_d	Driving pressure
ΔP_e	Entrance pressure drop
ΔP	Pressure drop
Q	Volumetric flow rate
S_R	Recoverable shear
R	Radius
T	Temperature
t	Time
x_i	Acierno structural parameter
v_φ	Principle velocity component in cone and plate flow

Greek Symbols

$\dot{\gamma}$	Shear rate
$\dot{\gamma}_w$	Wall shear rate
γ	Shear strain
$\dot{\gamma}_c$	Critical shear rate for onset of extrudate distortion
$\dot{\varepsilon}_e$	Approximate extensional strain rate
ε_b	Biaxial strain
$\dot{\varepsilon}$	Uniaxial extensional strain rate
$\dot{\varepsilon}_b$	Biaxial extensional strain rate
$\underline{\Delta}$	Strain rate tensor
λ	Relaxation time

η	Shear viscosity
η_o	Zero-shear viscosity
η^*	Complex viscosity
η_E	Uniaxial extensional viscosity
η_E^+	Uniaxial stress growth function
η_b	Biaxial extensional viscosity
η_b^+	Biaxial stress growth function
ρ	Density
σ_e	Approximate extensional stress
Ω	Angular velocity
θ	Cone angle
δ	Phase angle
ω	Angular frequency
$\pi_{\theta\theta}$	Pressure normal to plate surface in cone and plate flow
$\tau_{\theta\varphi}$	Shear stress in cone and plate flow
τ_w	Wall shear stress

Chapter 1

INTRODUCTION

1.1 Overview

The large scale commercial introduction of Linear Low Density Polyethylene (LLDPE) by Union Carbide Corporation (UCC) in 1977 created a great deal of interest in the new processing technologies that would be required to efficiently manufacture products from this material. The generally superior mechanical properties of end products as well as the favourable process economics of LLDPE served to accelerate these efforts.

An area of particular importance has been the utilization of LLDPE to produce plastic films using the tubular film blowing process. In this process, molten polymer is extruded through a narrow gap (on the order of 1 mm) annular die. The molten polymer tube is then drawn

upward by a take-up device. Air is introduced into the bubble at the bottom of the die so that a slight positive pressure exists inside the bubble, inflating the bubble. Around the periphery of the bubble, where it exits the die, cold air is introduced and flows cocurrently along the bubble, cooling and eventually solidifying the tubular film. Thus, the molten polymer experiences both shearing and extensional flows. A schematic of this process is shown in Figure 1.

One of the most commonly used polymers in the blown film process is low density polyethylene (LDPE). The molecules of this material differ from those of LLDPE in that they contain numerous long branches, which may be as long as the main molecular chain [1], while LLDPE has no long branches. As a result of this as well as other differences, the two materials exhibit dramatically different rheological behavior and, thus, processing characteristics. In order to effectively design new blown film equipment, or to modify existing equipment, a clear understanding of the rheological behavior of LLDPE is required. In addition, an understanding of how the rheology of different types of LLDPE film resins differ is essential if newly designed film blowing lines are to be sufficiently versatile to run a variety of LLDPE resins.

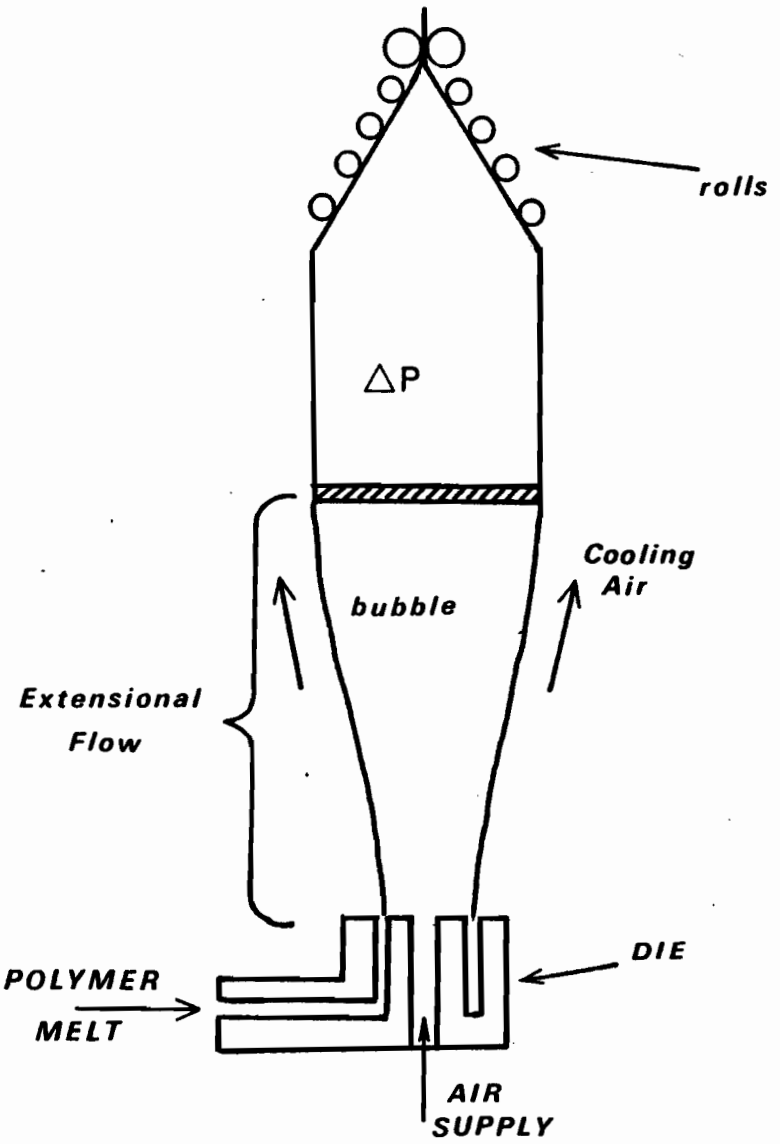

Figure 1. A schematic of the film-blowing process.

It is the objective of this work to study those rheological properties of three, superficially, similar LLDPE film resins and an LDPE film blowing resin that are thought to be of importance in determining their processing characteristics. The properties of importance fall into four broad categories.

1.1.1 Steady Shear Properties

Steady shear is the primary mode of deformation experienced by the molten polymer as it travels through the extruder and subsequently through the annular die. A knowledge of the shear rheology of a material gives some insight into the power requirements of the extruder drive, and of the die design in order to ensure uniform flow with minimum pressure drop.

1.1.2 Dynamic and Elastic Properties

A knowledge of the elastic and viscous response of a polymer to small, periodic deformations yields information on the manner in which stresses in the material decay with time after deformation. This information is important, at least qualitatively, for ranking materials in terms of their ability to retain their molecular orientation while solidifying. The extent of orientation is an important

factor in determining the mechanical properties of the solidified film. The elastic property of particular interest in the film blowing process is the tendency of the molten polymer tube to swell as it exits the die. This behavior is a result of the partial recovery of the strain imparted to the melt as it flows through the die. Depending on the amount of swell the melt exhibits, the ratio of the takeup speed to extrusion rate must be controlled in order to produce films of the desired thickness [2].

1.1.3 Flow Instabilities

At a given temperature, molten polymers exhibit flow instabilities at a critical value of the shear rate. These instabilities may manifest themselves as a distortion of the extruded molten polymer or as fluctuations in the pressure drop through the die, or as a combination of the two. In any case, they may limit the production rate of the film blowing process. If these phenomena are to be minimized, an understanding of the conditions under which they occur for a particular material is essential.

1.1.4 Extensional Flow

After exiting from the annular die, the melt is subjected to stretching in two directions: the machine

direction due to the windup device, and in the transverse direction due to the pressure difference between the bubble interior and exterior. This is known as unequal biaxial extension. How the material responds to such stretching is important in determining how the polymer molecules are oriented and how thin a film the melt can be made into.

It is hoped that a knowledge of the rheological properties of the materials to be studied will provide some insight into their processing behavior. Summarized below are the primary and secondary objectives of this work.

1.2 Objectives

A. Primary Objectives:

1) Measure the steady shear properties of the four resins. Those properties to be measured are the shear viscosity and, at low shear rates, the first normal stress difference. The latter being a measure of the elasticity of the melt.

2) Measure the elastic and viscous response of these resins to small strain periodic deformations. These are referred to as the linear viscoelastic properties of the materials.

3) Measure the swelling behavior of these materials after being subjected to steady shear.

4) Investigate the conditions under which flow instabilities occur.

5) Compare the materials response as determined in objectives 1 and 2 with the predictions of the model proposed by Acierno et al [3].

These properties will be measured at 190, 210 and 240 ^{0}C in the case of the three LLDPE resins and at 190 ^{0}C for the LDPE resin.

B. Secondary Objective:

Measure the biaxial extensional rheology of these materials using equipment developed at McGill by Rhi-Sausi [4] and subsequently modified by Yang [5].

Chapter 2

OVERVIEW OF LINEAR LOW DENSITY POLYETHYLENE

2.1 Manufacturing of LLDPE

In commercial terms, the four leading LLDPE technologies are those of Du Pont Canada, Union Carbide Corporation(UCC), Dow Chemical and, to a lesser extent, Phillips Petroleum. The first three processes are based on the copolymerization of ethylene with an α-olefin using Ziegler-Natta catalysts; Phillips having developed its own class of metal oxide catalysts. These processes are noted for their low operating pressures compared to the older process for the production of highly branched LDPE. This branched resin is produced in tubular or autoclave reactors by free radical polymerization at pressures as high as 3000 atm and temperatures between 100 and 200 ^{0}C [6]. In contrast, LLDPE resins generally possess little branching. Side chain length is controlled by the

choice of comonomer. Side chain frequency is controlled by the concentration of comonomer used during copolymerization. The distribution of side chain groups along the main molecular chains is influenced by the nature of the catalyst used. These factors influence the solid state properties of the resin end products, but have little effect on the melt rheology [7,8].

LLDPE was first brought onto the market by Du Pont Canada in the early 1960's, with Phillips following in 1970; their products were not as commercially successful as other polyethylenes available at that time, although Du Pont did grant several licences for this process [9]. Du Pont's Sclair solution process operates at relatively high (100 atm) pressures and temperatures and is very flexible with respect to product density and choice of comonomer. Originally Du Pont utilized primarily 1-butene as a comonomer, but has recently begun using 1-octene as well [10]. The popularity of this process has been due to the very high (>95%) conversion rates attainable, as well as the wide range of products that can be produced using a single catalyst system. The Phillips process is an emulsion type process that operates at comparatively low pressures (20 atm) and at a sufficient temperature to allow dissolution of the polymer in the reaction medium. This process utilizes 1-hexene as a comonomer. The resulting product is of a somewhat higher

density than those produced in the other LLDPE processes [11].

The sudden growth in the importance of LLDPE as a commodity resin may be attributed to the introduction of the Unipol process by Union Carbide Corporation (UCC) in 1977. The advantage of this process is that it does not require any solvents and thus avoids the processing equipment required for their recovery and purification. Polymerization takes place in a fluidized bed. The catalyst is the bed material, and an operating pressure of about 20 atm is used. The ethylene-comonomer mixture is fed into the bed and serves to fluidize the catalyst. Conversion of the reaction mixture is on the order of 3% per pass, necessitating the recycling of large amounts of gas. This process can use a variety of comonomers, with 1-butene being the most common, although newer grades with longer comonomers have been introduced. Unlike the Du Pont Canada and Phillips processes which yield a product in pellet form, the Unipol product is granular but may be pelletized in a later stage [12].

In 1977 Dow Chemical introduced its solution phase Dowlex process for LLDPE manufacture. This process operates at a pressure of about 25 atm. This limits the choice of comonomer to C7 to C14 α-olefins. Lighter α-olefins would be too volatile to remain in solution at typical operating

conditions [13]. Since these monomers are more expensive than 1-butene or 1-hexene, Dow's production costs are generally higher than those of competing processes that are capable of using 1-butene [9].

These technologies for the production of LLDPE are quite similar to those used for HDPE production. The main factor distinguishing the two technologies is the requirement for a relatively high comonomer content in the LLDPE polymers (3-12wt%). The rate of polymerization of the comonomer is lower than that of ethylene and the ratio of comonomer to ethylene in the reactor must therefore be several times higher than that required in the polymer. This requirement places a limitation on the type and quantity of comonomer that can be used in a particular process. For example, in the Unipol process the monomer mixture must be in the gaseous state; thus, the comonomer must be sufficiently volatile so that it does not condense under operating conditions. Similarly, in a solution process the operating pressure must be high enough to keep sufficient comonomer in the liquid phase, and lower boiling comonomers would require higher operating pressures [13].

The primary advantage the various LLDPE processes have over the conventional LDPE process is their ability to operate at substantially lower pressures, with the attendant

benefits. In Table I [13] a summary of the comparative costs of the Dow, Du Pont, UCC and conventional LDPE processes is given. The UCC process yielding granular product has the lowest capital cost, followed by those of Dow, Du Pont Canada, pelletized product UCC and, lastly, the high pressure LDPE process. There is some disagreement in the published literature regarding the capital and operating costs associated with the various processes. According to UCC a Unipol plant can be constructed for only 30% of the cost of a conventional high pressure process [14]. In contrast, Imhausen et al. [15] claim that their company's (Imhausen-Chemie GmbH) LDPE process is lower in both capital and operating costs than a Unipol process producing pelletized product, and has a capital cost 25% greater than a Unipol process yielding granular product. These authors cite the high cost of the catalyst and comonomer and the higher marketing and research costs associated with the newer LLDPE processes. Imhausen et al. argue that the cost savings inherent in operating at lower pressures are somewhat offset by the cost of additional equipment required for feed purification.

In addition to the relatively well established technologies discussed, new processes and products are being developed at competative costs. Chimie de France (CdF) has developed a technology that permits operators of high

LOW DENSITY POLYETHYLENE PRODUCTION COSTS

(100 000 metric tons/yr; .915 g/cm^3)

Process	Fixed Investment, U.S. Gulf Coast million $, mid-1980
High pressure tubular reactor, LDPE	74.9
Dow solution process, LLDPE	46.5
Du Pont, Canada solution process, LLDPE	51.5
Union Carbide gas phase, LLDPE	
pellets	52.5
granules	39.6

Table 1

pressure LDPE plants to modify their processes to produce LLDPE resins. The capital costs of this retrofit process are about 45% lower than those of the gas and liquid phase processes previously discussed. It also utilizes Ziegler-Natta catalysts, but as a result of its high operating pressures has operating costs about 25% above those of the Unipol process, and comparable to those of the Dow and Du Pont Canada processes [16]. B.P. Chemicals has developed its own process based on the conversion of a gas phase fluid bed process for HDPE production. They report that for a cost of roughly U.S.$1 million this process can be modified to produce LLDPE. The comonomer used is 4-methyl-1-pentene [17].

2.2 Solid State Properties

It has been found that the length, number and distribution of comonomer side chains have a profound influence on the microstructure and mechanical properties of LLDPE. The density of LLDPE is determined by the amount of comonomer in the polymer, decreasing as the content is increased [13]. A smaller amount of a longer chain comonomer is required than of a shorter chain comonomer to achieve the same density [7]. The absence of long chain branching results in a greater degree of crystallinity in LLDPE as compared to

LDPE resins; this results in a higher melting range. Since any branching tends to reduce crystallinity, increasing the level of comonomer tends to reduce the melting point of the resin [18]. The superior mechanical properties of LLDPE over LDPE have contributed to its popularity. The extent of improvement in such properties is controlled by the length, frequency and distribution of the comonomer branches [19]. A summary of the mechanical properties of some LLDPE (two of which are the subject of this study) film resins compared to those of LDPE and HDPE film resins is given in Appendix A. The well documented trend has been for the mechanical properties to improve as the comonomer length is increased [8,18,19]. Depending on the process used, optimal mechanical properties are achieved with comonomers of 8 to 12 carbon atoms [13,20]. A notable deficiency of LLDPE resins, when they are used to make films, is their greater haze compared to LDPE films; this somewhat limits their use to products were film clarity is not of importance [9].

Workers at Du Pont Canada [18] found that the distribution of comonomer between the molecules of copolymer affected end product mechanical properties. They noted that LLDPE resins that had a homogeneous distribution of comonomer exhibited reduced haze levels in films, as well as higher impact strengths for other extruded articles, when compared to heterogeneous copolymers. In addition, they showed that

both the polymer density and melting point increase as the comonomer distribution becomes more heterogeneous for a given comonomer concentration. The superior mechanical properties of LLDPE as compared to LDPE and HDPE have enabled resin processors to make thinner and lighter products that still have acceptable mechanical properties. Conversely, products of the same thickness or weight but with superior mechanical properties can be produced using these materials.

2.3 Processing Behavior

With the introduction of any new resin some modifications to existing process technologies must be made to account for differences in resin rheology and thermal properties. Because of its commercial importance and sensitivity to variations in resin properties, the modifications to film-blowing processes required to economically utilize LLDPE resins will be considered.

The main difficulties, in terms of process modifications, arise when one tries to process LLDPE on equipment designed to process LDPE resins. Unlike most LDPE resins, which tend to exhibit a quite rapid decrease in viscosity at processing shear rates, LLDPE resins exhibit a much less pronounced viscosity reduction at comparable shear

rates. This behavior is typical of linear, narrow molecular weight distribution resins [9]. Because of its increased viscosity, the power requirements to extrude LLDPE are greater than for LDPE, and LLDPE will exhibit a greater temperature increase due to viscous heating, at a given shear rate [21]. However, since plastics extruders operate on the principal of drag induced flow [2] a more viscous material like LLDPE will generally have a higher specific output (kg/hr-rpm).

To efficiently extrude LLDPE, new screw designs have been developed. To minimize viscous heating and reduce extruder drive power requirements, Kurtz et al. [21] suggested using screws shorter than those normally used for LDPE extrusion as well as using deeper channels on these screws. Deeper channels will reduce the viscous heating experienced by the melt. Normally in extruders, the channel depth is progressively decreased as the extruder exit is approached in order to generate pressure. Miller [22] suggested progressivly decreasing the flight spacing as the exit of the extruder is approached, thus achieving the pressure buildup in the melt without having to decrease the channel depth. The use of deep channels, however, can result in the presence of unmelted solids at the end of the flighted sections. The melting must therefore be completed by a barrier-type mixing head attached to the end of the screw.

To further reduce the viscosity of these materials they are generally extruded at higher temperatures than LDPE-typically 200 to 250 ^{o}C in film applications.

Due to the high shear stresses developed in the film die, narrow molecular weight distribution resins such as LLDPE experience a phenomenon known as sharkskin as they exit the die. This is a surface irregularity characterized by a series of ridges perpendicular to the direction of flow. It usually occurs at a shear stress lower than that at which LDPE exhibits distortion. Two simple, but not always practical, ways to eliminate this effect are to reduce the throughput of resin through the die or to increase the temperature at which the resin is processed. More effective methods have included using wider die gaps as well as having the die either converge or diverge just at the exit of the die [7].

A material's extensional viscosity is a measure of its resistance to elongation. Thus, a melt with a low extensional viscosity requires less force to elongate it. All LLDPE resins have lower extensional viscosities than LDPE resins. In the film blowing process, a low extensional viscosity permits the production of thinner films. Associated with this lower extensional viscosity, however, are problems with bubble stability. When the polymer bubble

is formed, it must be cooled so that the polymer will solidify. This is commonly done by having an air stream impinge on the bubble. An LLDPE melt can be deformed more easily than an LDPE melt, and it is more sensitive to air flows. An air flow that impinges directly on the bubble can create a force strong enough to destabilize it [21]. Air rings, which guide the flow of cooling air, have been designed to direct the air flow so that it is essentially parallel to the bubble surface. These designs permit sufficient cooling of the generally hotter LLDPE bubble and, because of the air flow pattern, also aid in stabilizing the bubble. A more complete review of air ring technology is presented by Strater [23].

Although LLDPE can be processed at rates comparable to those attained with LDPE on suitably modified equipment, most resin processors are compromising and using blends of LLDPE and LDPE. Speed [24] found that as LDPE is added to LLDPE, the onset of flow instabilities occurs at higher shear stresses and the viscosity is reduced. Furthermore, the force required to stretch the molten bubble rapidly increases as LDPE is added to LLDPE, so that at about 35 wt% LDPE in LLDPE the stretching force is near that for pure LDPE. In general it was found that the mechanical properties increased almost linearly as LLDPE was added to LDPE [24].

Chapter 3

RHEOLOGY OF MOLTEN PLASTICS

3.1 Viscometric Functions

3.1.1 Introduction

A viscometric flow is one in which the deformation experienced by a given element of fluid is indistinguishable from steady simple shear [25]. When a polymeric liquid is sheared in a viscometric flow the polymer molecules experience some orientation in the flow direction. This departure from the random orientation distribution gives rise to normal stress differences. Referring to Figure 2, this implies that the normal stresses on a fluid element are unequal.

$$\tau_{11} \neq \tau_{22} \neq \tau_{33}$$

Thus to completely define the state of stress of a material

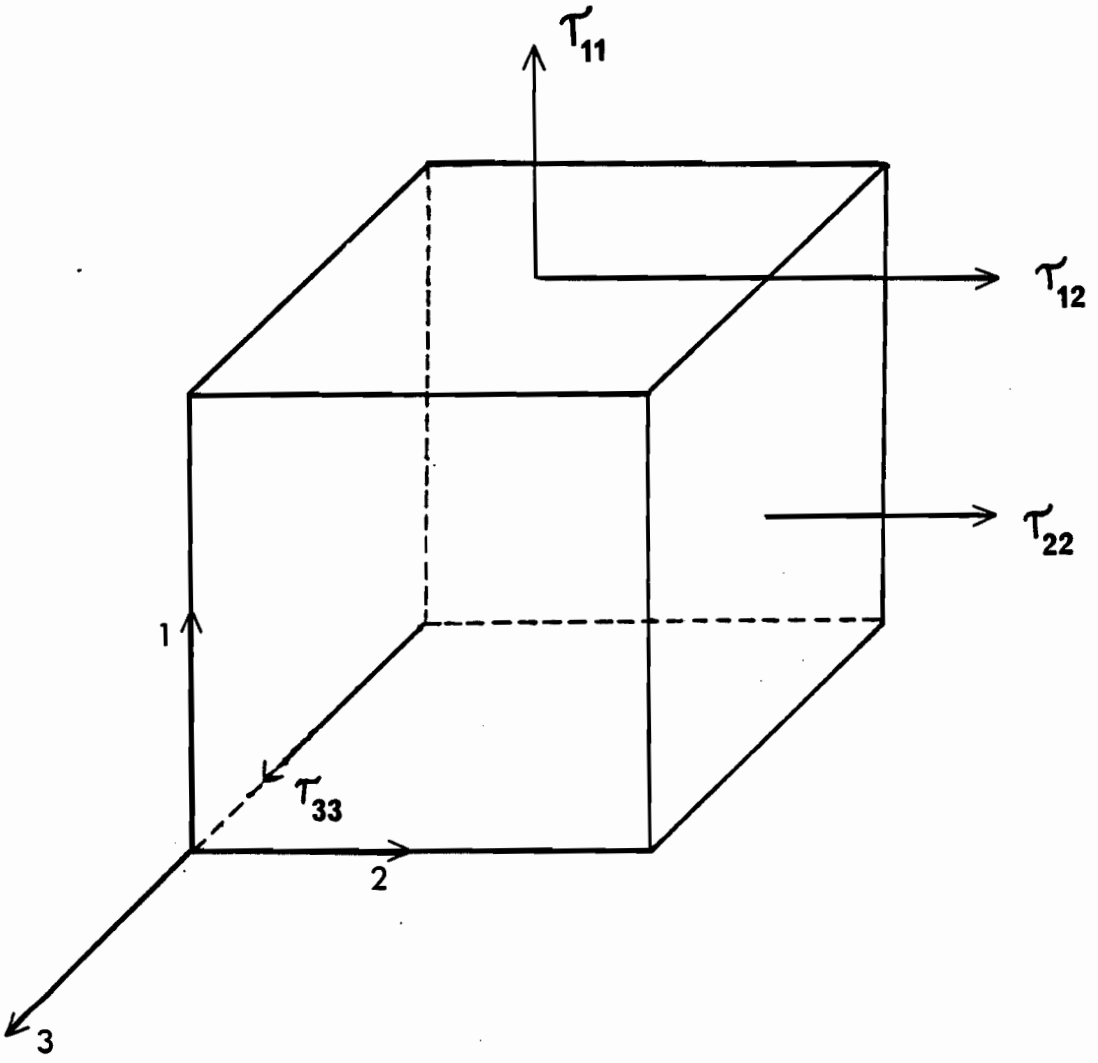

Figure 2. Stresses on a fluid element.
Axis 2 represents flow direction.

sheared in a viscometric flow both the shear stress, τ_{12}, and the normal stresses are required. However, for an incompressible liquid, only differences between normal stress components are rheologically significant [25]. Thus, three independent viscometric functions can be defined;

$$\eta(\dot{\gamma}) \equiv \tau_{12} / \dot{\gamma} \qquad (1)$$

$$N_1(\dot{\gamma}) \equiv \tau_{11} - \tau_{22} \qquad (2)$$

$$N_2(\dot{\gamma}) \equiv \tau_{22} - \tau_{33} \qquad (3)$$

The first function is called the viscosity, while the remaining two are called the first and second normal stress differences. All three are functions of the shear rate, $\dot{\gamma}$. Viscometric flows are a subset of what are commonly referred to as shear flows. A shear flow is defined to be a flow for which the distance between any two neighbouring particles in a shearing surface remains constant. Furthermore the distance between any two neighbouring shearing surfaces is constant. Bird [26] gives two additional criteria for the existance of a viscometric flow:

1) The lines of shear must be material lines.
2) The shear rate, $\dot{\gamma}$, is independent of time for a given particle.

The second criterion is self explanatory, while the first warrants further explanation. For any shear flow, one can

define lines of shear which, on a given shearing plane, are tangent to the direction of motion of a fluid particle. If these lines of shear are comprised of the same fluid particles at all times, they are referred to as "material lines" [26].

Using these definitions, it becomes apparent that there are several ways of generating a viscometric flow in the laboratory. The best known being;

(a) Laminar tube flow.

(b) Couette flow.

(c) Torsional flow.

(d) Cone and plate flow.

(e) Drag induced flow between parallel plates.

These flows are discussed in detail by Bird [26].

It is the task of the experimental rheologist to select from amongst these, a flow field that will readily yield values of the viscometric functions. The selection criteria include the type of material under investigation, any mechanical design limitations of the apparatus, and the shear rates at which data are desired.

3.1.2 Controllability of Flows

The primary problem associated with measuring the viscometric functions of a polymeric material is a lack of knowledge of the rheological constitutive equation of the material. Thus the viscometric flow selected must be completely controllable if all three viscometric functions are to be measured. This means that by prescribing the boundary conditions of the flow, the assumed kinematics of the flow satisfy Cauchy's equation regardless of the liquid's constitutive equation [25]. The best known example of such a flow is drag induced flow between parallel plates. Unfortunately, no commercial instruments are available that can generate this type of flow field, although several experimental devices have been described [27,28].

Laminar tube, Couette and torsional flows are all examples of "partially controllable" flows. These flows are characterized by having streamlines whose orientation is material independent, but which generate a shear field (and thus a stress field) that is not uniform in space and is dependent on the material's rheological properties. By measuring shear stresses at the solid boundaries, and with some data manipulation, values of the non-Newtonian shear viscosity can be obtained. The most commonly used of the

three flows, particularly for measurements of fluid viscosity at higher($\dot{\gamma}$ >1 s^{-1}) shear rates, is laminar tube flow. It is generally accepted that partially controllable flows are not capable of yielding reliable values of the normal stress differences [25]. However, this is still a subject of controversy [25,29,30].

In addition to controllable and partially controllable flows is a third class of flows which are easily generated and that yield values of the normal stress differences. This third class is referred to as "approximately controllable" [31]. Such flows are controllable when certain terms in Cauchy's equation can be neglected. The best known example of such a flow in experimental rheology is cone and plate flow.

3.1.3 Cone and Plate Flow

Cone and plate flow is obtained in the region bounded by a flat circular plate and a convex cone whose apex is in initial contact with the plate. In practice, however, the tip of the cone is truncated and a small gap is maintained between the two surfaces. This is to prevent damage to either of the surfaces, which would occur if they were to rub against each other. A schematic of the cone and plate geometry is shown in Figure 3. In the course of an

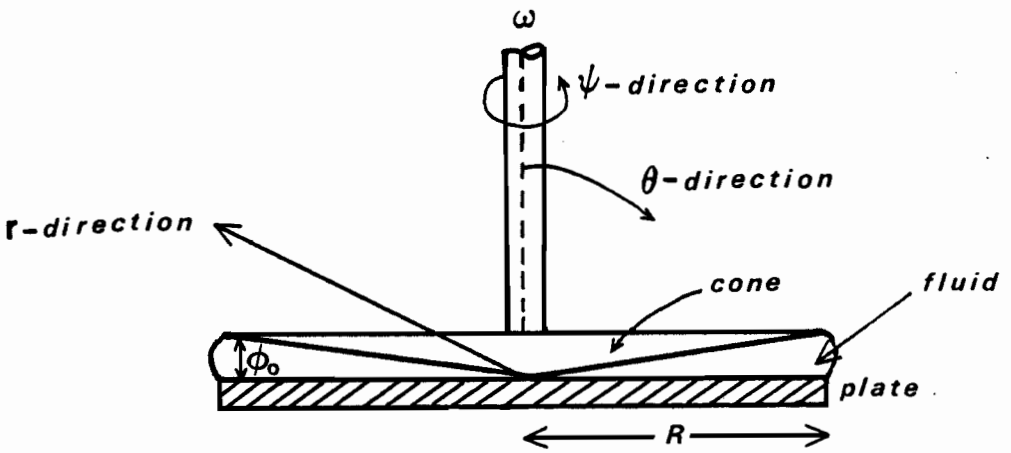

Figure 3. Schematic of cone and plate geometry.

experiment, either the cone or the plate is made to rotate at a constant angular speed while the other fixture is held stationary.

To make such a complex flow amenable to analysis, certain simplifying assumptions are required. The key ones are listed below.

1) Inertial effects are negligible (this allows one to neglect the acceleration terms in the equations of motion).

2) The cone angle is small (this allows one to assume that the shear rate and thus the stresses are uniform throughout the flow field).

3) The free surface of the sample at the edge of the gap is spherical, with a radius of curvature equal to the radius of the flat plate.

4) Surface tension effects at the liquid free surface are negligible.

With these assumptions, the following expressions describing the velocity field and viscometric functions can be derived [30,32].

$$v_\psi = \Omega r \tag{4}$$

$$\dot{\gamma} = \Omega / \phi_0 \tag{5}$$

$$\tau_{\theta\psi} = 3M / 2\pi R^3 \sin^2 \phi_0 \tag{6}$$

However, since $\phi_0 << 1$ rad, $\sin^2(\phi_0)$ is approximately unity, equation (6) simplifies to,

$$\tau_{\theta\psi} = 3M / 2\pi R^3 \tag{7}$$

where M denotes the torque exerted on the stationary fixture. To calculate the normal stress differences from the total normal thrust, F, which acts to separate the cone and plate, the following expressions can be derived:

$$N_1(\dot{\gamma}) = \tau_{\psi\psi} - \tau_{\theta\theta} = 2F / \pi R^3 \tag{8a}$$

$$N_2(\dot{\gamma}) = \tau_{\theta\theta} - \tau_{rr} \tag{8b}$$

$$N_1(\dot{\gamma}) + N_2(\dot{\gamma}) = -\partial \pi_{\theta\theta}(r) / d \ln r \tag{9}$$

The term $\pi_{\theta\theta}(r)$ is the local pressure on the plate. The total torque, M, and the total normal thrust, F, can, with some care, be measured; but, the measurement of the plate pressure profile is a more difficult task. To measure this profile, very small pressure transducers must be flush-mounted in the plate at several radial positions.

The equations presented above will adequately describe the behavior of a liquid in cone and plate flow as long as the assumptions listed are valid. If any are invalid, substantial errors in the values of the viscometric functions

can arise. Detailed discussions of the errors introduced if these assumptions are not applicable are given by Dealy [25] and Garcia-Rejon [33].

3.1.4 Capillary Flow

In most polymer processing operations, the melt is subjected to comparatively high shear rates, up to $10^5 s^{-1}$ in some processes. Primarily because of the ease with which it can be generated, capillary flow has found widespread use as a method for obtaining high shear rate viscosity data. The characteristic feature of the method is its use of a very narrow capillary through which the material is forced, with the pressure drop being recorded at a given flow rate. Using a narrow capillary offers two main advantages. Firstly, for materials of low viscosity an easily measurable pressure drop is generated in a relatively short tube; secondly, a narrow tube allows the viscous heat generated in the flow of viscous materials to be dissipated more quickly.

The polymer forced through the tube may be subjected to either a fixed wall shear stress or a fixed shear rate. In the former case, the volumetric flow rate of polymer exiting the capillary is measured and related to the wall shear rate, while in the latter the pressure drop across the capillary is measured at a given wall shear rate. In developing the

mathematical framework with which to analyze capillary flow of a non-Newtonian liquid, the assumptions made regarding the nature of the flow are similar to those associated with Hagen-Poiseuille flow. Beyond the entrance of the tube, for a Newtonian liquid the following expressions apply.

$$\tau_w = -\Delta P \cdot R / 2L \tag{10}$$

$$\dot{\gamma}_w = 4Q / \pi R^3 \tag{11}$$

Since equation (10) is derived from a force balance it is applicable regardless of the rheology of the liquid. The expression for the wall shear rate, however, is strictly applicable only to Newtonian liquids. For the case of a non-Newtonian liquid an expression relating the wall shear rate to measurable properties, such as the volumetric flow rate and wall shear stress, is required. Starting with the definition of the volumetric flow rate in a tube,

$$Q = 2\pi \int_0^R v_z r \, dr \tag{12}$$

and integrating by parts, we obtain the following:

$$Q = -\pi \int_0^R \left(\frac{dv_z}{dr}\right) r^2 \, dr \tag{13}$$

The derivative in the integrand of equation (13) is simply the definition of the shear rate. We also have available the following relationship between the wall shear stress, τ_w, and the shear stress at any radial position.

$$\tau_{rz} = \tau_w \cdot \frac{r}{R} \qquad (14)$$

This can be substituted into equation (13) and the variable of integration changed from r to τ_{rz}; for the case of non-Newtonian liquids the shear rate, $\dot{\gamma}$, must be treated as a function of the shear stress [26]. By differentiating equation (14) with respect to τ_w, the following relation is obtained.

$$\dot{\gamma}_w = \frac{1}{\tau_w^2} \frac{d}{d\tau_w} \left(\frac{\tau_w^3 Q}{\pi R^3} \right) \qquad (15)$$

Thus by plotting the volumetric flow rate against the wall shear stress, the wall shear rate at each shear stress can be determined. The value of the non-Newtonian viscosity is then found using the following expression.

$$\eta = \tau_w / \dot{\gamma}_w \qquad (16)$$

Many polymeric liquids exhibit what is known as "power-law" behavior at higher shear rates. This implies the following relationship between wall shear stress and shear rate.

$$\tau_w = k \dot{\gamma}_w^n \qquad (17)$$

For this special case, the following expression can be derived[25].

$$-\frac{\Delta P \cdot R}{2L} = k \left(\frac{3n+1}{4n} \right)^n \left(\frac{4Q}{\pi R^3} \right)^n \qquad (18)$$

Thus one can plot $-(\Delta PR/2L)$ against $(4Q/\pi R^3)$ on a logarithmic scale and obtain values of k and n from the intercept and slope of the resulting straight line.

The methods outlined above would work satisfactorily if the pressure drop in the capillary were measured using pressure transducers mounted along it's length. In most capillary rheometers, however, some sort of cylindrical plunger is used to force the polymer through the capillary, and the force required to do this is measured. Using these methods one must consider contributions to the driving force in addition to the fully developed flow pressure drop. Dealy [25] summarizes other factors that can contribute to the driving force for elastic liquids.

The two major contributions (aside from the pressure drop in the fully developed flow region) to the measured driving force are the pressure drops associated with the entrance and exit regions of the capillary. In the entrance region large stresses are developed due to the funneling effect as the fluid enters the capillary from the larger diameter polymer reservoir. The excess pressure drop is due to the large extensional stresses and, in some cases, recirculating eddies present [34-36] at the entrance; as well as to the hypothesized rearrangement of the velocity profile near the capillary exit [37].

Bagley [38] has suggested a procedure whereby the excess entrance pressure drop can be estimated. The procedure involves making measurements of the total pressure drop through capillaries of different lengths, but with identical entrance geometries. These capillaries should be long enough so that a region of fully developed flow exists. An "end correction", e, is then defined as follows,

$$\tau_w = P_d/2\left(\frac{L}{R} + e\right) \qquad (19)$$

where P_d is the measured driving pressure. Physically, e, can be considered to be the dimensionless length of fully developed capillary flow that would yield a pressure drop equal to that due to entrance effects. By making measurements of P_d for capillaries of different L/R ratios, and plotting P_d versus L/R with $\dot{\gamma}$ as a parameter, values of "e" can be obtained. The plots should be linear, and by extrapolating them to a zero driving pressure, one obtains a value of "e" as the intercept on the abscissa.

3.2 Linear Viscoelasticity

3.2.1 Description

To this point, only the viscous properties of polymeric materials have been considered. Also of importance are the

viscoelastic properties of molten polymers. The viscoelasticity of these materials is due to the fact that the polymer molecules not only interact by simple elastic collisions, as do gases and simple liquids, but also form temporary networks by wrapping around one another. These temporary entanglements play a dominant role in determining both the viscous and viscoelastic behavior of molten polymers. As the material is deformed, the number or density of entanglements is diminished. In addition, viscoelastic behavior is exhibited by dilute polymeric solutions in which molecular entanglements do not occur. For these materials, viscoelastic behavior is a result of the molecular orientation caused by an applied strain.

Linear viscoelasticity is a class of behavior often observed in deformations involving very small strains or strain rates. In this limit, the strain is sufficiently small so that the molecular orientation and entanglement density are not affected; or is sufficiently slow so that the rate of entanglement creation due to thermal motion is sufficient to replace those entanglements destroyed by deformation. For dilute solutions, linear viscoelastic behavior is exhibited when the strain is too small to alter the molecules random orientation distribution; or slow enough so that molecular orientation and the return to a random conformation due to thermal motion occur at the same rate.

The advantage of the use of linear viscoelasticity to characterize a material is that the representation of the material functions is simplified by the disappearance of the strain or strain rate as a parameter [25].

Two types of experiments can be used to determine the material functions that describe linear viscoelastic behavior. These are:

(i) Transient experiments (time domain).

(ii) Oscillatory shear experiments (frequency domain).

In the first, the material's stress response to a suddenly imposed strain or stress is measured as a function of time. In oscillatory shear the fluid is subjected to sinusoidal shearing. The shear strain is given by:

$$\gamma = \gamma_0 \sin(\omega t) \qquad (20)$$

The shear rate in the gap is thus:

$$\dot{\gamma} = \dot{\gamma}_0 \cos(\omega t) \qquad (21)$$

were ω is the frequency and $\dot{\gamma}_0$ the strain rate amplitude. For a purely viscous liquid, the stress recorded at the stationary plate is exactly in phase with the strain rate:

$$\tau_{viscous} = \eta \dot{\gamma}_0 \cos(\omega t) \qquad (22)$$

However, for a purely elastic material the stress response is exactly in phase with the strain:

$$\tau_{elastic} = G \gamma_0 \sin(\omega t) \qquad (23)$$

where G is the modulus of elasticity. Since molten polymers are viscoelastic, their stress response will be some combination of those given in equations (22) and (23).

The following expressions can be used to decompose the material's stress response into in-phase (viscous) and out-of-phase (elastic) components.

$$\tau = \eta' \dot{\gamma}_0 \cos(\omega t) + \eta'' \dot{\gamma}_0 \sin(\omega t) \qquad (24)$$

The η' term being the in-phase component and η'' being the out-of-phase component. These material functions can be transformed to yield other functions [39]. The most commonly used being the storage modulus:

$$G' = \omega \eta'' \qquad (25)$$

and the loss modulus

$$G'' = \omega \eta' \qquad (26)$$

The phase angle between the strain and stress oscillations is given by the following expression.

$$\delta(\omega) = \tan^{-1}(G'/G'') \qquad (27)$$

Using the definition of the phase angle, equations (22) and (23) may be represented by the following expression:

$$\tau = \tau_o \sin(\omega t + \delta) \qquad (28)$$

where τ_o is the amplitude of the shear stress.

3.3 Biaxial Extension

3.3.1 Description of Extensional Flows

In general, an extensional flow is one in which the velocity field is given by

$$u_i = a_i x_i \qquad (29)$$

in a Cartesian coordinate system. In steady extension the a_i coefficients are constants. For an incompressible fluid the continuity equation reduces to,

$$\frac{\partial u_i}{\partial x_i} = 0 \qquad (30)$$

and thus,

$$\sum_i a_i = 0 \qquad (31)$$

In other words, an extensional flow is a flow in which the rate-of-strain tensor has only diagonal terms; for this reason they are often referred to as shear free flows [26]. Different categories of extensional flows are defined by specifying the a_i's in equation (29). Uniaxial extension was one of the first types of extensional flows to be studied. Its velocity distribution, in cylindrical coordinates, is given by the following equations,

$$\begin{aligned} v_z &= \dot{\epsilon} z \\ v_r &= -\tfrac{1}{2}\dot{\epsilon} r \\ v_\theta &= 0 \end{aligned} \tag{32}$$

where, $\dot{\epsilon}$, is defined as the uniaxial strain rate. For a uniform cylindrical sample of original length, L_o, $\dot{\epsilon}$ is given by the following expression.

$$\dot{\epsilon} = \frac{1}{L}\frac{dL}{dt} \tag{33}$$

If $\dot{\epsilon}$ is time independent, the following material function can be defined,

$$\eta_E(\dot{\epsilon}) = \frac{(\tau_{zz} - \tau_{rr})(\dot{\epsilon})}{\dot{\epsilon}} \tag{34}$$

This is referred to as the extensional viscosity. For the case of a stress growth experiment, where a steady state stress has not been attained, a uniaxial stress growth coefficient can be defined.

$$\eta_E^+(\dot{\epsilon}, t) = \frac{(\tau_{zz} - \tau_{rr})(\dot{\epsilon}, t)}{\dot{\epsilon}} \tag{35}$$

In many polymer processing operations, the molten polymer is

subjected to both shearing and extensional strains. In terms of annual production, one of the most important of these processes is the blown film process [30]. In this process the molten polymer is subjected to a complex unequal biaxial extensional flow, as a opposed to uniaxial extension which is the primary mode of deformation, for example, in fiber spinning.

The special case of equal biaxial extension is described below. Consider the liquid disk shown in Figure 4. At time t=0 the disk is in its undeformed state; at time t the disk is stretched in the radial direction in such a way that in cylindrical coordinates there are only two non-zero velocity components.

$$v_r = \dot{\epsilon}_b r$$
$$v_z = -2\dot{\epsilon}_b z \qquad (36)$$

Thus, the velocity component, v_z, will be a function of only z, and the velocity component, v_r, will be a function of only r [4]. What we are actually observing is radial extension and simultaneous uniaxial compression. Taking this point of view, the radial strain rate, for a sample in the shape of a circular disk having radius R, can be defined as follows.

$$\dot{\epsilon}_b = \frac{1}{R}\frac{dR}{dt} \qquad (37)$$

with the total biaxial strain at time t being defined as,

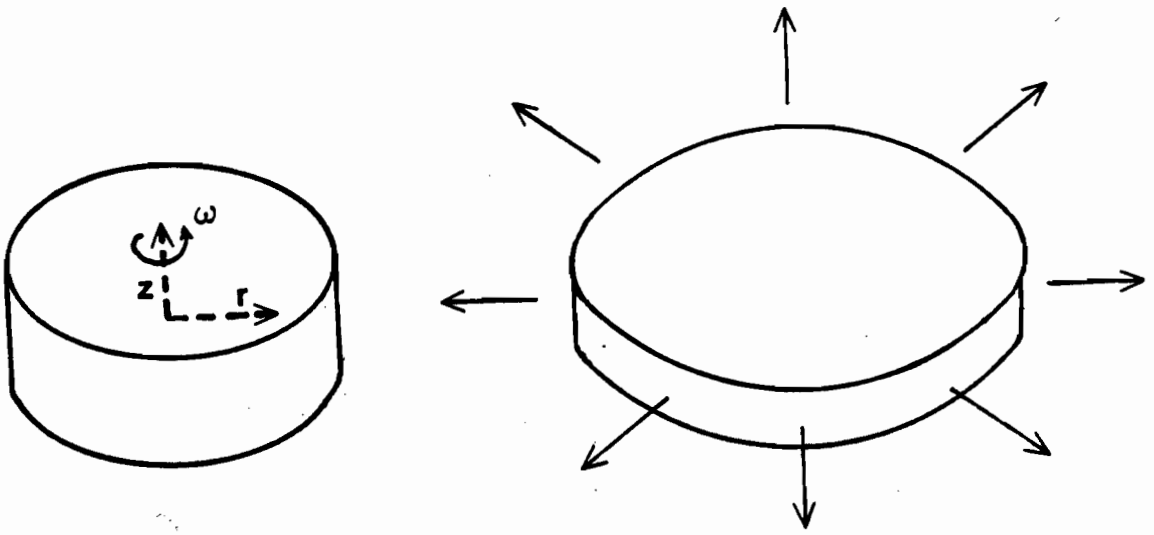

before extension

after extension

Figure 4. Equal biaxial stretching of a fluid disk.

$$\epsilon_b = \ln\left(\frac{R}{R_o}\right) \qquad (38)$$

We can consider this flow to be generated by a radial, tensile stress rather than an axial compressive stress [25]. Thus, the biaxial extensional viscosity is defined as follows [25].

$$\eta_b(\dot{\epsilon}_b) = \frac{(\tau_{rr} - \tau_{zz})(\dot{\epsilon}_b)}{\dot{\epsilon}_b} \qquad (39)$$

This definition presupposes that the stress difference given in the numerator of equation (39) has reached a steady state value. For the case of a stress growth experiment, in which a steady-state value has not been attained, a biaxial stress growth coefficient can be defined [40].

$$\eta_b^+(\dot{\epsilon}_b, t) = \frac{(\tau_{rr} - \tau_{zz})(\dot{\epsilon}_b, t)}{\dot{\epsilon}_b} \qquad (40)$$

3.3.2 Biaxial Extension Rheometry

Four methods have been used for the study of biaxial extension in elastic liquids, although no commercially manufactured instruments are yet available.

Meissner [41] has developed a device that uses a set of eight rotary clamps arranged in a circle to grip a circular sheet of molten polymer. As the clamps rotate at a controlled speed, the sample is stretched in all directions. Eight pairs of automated scissors cut the sheet of molten

polymer between the clamps at frequent intervals. This cutting produces eight strips of polymer that can be wound up on rollers. By controlling the rotational speed of the rotary clamps, the desired strain rate can be achieved. Measurement of the tensile force on the clamps permits a determination of the stress. The main drawbacks of this instrument are its mechanical complexity and its large thermal inertia, which requires long heat up times when working with thermoplastic polymers [42].

The idea of using a so called "lubricated squeezing flow" to generate equal biaxial extension was orginally put forth by Stevenson [43]. A device based on this idea was developed and tested by Chatraei and Macosko [44]. This instrument consists of two parallel disks, between which is held a sample of the material to be investigated. In an experiment, the lower disk is stationary, while the upper one is forced downwards, thus squeezing the sample. Ordinarily, this would generate a shear flow within the gap, but by placing a thin layer of low viscosity liquid between each disk and the sample, a flow that is almost purely extensional in character can be obtained. Numerical simulation studies indicate that shear dominates over extension when the viscosities of the two liquids are of the same order of magnitude. Extensional flow is well approximated in the "core liquid" when its viscosity is more than 100 times that

of the thin lubricating layers on both of the disks [45]. The main limitation of this technique is the fact that for extensional strains of more than about 1 (as defined in equation 38), the lubricant liquid tends to flow out from between the disks making the assumption of extensional flow invalid [46].

The idea of approximating biaxial extension by bubble inflation seems to have orginated in connection with work done on the elastic properties of rubbers [47]. The biaxial extensional properties of elastic liquids were first measured using this technique by Denson [48]. Rhi-Sausi and Dealy [49] developed an instrument based on this principle for use with molten thermoplastics.

Essentially, the method involves the inflation of a thin circular disk of the sample into a bubble. If one imagines for a moment that the circular region near the pole of the bubble is equivalent to the disk depicted in Figure 4, it can be seen that biaxial extension is approximated in the region near the pole. By measuring the rate of separation of material points near the pole of the bubble, and monitoring the pressure difference across the sample surface, estimates of the extensional strain and stress can be obtained [5]. Because of gravitational effects, liquid samples must be immersed in a medium of comparable density. Furthermore,

because of the fragility of the inflated bubble of the molten polymer, it is important that convection currents caused by thermal gradients in the supporting medium are eliminated.

Lastly, it has been suggested that lubricated flow in a divergent channel generates equal biaxial extension, but only away from the channel wall [50]. It is proposed that birefringence can be used to infer the stress in this region. Of course, the melt must be transparent to use this technique [51].

3.4 Extrudate Swell

3.4.1 Explanation of Phenomenon

The term "extrudate swell" is used to describe the increase of the diameter of a liquid stream as it emerges from a circular channel. This behavior is exhibited by elastic as well as inelastic liquids. The magnitude of this swell is quite small for the latter case, causing a 12% increase in diameter for a Newtonian liquid at low Reynolds numbers [52]. Elastic liquids such as polymer melts exhibit a similar increase in diameter at very low shear rates but may swell to 2-4 times the tube diameter at higher shear rates

[2]. For the case of a noncircular channel, the shape of the extrudate also changes [30]. The extrudate swell for flow from a circular die is defined by the following expression:

$$B = D/d \qquad (41)$$

where the meaning of these symbols is given in Figure 5.

For viscoelastic liquids extrudate swell is primarily a result of the gradual recovery of some of the strain imparted to the liquid as it travels through the particular flow geometry [53]. Depending on the material and processing conditions the so called "equilibrium swell" may only be attained after a period of 10 minutes or more.

Considering the case of equilibrium swell, for a particular polymer the extrudate swell is a function of wall shear rate, $\dot{\gamma}$, the L/D ratio of the circular tube, and the liquid temperature,T. The geometry of the entrance of the tube can also affect the extrudate swell when the L/D is not too large [30].

It has been found that the swell ratio decreases as L/D increases, becoming essentially independent of L/D at values greater than about 20 for polyethylene [30] and about 10 or less for polystyrene [54]. It is believed that this phenomenon is due to a characteristic of viscoelastic fluids known as fading memory. At the tube entrance, the material

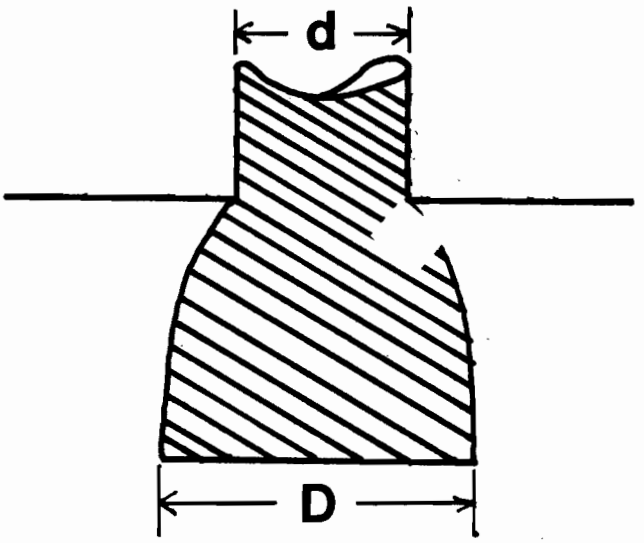

Figure 5. Capillary extrudate swell.

is subjected to an extensional strain field [36] which generates an axial normal stress within the material. When the liquid exits from the tube, these extensional stresses cause it to recoil resulting in an increase in diameter. Since viscoelastic liquids exhibit stress relaxation with time, the contribution these extensional stresses make to the materials swell diminishes when longer tubes are used. Lodge [55] observed that an elastic liquid which had not been subjected to the extensional strains associated with tube entry flow also swelled upon exiting from the tube. In shearing flow the long polymer molecules are oriented and stretched in the flow direction. As a result, an axial normal stress, τ_{zz}, (refer to Figure 6) is generated. When the liquid exits the tube, the shear strain that it had experienced is partially recovered (elastic recoil) resulting in an increase in extrudate diameter.

In the linear viscoelastic region the amount of shear strain recovered by a liquid after shearing can be defined [25],

$$S_R = (\tau_{zz} - \tau_{rr}) / 2\tau_{rz} \qquad (42)$$

where S_R is known as the recoverable shear. This expression is often found to fit experimental data in the materials non-linear viscoelastic region as well [25]. If this expression is valid, then extrudate swell can be related to

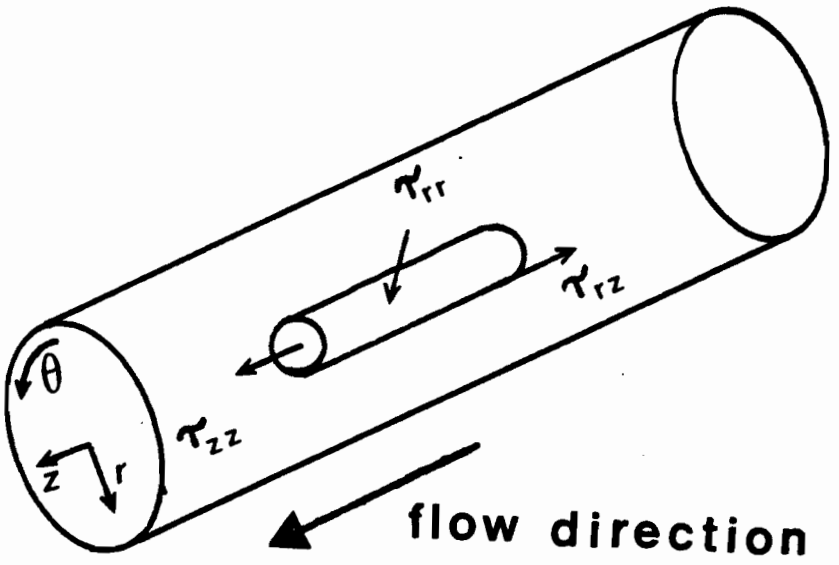

Figure 6. Stresses on a fluid element in capillary flow.

the normal stress difference at a particular shear rate. Furthermore S_R and thus extrudate swell are also increasing functions of shear rate.

Since extrudate swell is primarily due to elasticity it is not unexpected that for a given material and shear rate, the amount of swell decreases with increasing temperature [30].

The molecular structure of a molten polymer plays a central role in determining its swell characteristics. The properties that have been found to have the most dramatic effect on swell characteristics include molecular weight(MW) and molecular weight distribution(MWD). For most polymeric materials - polyolefins and polystyrene having recieved the most attention- the extent of swell increases with both MW and the broadening of the MWD [53,56]. For highly branched polymers, notably low density polyethylene(LDPE), swell increases with increasing frequency of long chain branching [57-59]. In addition any molecular characteristics that have an effect on material elasticity will also affect its swell characteristics.

3.4.2 Measurements Methods

Two broad classes of methods have found common use in making extrudate swell measurements. In the first method, a

short length of polymer is extruded into ambient air which quenches it. The diameter of the extrudate is then measured to yield a value of the swell. This method has three major shortcomings:

1) The extrudate solidifies before the equilibrium swell is achieved.

2) The swelling that takes place does so under non-isothermal conditions and while the polymer is undergoing a change of phase.

3) Since the density of the polymer is much greater than that of air, some sagging of the extrudate will occur.

All three of these factors will cause the equilibrium swell to be underestimated [60-62]. In the second method, the polymer is extruded into a heated chamber, maintained at a temperature above the polymers melting range, where it is allowed to swell completely, before its photograph is taken. As a further refinement of this method, the chamber into which the sample is extruded is filled with an inert liquid whose density approximates that of the molten polymer [62].

3.4.3 Predictive Methods

Three approaches have been used to predict the extrudate

swell of an elastic liquid.

1) Rubber elasticity theory.
2) Overall momentum balance.
3) Numerical simulation.

Models of the first type [63-66] assume that the liquid experiences an instantaneous rubber-like recovery of the strain it had been subjected to within the capillary. These models thus attempt to relate swell to the recoverable shear, S_R, which is approximated by equation (42). These models are not capable of predicting the ultimate swell of a liquid since this takes a finite period of time, after extrusion, to be achieved. One model of this type that has been used to predict swell [67] is that of Tanner [66].

$$S_R = \left\{2B^6 - 2\right\}^{1/2} \qquad (43)$$

This model (in fact, all models of this type) assumes that all of the swell exhibited by the liquid is due to the recovery of shear strain. Thus it is only applicable to capillaries that are long enough that the entrance region deformation of the material has been "forgotten".

The momentum balance approach to predicting extrudate swell was put forth by Metzner [68]. The method is conceptually quite simple; a momentum balance (in the flow

direction) is made on a control volume of fluid with boundaries just up and downstream of the capillary exit. In addition to the inertia term contributions, the axial stresses acting on the control volume are considered. This inclusion of liquid elasticity led to good agreement between model predictions and swell of polymer solutions. However, Graessly [54] used this approach to predict the first normal stress difference from extrudate swell, and found the model predictions to be low by a factor of 10^7.

Both finite element and finite difference methods have been applied to the problem of swell prediction. These methods involve the simultaneous solution of the transport equations of mass and momentum using a specific constitutive equation. The major difficulty associated with these approaches is the stress discontinuity associated with the exit of the die. A complete review of the various techniques and their limitations is presented in the text by Tanner [69].

3.5 Extrudate Distortion

The commercial viability of most polymer processes is dependent on the achievment of high production rates, and achieving high production rates frequently entails subjecting

the molten polymer to high shear stresses as it passes through various dies and channels. At a limiting value of the extrusion shear stress, the extruded polymer will experience some form of physical distortion. Depending on the type of polymer and the shear stress, this distortion may be a uniform surface roughness or a highly irregular deformation of the entire extrudate; the former being referred to as sharkskin and the latter being known by the more general term "melt fracture". In fact, there are at least four distinct types of extrudate distortion. Simplified sketches of the various types are presented in Figure 7. Type I is an example of the shark-skin distortion typical of linear, narrow MWD polymers. Type II is characteristic of the incipient distortion observed with branched polymers, Type III is observed with branched and linear polymers at shear stresses well above the incipient range and is referred to as "melt fracture", and Type IV is actually a combination of either Type I and Type III alternating with comparatively smooth, glossy regions. Type IV is referred to as stick-slip flow and generally occurs over a range of shear stresses in linear polymers.

Because of its experimental simplicity, most of the work on extrudate distortion has been carried out using circular dies. Work has also been done on the extrudate distortion associated with slit and annular dies [7,30,70,71].

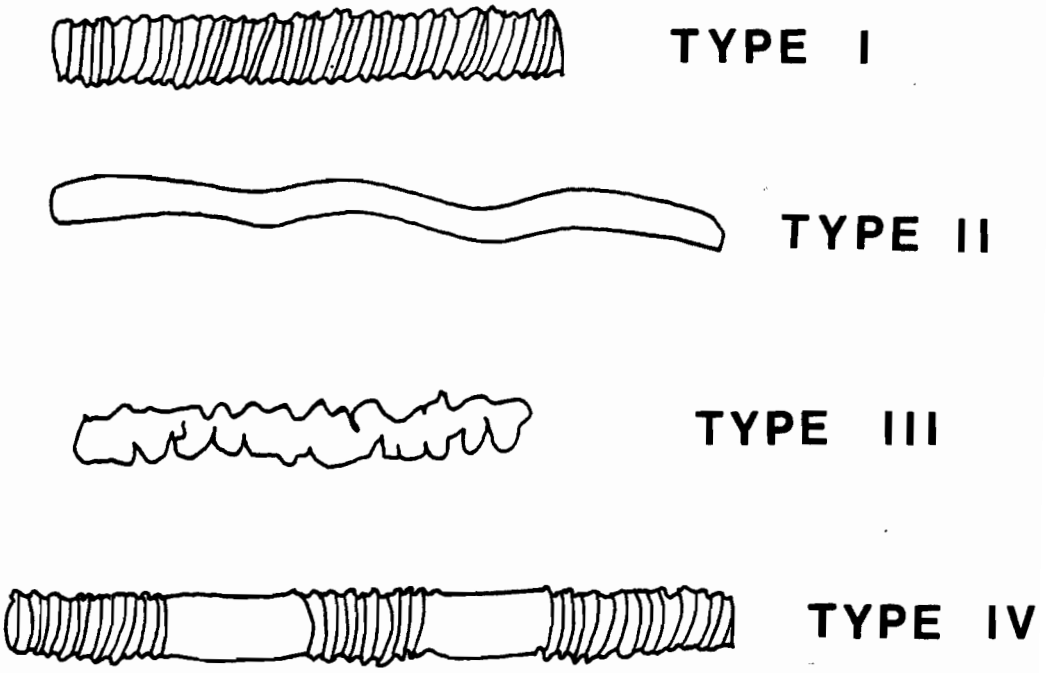

Figure 7. Various types of flow instabilities.

Despite all the work done, the underlying causes of the various types of extrudate distortion are not clearly understood. It is known, however, that fluid inertia is not a factor since Reynolds numbers as low as 10^{-5} have been associated with distortion [72]. Thermal effects can also be discounted on the basis of calculations made by Lupton [73], which showed that shear heating under conditions in which they observed extrudate distortion will lead to a temperature rise of only 2 or 3 °C. It is generally agreed that extrudate distortion is due to the elastic nature of the material. This has led to the correlation of the recoverable shear, S_R, with the onset of distortion. The definition of S_R is that given in the previous section on extrudate swell. Bagley [74] found that the value of S_R was fairly constant at about 7 units for several different polymers. Vlachopoulos [75] found that the value of S_R varies from about 2 to 66 depending on the polymer and its MW and MWD. These discrepencies may be at least partially attributed to the absence of any reliable measurements of either the shear modulus or the first normal stress difference at the shear rates where melt fracture is observed, and to the variety of methods that are used to estimate these material properties. The use of S_R, however, gives no insight into the underlying mechanism of extrudate distortion [76].

It has been suggested [77,78] that the onset of extrudate distortion coincides with the power law index reaching a value of between .28 and .40. This criterion is remarkably insensitive since it reflects the shear behavior of many molten polymers over many decades of shear rate [72]. Bartos [79] (suggested that the ratio of the shear viscosity to zero-shear-rate viscosity might be a criterion for the onset of distortion. However, his own data and the work of Cogswell [80] do not lend support to this hypothesis.

Molecular structure has been shown to have a significant effect on the conditions under which extrudate distortion occurs as well as on the types of instabilities exhibited. Vlachopoulos [75] studied four different polymers (polystyrene, polypropylene and high and low density polyethylenes) and found that the critical shear stress at which distortion was first observed was on the order of 10^5 Pa in all cases. The value of the critical wall shear stress was found to be an inverse function of the the molecular weight and independent of the MWD. Conversely, other workers have found the critical shear stress to be independent of molecular weight [81,82].

Branched polymers such as LDPE tend to exhibit type II and III instabilities. The distortion of the extrudate with such materials tends to be lessened by increasing the length

of the tube. This would suggest that the instabilities originate near the entrance of the die. Flow visualization studies carried out by Ballenger [83] showed that with LDPE, large eddies exist in the corners formed at the junction of the rheometer barrel and the capillary die. Extrudate distortion tends to occur in conjunction with the oscillation of these eddies. As the flow rate is increased, jets of polymer melt seem to "spurt" randomly from these eddies into the capillary die. This behavior has also been observed with polystyrene [83]. Apparently the tapering of the entrance of the capillary reduces both the size of these eddies as well as their tendency to oscillate [72].

Sharkskin extrudate distortion is typical of unbranched polymers such as HDPE. A narrow MWD gives rise to a more pronounced degree of sharkskin [84]. Studies by Benbow [85] and Vinogradov [86] indicated that sharkskin is initiated at the die exit and is associated with a high local stress at the point where the melt separates from the die wall. More recently, Weill [87] suggested that sharkskin in HDPE originates in the entry region of the capillary where the axial pressure gradient is greater than in the fully developed region of the capillary.

It has been suggested that extrudate distortion is initiated by slippage of the polymeric liquid at the wall of

the tube. Studies by den Otter [88] indicate that during distortion of LDPE, no slip at the wall is observed. However, slippage is observed in linear polymers such as HDPE. With such linear polymers, a transition from sharkskin to an oscillating flow (type IV instability) is observed as the shear stress is increased. This oscillating flow is often referred to as stick-slip flow [87]. This phenomenon seems to be related to the intermittent loss of adhesion between the polymer and the wall. Vinogradov [89] argues that the intermittent slip is due to the greater elasticity and lessened fluidity exhibited by the liquid at higher strain rates. As a result this suddenly more elastic liquid is unable to support the shear stress and separates, leaving a thin layer of polymer still attached to the tube wall. This is known as cohesive rather than adhesive failure.

The regions of the extrudate where the polymer has slipped are generally quite smooth, while those where adhesion is maintained will exhibit either type I or III distortion. A discontinuity in the flow curve of materials which exhibit stick-slip behavior is common. Referring to Figure 8, this is shown for the case of HDPE. At flow rates between points A and B oscillations in pressure are observed (represented by the horizontal lines) and the extrudate exhibits stick-slip behavior. Curiously, when the flow rate at point B is reached, a sudden drop in pressure is observed

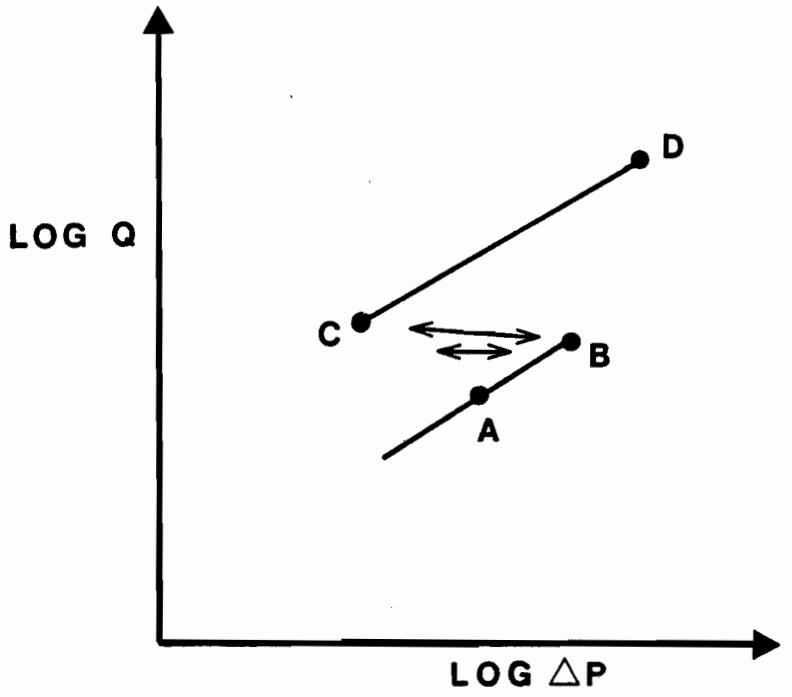

Figure 8. Flow curve for a HDPE.

with no associated change in flow rate. Between points C and D, a continuous slip flow is observed and beyond point D a type III distortion typical of branched polymers is observed. Uhland [90] found that by roughening the wall of the tube or raising the temperature the onset of slippage (point A) could be delayed. He also observed that extreme tapering of the capillaries inlet region removed the pressure oscillations associated with stick slip flow, but had no effect on the upper branch of the flow curve.

3.6 Molecular Structure Effects

3.6.1 Introduction

Not surprisingly, the molecular structure of a polymeric material plays a dominant role in determining its rheological behavior. The macroscopic response of the material to an imposed stress or strain is dependant on how the molecules interact with one another. Clearly,then, variables such as chemical structure, average chain length(average molecular weight), distribution of chain lengths(molecular weight distribution) and number of long chain branches are important.

Before proceeding, a few definitions used to describe the molecular characteristics of a particular polymer are presented. Various expressions have found common use for defining the average molecular weight of polymeric materials. The differences between them lie in the extent to which they weight the different weight fractions of the polymer to obtain an average. Four expressions for the average molecular weight that are frequently used are presented below.

$$M_n = \int_0^\infty M \varphi(M) dM \qquad (44)$$

$$M_w = \int_0^\infty M^2 \varphi(M) dM / M_n \qquad (45)$$

$$M_z = \int_0^\infty M^3 \varphi(M) dM / M_w \qquad (46)$$

$$M_{z+1} = \int_0^\infty M^4 \varphi(M) dM / M_z \qquad (47)$$

Here $\varphi(M)dM$ represents the normalized number distribution of molecular weights; i.e. $\varphi(M)dM$ is the fraction of chains having a molecular weight between M and M+dM. By using higher powers of each molecular weight, as in equations (45), (46) and (47), the high molecular weight fractions contribute more to the value of the molecular weight than do the lower weight fractions. Thus, the values of M_z and M_w relative to that of M_n are indicators of the breadth of the molecular weight distribution. In fact a commonly used measure of polydispersity is the ratio of (45) to (44), which is called the polydispersity index [2]. An additional index of

polydispersity is defined by equation (48).

$$MWD = M_{z+1} M_z / M_w M_n \qquad (48)$$

Techniques have also been used to characterize the extent to which branches are present [91,92]. Many polymers, notably polyethylene, may contain short and long chain branches, the former being characteristic of HDPE and the latter of LDPE. Typically, the extent to which branches are present is expressed by giving the number of methyl groups present per 1000 carbon atoms. Unlike these two materials, LLDPE has very little branching.

Differences in these molecular parameters reveal themselves in the response of the melt to shear and extensional flows, as well as in phenomena where elasticity is exhibited.

3.6.2 Shear Flow

Some of the earliest work in this area addressed the problem of relating viscosity to molecular weight. Several workers have found that for linear polymers, (that is, those with little branching) at shear rates low enough so that the polymer behaves as a Newtonian liquid, the viscosity is directly proportional to the molecular weight. At a certain molecular weight, M_c, the viscosity begins to increase much more rapidly with M, being proportional to approximately $M^{3.4}$

[30] for monodisperse polymers. The value of M_c is dependent on the molecular structure of the polymer. It is believed that this increased sensitivity of viscosity to molecular weight is a result of a change in the mechanism by which the molecules act to cause a resistance to flow. Below M_c the polymer molecules flow over one another and form few temporary entanglements when subjected to a shear strain. Above M_c , however, these temporary entanglements become more numerous and thus tend to have a greater impact on the resistance to flow [30].

As was mentioned in a previous section, the shear-thinning behavior of molten polymers can be attributed to the destruction of temporary entanglements as the material is strained. Thus, for polymers of sufficient molecular weight for temporary entanglements to be the dominant source of resistance to flow, one finds that increasing the molecular weight lowers the shear rate at which non-Newtonian behavior is first observed [93]. It has also been observed that the non-Newtonian regime commences at lower shear rates as the molecular weight distribution of the polymer is broadened [30,94]. Studies carried out on polyethylenes have shown that shear viscosities of highly branched samples are somewhat lower than those of linear polymers of comparable molecular weight [95]. In addition, it has been observed that highly branched polyethylene tends to depart from Newtonian flow at

lower shear rates than do comparable weight linear polyethylenes [30]. Peticolas [96] found that HDPE, which has only short-chain branches, has a melt viscosity only slightly lower than linear polymers of the same weight average molecular weight indicating that short branches have little effect on material rheology in shear.

3.6.3 Extensional Flow

The effect of molecular parameters on extensional flow behavior has recieved considerable attention in the last several years. Owing to the importance of polyethylenes in the film-blowing process, where extension is the dominant mode of deformation, most of the work carried out has been with these materials [97-102]. Some studies with polystyrene have also been carried out [103,104]. No studies have been published detailing the interrelationship between molecular properties and material response in biaxial extension. The work published to date deals exclusively with uniaxial extensional flow [25].

For both LDPE and polystyrene, it has been found that a broadening of the molecular weight distribution leads to a pronounced maximum in the steady-state elongational viscosity. An increase in the weight average molecular weight, for samples of equivalent polydispersity, results in

an increase in the value of the steady-state extensional viscosity [98,105]. Muenstedt et al. [98] and Utracki et al. [101] compared the behavior of branched and unbranched polyethylenes in uniaxial extensional stress growth (LDPE and HDPE in the former case and LDPE and LLDPE in the latter). Both workers observed that in the case of the branched polymer, beyond a certain critical value of the extensional strain rate, the value of the extensional stress growth function did not reach a steady state value. This continuous increase in viscosity is frequently referred to as "strain hardening" or "unbounded stress growth". This proceeds until the sample ultimately breaks. This behavior is not apparent in HDPE or LLDPE, the latter containing short chain branches.

3.6.4 Elastic Properties

Two manifestations of material elasticity have recieved a great deal of study in regards to the effect of molecular structure on them; extrudate swell and the first normal stress difference. As was mentioned in an earlier section, the extrudate swell of a polymeric liquid tends to increase as the molecular weight is increased. Broadening the molecular weight distribution or increasing the amount of long chain branching has the same effect. The above conclusions have been found to hold true for the first normal

stress difference [30]. Han [30] concludes that, in general, fluid elasticity is increased by the presence of long chain branching, and by increased polydispersity and molecular weight.

3.7 Network Theories

3.7.1 Introduction

Two broad classes of constitutive equations have been developed in an attempt to predict the response of a viscoelastic liquid to an arbitrary strain field. The first includes those equations that are based on rational or continuum mechanics. This approach begins with a hypothesis regarding the relationship between stress and strain for a material and leads to a general form of the constitutive equation. Constraints are placed on the form of the equation to ensure that the predicted fluid response is reference frame independent [26,106] and an emperical assumption regarding the fluids behavior must be introduced. The second approach begins by considering the nature of the material's molecular structure and then developing a macroscopic constitutive equation. Rather than yielding a general model,

this approach results in models that are quite specific and depend on the assumptions made regarding the material's structure. Network theories are examples of models that have such a molecular basis.

Network theories view a polymer as consisting of a highly entangled network. The network interconnections, or entanglements, are analagous to chemical crosslinks, but are temporary in nature. The molecular segments between the entanglements are the network strands. At equilibrium the concentrations of strands and entanglements are constant, although they are continuously being created and destroyed by the thermal motion of the molecules and by the deformation process [107]. The response of the melt to an imposed strain is dictated, to a large extent, by the kinetics of the destruction of entanglements. One of the first network theory models was suggested by Lodge [108]. A complete discussion of this model is presented by Tsang [106]. A few of its most important features are worth noting, however. The model makes two assumptions that are quite unrealistic when dealing with molten thermoplastics: 1) when the liquid is subjected to a deforming strain, the molecular entanglement junctions move as if they were macroscopic points in the liquid; thus the microscopic motions of the junctions are assumed to have no effect on the rheological response of the fluid-this is referred to as the "affine

junction motion" assumption; 2) the number of segments in the molecular network is unchanged by any deformation that the polymer may experience. The resulting equation is presented below,

$$\underline{\tau}(t) = \int_{-\infty}^{t} \sum_{i} \frac{G_{oi}}{\lambda_{oi}} e^{-(t-t')/\lambda_{oi}} \underline{C}^{-1}(t,t')\, dt' \qquad (49)$$

where λ_{oi}, and G_{oi} are the relaxation time and elastic modulus of the i^{th} type of entanglement in the polymer network. The tensor $C^{-1}(t,t')$ is the Finger strain tensor. The exponential term in the integrand permits the model to predict,at least qualitatively, the fading memory behavior exhibited by all viscoelastic materials. The model predicts the existance of normal stress differences in shear flow (a nonlinear viscoelastic effect), but does not predict the shear thinning behavior of molten polymers. Some efforts have been made to use a strain rate dependent memory function that could account for the strain rate dependence of the segment creation and loss rates [109]. Other workers found that better results could be obtained with models that incorporate a strain, as opposed to strain-rate, dependent memory function [110]. A model of this type was found to predict most viscoelastic behavior with the notable exception of transient normal stress growth data [111].

3.7.2 Acierno's Model

A novel approach to account for the change in network structure upon imposition of a strain is that taken by Acierno et al. [3]. The model begins with the equation used in the Lodge model, but given in its differential form. In this form it is known as the contravarient Maxwell model. However, the new model utilizes values of relaxation times and elastic moduli that are functions of a structural parameter accounting for the reduction in the entanglement density as the material is strained. The value of this structural parameter is found by solving a differential equation relating the time rate of change in the normalized number of entanglements to the stress field in the material. The equations comprising the model are presented below.

$$\underline{\tau} = \sum_i \underline{\tau}_i \tag{50}$$

$$\lambda_i \frac{\overset{\nabla}{\underline{\tau}}_i}{\partial t}(\underline{\tau}_i/G_i) + \frac{1}{G_i}\underline{\tau}_i = \lambda_i \underline{\Delta}_i \tag{51}$$

$$G_i = G_{oi} x_i \quad ; \quad \lambda_i = \lambda_{oi} x_i \tag{52}$$

$$\frac{dx_i}{dt} = \frac{1 - x_i}{\lambda_i} - \frac{a x_i}{\lambda_i}\left(\frac{tr(\underline{\tau}_i)}{2G_i}\right)^{1/2} \tag{53}$$

Equation (50) is simply a spectral decomposition of the stress tensor; it accounts for the fact that the response can be described by an arbitrarily large number of simple viscous and elastic components. Equation (51) for the stress is a contravarient Maxwell model with time dependent moduli, G_i, and relaxation times, λ_i. In equation (52), λ_{oi} and G_{oi} are the

equilibrium values of λ_i and G_i - that is, the values that describe the mechanical behavior of the fluid in the limit of linear viscoelasiticity. The scalar quantity, x_i , is the structural parameter that describes how far the liquid is from its equilibrium state. It is defined as follows,

$$x_i = n_i / n_{io} \qquad (54)$$

where n_{io} is the average number of entanglements per molecule at equilibrium, and n_i is the number of entanglements at some time,t, after the material has been deformed. Thus at equilibrium, $x_i = 1$. The subscript, i, is related to the occurrence of junctions of varying degrees of complexity, each of which corresponds to a different relaxation time. Equation (53) is the kinetic equation mentioned earlier. The second term on the right hand side gives the rate of destruction of entanglements due to the existing stress, while the first term gives the rate of entanglement formation due to thermal motion [112]. This equation also contains a single adjustable parameter,a, which can be found by fitting steady shear data [113].

Garcia-Rejon [113] obtained simple shear and uniaxial extension data for three HDPE blow molding resins and for a copolymer resin. He concluded that the model was capable of predicting both the linear and nonlinear effects present in uniaxial stress growth experiments. In addition the model

successfully predicted the response to steady shear flow. Tsang [106] found that the model could fit quite well his low shear rate viscosity and first normal stress difference data, but that different values of the adjustable parameter,a, were needed to fit the entire viscosity curve, especially at high shear rates. Tsang observed only a qualitative agreement between the model predictions and behavior in uniaxial extension.

3.8 Polymer Degradation and Stabilizing Agents

Degradation can be considered to be any type of chemical modification of a polymer chain and can involve the main-chain backbone and/or side groups [114]. These modifications are chemical in nature; that is, primary valence bonds are broken. This may result in a reduction in mean molecular weight, or an increase in weight as a result of crosslinking.

High thermal stability in polymers permits processing to be carried out at high temperatures. As a result of the associated reduction in the melt's resistance to deformation, processing rates may be increased, with little increase in extrusion power. Of course the advantages of increasing production rates must be weighed against the higher energy

costs associated with higher processing temperatures. Superior thermal stability also improves product quality as a result of the elimination of the deleterious effects of degradation on physical properties [115].

It is well known that the mechanism of polyethylene thermal degradation can be described by a free radical chain reaction. The following series of simplified equations can be used to describe a typical reaction sequence [115].

a) Initiative Step: Production of free radicals.

(Polymer) R-H ------> R* + H*

b) Propagation Step: Radicals interact with oxygen and polymer chain.

R* + O_2--------> ROO*

ROO* + R-H --------> ROOH + R*

c) Termination Step: Deactivation of free radicals.

R* + R* ------> R-R

R* + ROO* ------> ROOR

$$ROO^{*} + ROO^{*} \longrightarrow ROOR + O_2$$

Recombination of chain radicals in the termination step can produce crosslinks or molecular enlargements. The overall effect of these reactions is that oxygen combines with polymer chains to form carbonyl compounds which accumulate and give rise to characteristic yellow and brown discolourations [115].

The overall thermal oxidative process depends on the rate of hydrogen abstraction from polymer chains. The most stable bonds; that is, those that are least susceptible to hydrogen abstraction; are those of the -CH- type in the alpha position of aromatic groups.

Stablest C-H bond.

Lower bond stabilities are observed for tertiary, secondary and finally primary substituted carbon atoms. That is,

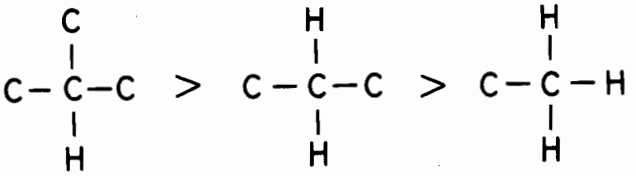

Decreasing bond stability.

This seems to account for the observation that the rate of

thermal decomposition is greater for polyethylenes with a higher degree of branching [116].

The breakdown of chemical bonds that initiates the degradation process cannot be prevented by any external means. Additives can only exert a retardative affect on the degradation process. Retardative stabilization can be achieved by any of the following mechanisms [114].

a) Intervention directly in the degradation reactions to produce inactive species and to reduce the concentration of reactive species, so that the resultant overall rate for the degradation process is decreased.

b) Removing, deactivating or promoting competition for sources that have a catalytic effect on the degradation process (such as oxygen).

A method often used in rheological experimentation is to surround the material sample by an oxygen free atmosphere. Even with this precaution, oxygen entrapped in the course of sample preparation often necessitates the use of stabilizing agents.

There are basically two classes of stabilizers used with

polyolefins. Those in the first class generally act to reduce the rate of the propagation step. These are known as primary stabilizers. They perform their function by intervening directly with the degradation reactions to produce inactive species by forming highly stable bonds. Often these compounds contain aromatic rings in their structure, which form highly stable bonds due to their resonance stabilized structure [115]. Since this type of stabilizer reacts with radicals to inhibit degradation, it will eventually be consumed by the chain propagation species.

The major source of the discolouration that often accompanies polymer degradation is the formation of peroxide compounds. The second class of stabilizers contain phosphite compounds that act to break down these peroxides. A synergistic effect can be achieved by using a stabilizer that is a blend of both these types of stabilizer [115].

3.9 Previous Work on LLDPE Rheology

The absence of long chain branching and the relatively narrow molecular weight distribution of LLDPE resins are

primarily responsible for the different rheological behavior of these materials as compared to their most important commercial competitor, LDPE [9,117]. In the film-blowing process, the rheological properties in shear and extensional flows as well as the elastic properties of a resin are of importance.

One of the earliest published studies comparing the rheology of LLDPE and LDPE film resins was that of Garcia-Rejon [33]. The LLDPE resin studied was manufactured by Du Pont Canada Ltd. using a solution phase polymerization process; the comonomer was not specified. One of the LDPE resins was also manufactured by Du Pont Canada and the other by Union Carbide Canada. The LLDPE had a melt index of 1.6 g/10 min while both LDPE resins had melt indices of 2.0 g/10 min.

Both of the LDPE resins had higher zero shear viscosities than the LLDPE resin, but at shear rates greater than about 0.7 s^{-1}, the viscosities of the LDPE resins began to decrease more rapidly than that of the LLDPE as the shear rate was increased. It is thought that this is a result of the greater resistance to deformation of the branched materials initially due to the entanglements caused by branching, while at higher shear rates these same branches become disentangled [30]. Thus at the higher shear rates

corresponding to processing conditions, the LLDPE would be more viscous than either of the other resins. The LLDPE resin was also found to have lower values of the extrudate swell ratio than either of the LDPE resins. Patterson [118] also found this to be true in his studies of an LLDPE and an unspecified LDPE. These results are not unexpected, since the long chain branching characteristic of LDPE is known to increase extrudate swell [58]. Of interest is Garcia-Rejon's finding that of the three resins, the LLDPE exhibited the highest values of the first normal stress difference. In uniaxial extensional stress growth experiments, at strain rates of up to 0.026 s^{-1}, the LDPE resin generally exhibited a higher peak stress, although at a strain rate of 0.022 $s^{-1}$the LLDPE and LDPE exhibited similar behavior.

Kalyon and Moy [119] studied the effect of different comonomers on the rheology, processing behavior, and end product properties of films blown from LLDPE. They concluded that the uniaxial extensional viscosity of LLDPE resins increases as the number of C-atoms in the comonomer increases. They also found that of the resins studied, the one that contained a 1-octene comonomer had a lower viscosity than resins of the same melt index and similar density incorporating 1-butene or 1-hexene comonomers. Films of LLDPE in which the comonomer was 1-hexene had the highest tear and puncture resistances, while films made from resins

using 1-octene comonomer had the highest impact strengths.

Al-Bastaki [101,120] studied 5 wire coating resins, two of which were LLDPE (with unspecified comonomers), two were branched polyethylenes of somewhat higher density (0.932 g/cm^3 vs 0.92 g/cm^3 for LLDPE), and the fifth was a linear polyethylene of density 0.932 g/cm^3 and of high polydispersity (18.3). One of the LLDPE resins (his W1) had an unusually high polydispersity of 8.4, which is comparable to that of branched resins. The other LLDPE resin (his W5) had a more typical polydispersity value of 4.6.

Although lacking in long chain branching, W1, exhibited strong shear thinning and also did not exhibit a zero shear viscosity even at very low shear rates. Its viscosity curve was similar in appearance to those of the branched resins and the linear MDPE, although it had a somewhat lower viscosity at the lowest shear rates. Resin W5 was qualitatively similar to Garcia-Rejon's LLDPE resin, exhibiting a well defined zero shear viscosity that was substantially lower than the low shear viscosities of the other resins and that declined comparativley slowly with increasing shear rate so that at shear rates on the order of a few hundred s^{-1}, it had the highest viscosity of all the resins studied. These trends were observed both at 190 $^{\circ}$C and 220 $^{\circ}$C. Both of the LLDPE resins were found to have the lowest values of the

first normal stress difference of the resins studied, with W5 having substantially lower values than W1. One might thus conclude that, at least at low shear rates, these resins are less elastic than branched MDPE and the broad molecular weight distribution linear MDPE.

Al-Bastaki found at all strain rates that both of the LLDPE resins tended to achieve an apparent steady state value of the uniaxial extensional stress growth function followed by a sudden decrease in its value at longer times. This behavior was most pronounced in the case of resin W5. In contrast, the branched resins were found to display a rapid increase in the value of the stress growth function at strain rates above 0.05 s^{-1}, with no steady state value of this function being attained. In addition, resin W5 had much lower values of the extensional stress growth function (equal to the extensional viscosity when steady state obtained) than any of the other resins. The stress growth functions and viscosities of W1 were comparable in magnitude (except for the regions of unbounded growth for the branched resins) to those of the other resins. Both of these LLDPE resins were found to have the lowest values of the storage modulus (another measure of material elasticity) at all angular frequencies of the resins studied. Measurements of the extrudate swell characteristics indicated that the LLDPE resins swelled less than the branched resins and to the same

extent as the other linear resin. However, a great deal of scatter exist in these data, and the results are not conclusive.

Saini and Shenoy [121,122] studied the low shear rate and linear viscoelastic properties of an unidentified LLDPE resin. The important conclusion drawn was that this class of resins does not shear thin to the extent that branched LDPE and linear HDPE do.

Attala and Bertinotti [123] measured the shear, extensional behavior and extrudate distortion phenomena of a film-grade LLDPE (1-butene comonomer) and a film-grade, branched LDPE resin. As had been found in the previously discussed work, the LLDPE resin had a lower viscosity at low shear rates but a higher viscosity at shear rates above 2 s^{-1} than the LDPE resin. Considerable differences were exhibited by the two polymers in their extrudate distortion phenomena. Firstly, at a given temperature, distortion occurred at much lower shear rates for the LLDPE than for the LDPE. In addition, the LLDPE exhibited two types of distortion. At lower shear rates sharkskin (Type I) was first observed, increasing in severity with shear rate, and then disappearing completely in favor of an extrudate with a glossy smooth surface. This sudden disappearance of the surface roughness was accompanied by an increase in the apparent shear rate

with no associated increase in the shear stress. At higher shear rates, the gnarled type of extrudate distortion (Type III) typical of LDPE was observed. This sort of behavior is apparently quite typical of linear, narrow molecular weight distribution polyethylenes [84,124].

Using a method suggested by Cogswell [125,126] based on the measurement of the entrance pressure drop through a capillary, these authors found that the approximate extensional viscosity of the LLDPE resin was lower than that of the LDPE resin.

Han and Kwack [127,128] compared the processing behavior and rheology of LDPE and LLDPE resins on a pilot scale film blowing line. Measurements of these materials' extensional flow behavior indicated that the LLDPE resins did not exhibit the strain hardening behavior typical of LDPE at the higher strain rates associated with processing conditions. They termed the critical machine direction stress at which the film bubble breaks the "ultimate melt strength", and found that the stretching of the film caused the stress to build up much faster in the case of the LDPE than for the LLDPE. Thus, films of LLDPE could be subjected to greater draw down without breaking, making it possible to produce thinner films. This behavior in processing is due to the lack of strain hardening of these resins. Han and Kwack also noted

that unlike LDPE resins, LLDPE showed a very weak dependance of transverse direction stress on the bubble blow up ratio. They hypothesized that this difference in extensional rheology was primarily due to the narrower molecular weight distribution and absence of long chain branching in the LLDPE's. In studies with different LDPE's [128] they found that resins with less long chain branching and narrower weight distributions exhibited less strain hardening and could thus be drawn into thinner films; the behavior of LLDPE's follows this trend.

Utracki et al. [129] studied the contrasting behavior of LDPE, HDPE and LLDPE resins when subjected to high shear flows through capillaries. Unlike the LDPE resin both the LLDPE and HDPE resins exhibited a sharkskin type of flow instability at critical values of the wall shear stress (240 kPa for the LLDPE's). One of the LLDPE resins experienced the so called "stick-slip" flow and the associated pressure drop oscillations. Although this behavior was also exhibited by one of the HDPE resins it did not occur with the LDPE resins studied.

Vasudevan et al. [130] compared the film processing characteristics of a newly developed broad-MWD LLDPE resin to several other LLDPE's, one of which was resin 31 (GRSN-7047) of the present study. It was found that this broad-MWD resin

was less susceptible to flow instabilities such as sharkskin than conventional LLDPE's and tended to shear thin more rapidly as well. In addition, the broader MWD resin tended to exhibit some strain hardening in extension, and thus would break at a lower strain rate than an LLDPE such as resin 31. This newly developed LLDPE tends to have higher machine and cross direction film strengths than narrow-MWD LLDPE's.

Winter et al. [131] studied the behavior of an LLDPE and an LDPE resin in steady and oscillatory shear as well as in biaxial extension using the lubricated squeezing flow method. They concluded that the flow behavior of LLDPE is dominated by relatively short relaxation times.

Because of the higher temperatures used in the processing of LLDPE resins, precautions to prevent thermal degradation must be considered. Capolupo [132] studied the stabilization requirements of LLDPE resins. She concluded that without the addition of stabilizing packages, commercially available LLDPE resins experienced discoloration as well as reductions in melt index after repeated passes through a Brabender extruder. This reduction of melt index is indicative of a cross-linking type degradation. She found that the ideal stabilizing system should consist of both primary and secondary antioxidants in order to prevent discoloration of the polymer.

In a recent paper, Acierno et al. [133] studied the relationship between the molecular weight and rheology of LLDPE resins (all with 1-butene comonomer) of similar polydispersity. They observed the following the relationship between weight average molecular weight M_w and zero shear viscosity,

$$\eta_o = 9.45 \times 10^{-16} M_w^{3.67} \qquad (55)$$

A power law relation between M_w and the Newtonian apparent shear rate at which extrudate distortion was first observed was also found.

$$\dot{\gamma}_c = a M_w^b$$
$$a = 3.75 \times 10^{-71} \exp[-.28T] \qquad (56)$$
$$b = -16.945 + .031T$$

Where T is the extrusion temperture. The L/D of the capillary was found to have little effect on the value of $\dot{\gamma}_c$. Nonisothermal elongational flow experiments were also carried out by drawing an extruded filament through a series of pullies and then through two variable speed counterrotating wheels. A strain gauge is used to detect the force exerted by the filament on the first pulley. At a given shear rate, the speed of the rotating wheels is gradually increased until the filament finally breaks, the force reading on the first pulley when this occurs is known as the "melt strength" (MS). The "breaking-stretching ratio"

(BSR) is the ratio of the linear speed of the rotating rolls to the extrusion speed at the die. The MS was found to increase with M_w, while BSR decreased with M_w.

Chapter 4

EXPERIMENTAL PROCEDURES

4.1 Materials Studied

In the course of this work four film grade polyethylene resins were studied. Resins 30, 31 and 33 were linear low density polyethylenes (LLDPE), resin 32 being a branched low density polyethylene (LDPE).

Resins 31 and 33 were manufactured using Union Carbide's low- pressure gas phase fluidized-bed process. Both of these resins incorporate a 1-butene comonomer. Resin 30 is produced by Dow Chemical using a solution phase polymerization process. In this case a 1-octene comonomer is used. Resin 32 is also manufactured by Union Carbide by free radical polymerization of ethylene in a tubular reactor at extremely high pressures (1000 to 3000 atm.). This resin is highly branched, unlike the LLDPE's which have a

SOME PROPERTIES OF THE RESINS STUDIED

Resin #	30	31	32	33
Commercial Name	Dowlex 2045	Unipol grsn-7047	DYNJ-4*	Unipol gers-6937
Manufacturer	Dow Chemical	Union Carbide	Union Carbide	Union Carbide
Resin type	LLDPE	LLDPE	LDPE	LLDPE
Comonomer type	1-octene	1-butene	None present	1-butene
Density (g/cm^3)	.920	.918	.919	.918
Melt Index (g/10 min.)	1.0	1.0	.75	.50
M_n	24600	35400	9270	35000
M_w	93100	115000	140000	112600
M_w/M_n	3.78	3.25	15.1	3.22

* Unmodified version of DFDY-2247

Table 2

characteristic linear backbone with very little branching.

A summary of some of the resin properties is given in Table 2. Plots of the molecular weight distributions of the LLDPE resins are given in Appendix B. For those unfamiliar with some of the tabulated properties, refer to any of the standard texts on polymer science [1,6].

4.2 Resin Stabilization

4.2.1 Degradation Studies

The experiments performed to assess whether the materials under study degraded during the course of a rheological experiment were quite simple. The compression molded samples of the resin-stabilizer blend were tested using a Rheometrics Mechanical Spectrometer (RMS) at temperatures of up to 240 °C. This instrument was used in the time sweep mode. Thus configured, the sample material's linear viscoelastic properties in oscillatory shear can be measured as a function of time. In the course of some preliminary work, it was found that the linear viscoelastic property which was most sensitive to thermal degradation was the storage modulus, G'. The criterion used in judging if a particular stabilizer concentration adequately retarded

degradation was whether the value of G′ measured at the start of the time sweep had varied by more than 5% after 45 minutes. Since the presence of oxygen has a deleterious effect on resin stability, nitrogen was used in the RMS forced-convection oven in all cases.

4.2.2 Blending Procedures

Two different blending procedures were used to incorporate the stabilizer into the resins. This was necessary because the two Unipol resins were in granular form, while the Dowlex and LDPE resins were pelletized. The stabilizer used was Irganox B561, which is a blend of 20% Irganox 1010 and 80% Irgofos 168. This material has been found to be particularly well suited for use with polyolefins. It is manufactured by Ciba-Geigy and is supplied as a fine white powder.

A simple, yet effective, procedure for dry blending the granular resins and stabilizer involved placing the appropriate amounts of the two components in a 4 litre jar and vigorously shaking the contents for approximately 5 minutes. This method was found to give excellent batch to batch reproduceability of results.

The great disparity in particle size between the pelletized resins and the stabilizer precluded the use of dry

blending. In this case a relatively concentrated solution of the stabilizer was prepared in chloroform and slurried with the polymer pellets to yield the desired blend of polymer-stabilizer when the mixture was evaporated to dryness. It was found that incomplete removal of the chloroform accelerated the degradation of the polymer samples at the experimental temperatures used. To ensure adequate drying, the polymer-stabilizer mixture was left in a high vacuum oven at 50°C for 48 hours.

4.3 Low Shear Rate and Oscillatory Shear Experiments

4.3.1 Apparatus

In this study a Rheometrics Mechanical Spectrometer (RMS), model 605, was used to measure the low shear viscosity and first normal stress functions as well as the linear viscoelastic dynamic properties of the materials studied. This instrument is a rotational rheometer, the first prototype of which was designed by Macosko and Starita [134] in 1970. This device is particularly well suited to material characterization studies because of its versatility. This is due to its use of a transducer system capable of measuring both torque and normal force. Furthermore its microprocessor-controlled drive system allows it to generate

both steady and oscillatory shear flows.

In performing these experiments either cone and plate or parallel plate fixtures can be used. In this work the former was used for steady shear experiments and the latter for oscillatory shear experiments. The upper fixture is mounted on the end of the shaft of a servo-controlled rotary actuator equipped with a high precision bearing. The motion of this shaft is controlled by a closed loop system based on a high precision tachometer. With this drive system the upper fixture can be driven at angular velocities of 0.01 to 100 rad/s, or, while in the oscillatory mode, at frequencies from .016 to 20 Hz [25,135]. The cone and plate fixtures used were of 2.5 cm diameter. The cone angle was 0.04 radians. The parallel plate fixtures were also 2.5 cm in diameter. As is typical of cone and plate units, the apex of the cone is truncated to prevent any damage to the fixtures when the cone is rotated. The temperature of the sample held in the gap between the fixtures is maintained by a forced convection oven surrounding the fixtures. The sensing element used in the temperature control loop is a platinum resistance thermometer that measures the gas stream temperature. A better measure of the sample temperature is given by a thermocouple embedded in the upper test fixture. Because the force transducer, which is mounted directly below the lower fixture, is sensitive to temperature variations, it is

immersed in a constant temperature bath maintained at 35 ^{o}C.

4.3.2 Sample Preparation

Flat disks of 25 mm diameter were prepared by compression molding the resin pellets at 160 ^{o}C and about 2400 psig. The granular nature of the two Unipol resins made it difficult to make samples that were free of air bubbles. These materials were first extruded (after blending with stabilizer) using an Instron Capillary Rheometer (ICR), with the extrudate being cut into 3 mm pellets. For the pelletized resins, this additional procedure was unnecessary.

4.3.3 Viscometric Functions

As had been mentioned in chapter 3, there are three viscometric functions that completely determine the state of stress in steady simple shear. Of these three functions; the viscosity function, $\eta(\dot{\gamma})$, the first and second normal stress differences, $N_1(\dot{\gamma})$ and $N_2(\dot{\gamma})$; only the first two can be measured with relative ease. Measurement of the second normal stress difference requires a knowledge of the radial variations of the normal force acting downwards against the stationary plate. The RMS is incapable of measuring these variations.

Measurements of $\eta(\dot{\gamma})$ and $N_1(\dot{\gamma})$ were made at shear rates ranging from .025 s^{-1}up to the onset of sample edge distortion (edge fracture). Depending on the material and temperature this occurred at from .25 to 1.585 s^{-1} Experiments were carried out at 190, 210 and 240 ^{o}C.

To carry out an experiment, the cone and plate fixtures were installed and the oven allowed to heat to the desired temperature. When this temperature was reached, the gap between the cone and plate was set at the prescribed distance of 50μm. It is imperative that the gap be set at the temperature at which the experiment will be performed to minimize errors due to thermal expansion. The method used in setting the gap is that described by Pangalos [136]. Once the gap is set, the convection oven gas supply is switched from air to nitrogen and the sample is inserted. Since the sample is about 5 times thicker than the gap spacing, the upper fixture must be gently pushed down to achieve the final gap setting. Prior to commencing the experiment, the molten polymer squeezed out from between the fixtures must be carefully scraped off.

Once the oven temperature has stabilized and the normal force in the sample has relaxed (this may take up to 30 minutes at 190 ^{o}C) the experiment is started. The sample is sheared at a sequence of predetermined shear rates. At each

shear rate the torque output is monitored until a steady value is reached; this value is stored by the system electronics and is subsequently converted into a value of the viscosity. The same procedure is simultaneously followed in measuring $N_1(\dot{\gamma})$, except that the transducer's normal force output is used. When the measurement is completed, the instrument's control system selects the next shear rate and the sequence is repeated.

4.3.4 Oscillatory Shear Functions

The procedure for making these measurements is quite similar to that outlined in the previous section. In this case the input parameters include not only the frequencies at which measurements will be made, but also the amplitude of the oscillations. It is important that the amplitude be large enough to give an easily measureable torque reading but not be so large to cause the material to exhibit non-linear viscoelastic behavior. The amplitude at which non-linear behavior begins varies from one material to another and must be determined.

Using the dynamic torque signal from the transducer the phase angle and amplitude ratio are determined. Using this information a variety of linear viscoelastic functions can be calculated [39].

4.4 Capillary Rheometer Studies

4.4.1 Apparatus

The capillary flow instrument used was an Instron Capillary Rheometer (ICR). This instrument consists of an electrically heated resevoir or barrel, into the end of which can be mounted a capillary die. This assembly is mounted underneath the crosshead of an Instron mechanical testing machine. A hardened stainless steel plunger of diameter slightly less than that of the barrel is connected to a load cell mounted on the moveable cross-head. The plunger descends at a constant velocity and is fitted with a Teflon o-ring to prevent leakage of polymer between the plunger and the resevoir. The load cell measures the force required to push the molten polymer through the capillary.

The crosshead speed can be varied from 0.05 to 50 cm/min in discrete intervals. The dimensions of the capillaries used in this work are listed in Table 3.

4.4.2 Viscosity Measurement

The desired capillary is installed below the barrel, and the entire assembly allowed to come to the operating

CAPILLARIES USED FOR VISCOSITY DETERMINATION

Diameter (cm)	L/D	Entrance Angle (rad)
0.132	5	$\pi/2$
0.132	10	$\pi/2$
0.132	20	$\pi/2$
0.132	40	$\pi/2$

Table 3

temperature. While this is taking place, the load cell can be calibrated by suspending weights from it. When the barrel temperature has stabilized at its equilibrium value (this typically takes 2 to 3 hours) the polymer pellets (or granules) are introduced into the barrel. To prevent the occurrence of air bubbles in the molten polymer, only small amounts of polymer should be added to the barrel followed by packing of the polymer with a narrow brass plunger. When the barrel is full, about 10 minutes should be allowed for the polymer temperature to equilibriate. At this time the plunger is lowered into the barrel and the desired crosshead speed set. Polymer is extruded until a steady force value is measured by the load cell, a new crosshead speed is then selected and the procedure repeated. In this way measurements at a number of shear rates can be made with one filling of the barrel. The force measurement and crosshead speed data are then analyzed according to the procedures outlined in Chapter 3 to yield values of wall shear stress and wall shear rate from which the melt viscosity can be calculated.

4.5 Extrudate Swell Measurements

4.5.1 Apparatus

The apparatus used to measure swell behavior was developed several years ago at McGill by Utracki et al. [61] and modified by Garcia-Rejon [113]. It's most notable features are that it permits swell to be measured isothermally and in the absence of extrudate sag. Several detailed descriptions of the apparatus are available, most notably those of Al-Bastaki [120] and Orbey [137], thus only a somewhat abbreviated description of the apparatus will be given.

The apparatus consists of a section of stainless steel pipe, of 15 cm diameter and 25 cm in length, with a stainless steel plate welded to its base. An immersion heater controlled by a Fenwal 524 temperature controller is mounted on this base. A vertical section of the pipe is cut away to permit the mounting of a pyrex viewing port. A two piece cover made of maronite (a compressed board comprised of asbestos fibres) and stainless steel fits on top of the vertically mounted pipe. This cover can hold up to 6 clear pyrex test tubes. The test tubes are filled with a mixture of silicon based oils whose density is slightly less than that of the molten polymer to be studied. Based on the results of previous workers [113,137] it was felt that a mixture of a 2 cS and 5cS Dow Corning 200 series silicon oils would be suitable. It was found that at a temperature of 135 ^{o}C a mixture of about 63% 2 cS and 37% 5 cS oils gave

practically neutral buoyancy to a molten sample of any of the four polyethylenes studied. The test tubes filled with this oil are in turn submerged in 50 cS (used because of it's lower cost) silicon oil which serves as a heating medium.

The use of this technique requires that certain precautions be taken to ensure reliable results. Due to the higher volatility of the 2 cS compared to the 5 cS oil, the percentage of 2 cS oil in the mixture decreases over a period time, raising the mixtures specific gravity. This causes the extrudates to float rather than hang freely, making it impossible to photograph them. Thus, additional 2 cS oil should be added periodically. Since the bath temperature is 135 ^{o}C in all cases, the swell values must be corrected to the extrusion temperature. The swell ratio at the extrusion temperature can be approximated by means of a density correction based on the assumption of isotropic shrinkage. The following relation is used,

$$B = B_o(\rho_o/\rho)^{1/3} \qquad (57)$$

where B and ρ are the extrudate swell and density at the extrusion temperature and B_o and ρ_o are the values at the bath temperature.

4.5.2 Experimental Procedure

The oil in the bath is heated to the desired temperature. Typically, it takes about 45 minutes for the temperature inside the test tubes to reach its steady state. While the oil is heating, the ICR is allowed to heat up as well. Han [30] has noted that for polyethylenes the dependance of swell on the die L/D ratio ceases for L/D greater than about 20. Thus a 0.132 cm diameter die with an L/D of 40 was used. Once the oil temperature has stabilized and polymer loaded into the ICR barrel and allowed to heat up; a crosshead speed is selected, and polymer is extruded until a steady stress is measured by the load cell. At this point the bath assembly is slid forward so that the mouth of one of the test tubes is aligned with the die exit. A 9 to 10 cm strand of polymer is then extruded into the oil filled test tube. The crosshead is then stopped and the sample held in place by a pair of sliding clamps. The sample is allowed to remain in the tube for about 12 minutes to ensure that it's equilibrium swell is achieved; it is then photographed. While this first sample is relaxing, three more experiments at different crosshead speeds are carried out. At the beginning and end of each sequence of photographs, a 0.127 cm diameter copper wire immersed in one of the test tubes is photographed to give a dimensional standard.

All photographs were taken with a Nikon F2 SLR camera using Tri-X-Pan 400 ASA Kodak film. Although this film is

quite sensitive, additional lighting was required. Thus, 2 75 W tungsten bulbs were used to illuminate the test tubes. These were mounted inside of two cylindrical arms welded to opposite sides of the chamber. The film was developed using a commercially available developer, Microdol-X. The negatives were were first analyzed by mounting them as slides and projecting them onto a wall. It was found that this procedure was not adequate since the projected images were too fuzzy to measure accurately. As an alternative, the negatives were analyzed using a Zeichert optical microscope.

Samara (156) has found that the Dow Corning 200 fluid silicone oils used in this study may cause swelling of the molten extrudate. This swelling is due to the diffusion of oil into the extrudate. He reported that during the 12 minute immersion of the extrudate, oil absorption may contribute up to 5 % of the total measured swell.

Chapter 5

RESULTS AND DISCUSSION

5.1 Degradation Studies

Preliminary testing indicated that all three of the LLDPE resins experienced some degradation at even the lowest experimental temperature of 190 ^{o}C when using an air atmosphere and without the addition of a stabilizer. The LDPE (resin 32) remained stable at 190^{o}C for up to 60 minutes when kept in a nitrogen atmosphere with no stabilizer added. The occurrence of degradation is indicated by an increase in the value of the storage modulus, G'. Other linear viscoelastic properties such as the dynamic viscosity, η', were found to be less sensitive to changes in material structure brought about by degradation. This is clearly shown in Figure 9 where, for resin 30, the value of η', increased by about 3% while that of G' increased by over 250%

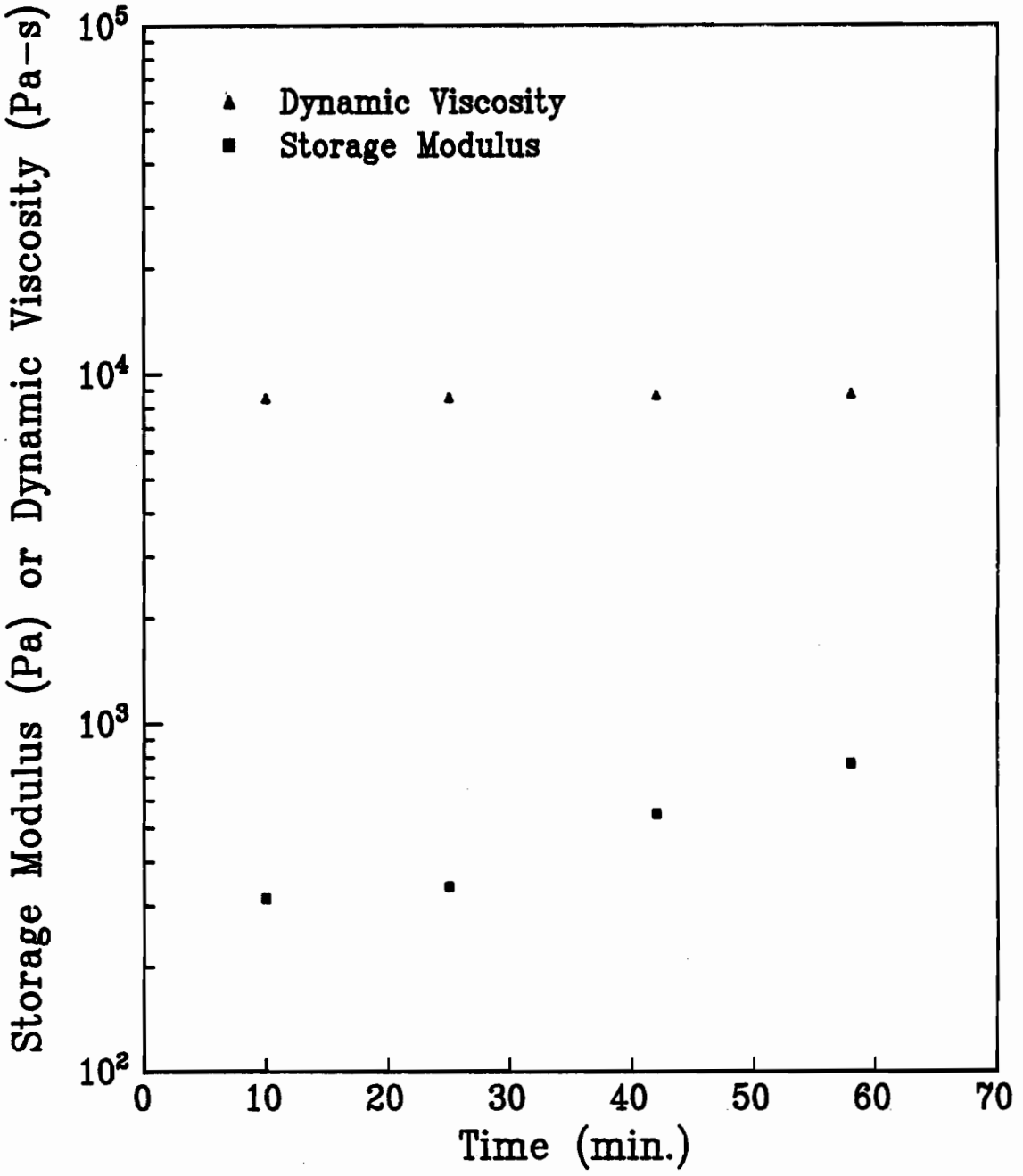

Figure 9: Rheological indications of thermal degradation. Dynamic viscosity and storage modulus of resin 30 at 240°C. No stabilizer, Nitrogen atmosphere.

over the same period of time. Similar behavior was observed for resins 31 and 33. These results indicate that the viscous properties of these materials are less sensitive to degradation than are the elastic properties, at least in the linear viscoelastic range. Furthermore, the increasing value of G' indicates that the material is becoming more elastic, which is likely due to cross-linking rather than to chain scission. As shown in Figures 10, 12 and 15, conducting the experiments under a nitrogen atmosphere did not sufficiently retard the degradative process.

In order to control degradation during the laboratory studies, a commercially available stabilizer, Irganox B561, was blended with the resins. Concentrations of .25%, .3% and .175% were required to stabilize resins 31, 33 and 30 respectively. In addition a nitrogen atmosphere was found to be necessary except in the case of resin 33 at 190 ^{o}C (see Figure 12). Referring to Figures 10, 12-13 and 15, it is clear that the addition of the stabilizer at these concentrations has no effect on the rheological properties of these materials.

It was not possible to stabilize resin 30 for more than about 15 minutes at 240^{o}C without increasing the stabilizer concentration to the point where it began to lead to an overall reduction in the value of the storage modulus. This

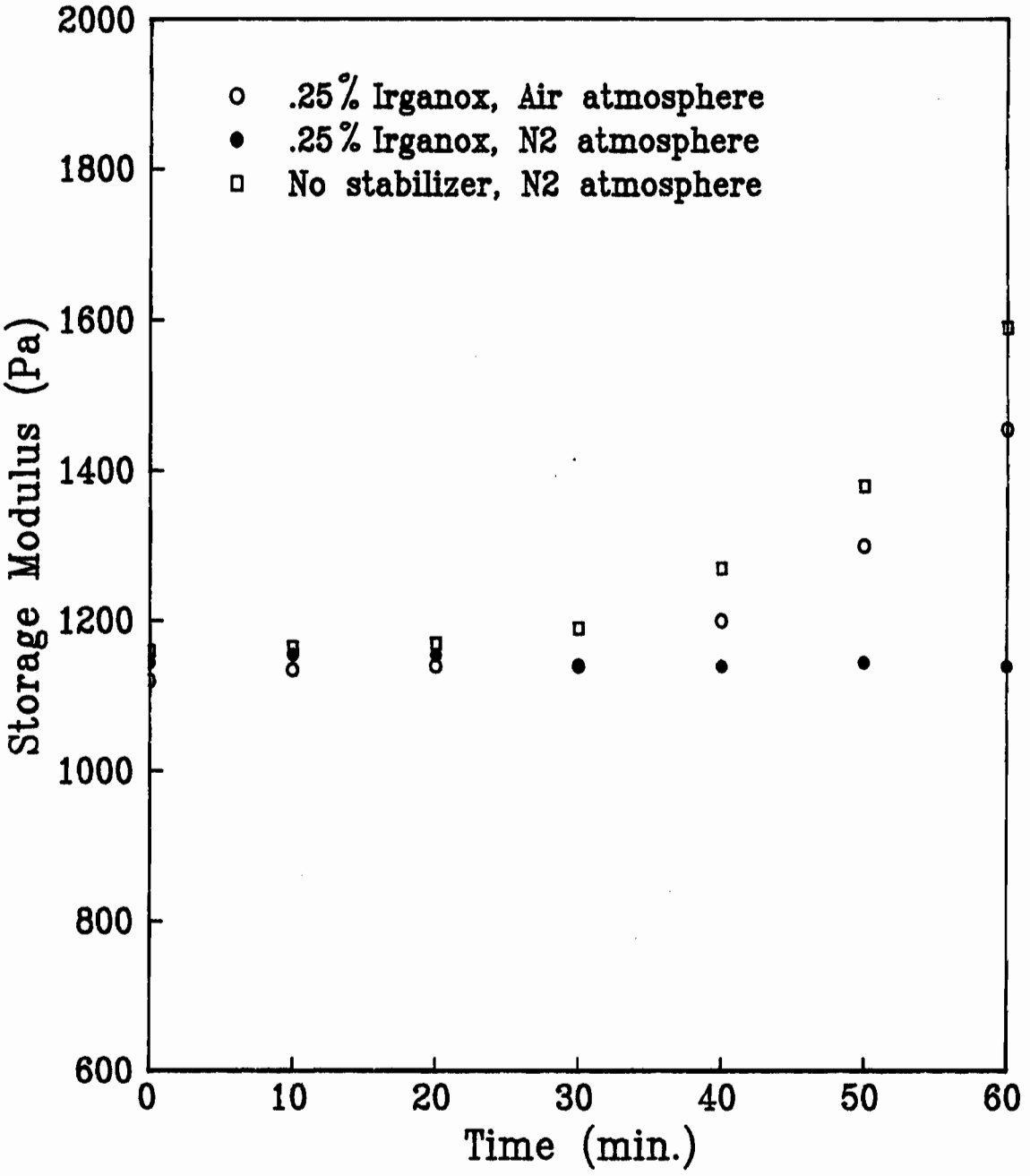

Figure 10: Degradation of resin 31 at 190°C. Effects of stabilizer and surrounding atmosphere on degradation.

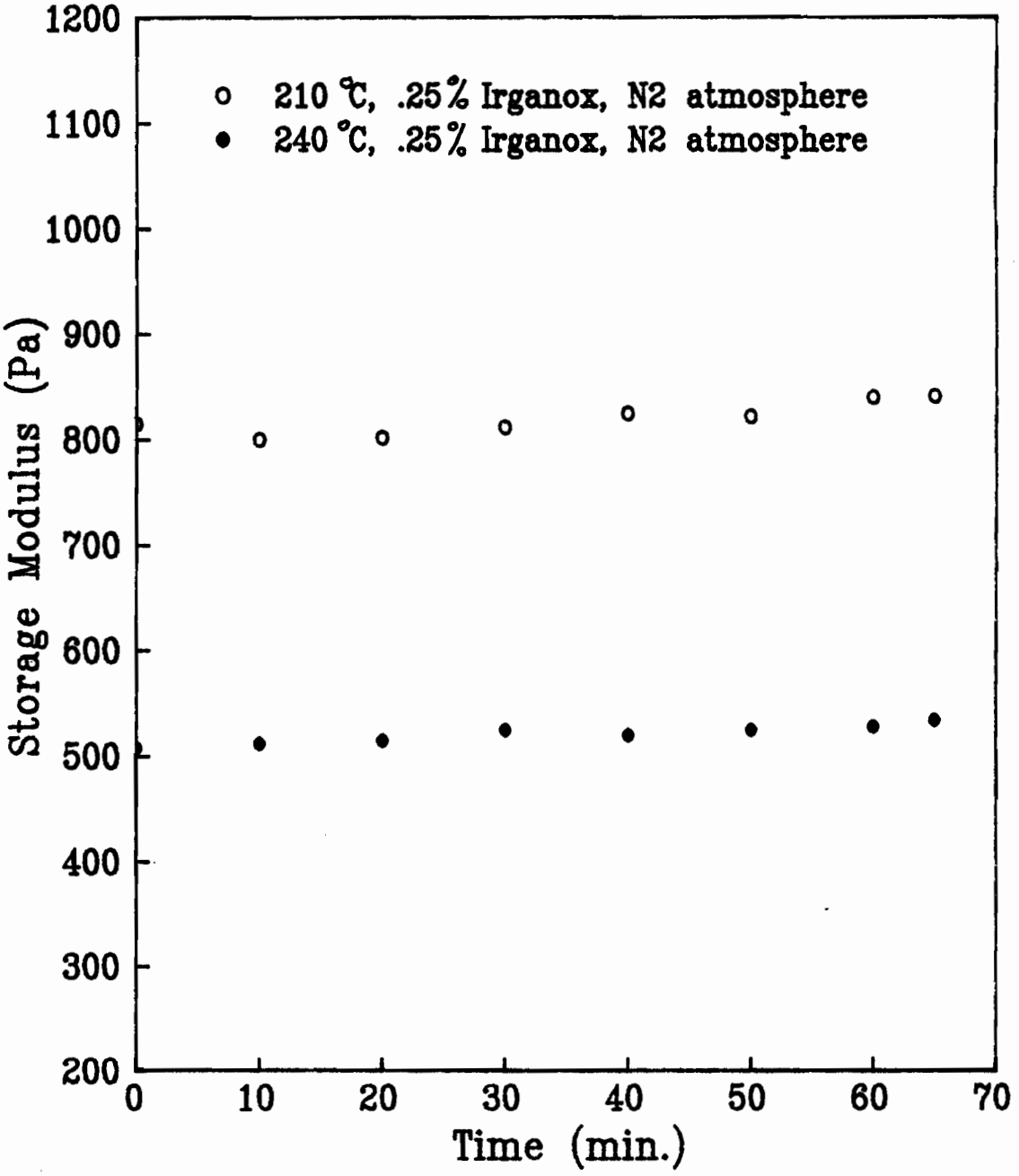

Figure 11: Degradation of resin 31 at 210°C and 240°C.

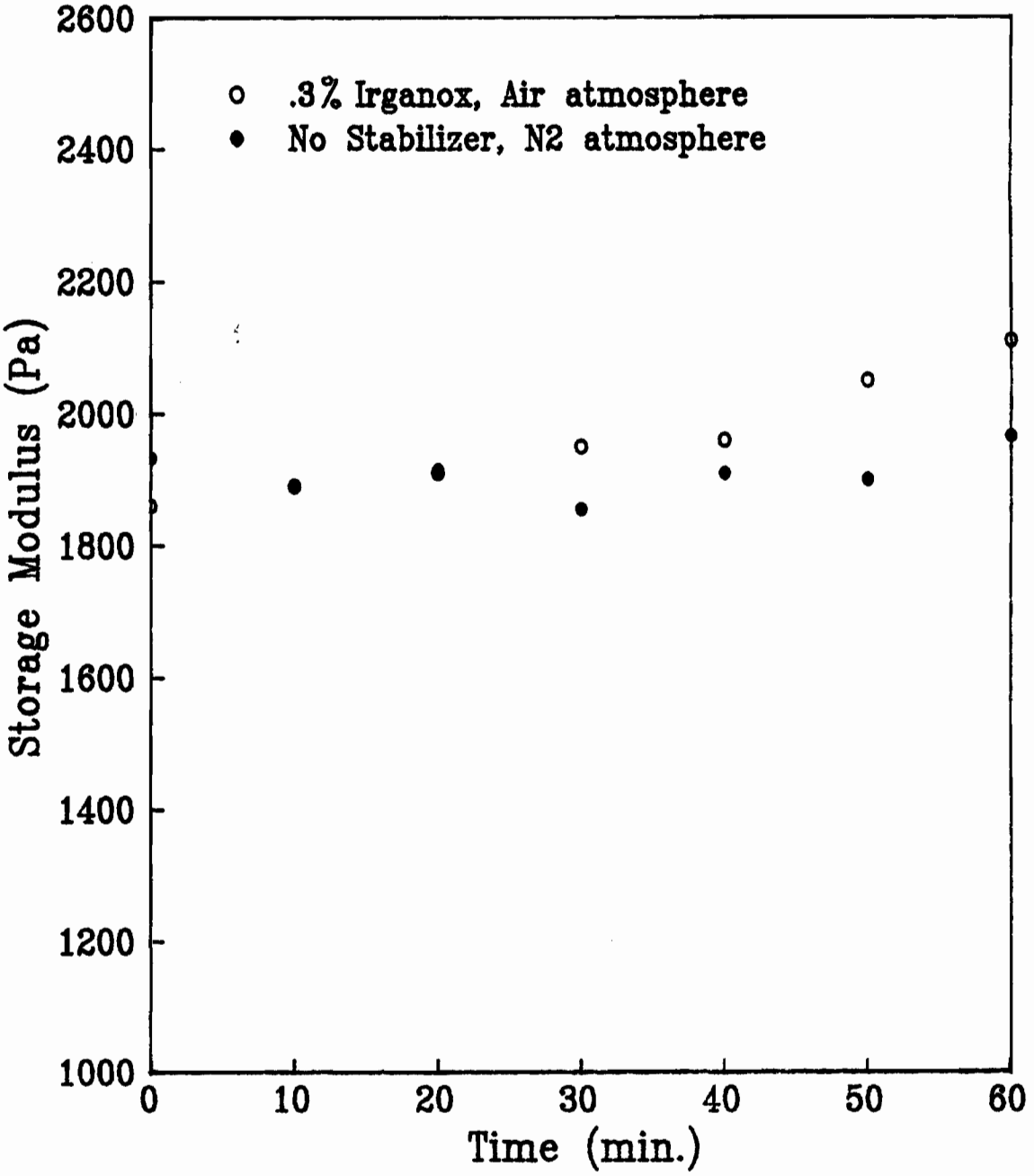

Figure 12: Degradation of resin 33 at 190°C. Effects of stabilizer and surrounding atmosphere on degradation.

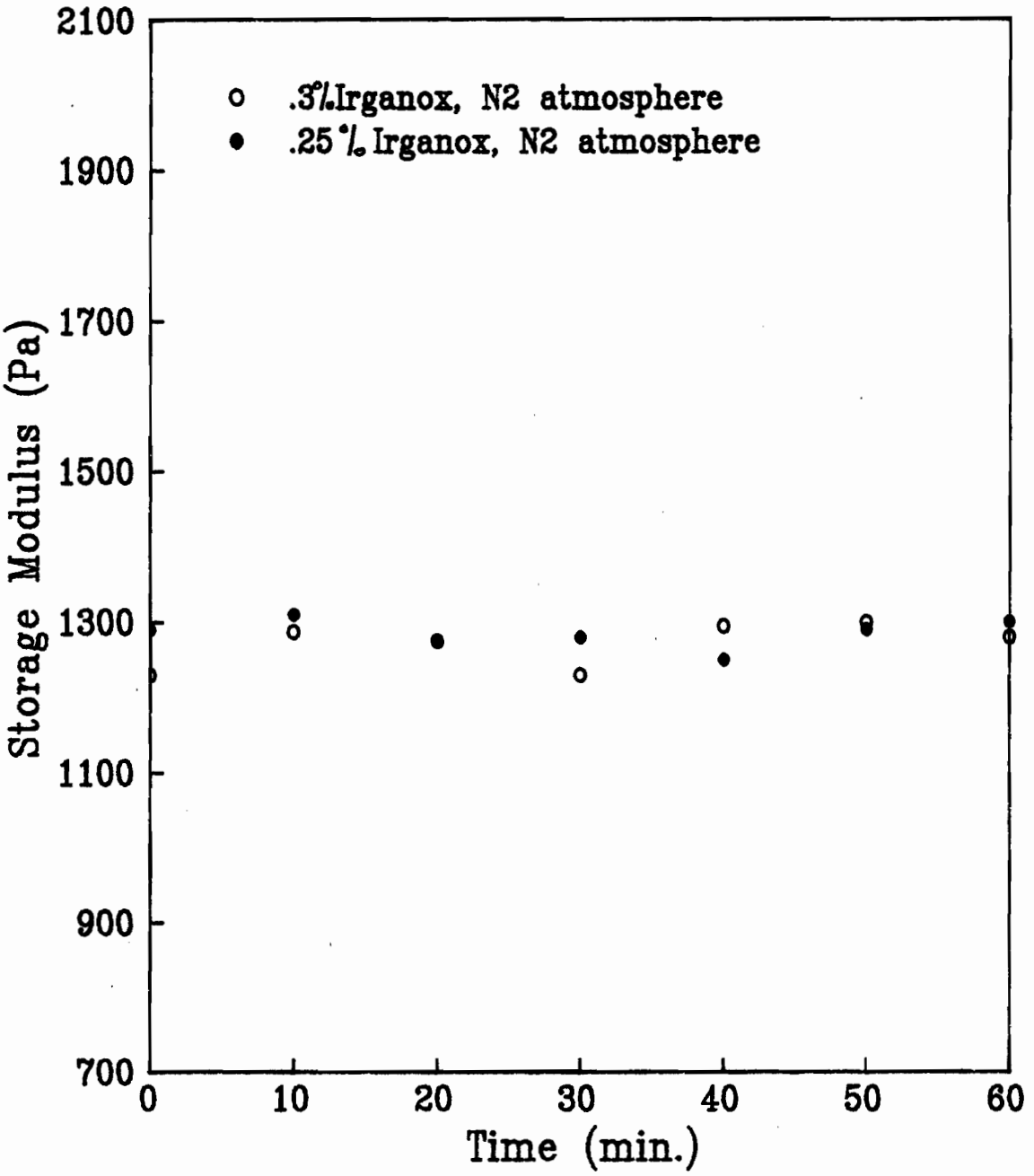

Figure 13: Degradation of resin 33 at 210°C. Effects of stabilizer concentration on storage modulus.

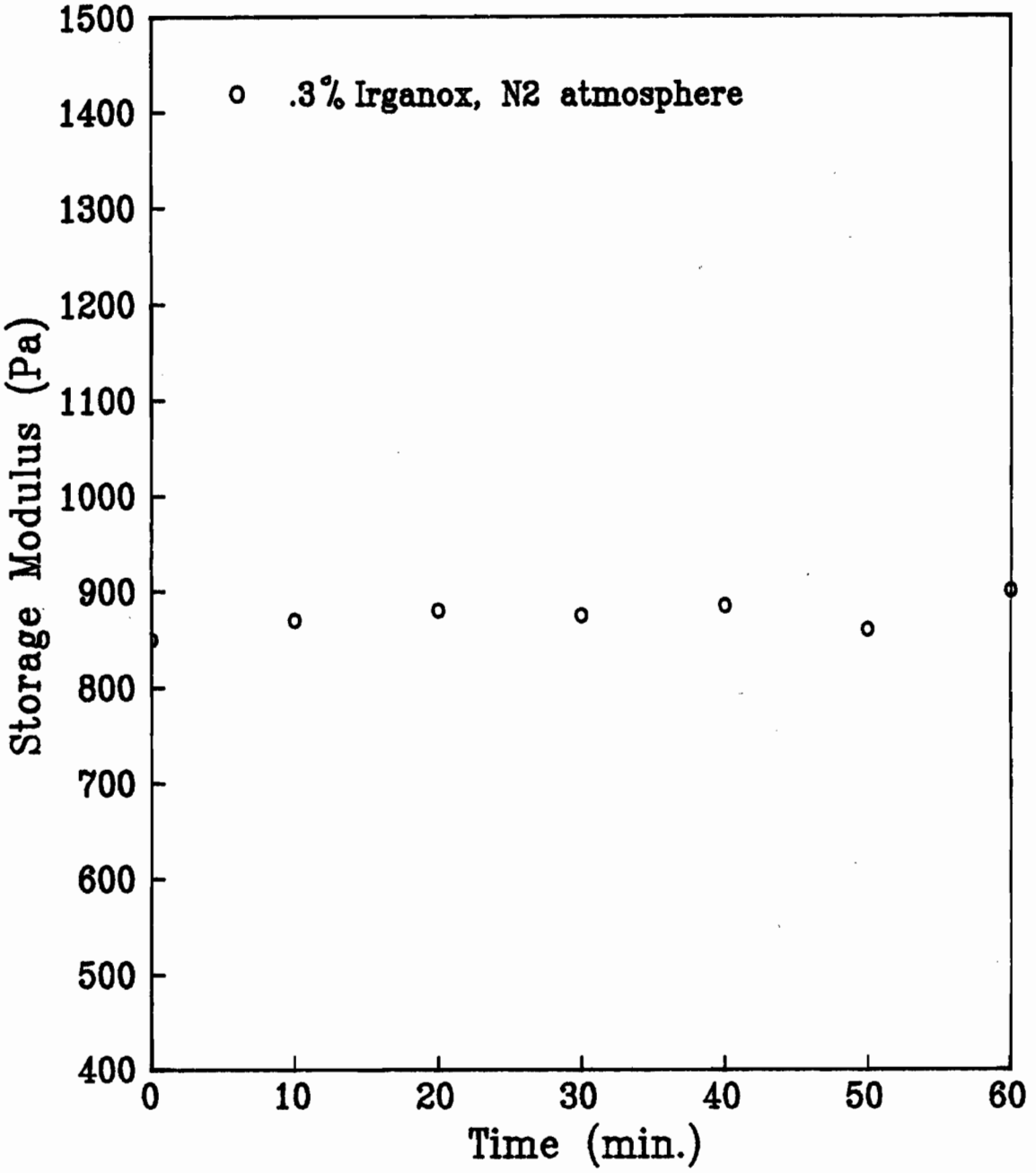

Figure 14: Degradation of resin 33 at 240°C.

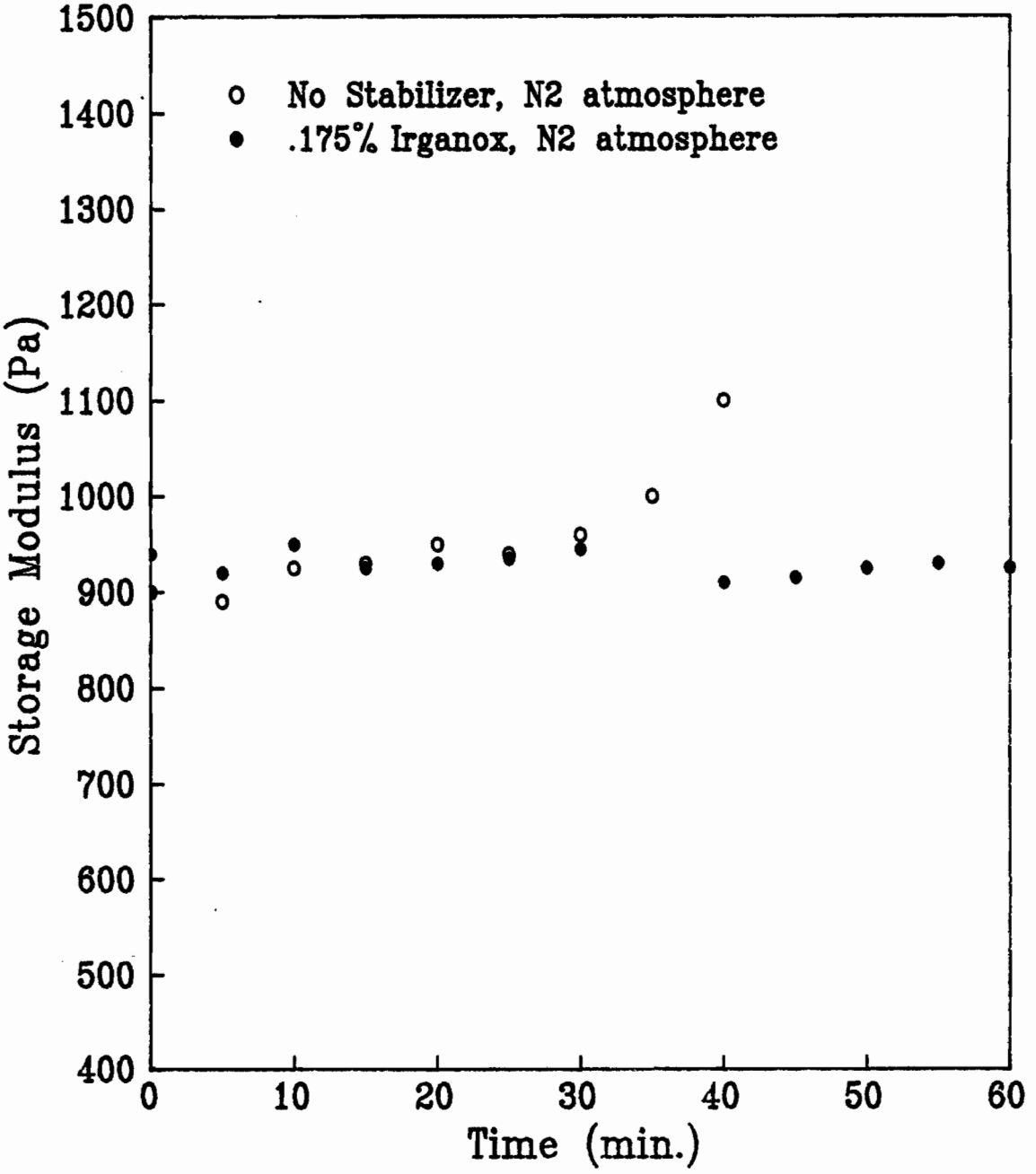

Figure 15: Degradation of resin 30 at 190°C.
Effects of stabilizer on thermal stability.

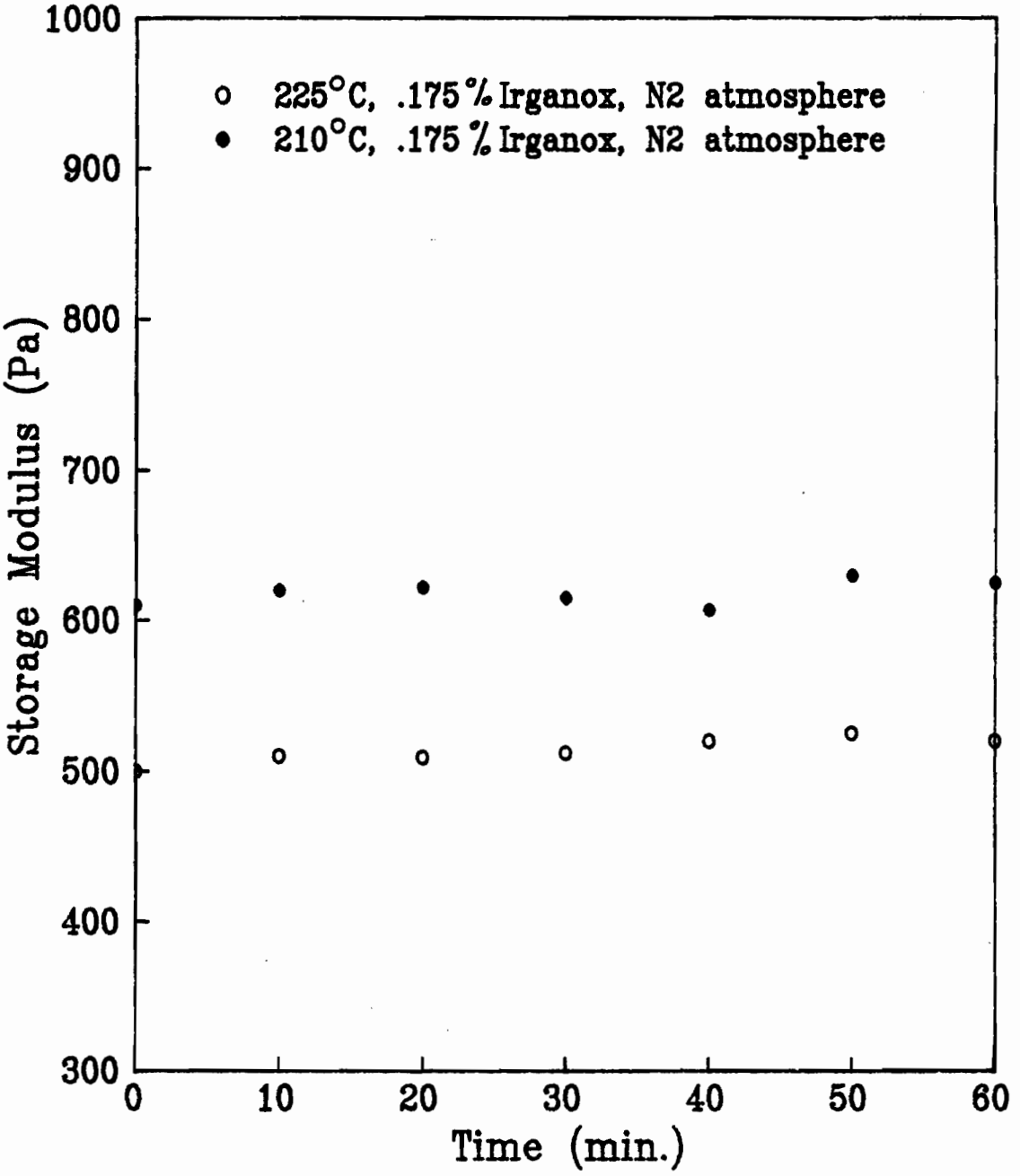

Figure 16: Degradation of resin 30 at 210°C and 225°C.

occurred at a stabilizer loading of about .35%. Thus, the highest temperature at which the low shear rate and oscillatory shear properties of resin 30 could be measured was 225^{o}C.

When measuring the low shear rate properties of all four resins two samples were required to cover the shear rate range. For each temperature it took up to 80 minutes to complete an experiment. This is due to the long times required for the normal stresses in the sample, created when the cone fixture is squeezed down on it, to relax completely, and for the normal stress fluctuations due to temperature fluctuations to cease. Oscillatory shear experiments typically took less than 15 minutes to perform. An interesting observation made by Gordon [138] and subsequently confirmed by the author was that allowing the stabilized LLDPE resins to remain in the barrel of the Instron Capillary Rheometer (ICR) at temperatures of up to 240^{o}C for as long as 30 minutes did not seem to affect the viscosity of the resins at high shear rates. This is surprising since the melt is exposed to air in this apparatus. This may be due to the fact that viscous properties are less sensitive to the type of degradation that occurs in these resins. It was thus possible to obtain high shear viscosity data for resin 30 at both 225 and 240^{o}C.

None of the three LLDPE resins seemed to be more susceptible to degradation than the others, however resin 30 could not be adequately stabilized with Irganox B561 at 240 ^{o}C. This finding indicates that Irganox B561 may not be a suitable stabilizer for this resin.

5.2 Steady Shear Properties

5.2.1 Viscosity and First Normal Stress Difference

The shear viscosity data presented in Figures 17-19 show the differences in behavior of the three LLDPE resins and most strikingly, the substantially different behavior of the LDPE resin. As has been observed by previous workers [22,62,120,123,131,139], the LDPE resin exhibited higher values of the shear viscosity than did the three LLDPE resins at low shear rates, while the latter all had higher shear viscosities at the higher shear rates. By extrapolating the low shear rate data of the LDPE in Figure 17 to higher shear rates (linear extrapolation on a log-log plot), the shear rates at which the viscosities of the LLDPE resins surpass the LDPE viscosity can be estimated. The shear rates at which this viscosity "cross-over" occurs are, .18, .65 and 5.5 sec^{-1} for resins 33, 31 and 30, respectively.

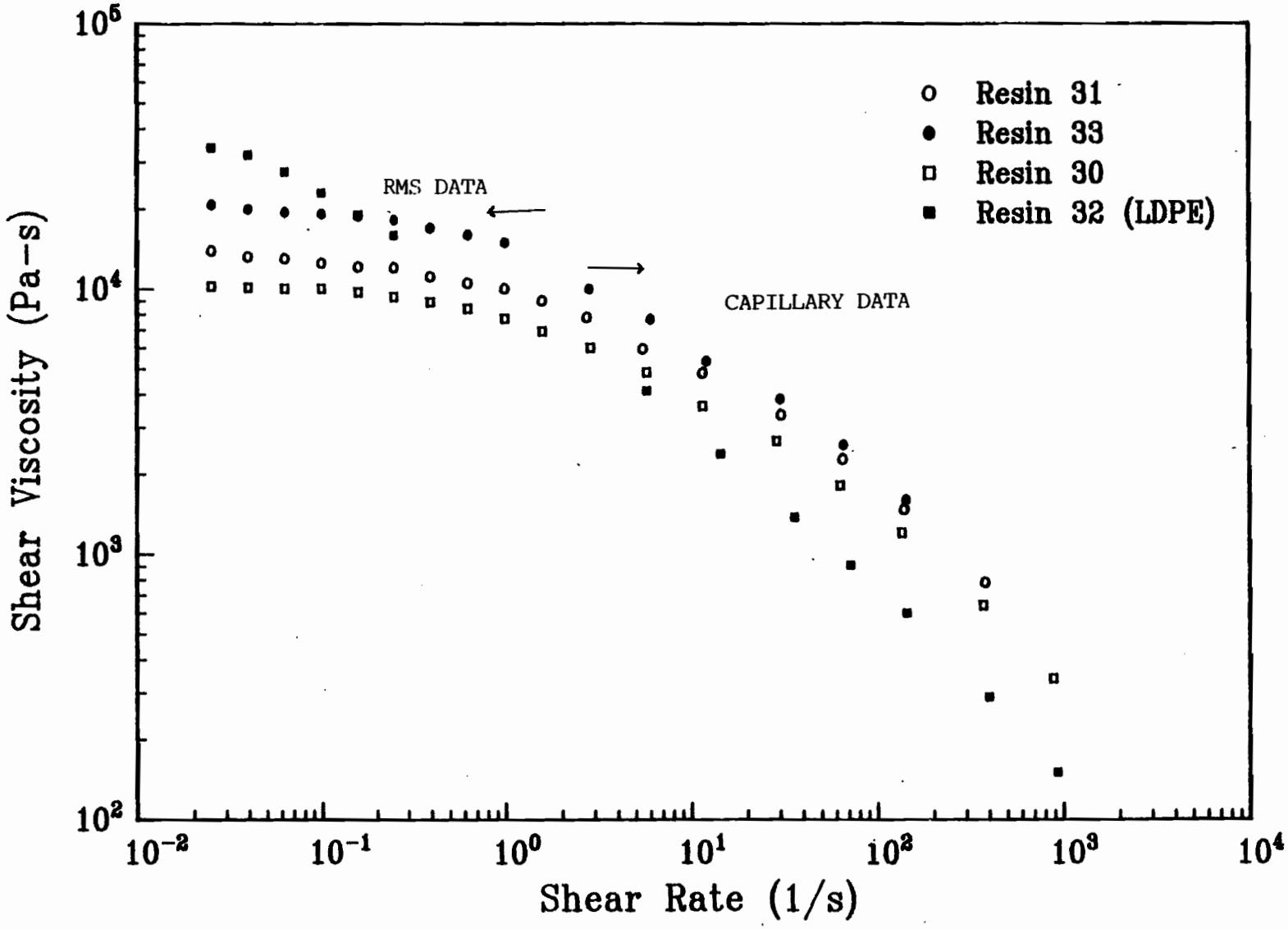

Figure 17: Shear viscosity, η, data at 190°C.

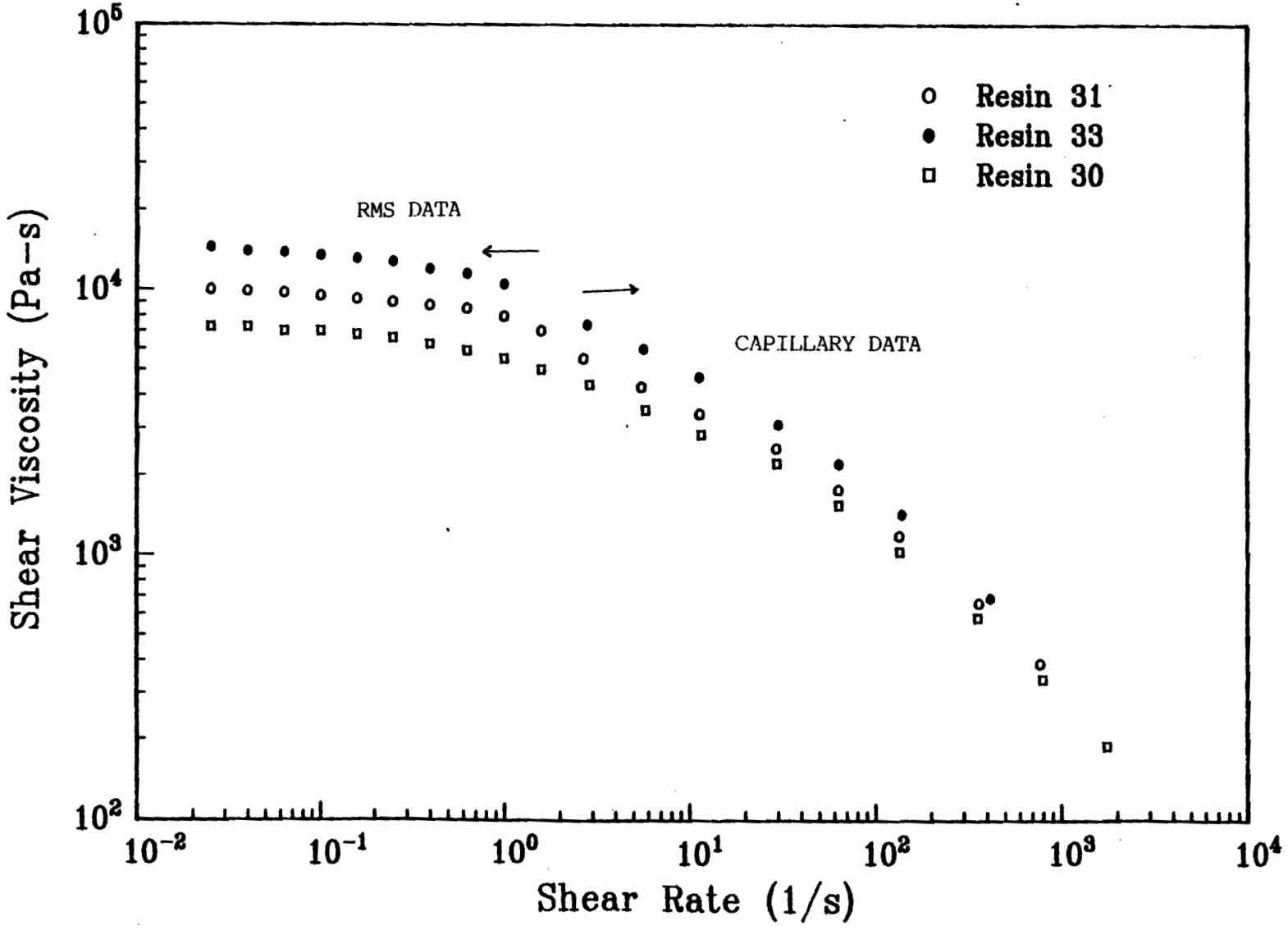

Figure 18: Shear viscosity, η, data at 210°C.

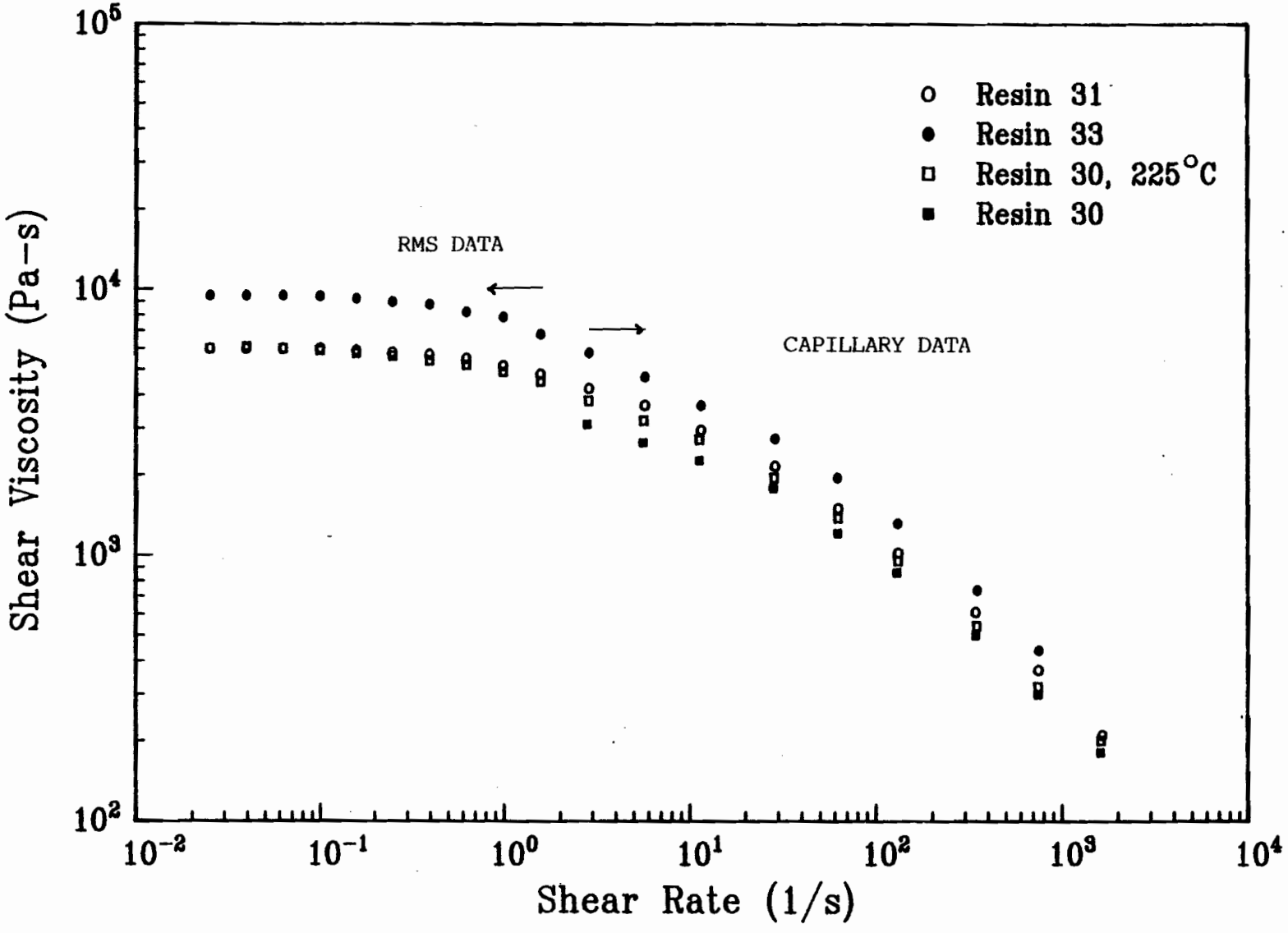

Figure 19: Shear viscosity, η, data at 240°C.

All three of the LLDPE resins exhibited fairly well defined values of the zero-shear viscosity at low shear rates. These values are presented in Table 4. At all temperatures, resin 33 had the highest value of the zero-shear viscosity followed by resins 31 and 30. The shear rates at which these materials exhibited a 5% or greater departure from the lowest shear rate (.02512 s^{-1}) viscosity are given in Table 5. Again, resin 33 seemed to experience a more rapid decrese in viscosity than did either of the other resins, followed by resin 31 and then by resin 30. Interestingly, this departure from the zero-shear value of the viscosity occurred at progressively higher shear rates for all three resins as the temperature was increased. This is readily explainable. The random molecular motions which result in the formation of entanglements occur more quickly at higher temperatures. By shearing a melt, entanglements are destroyed at a rate proportional to the shear rate. Thus, by increasing the melt temperature, the shear rate at which the rate of entanglement destruction surpasses the rate of entanglement formation is increased. When entanglement destruction is greater than entanglement formation, shear thinning occurs.

The values of the zero-shear viscosity of these resins at 190 and 210^{o}C are plotted against their weight average molecular weights in Figure 20. Resins 31 and 33, which have

ZERO SHEAR VISCOSITIES OF LLDPE RESINS

	η_o (10E-04 Pa-s)		
	190 °C	210 °C	240 °C
Resin 30	1.05	0.725	0.600★
Resin 31	1.40	1.00	0.600
Resin 33	2.15	1.45	0.950

★225 °C for resin 30

Table 4

SHEAR RATES AT WHICH VISCOSITY DEPARTS FROM ZERO-SHEAR VALUE ($\Delta\eta$ >-5%)

	190°C	210°C	240°C
Resin 30	0.1585	0.1585	0.1585★
Resin 31	0.100	0.1585	0.3981
Resin 33	0.0631	0.100	0.2512

★225°C for resin 30

Table 5

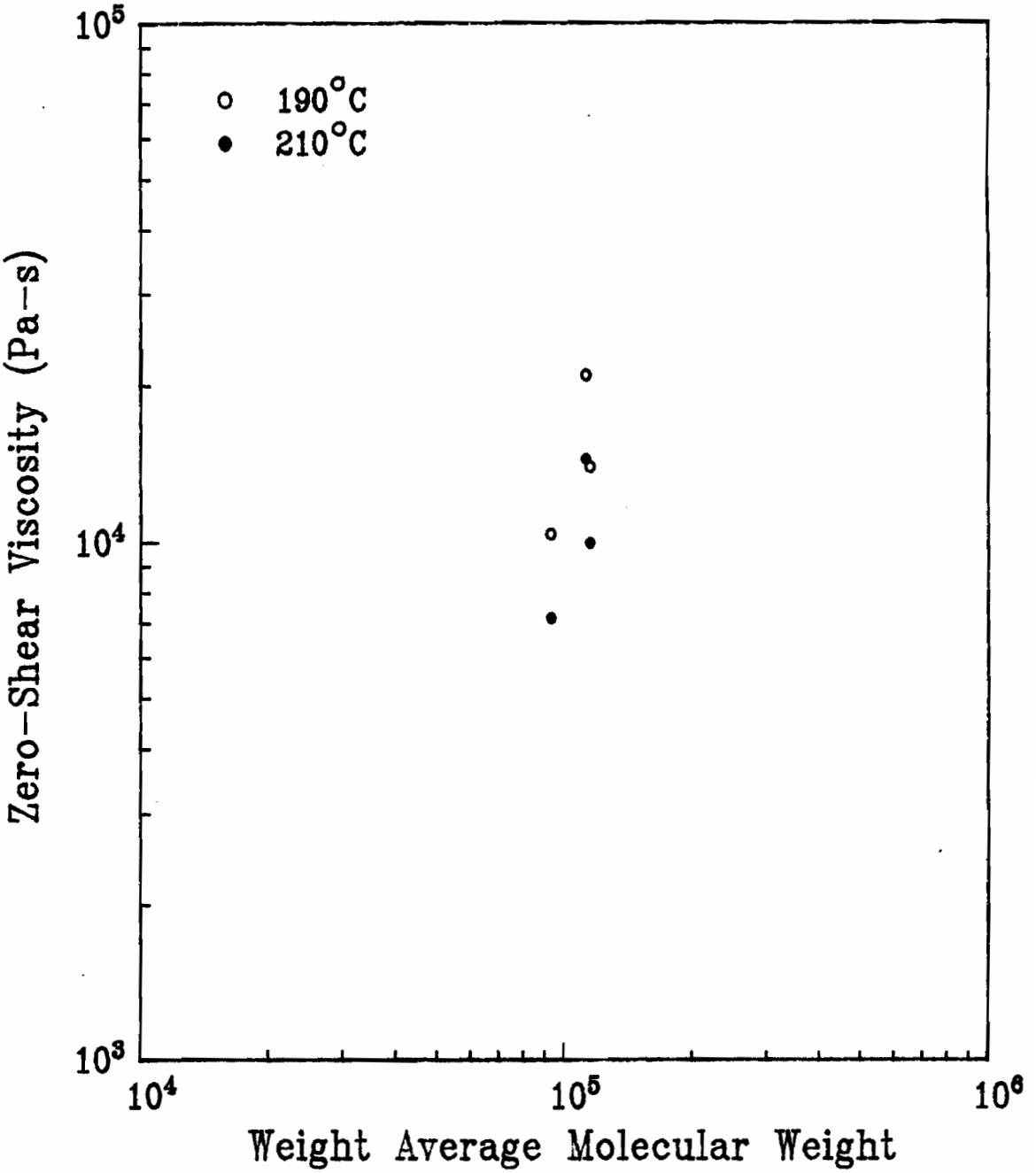

Figure 20: Relationship between zero shear viscosity, η_o, and weight average molecular weight, M_w, for the LLDPE resins at 190°C and 210°C.

comparable values of M_w(within about 2%) and M_n , differ in zero-shear viscosity by more than 30%. Thus, the frequently cited 3.4 power proportionality between zero-shear viscosity and molecular weight for monodisperse resins [30] does not seem to apply. These resins also have almost identical values of the polydispersity index with that of resin 31's being slightly higher. This difference in viscosity may be due to subtle differences in branching structure. Resin 30, with a weight average molecular weight about 20% less than that of the two other resins has a significantly lower value of the zero-shear viscosity.

One of the assumptions used to derive the rheometrical equations for cone and plate flow, which was used in making these measurements, is that the sample free surface is spherical and has a radius of curvature equal to that of the cone radius [25]. For polymeric liquids in particular, this assumption of edge sphericity becomes invalid as the shear rate is increased. It has been observed by Hutton [140] that at a limiting value of the shear rate, the liquid sample exhibits "edge fracture" at the liquid-air interface. Hutton suggested that this occurs when the elastic energy of the liquid becomes greater than the energy required to fracture it. Assuming the validity of this hypothesis, one would expect that more elastic melts would exhibit "edge fracture" at a lower shear rate than less elastic melts. This

phenomenon was observed with all four of the resins studied. Its presence was also indicated by a steadily decreasing value of the shear stress. The onset of fracture limited the shear rate at which the cone and plate geometry could be used. Resin 32 (LDPE) exhibited edge fracture at shear rates as low as .25 s^{-1} while the LLDPE resins experienced it at shear rates between 1 and 1.585 s^{-1} depending on the resin and temperature. Resin 33 seemed the most susceptible to edge fracture of the three LLDPE resins, with resins 31 and 30 having an apparently equal propensity for this phenomenon.

Despite the significant differences in the low shear rate viscosities of these resins, their viscosity curves at the higher shear rates, which are characteristic of processing conditions, tend to almost converge. This is particularly true for resins 31 and 33. An interesting difference between the behavior of the LDPE resin and the LLDPE resins at the higher shear rates, is that the former tends to enter the so called power law region at a lower shear rate than do the latter resins. In addition, the LDPE resin has a substantially lower viscosity than any of the LLDPE resins in the their power law regions (50 to 60% lower). As had been mentioned in an earlier section, this behavior is quite typical of materials such as LDPE with long chain branching and broad molecular weight distributions. Because of its convenience in engineering practice, the

following emperical expression is frequently used to fit viscosity data in the power law region.

$$\eta(\dot{\gamma}) = k\dot{\gamma}^{n-1} \qquad (58)$$

In this expression the value of the power law index, n, is a simple measure of the rapidity with which the materials viscosity decreases. In Figures 21-23, the power law regions of the viscosity curves are shown, and in Table 6 the values of the power law constants are given. The power law constants for the LLDPE resins are all between 12.5% and 22.5% greater than that of resin 32 indicating that the latter's viscosity decreases most rapidly with shear rate.

The normal stress difference data for these resins are presented in Figures 24-26. The expected rapid increase of the normal stress difference with shear rate is evident as is the inverse proportionality between it and temperature. At the low shear rates that were attainable with the cone and plate geometry, the following ranking of the resins according to normal stress differences was observed.

$$(N_1)_{32} > (N_1)_{33} > (N_1)_{31} > (N_1)_{30} \qquad (59)$$

Since N_1 is a measure of elasticity, this is also a ranking of the elasticity of the four resins at low shear rates. It is also an approximate measure of their tendency to exhibit edge fracture in cone and plate flow. Although it is difficult to

POWER LAW CONSTANTS

Resin 30

	n	k ($Pa-s^n$)
190°C	.400 ± .007	2.18E 04 ± 420
210°C	.372 ± .005	2.13E 04 ± 410
225°C	.407 ± .005	1.74E 04 ± 395
240°C	.410 ± .006	1.47 04 ± 379

Resin 31

	n	k ($Pa-s^n$)
190°C	.421 ± .007	2.49E 04 ± 515
210°C	.400 ± .008	2.18E 04 ± 485
240°C	.402 ± .008	1.87E 04 ± 415

Resin 33

	n	k ($Pa-s^n$)
190°C	.435 ± .005	2.98E 04 ± 380
210°C	.377 ± .004	2.68E 04 ± 406
240°C	.401 ± .004	2.40E 04 ± 406

Resin 32

	n	k ($Pa-s^n$)
190°C	.355 ± .006	1.36E 04 ± 252

Table 6

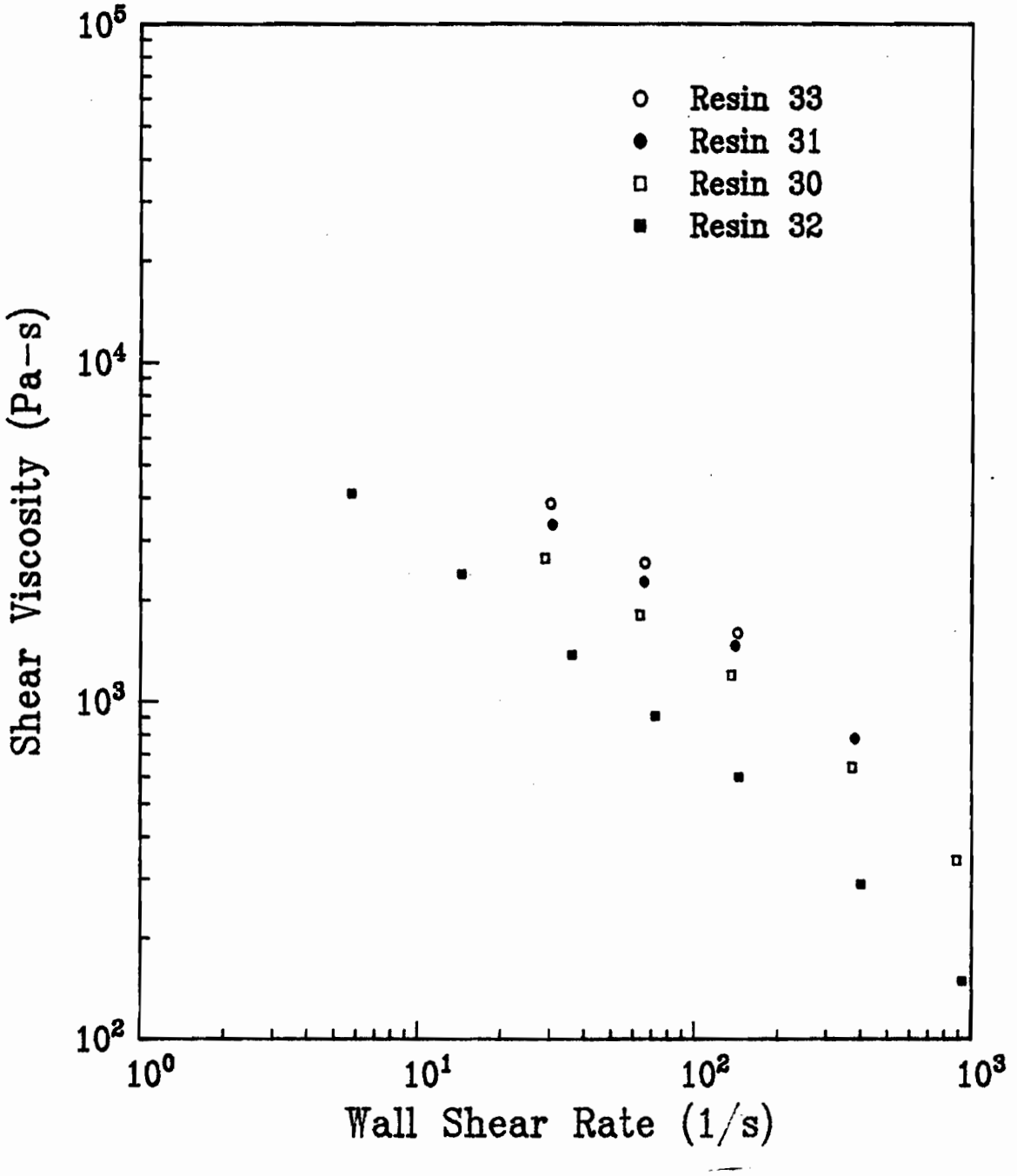

Figure 21: Power law regions of shear viscosity functions at 190°C.

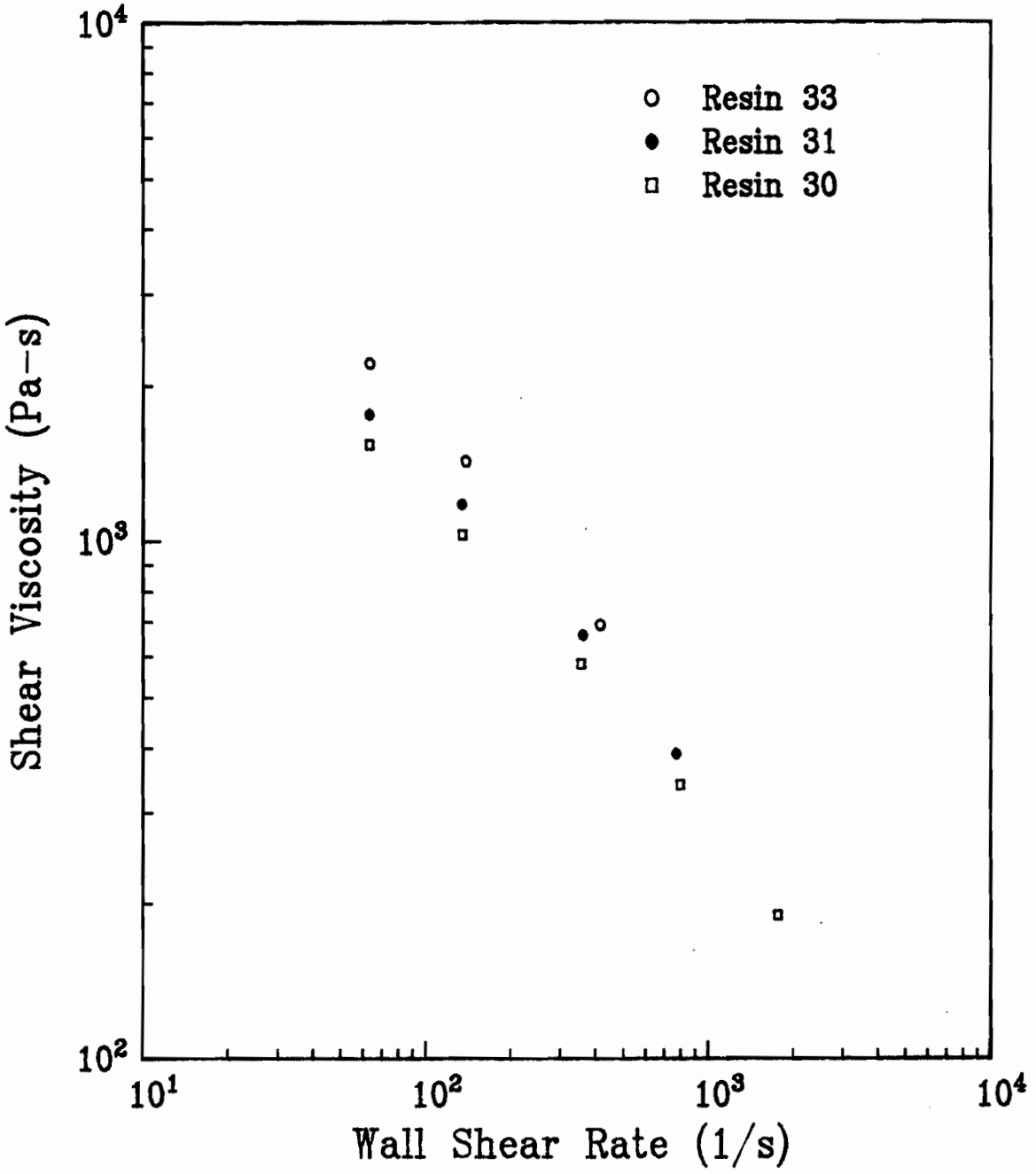

Figure 22: Power law regions of shear viscosity function at 210°C.

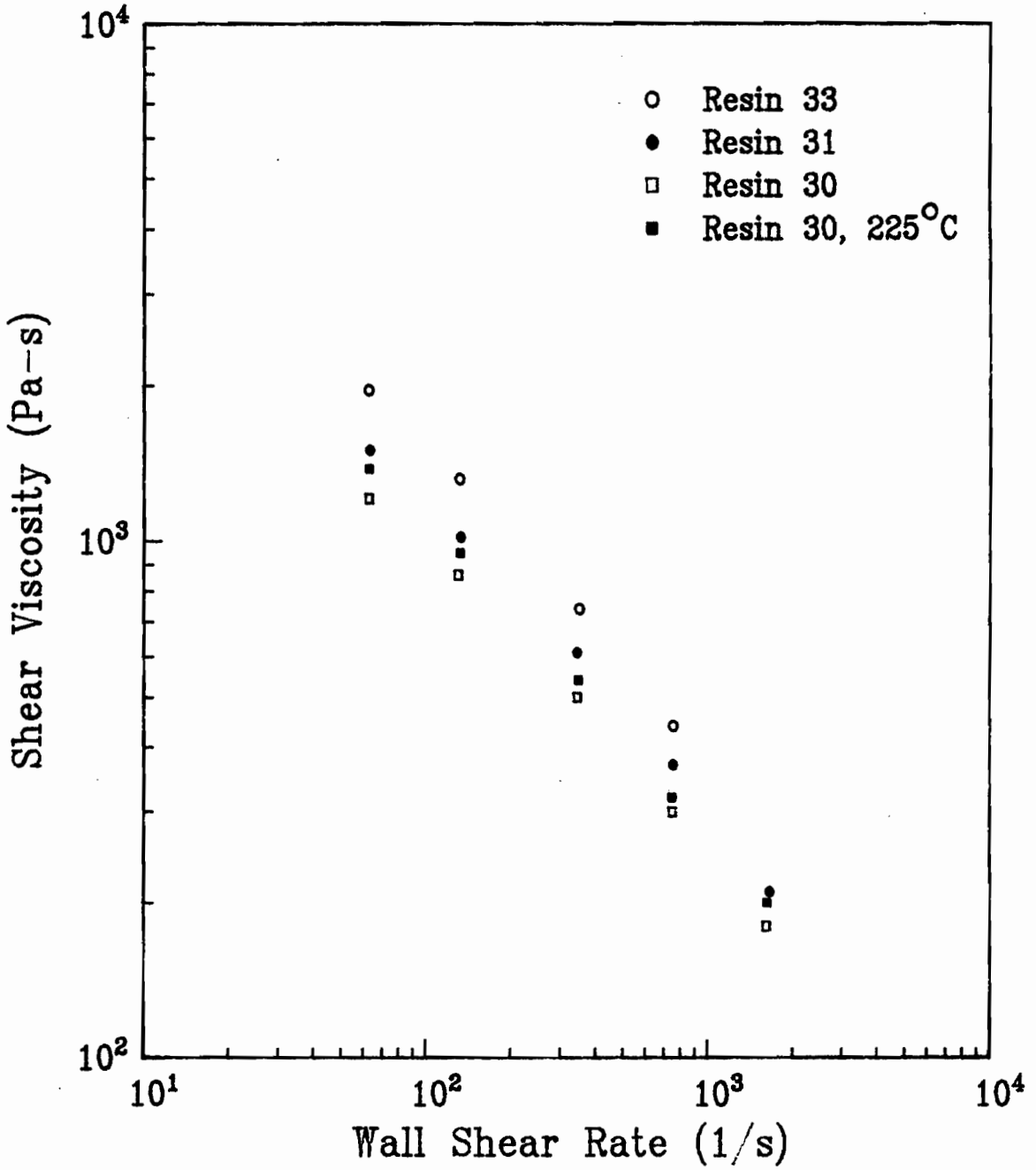

Figure 23: Power law regions of shear viscosity functions at 240°C.

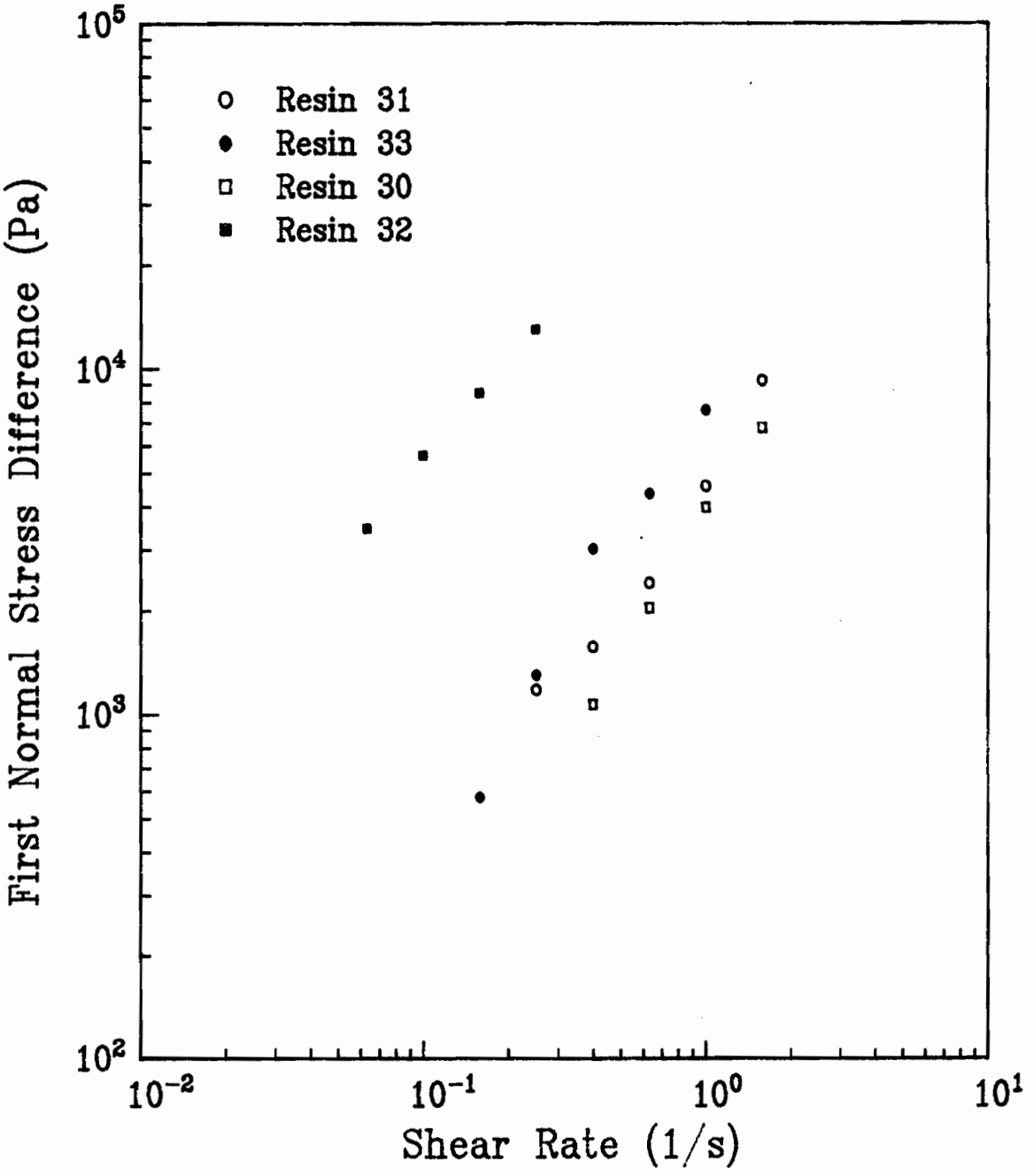

Figure 24: First Normal Stress Difference, N_1, data at 190°C.

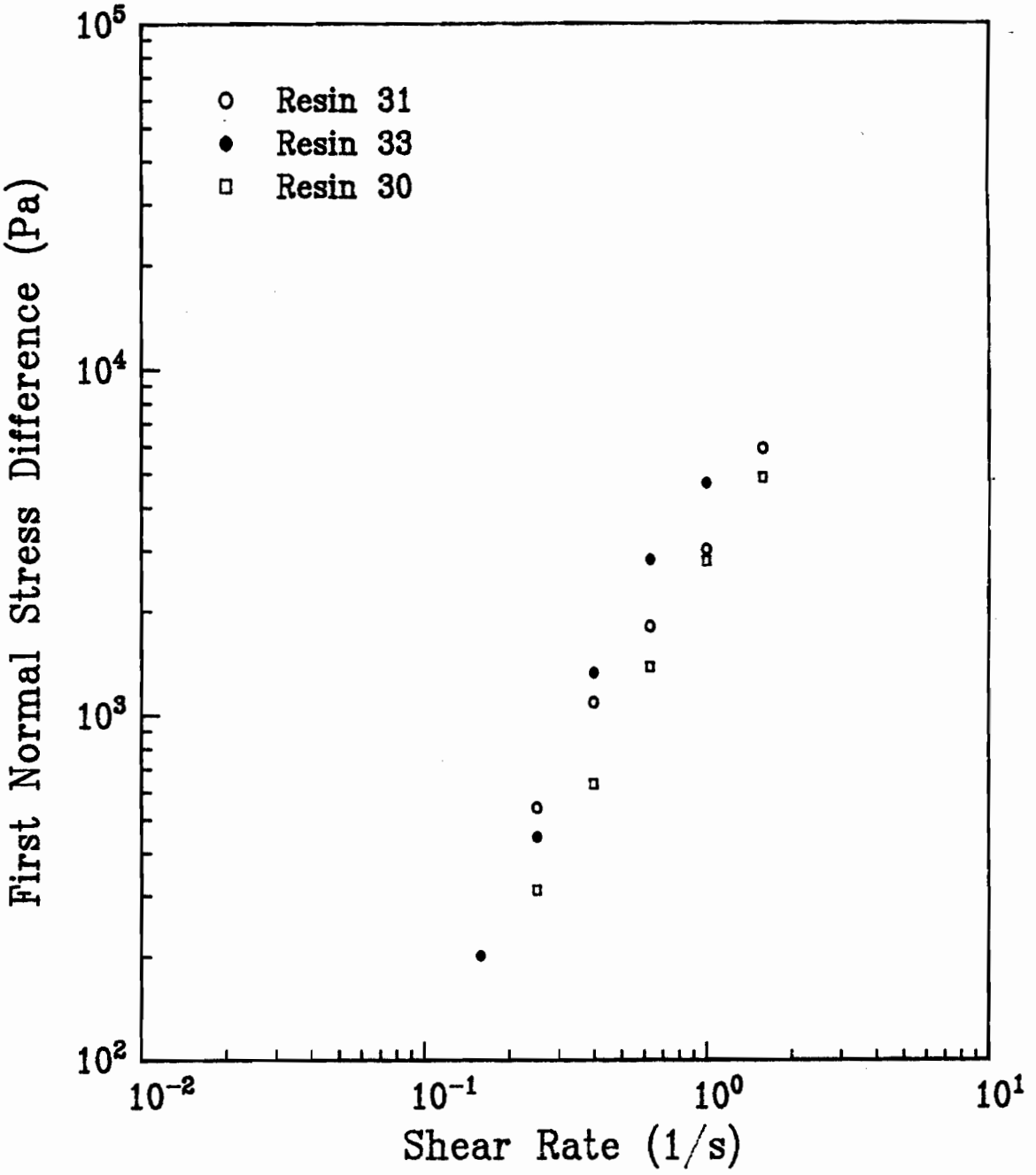

Figure 25: First Normal Stress Difference, N_1, data at 210°C.

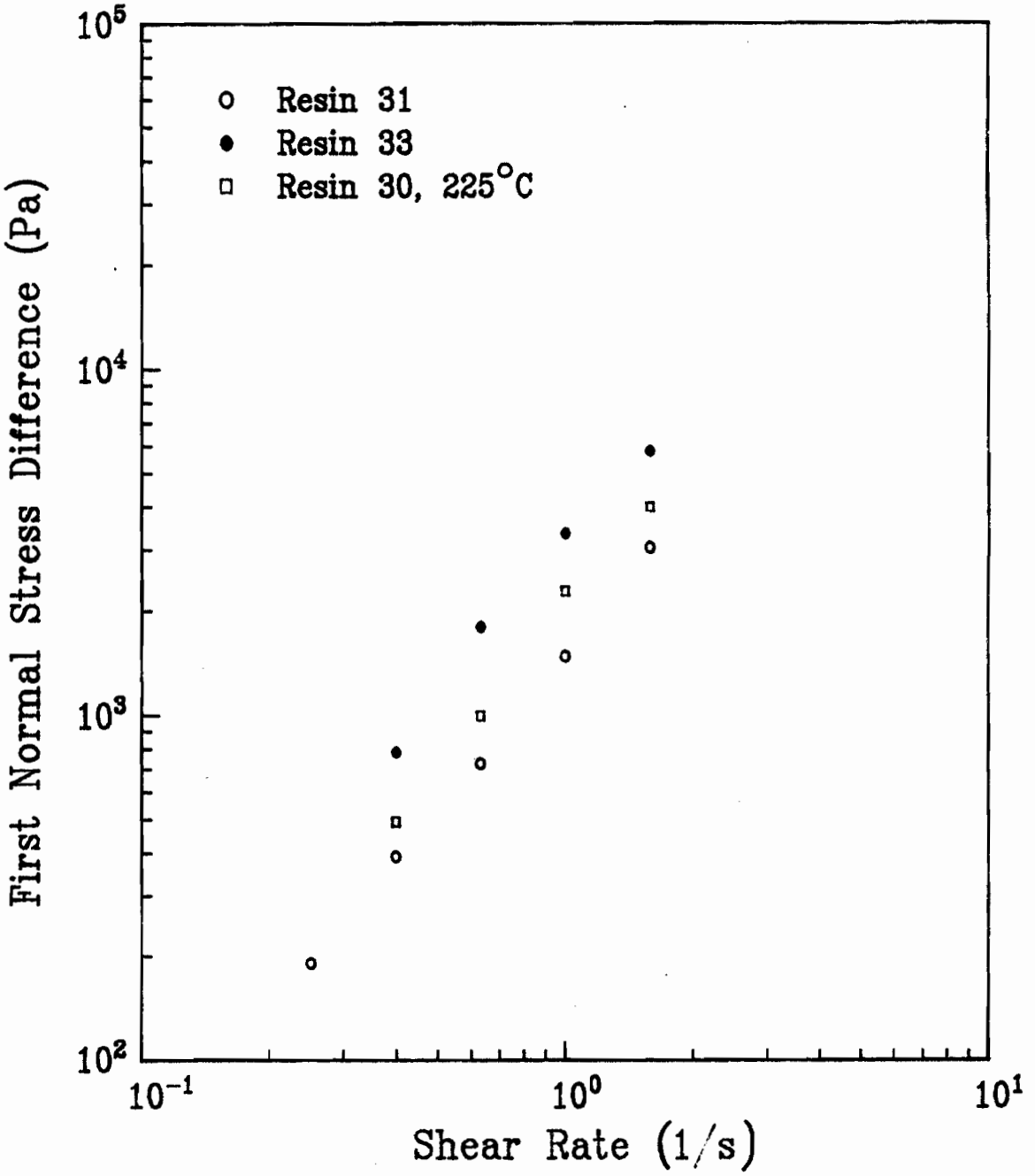

Figure 26: First Normal Stress Difference, N_1, data at 240°C.

draw conclusions regarding the reason for the variation in N_1 among the linear resins, it is quite likely that the higher values associated with resin 32 are a result of its long chain branching and rather wide molecular weight distribution [127]. The raw normal stress difference data for the materials studied are summarized in Appendix C along with the confidence intervals associated with them.

Although the shear viscosities of the LLDPE resins approach the linear viscoelastic limit known as the zero shear viscosity, the presence of normal stresses in shear indicates that the linear viscoelastic region has not in fact been attained, since linear viscoelastic theory predicts a zero value for the first normal stress difference [39].

5.2.2 Entrance Effects

In the flow of polymeric liquids in the entrance region of a capillary, large stresses are generated as a result of stretching along the liquid streamlines. An estimate of the pressure drop associated with this entrance flow can be obtained using a procedure suggested by Bagley [38]. For a given material and temperature, a plot of total pressure drop vs L/D of the capillary is made at constant values of the wall shear rate. An example of such a plot (hereafter referred to as a "Bagley plot") is presented in Figure 27.

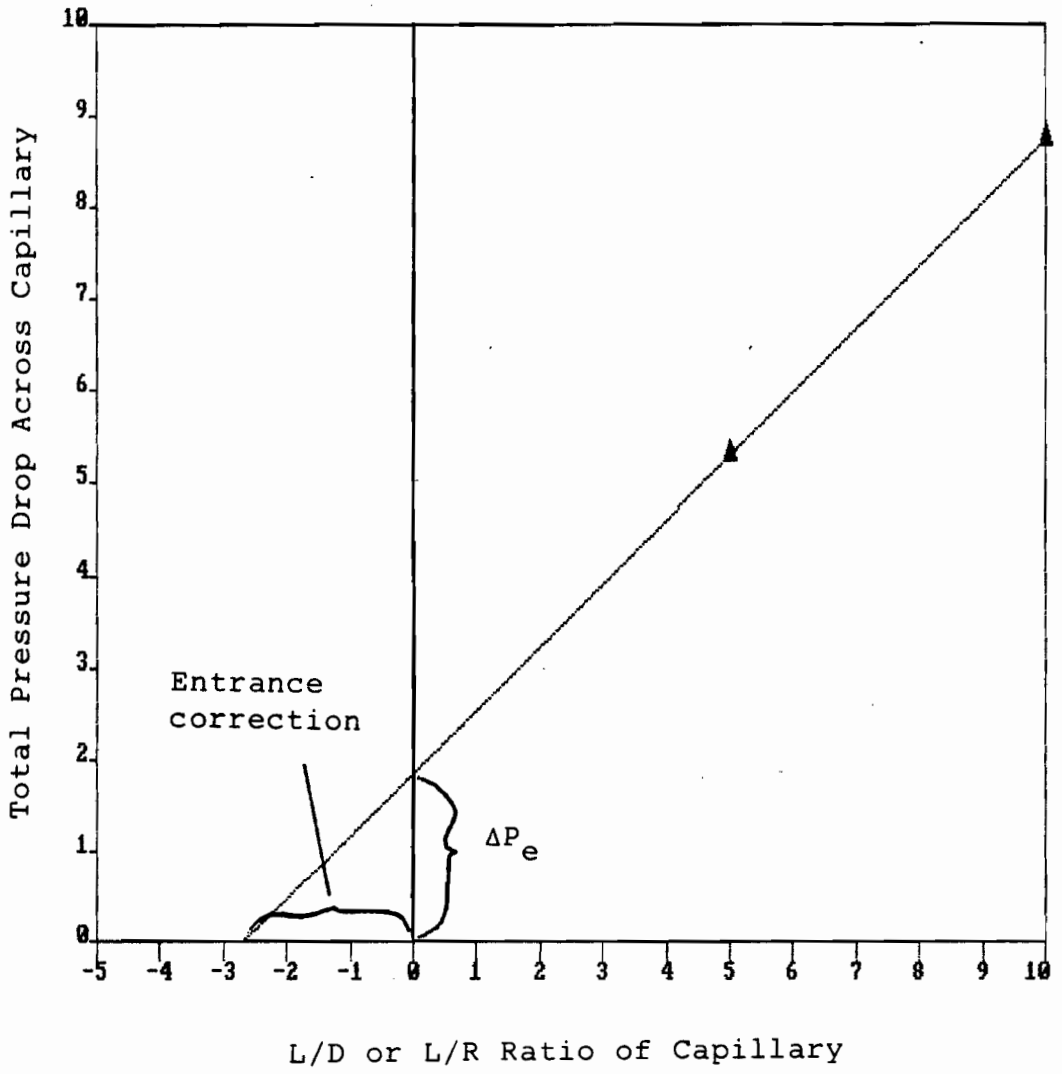

Figure 27: Example of a Bagley Plot.

The entrance pressure drop can be obtained by taking the pressure drop value for L/D=0. This large entrance pressure drop is due to both the viscous and elastic nature of the polymeric liquid, although Han [141] found that the viscous component of this pressure drop is generally less than 5% of the total pressure drop, indicating that the greater part of the entrance pressure drop is due to melt elasticity.

In Figures 28-30 the entrance pressure drop data obtained from the materials Bagley plots are presented. At these high strain rates, resin 33 exhibits the largest entry region pressure drop, followed by resins 31, 30 and 32. As expected, the magnitude of the pressure drop decreases with increasing temperature. These results are somewhat surprising in that LDPE resins such as the one being studied are generally considered to be more elastic than linear polyethylenes such as LLDPE [59] and would thus be expected to exhibit higher values of entry pressure drop. To eliminate temperature as a variable, these data were plotted with wall shear stress as the independent variable in Figures 31-33. It is apparent that the entrance pressure drop is essentially a linear function of the wall shear stress in the capillary, at least for the LLDPE resins. In Figure 33 it appears that the entrance pressure drop for resin 32 increases almost quadratically with the wall shear stress. Comparing all four resins at 190 ^{o}C in Figure 34, we find that

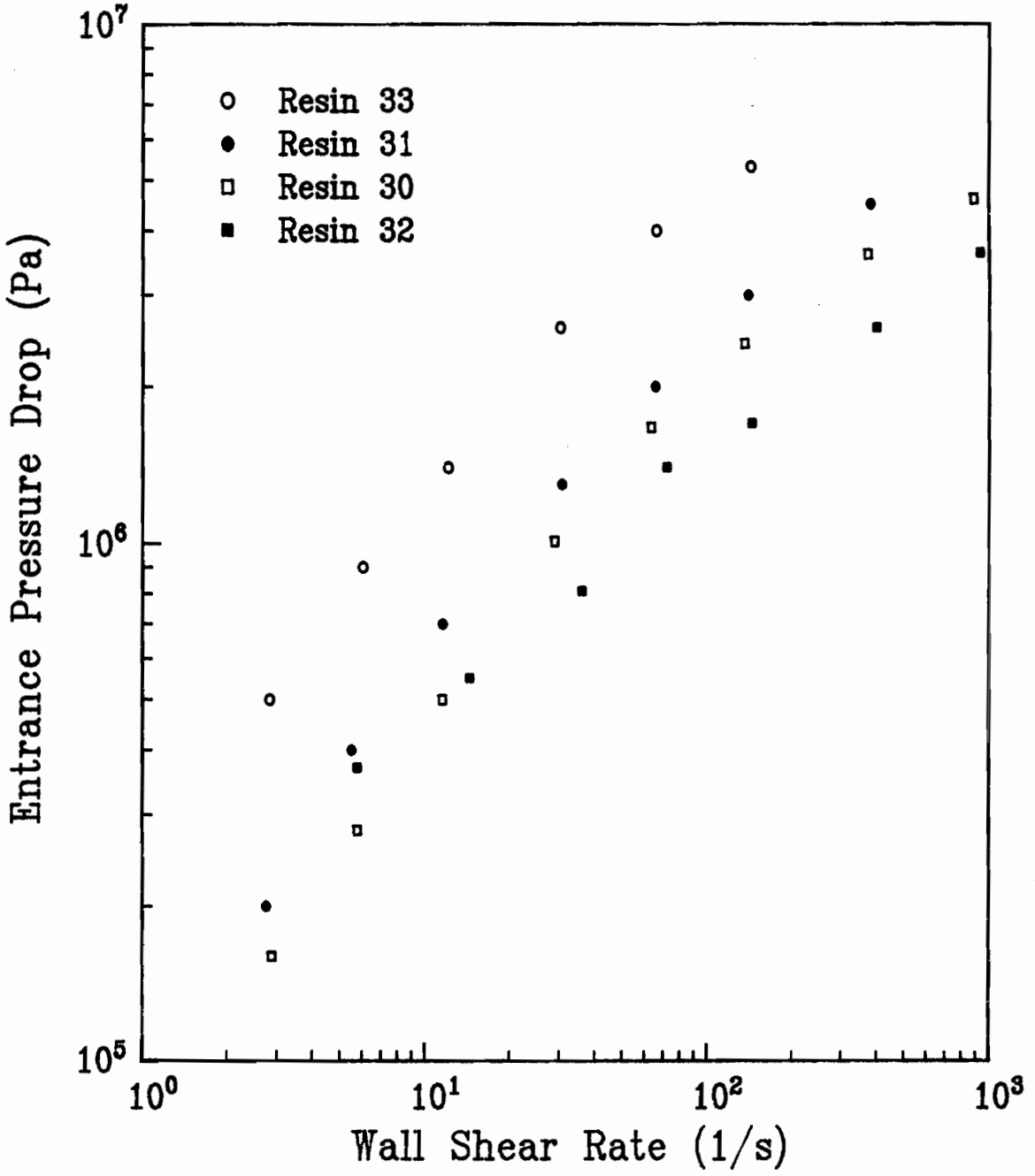

Figure 28: Entrance pressure drop, ΔP_e, as a function of wal shear rate, $\dot{\gamma}_w$, at 190°C.

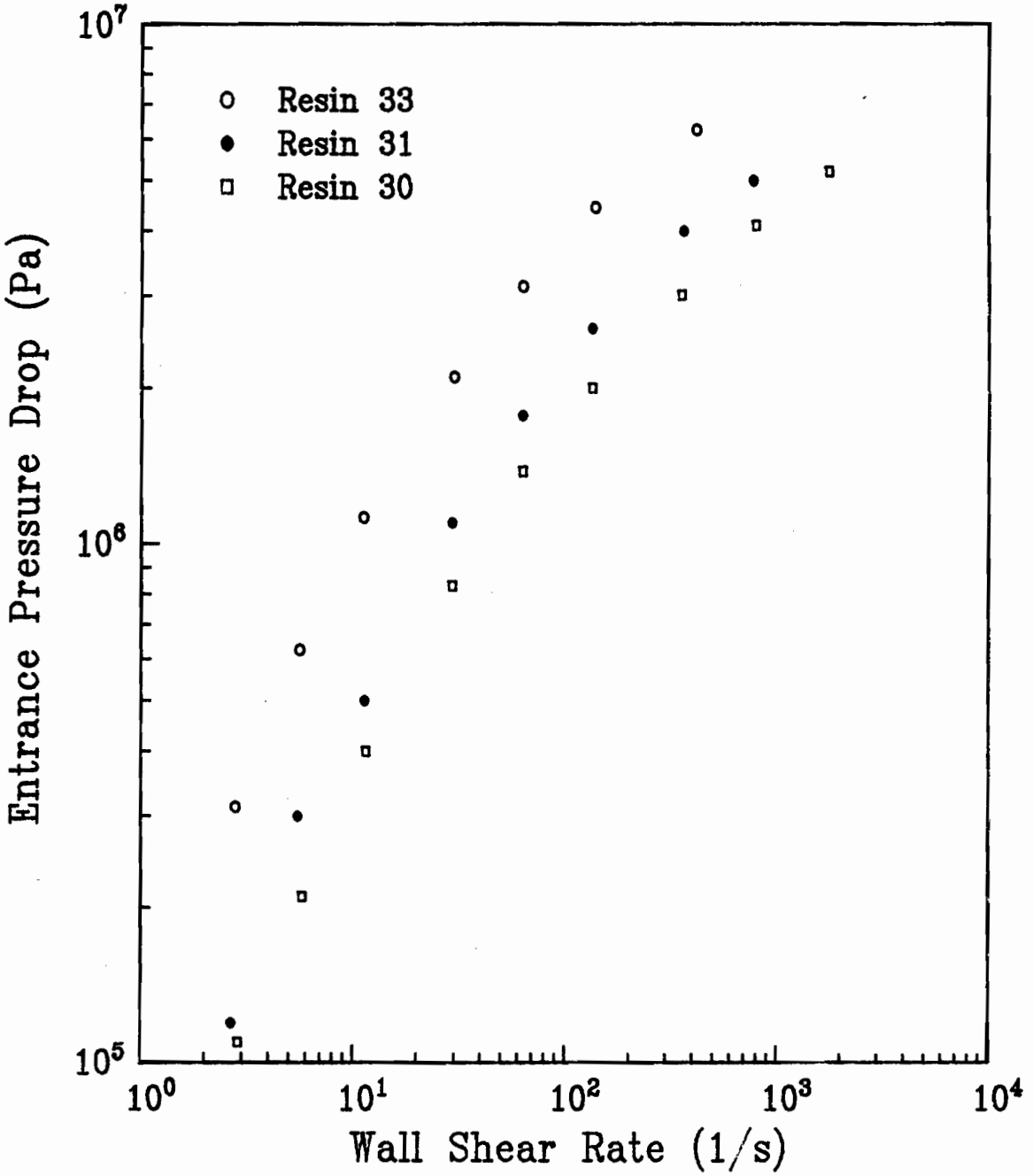

Figure 29: Entrance pressure drop, ΔP_e, as a function of wall shear rate, $\dot{\gamma}_w$, at 210°C.

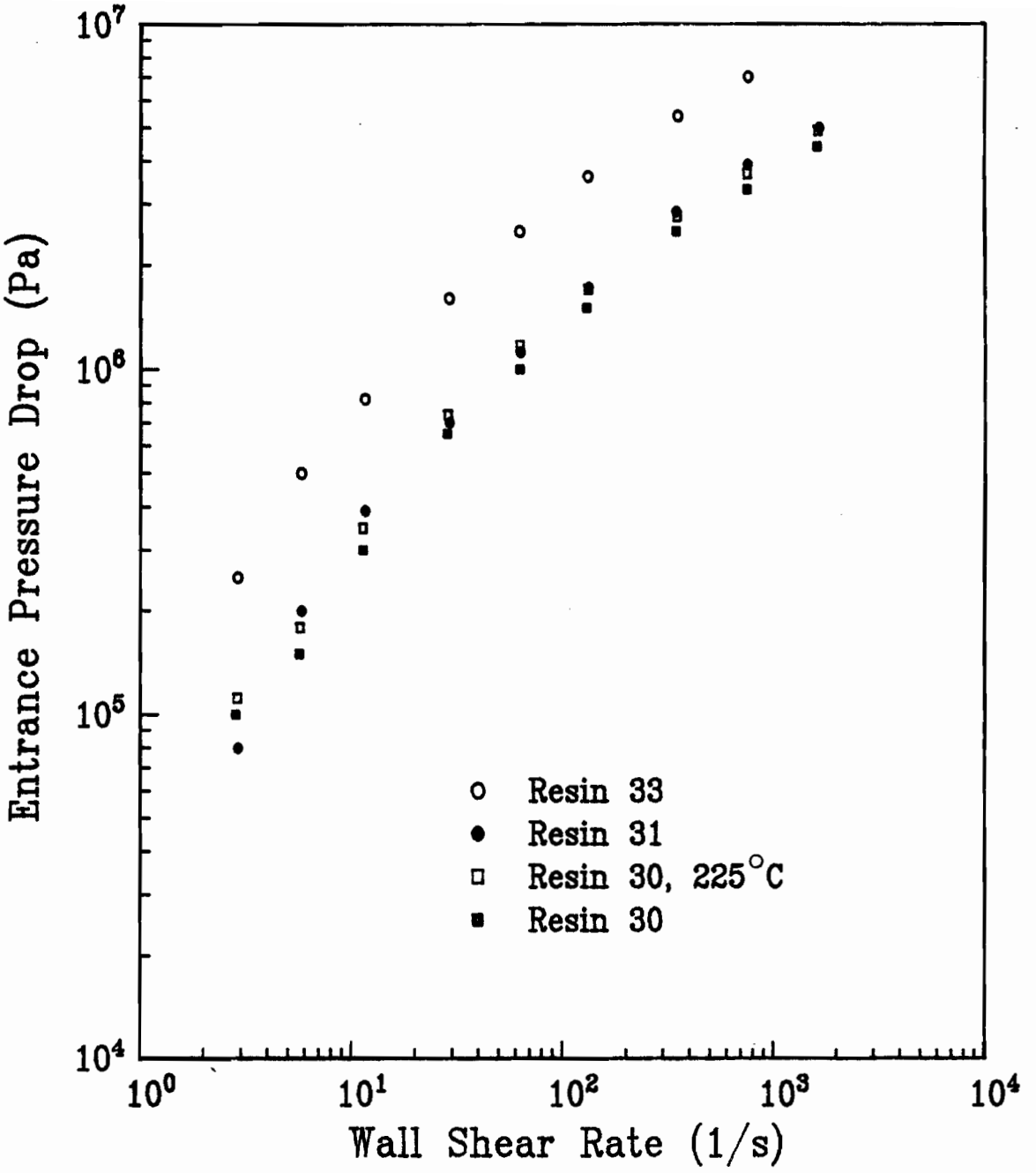

Figure 30: Entrance pressure drop, ΔP_e, as a function of wall shear rate, $\dot{\gamma}_w$, at 240°C.

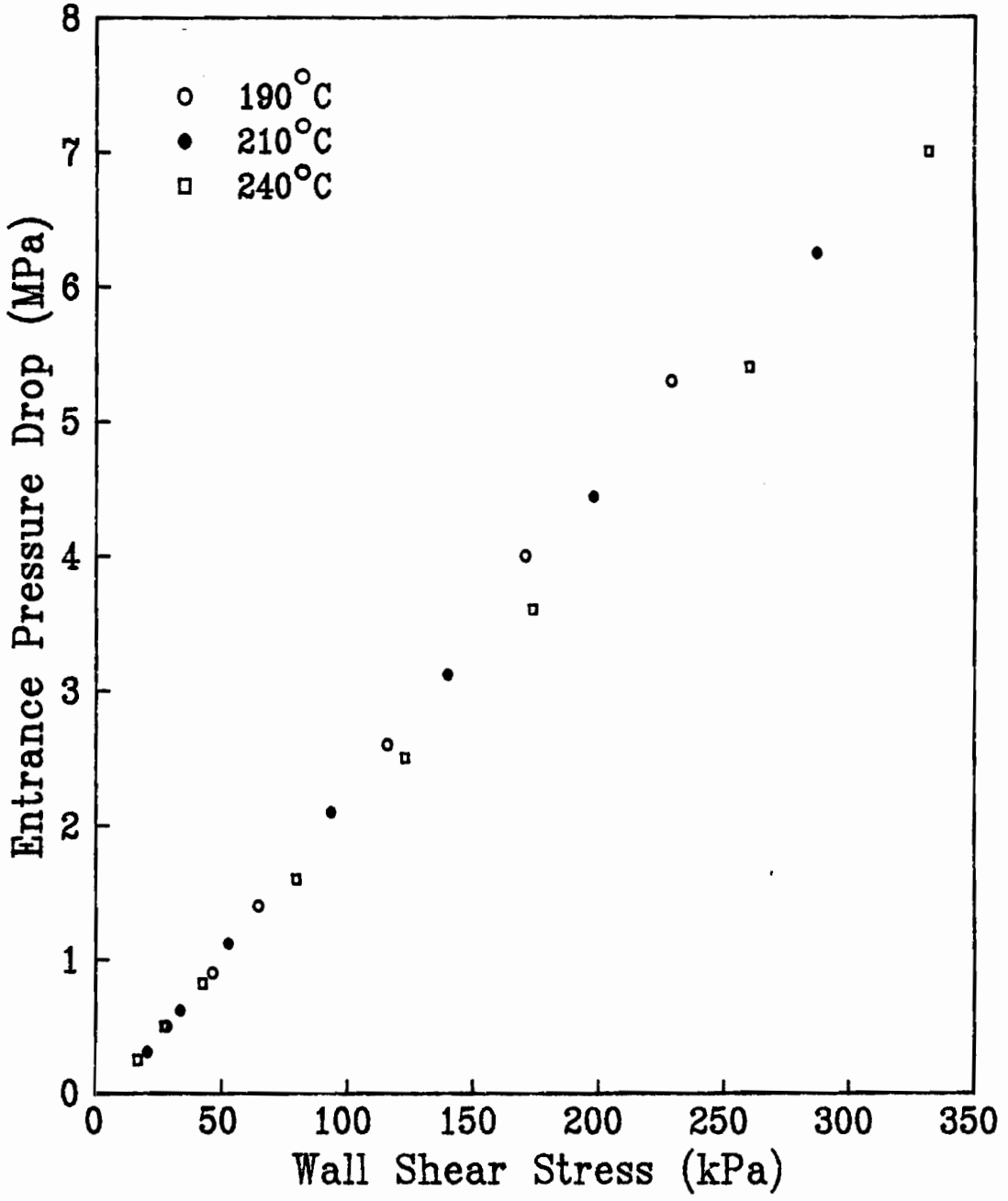

Figure 31: Entrance pressure drop, ΔP_e, as a function of wal shear stress, τ_w, for resin 33.

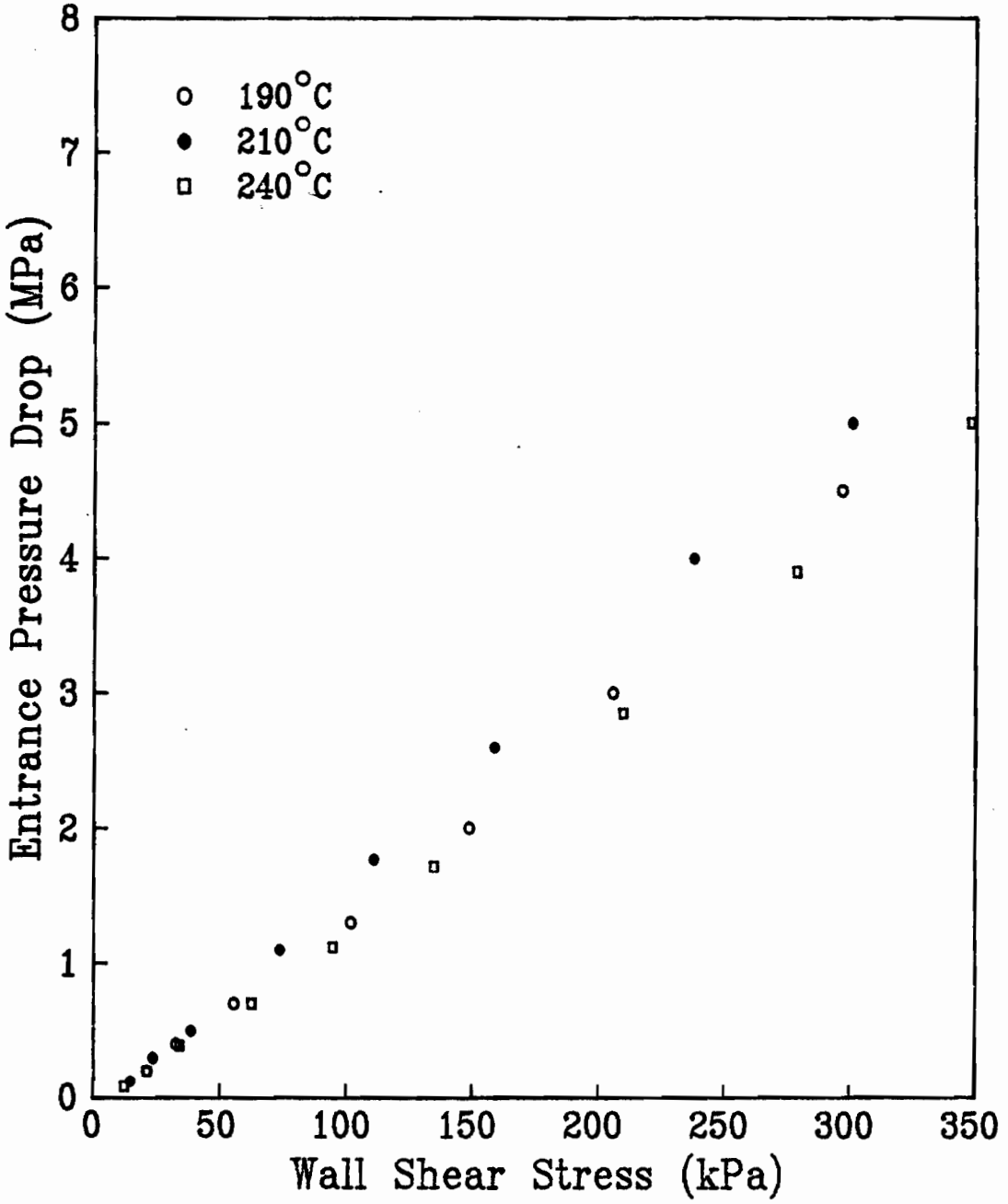

Figure 32: Entrance pressure drop, ΔP_e, as a function of wall shear stress, τ_w, for resin 31.

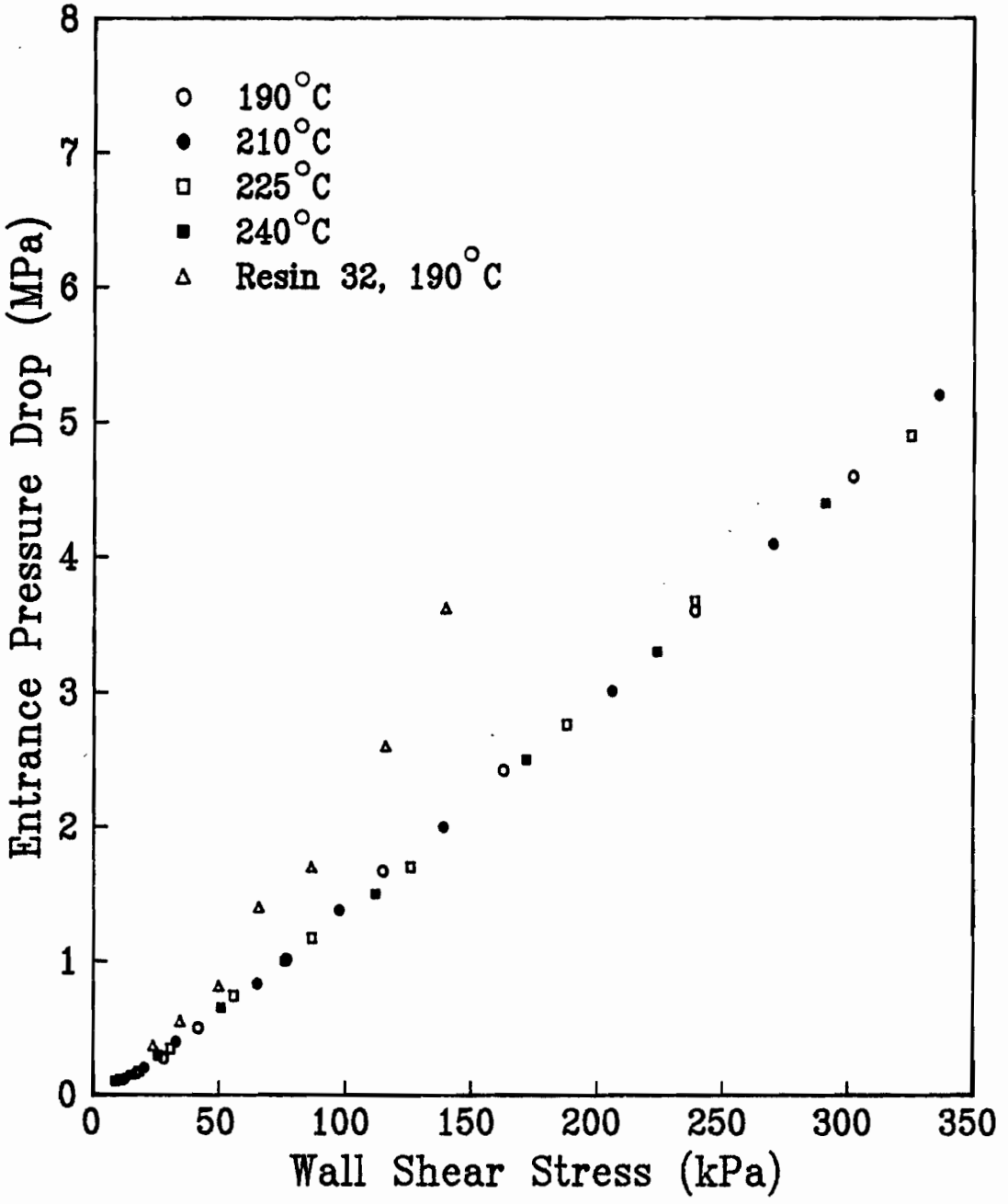

Figure 33: Entrance pressure drop, ΔP_e, as a function of wall shear stress, τ_w, for resins 30 and 32.

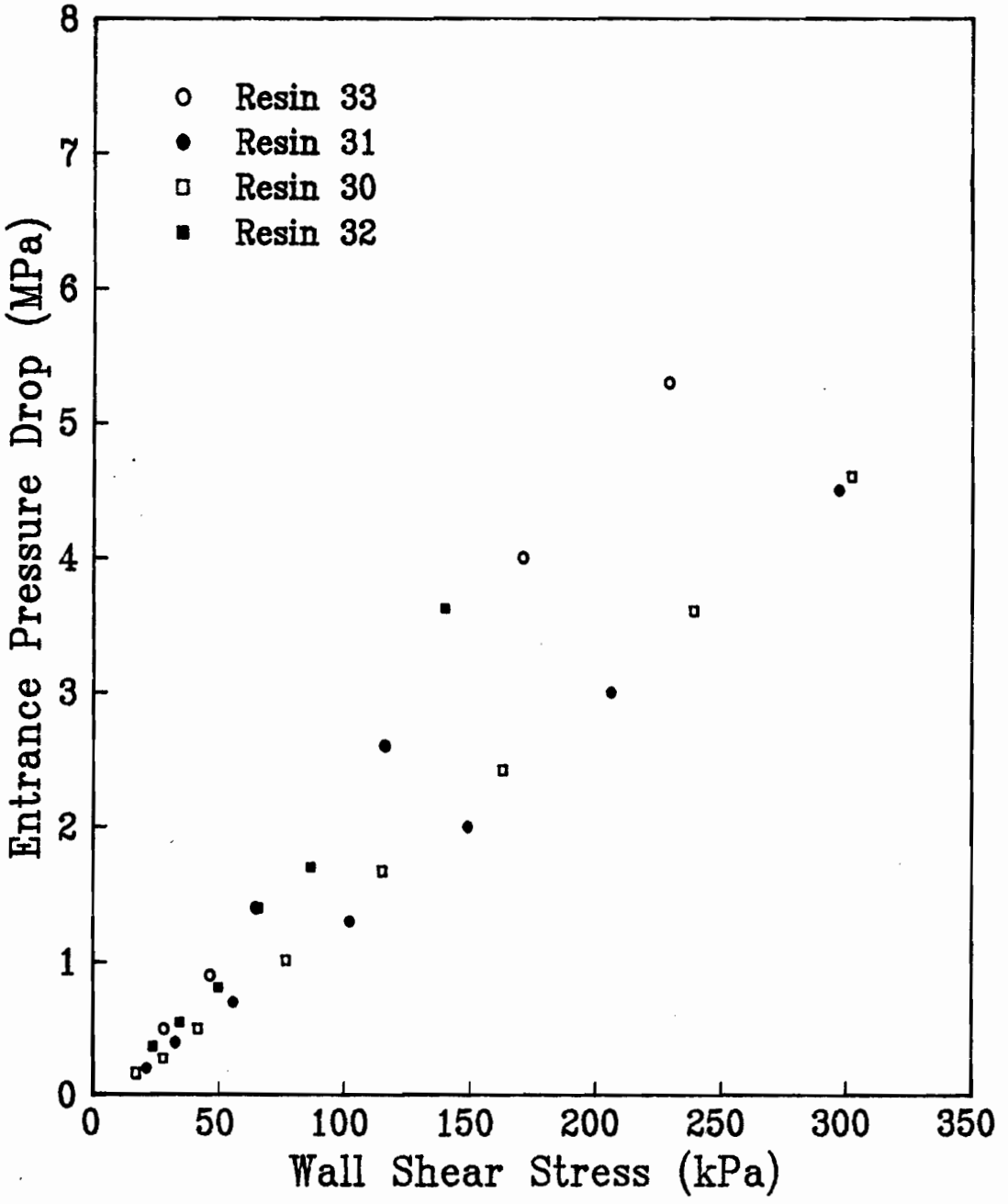

Figure 34: Entrance pressure drop, ΔP_e, as a function of wall shear stress, τ_w, for all four resins at 190°C.

in the experimental range covered, resins 32 and 33 have comparable entrance pressure drops with the former showing a more rapid increase with increasing shear stress. In addition, resins 31 and 30 also have comparable values at this temperature and have entrance pressure drops that do not increase as quickly with shear stress as do those of resins 32 and 33.

In calculating the value of the wall shear stress, the so called Bagley entrance correction must be determined (see Figure 27). As was discussed in the section of Chapter 3 entitled "Capillary Flow" this entrance correction represents the length of capillary that would be required to produce a pressure drop equivalent to the entry region pressure drop. In Figures 35-37 we find that all of the resins exhibit an increase in the magnitude of this term with increasing shear rate, and as expected, a decrease in its value with increasing temperature. Although the data are somewhat scattered, a few interesting trends are apparent. Most notable is the very high value of the entrance correction for resin 32 as compared to the LLDPE resins. If one were to look only at the value of the entrance correction term, it would appear that resin 32 is much more elastic than the most elastic of the copolymer resins (resin 33). In fact the larger value of the correction term is due both to the genuine elastic nature of the melt and its relatively low

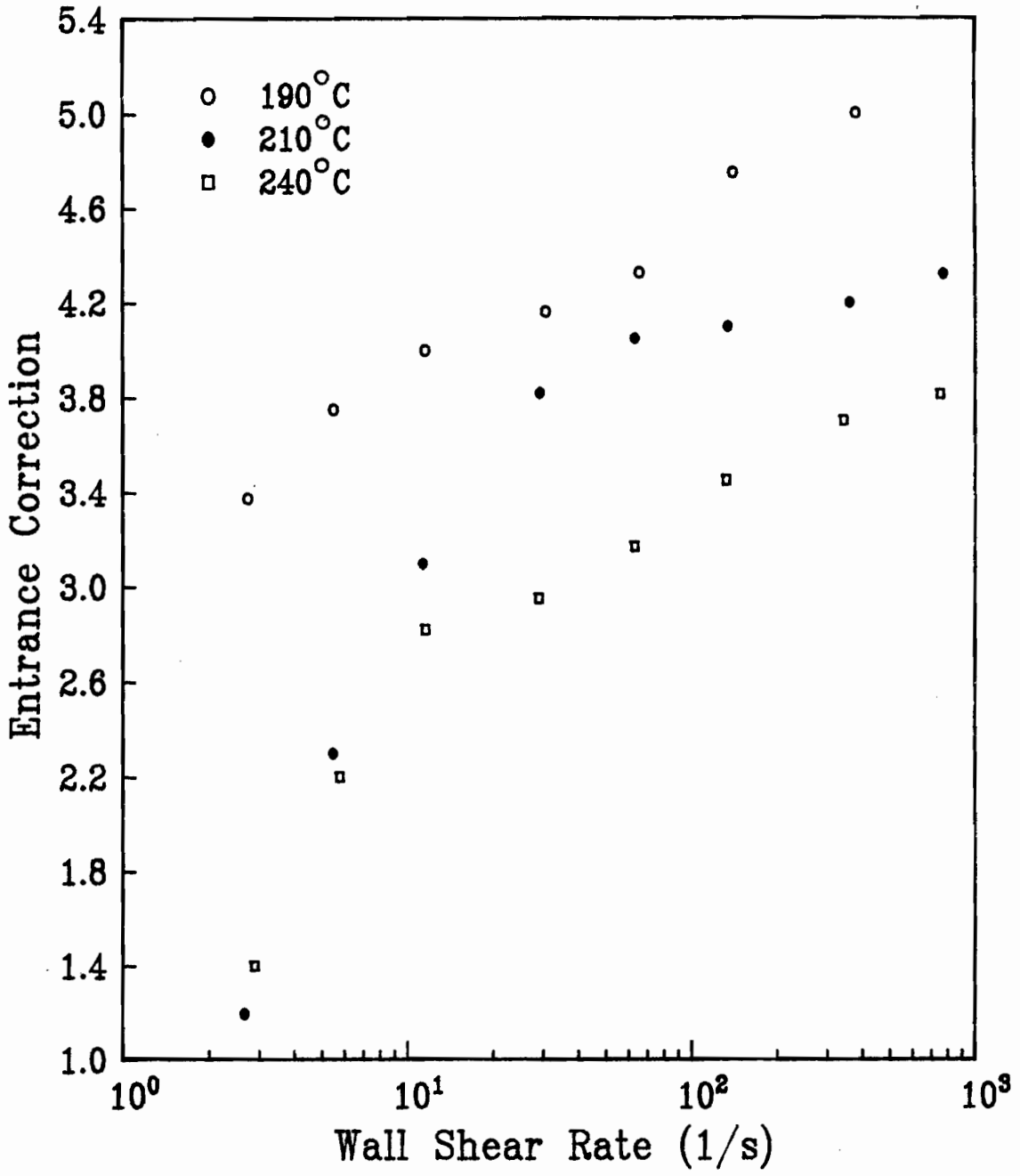

Figure 35: Bagley entrance correction as a function of wall shear rate for resin 31.

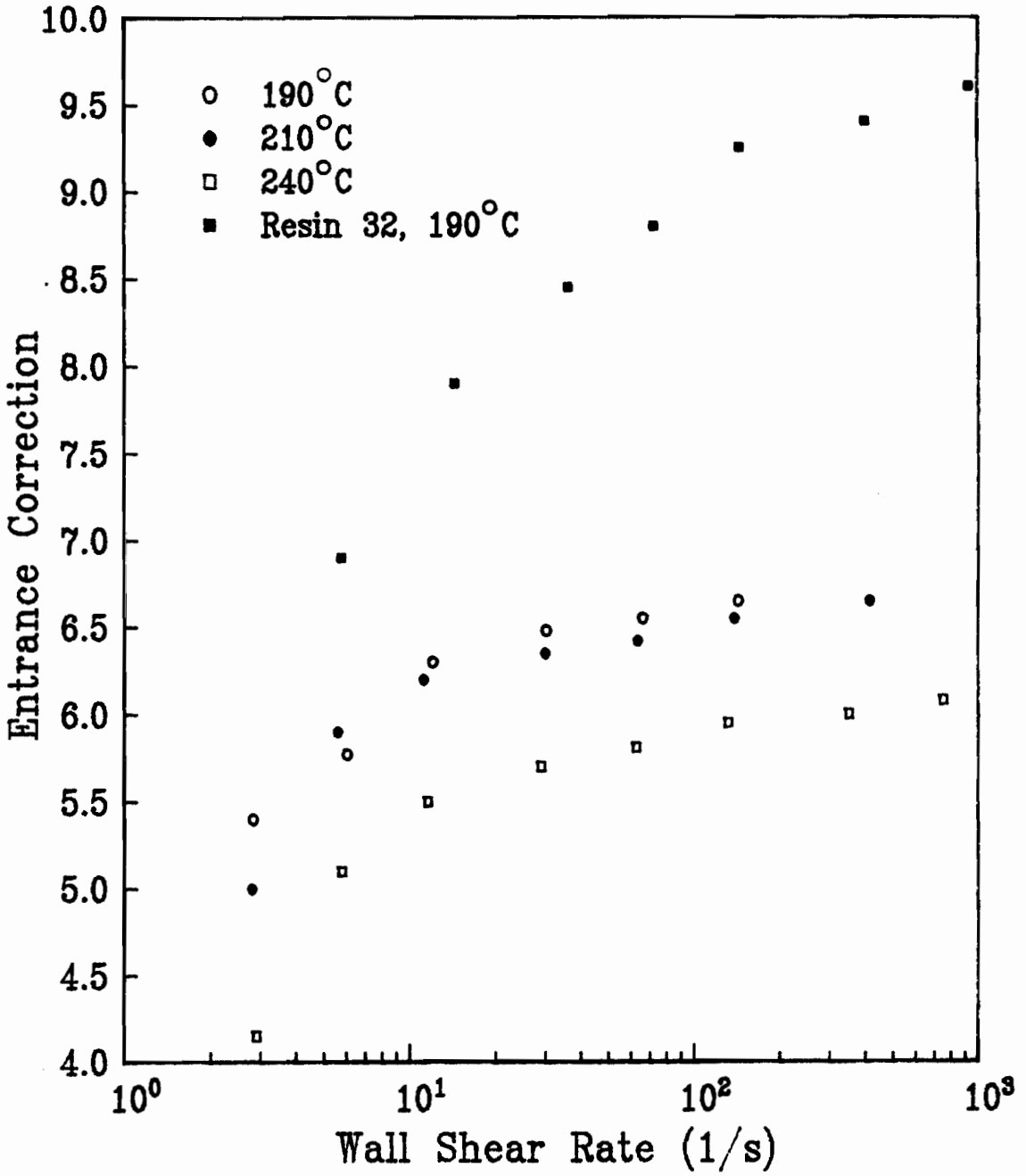

Figure 36: Bagley entrance correction as a function of wall shear rate for resins 32 and 33.

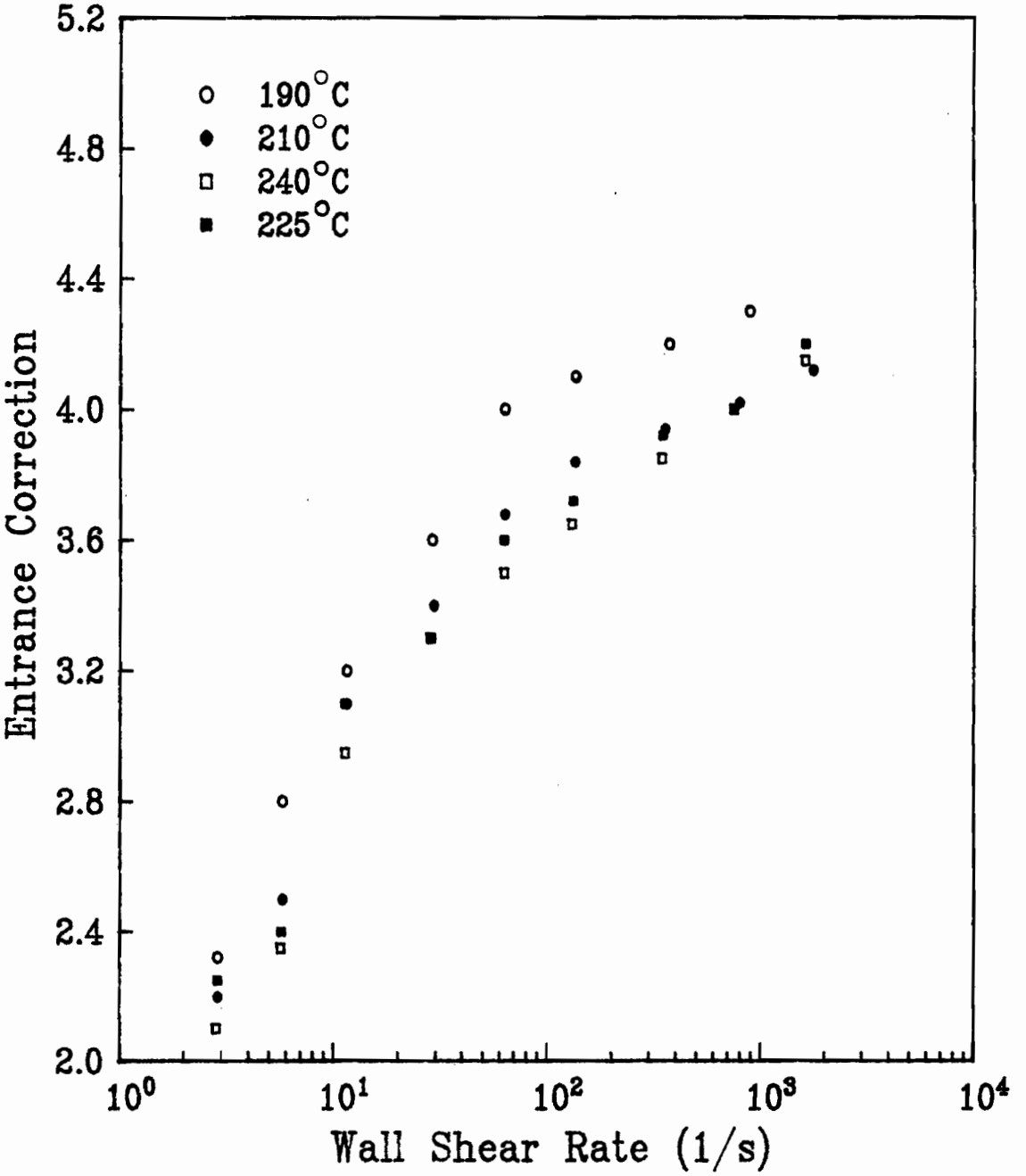

Figure 37: Bagley entrance correction of a function of wall shear rate for resin 30.

viscosity at a given shear rate in comparison to LLDPE resins. This is especially true in the case of resin 33. In general, the trends evident in the entrance pressure loss data of the LLDPE resins apply, with resin 33 exhibiting the largest values of the entrance correction followed by resins 31 and 30.

In the course of this study, viscosity data were obtained using a capillary of L/D=40, thus even if the entrance correction length values are in error by as much as 10%, the error introduced in equation (60) when calculating the value of the wall shear stress will be at most 2% for the case of resin 32 and 1.5% for resin 33.

$$\tau_w = \Delta P_{Total} / 4\left(\frac{L}{D} + e\right) \qquad (60)$$

Cogswell [125,126] suggested that an estimate of a polymer's extensional viscosity can be obtained from a knowledge of the entrance pressure drop. Cogswell assumed that the entrance pressure drop, ΔP_e, can be represented as a sum of two terms, one related to shear and the second to extension. He further assumed that the fluid follows streamlines that result in the minimum pressure drop. Shroff [142] modified Cogswell's analysis by using the true value of the wall shear rate in Cogswell's equations rather than the apparent (Newtonian fluid) value. The equations used are given below.

$$\sigma_e = \frac{3}{8}(n+1)\,\Delta P_e \qquad (61)$$

$$\dot{\epsilon}_e = \frac{4\eta(\dot{\gamma}_w)\,\dot{\gamma}_w^2}{3(n+1)\,\Delta P_e} \qquad (62)$$

These equations only apply in the power law region of the viscosity curve. Equation (61) gives a value of the average extensional stress, σ_e, and equation (62) gives the value of the average strain rate, $\dot{\epsilon}_e$. The ratio of the two gives an "apparent" extensional viscosity,

$$\eta_e = \sigma_e / \dot{\epsilon}_e \qquad (63)$$

In these equations n is the value of the power law index. The resulting curves of η_e as a function of $\dot{\epsilon}_e$ are shown in Figures 38-40. However, this procedure is immediately suspect since it indicates that resin 32 has the lowest extensional viscosity of the resins studied. It has been well established that LLDPE resins have lower extensional viscosities than LDPE resins [120,123,128]. In addition, Meissner [143] found (for LDPE) that the extensional viscosity increased with the extensional strain rate rather than decreasing, as shown in Figure 38. Similar behavior was observed by Utracki et al. [101], who observed that at high strain rates ($\dot{\epsilon} > .5\ s^{-1}$) the extensional stress exhibited unbounded growth until sample breakage occurred. Han et al. [144] measured the extensional viscosity of an LDPE using a fibre spinning technique [30] and found it to be independent

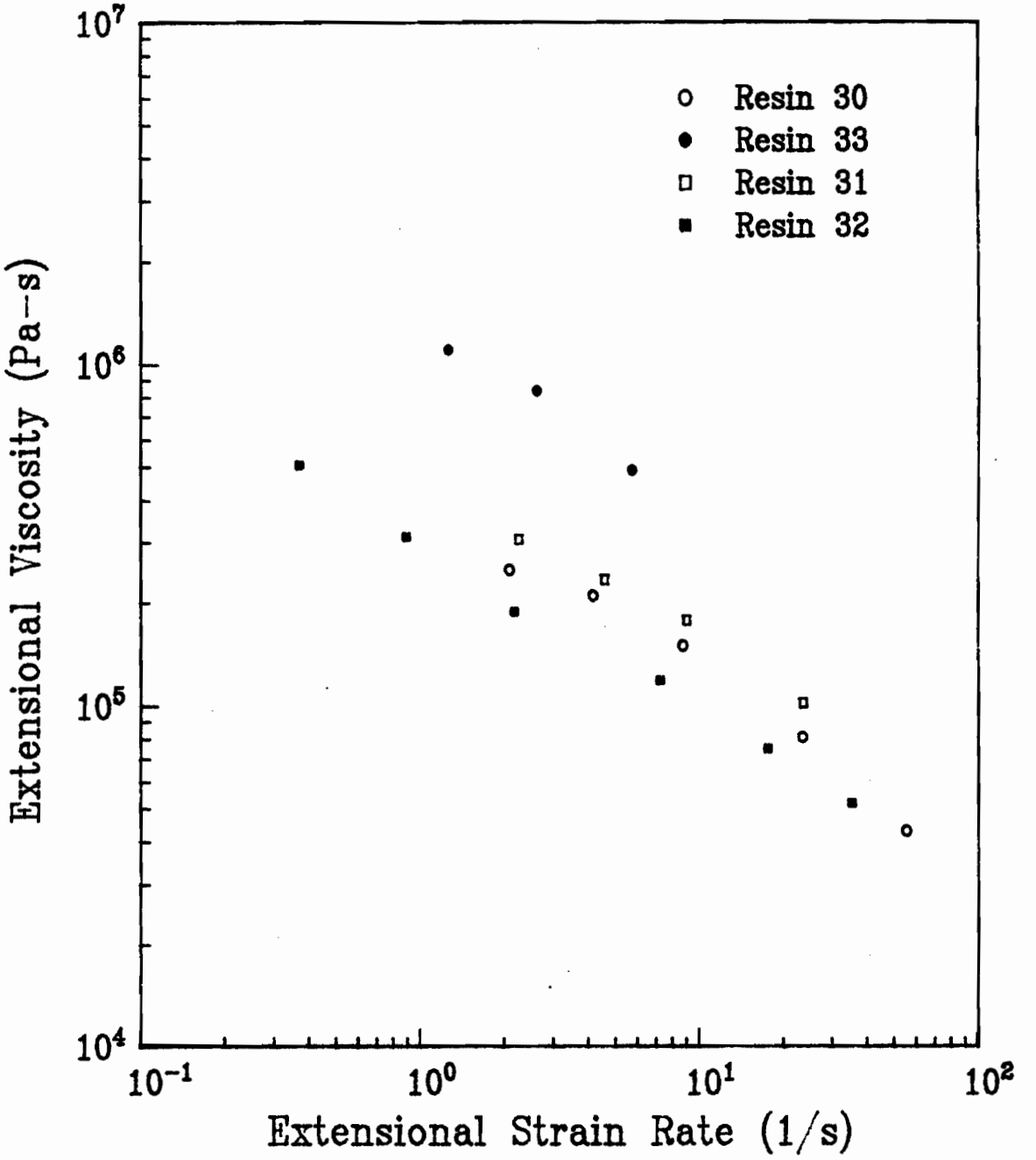

Figure 38: Estimation of the extensional viscosities, η_e, from the method of Shroff (142) at 190°C.

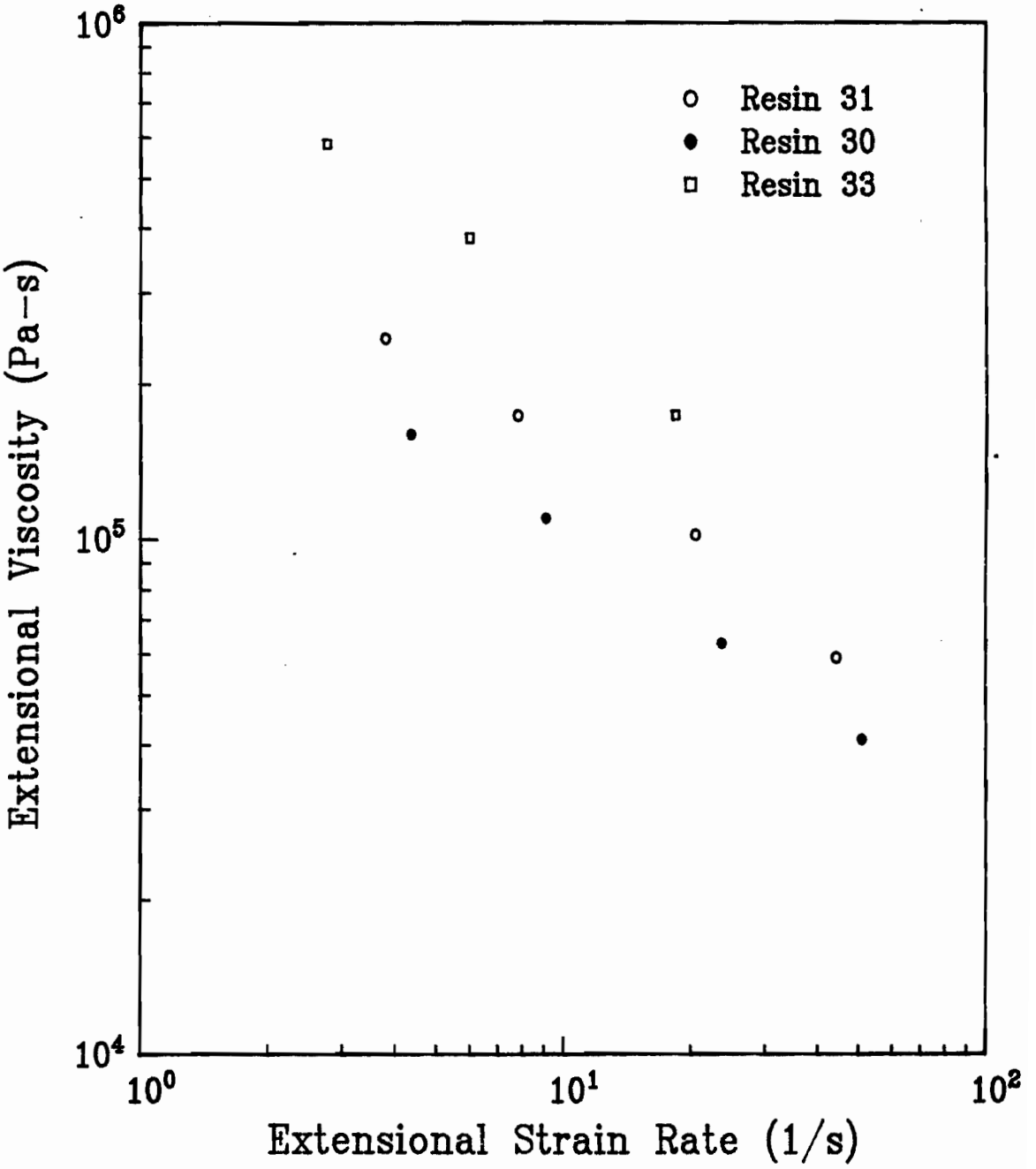

Figure 39: Estimation of the extensional viscosity, η_e, from the method of Shroff (142) at 210°C.

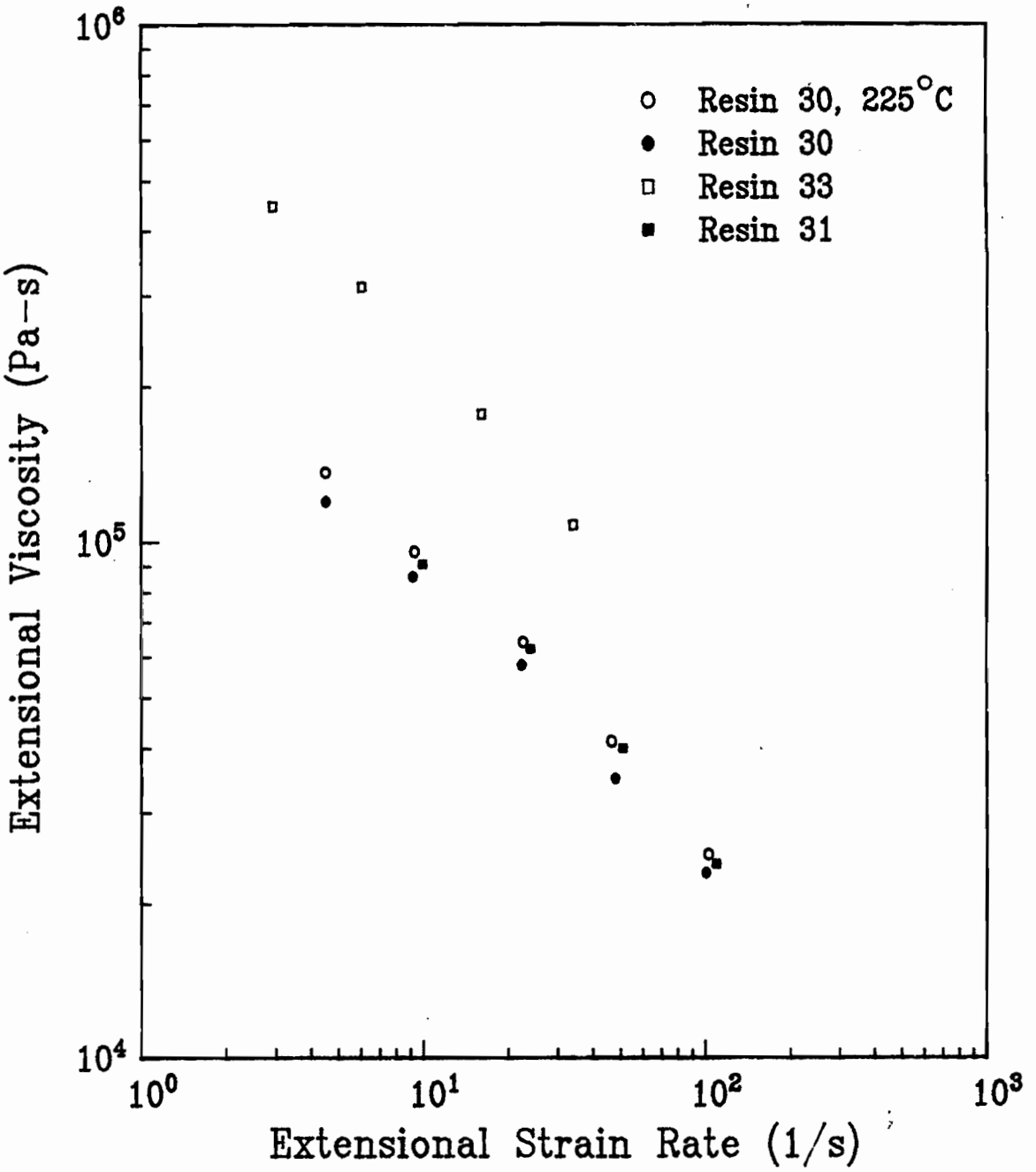

Figure 40: Estimation of the extensional viscosities, η_e, from the method of Shroff (142) at 240°C.

of the extensional strain rate. Conversely, linear HDPE was found to have an extensional viscosity that was a decreasing function of strain rate. Kwack et al. [128] observed similar behavior for LLDPE resins. The anomalous results for resin 32 obtained using equations (61) and (62) may be due to the peculiar recirculating entrance flow patterns that are characteristic of branched polyethylenes [35]. One would expect that as a result of this complex recirculating flow field, the assumption made in deriving equations (61) and (62) that stipulates that the fluid follows streamlines giving the minimum pressure drop is probably invalid. Indeed, in their paper discussing this estimation technique, Shroff et al. [142] also found that for the LDPE they studied this method erroneously predicted its extensional viscosity to decrease with strain rate.

Thus the results obtained for the LLDPE resins seem to be in at least qualitative agreement with those obtained for similar materials using more rigorous extensional rheometric techniques. The results presented in Figures 38-40 indicate that resin 33 has the highest extensional viscosity of the LLDPE's followed by resin 31 and then 30. These results appear to be contradictory to those of Kalyon and Moy [119] who found that the extensional viscosity of LLDPE increases with the carbon number of the comonomer-that is, a resin with a 1-octene comonomer would have a higher extensional

viscosity than one containing a 1-butene comonomer. In contrast, Kwack's results are in qualitative agreement with ours, finding that resins with shorter comonomers have higher extensional viscosities. However, these results may be fortuitous, since it is generally conceded that the comonomer branches play a minor role in determining LLDPE melt rheology [7].

It should be noted that the entry pressure drop data presented are extremely sensitive to the entrance geometry of the system from which they are obtained and are of use only for comparing the behavior of resins tested in a system with identical entrance geometry.

5.3 Oscillatory Shear Results

5.3.1 Storage and Loss Moduli

Prior to making measurements of these materials linear viscoelastic properties, strain sweeps were carried out to determine at what strain amplitudes the storage modului of these materials began to show a dependance on the strain amplitude. In Figure 41 plots of storage modulus vs strain amplitude are presented for the four resins. For the three LLDPE resins the strain amplitude dependance of the storage

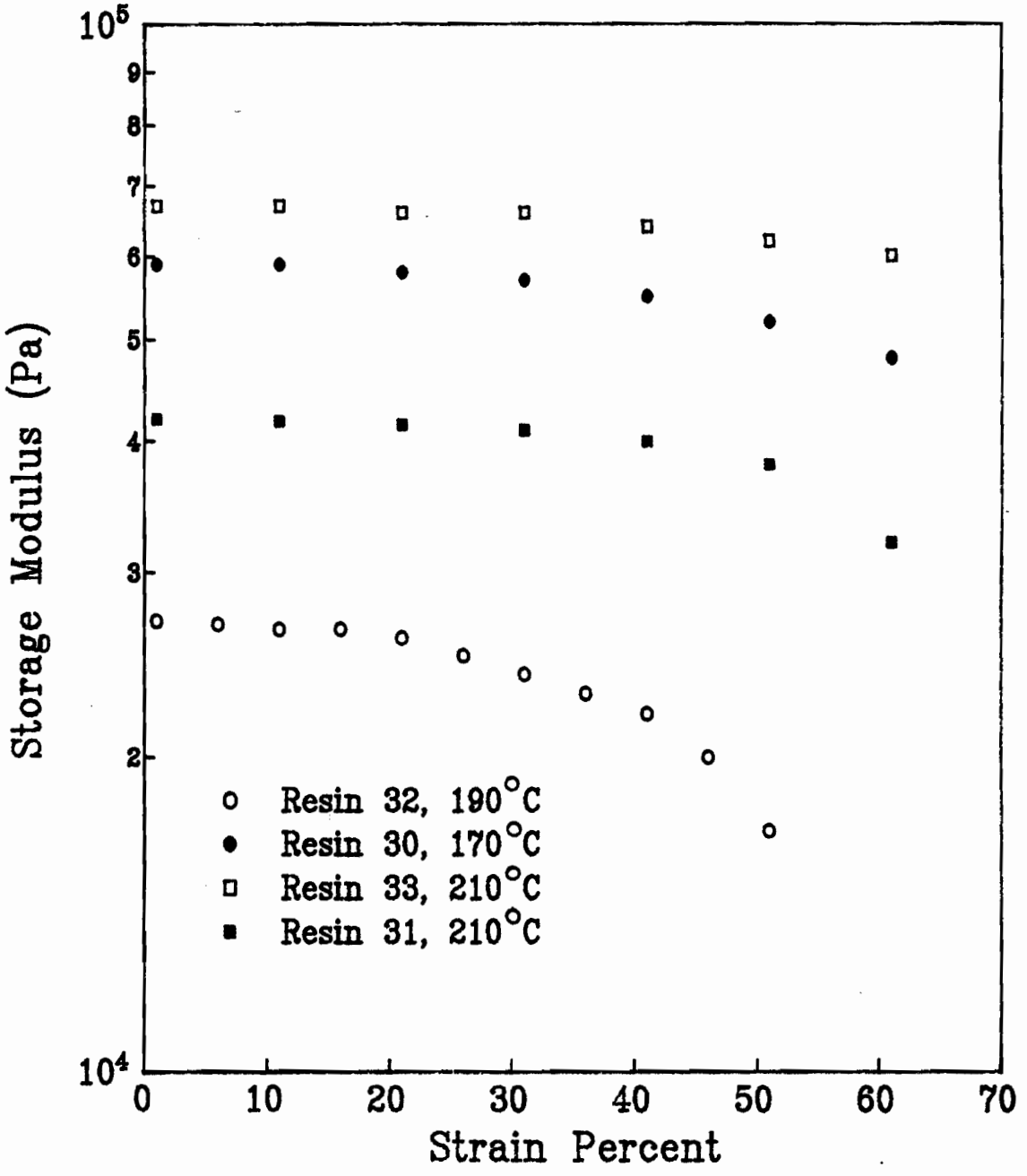

Figure 41: Strain amplitude dependence of linear viscoelastic properties.

modulus was first observed at strain amplitudes of about 25%. For the LDPE resin a strain amplitude dependance is apparent at an amplitude of about 15%. Thus, in all oscillatory shear experiments with the LLDPE resins, strain amplitudes of 10% were used, while for the LDPE resin a strain amplitude of 5% was used.

In Figures 42-44 the storage modulus data for the four resins are presented. In all cases the magnitude of the storage modulus increases with increasing frequency indicating that the materials are behaving more and more elastically. Furthermore as the temperature increases the value of the storage modulus decreases. Amongst the three LLDPE resins, resin 33 had the highest value of the storage modulus, followed by resins 31 and 30, indicating that resin 33 is the most elastic of the three. This trend was observed at all temperatures. At the higher frequencies the differences between the storage moduli of the LLDPE resins become somewhat less pronounced, particularly between resins 33 and 31. The behavior of resin 32 is markedly different from that of either of the other three resins. At low frequencies it is more elastic than the LLDPE resins while being less elastic at the higher frequencies. This difference in behavior between LLDPE and LDPE has also been observed by Huang and Campbell [145]. In the very slow deformation rate region where the first normal stress

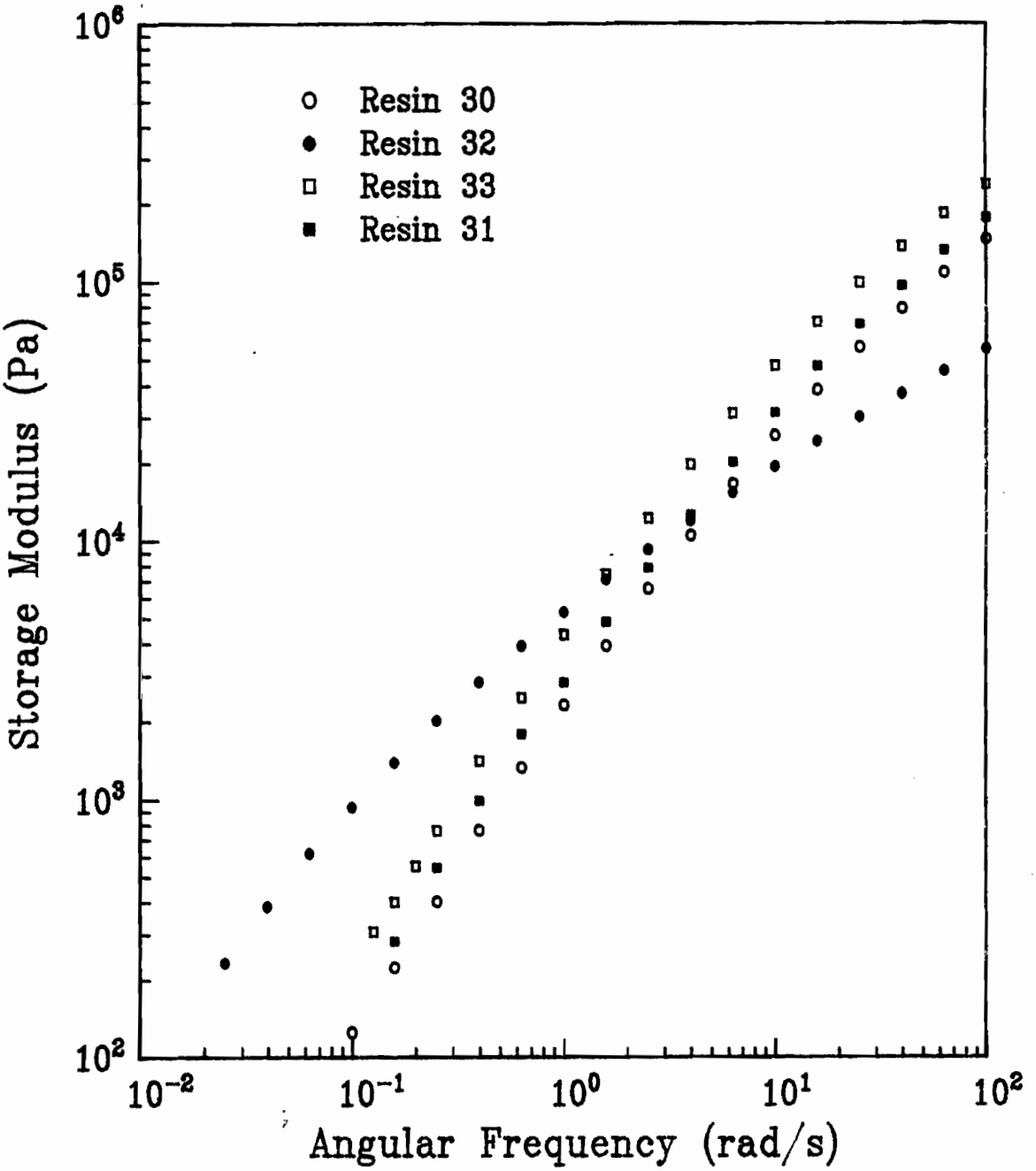

Figure 42: Storage modulus as a function of angular frequency at 190°C.

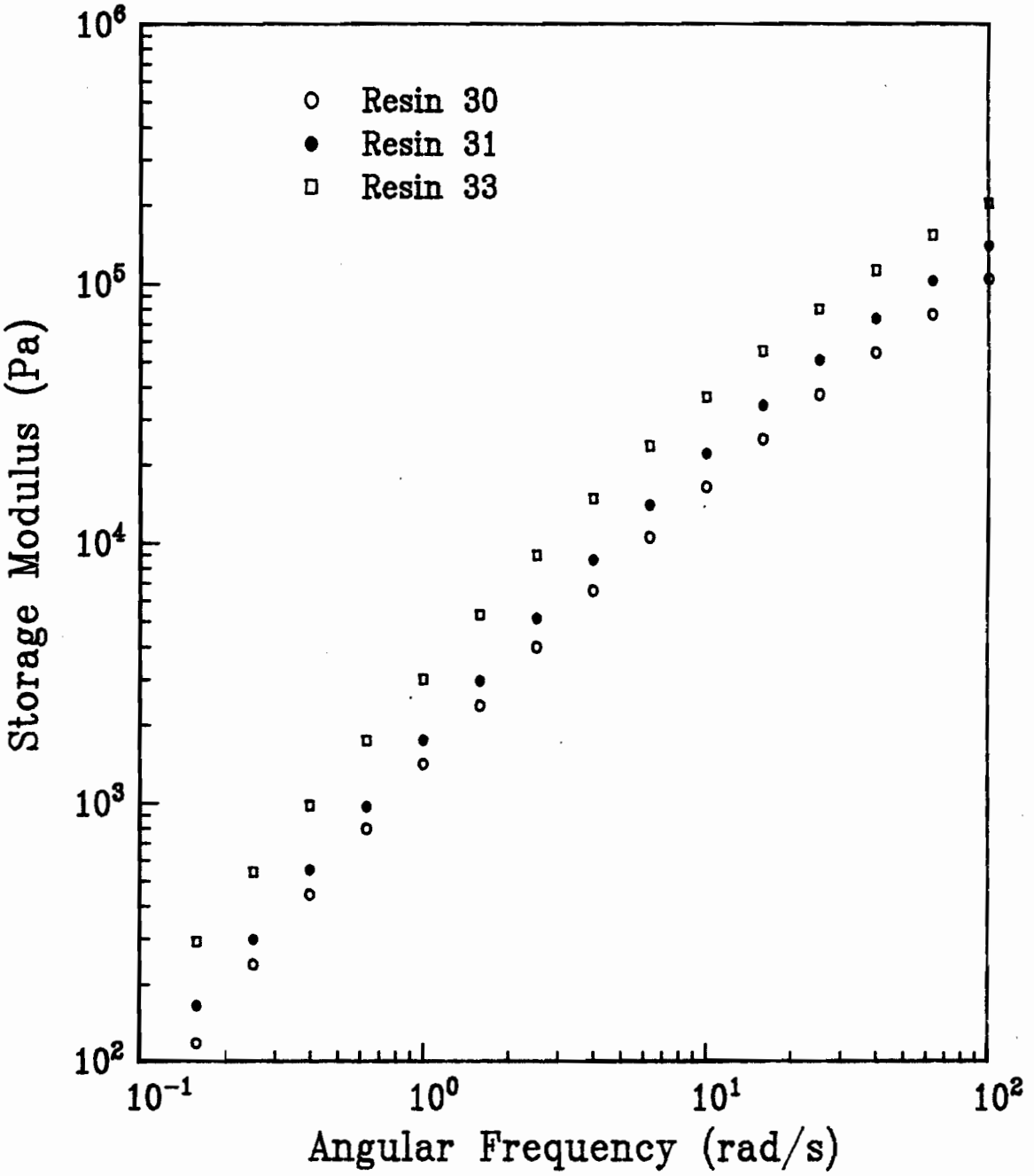

Figure 43: Storage modulus as a function of angular frequency at 210°C.

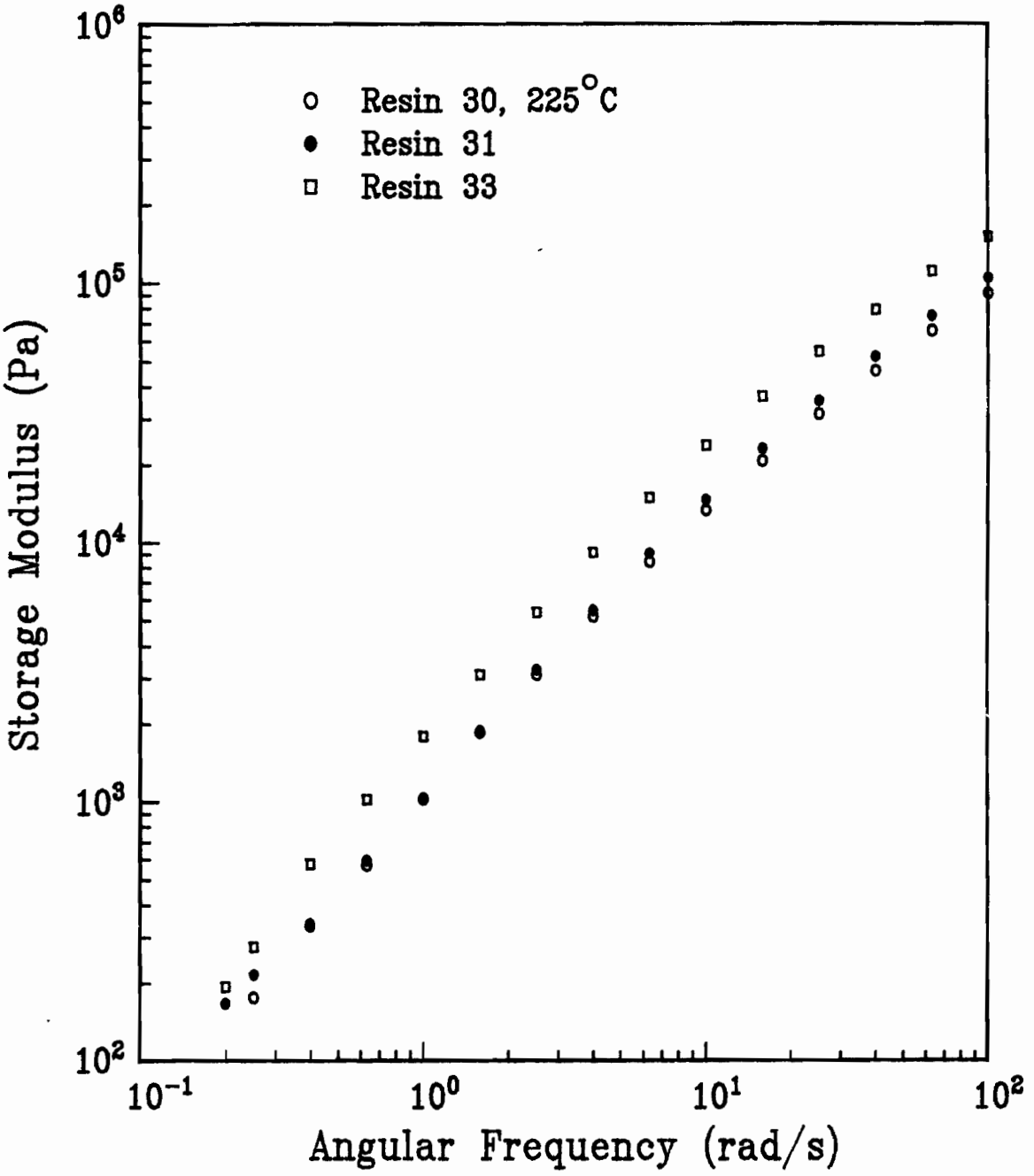

Figure 44: Storage modulus as a function of angular frequency at 240°C.

difference is proportional to the square of the shear rate the following behavior should be observed.

$$\lim_{\omega \to 0} \left(\frac{2G'}{\omega^2} \right) = \text{constant} \qquad (64)$$

This result implies that a plot of log G' versus log ω should approach a straight line with a slope of two at sufficiently low frequencies [39]. However, such behavior may not be observed at the lowest frequencies at which reliable measurements can be made. This is especially true of polymers having a broad molecular weight distribution [25]. Although this limit was not attained by any of the resins tested, the LLDPE resins approached it more closely than did the LDPE resin (32). At 190 ^{o}C at a frequency of about 0.15 rads/s, the LLDPE resin curves had slopes ranging between 1.28 and 1.1, while at the same frequency the curve of the resin 32 data had a slope of only about .8. The fact that the LLDPE resins approach the theoretical limit at higher frequencies than does the LDPE indicates that they have shorter relaxation times [131]. At very high frequencies elastic liquids will exhibit a storage modulus that is constant, the fluid acting like a perfectly elastic solid, which indicates that the fluid is being deformed so rapidly that there is not enough time for the molecules to rearrange themselves, thus allowing the stresses to relax before another deformation occurs. In light of this, one would

expect that a material with longer relaxation times would begin to exhibit a constant value of the storage modulus at a lower frequency than would a material with shorter relaxation times. At the higher frequencies, the storage modulus data for resin 32 can be seen to be leveling off while those of the LLDPE resins are still increasing quite rapidly. This further indicates that the LDPE resin has longer relaxation times than do the LLDPE resins. These longer relaxation times are due to the long disentanglement times of the long chain branches present in resin 32. This difference in relaxation times may be partially responsible for the fact that films blown from LLDPE tend to exhibit less shrinkage than LDPE films when subsequently reheated. Shrinkage is due to the molecular orientation imparted to the film when it is in the liquid state- below the bubble frost line. A material with shorter relaxation times would be expected to have less orientation remaining within it by the time it reaches the frost line.

The loss modulus data for these resins are plotted in Figures 45-47. As was the case for the storage modulus function, the LLDPE resins exhibit similar behavior of their loss moduli. Again, resin 33 has the largest values of this function at all frequencies and temperatures followed by resins 31 and 30, with the differences becoming less apparent at the higher frequencies. Resin 32 displays markedly

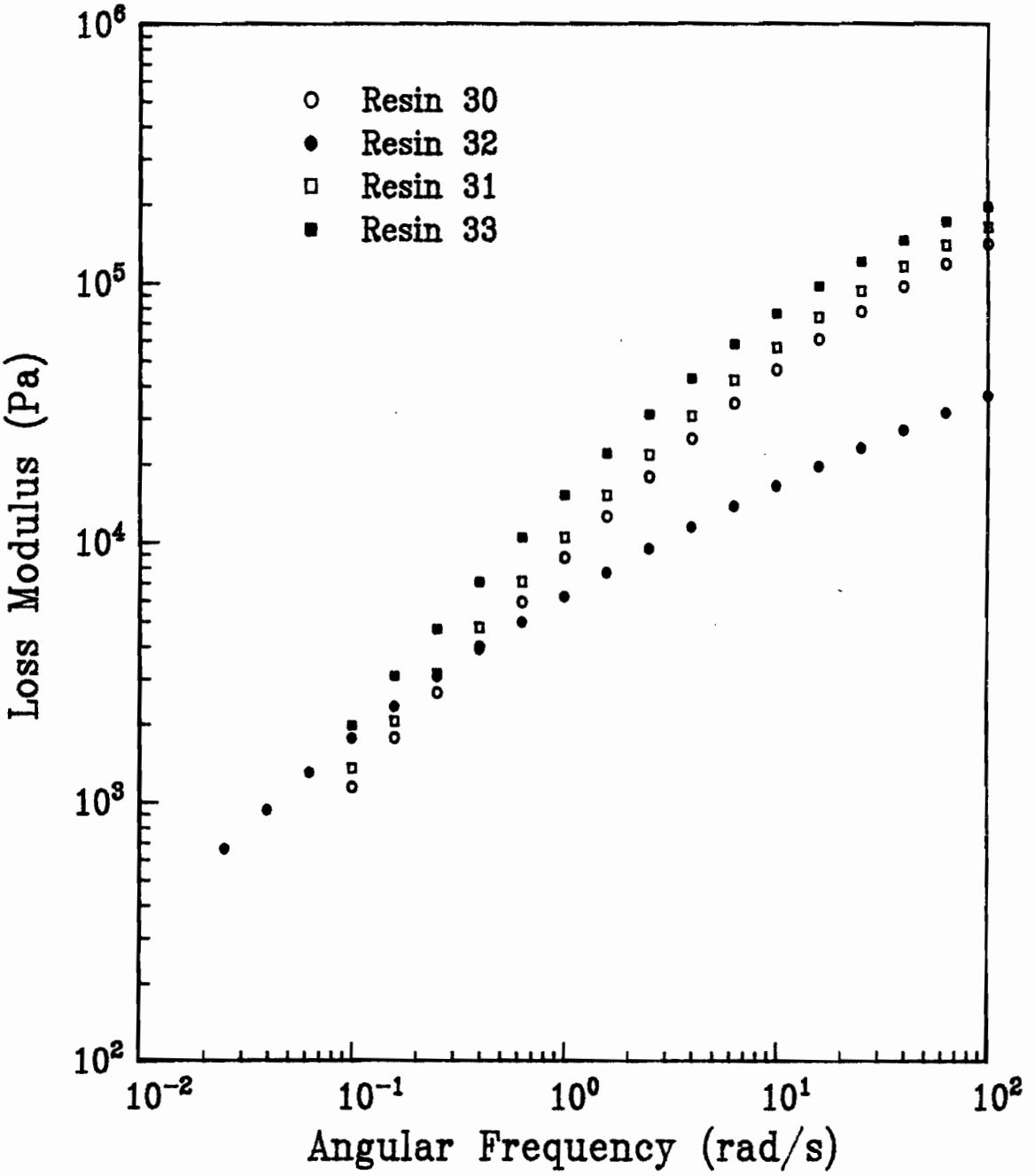

Figure 45: Loss modulus as a function of angular frequency at 190°C.

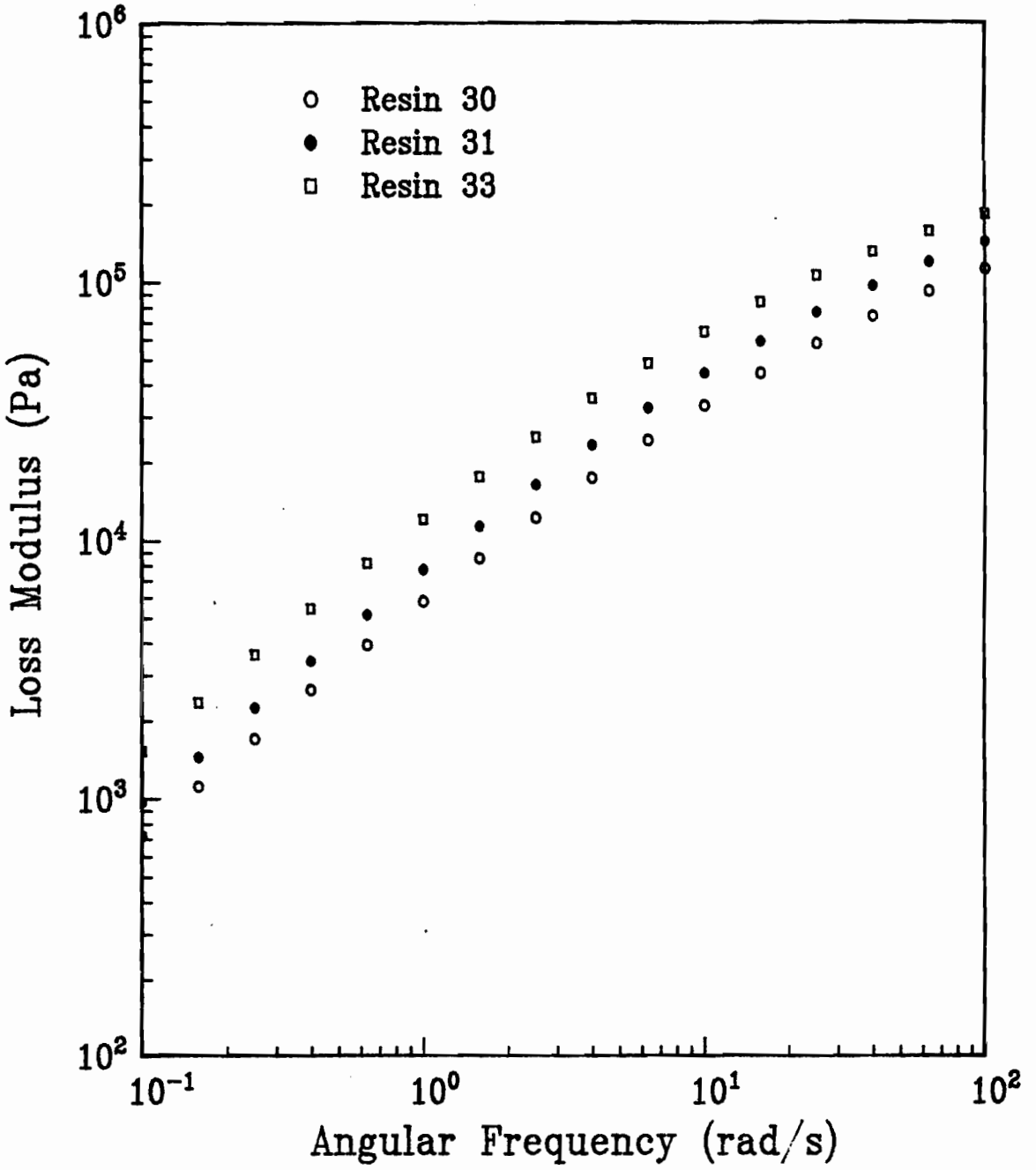

Figure 46: Loss modulus as a function of angular frequency at 210°C.

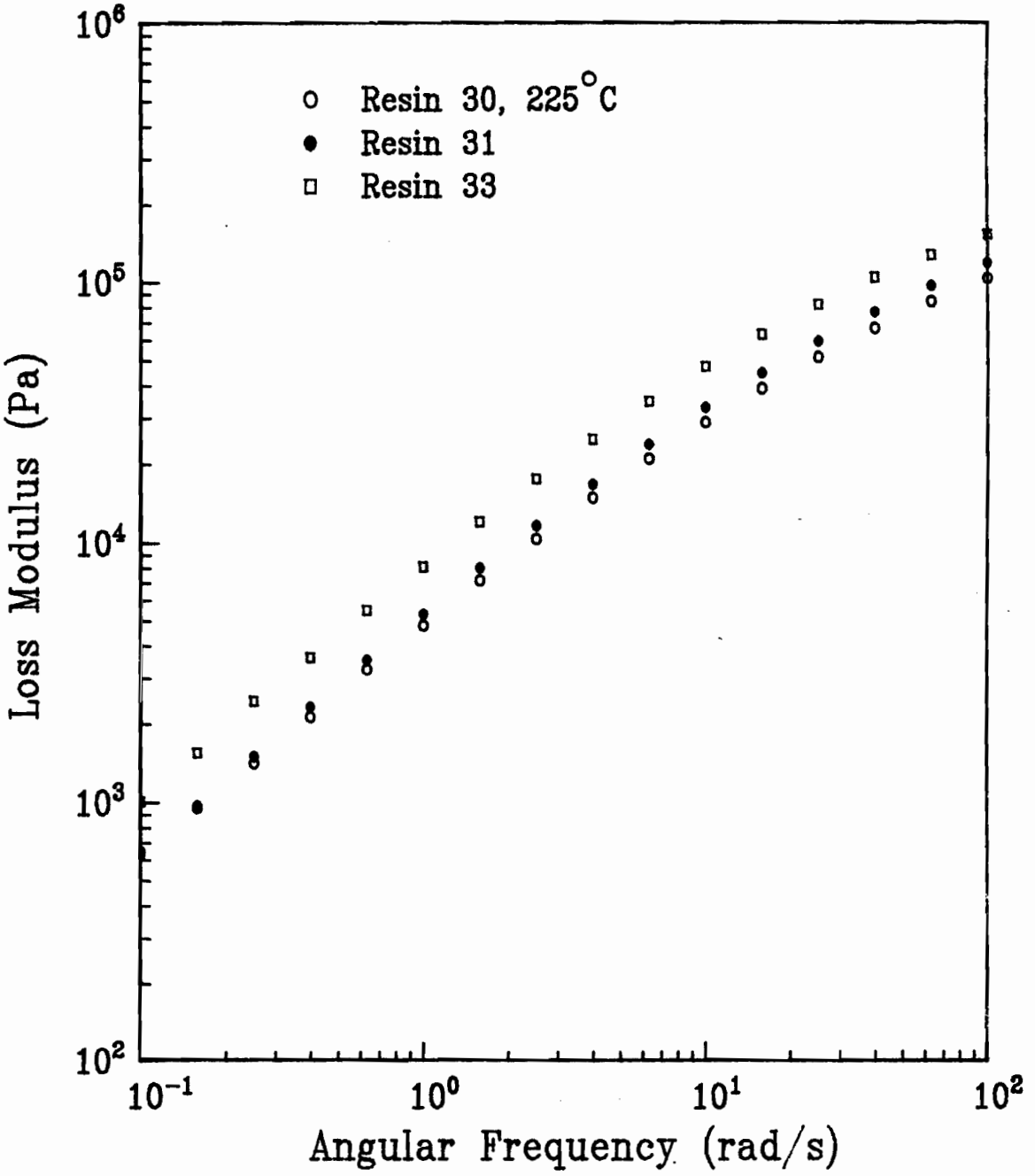

Figure 47: Loss modulus as a function of angular frequency at 240°C.

different behavior with a lower value of the loss modulus at high frequencies than the other resins and an apparently higher value at lower frequencies. Of interest are the relative magnitudes of the storage and loss moduli of a given material at a particular frequency. At frequencies low enough so that the flow is similar to steady shear, viscous dissipation of the stress is predominant, and the loss modulus is greater than the storage modulus. At higher frequencies where elasticity is predominant, the loss modulus has a lower value than the storage modulus.

5.3.2 Comparison With Steady Shear Data

Cox and Merz [146] first noted that at low shear rates and frequencies, in particular, the magnitude of the complex viscosity, $|\eta^*|$, is often equal to the shear viscosity, η , for equal values of the angular frequency, ω , and shear rate, $\dot{\gamma}$. The complex viscosity is defined below.

$$|\eta^*| = \left[(\eta')^2 + (\eta'')^2\right]^{1/2} \qquad (65)$$

In addition, theoretical work carried out by Coleman and Markovitz [147] predicts that at very low frequencies and shear rates the dynamic viscosity, η', also becomes equal to the shear viscosity. This result is not surprising since very low frequency, oscillatory shear subjects the liquid to essentially the same shear field as would a constant shear

rate experiment. The steady shear, dynamic and complex viscosities of the resins of this study are compared in Figures 48-57. For the LLDPE resins, the agreement between all three functions was generally quite good at the lower shear rates and frequencies. At the higher shear rates and frequencies, the dynamic viscosity gave consistantly better agreement with the shear viscosity than did the complex viscosity. The latter tends to have higher values than the shear viscosity. The opposite behavior was observed for resin 32, with better agreement between the complex and shear viscosities being observed at all shear rates and frequencies. In his work with LLDPE and LDPE resins, Utracki [129,148] reported similar behavior. These observations are of interest since they show that it is possible, in principle at least, to deduce the non-Newtonian viscous behavior of these materials from linear viscoelastic data.

5.3.3 Relaxation Spectra

The concept of a continuous relaxation spectrum presupposes a mechanical analog to a viscoelastic liquid comprised of an infinite number of Maxwell elements (dashpot and spring in series) placed in parallel. The equation describing the stress response of a single Maxwell element is given below.

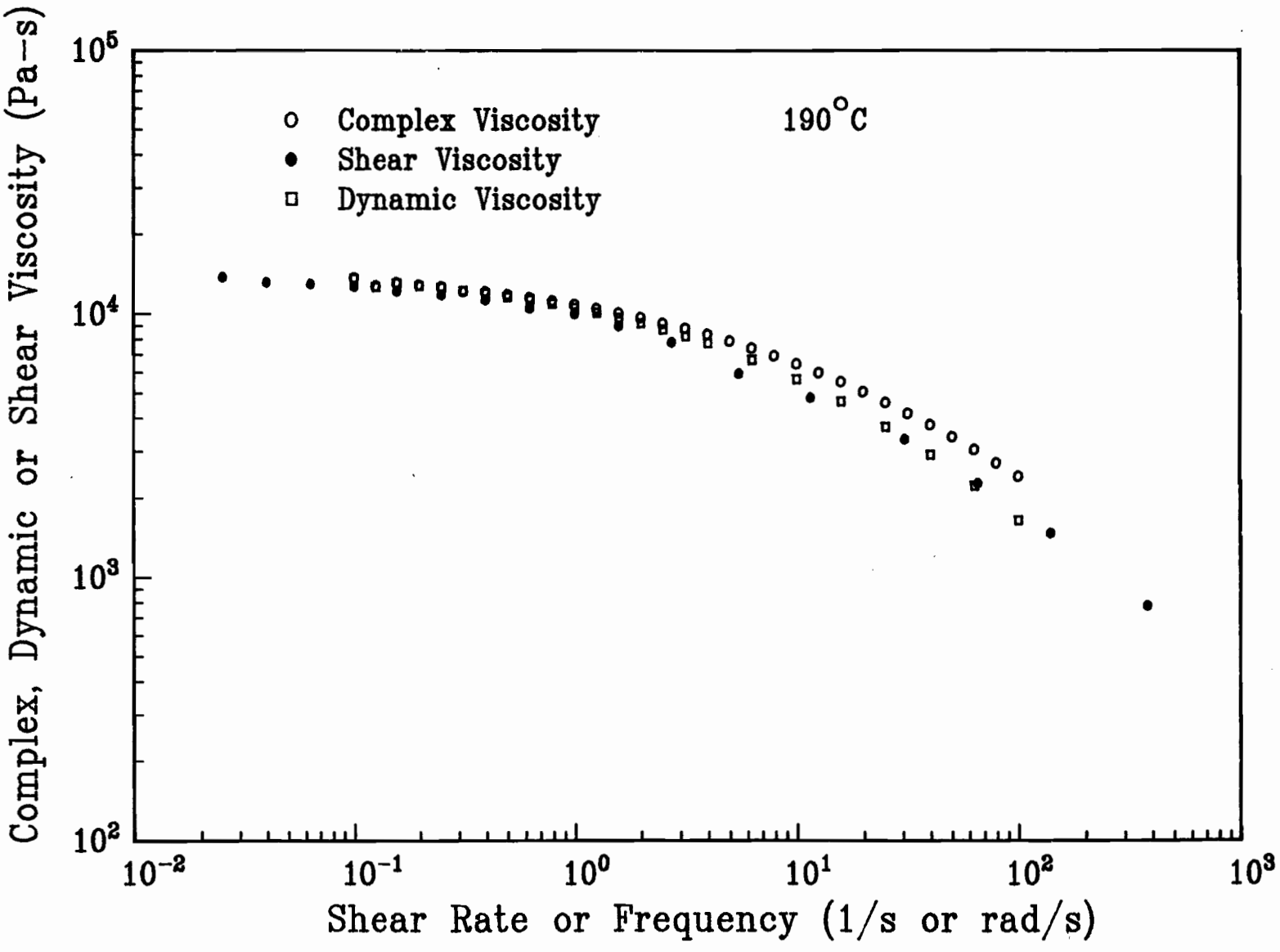

Figure 48: Comparison of shear, dynamic and complex viscosities for resin 31 at 190°C.

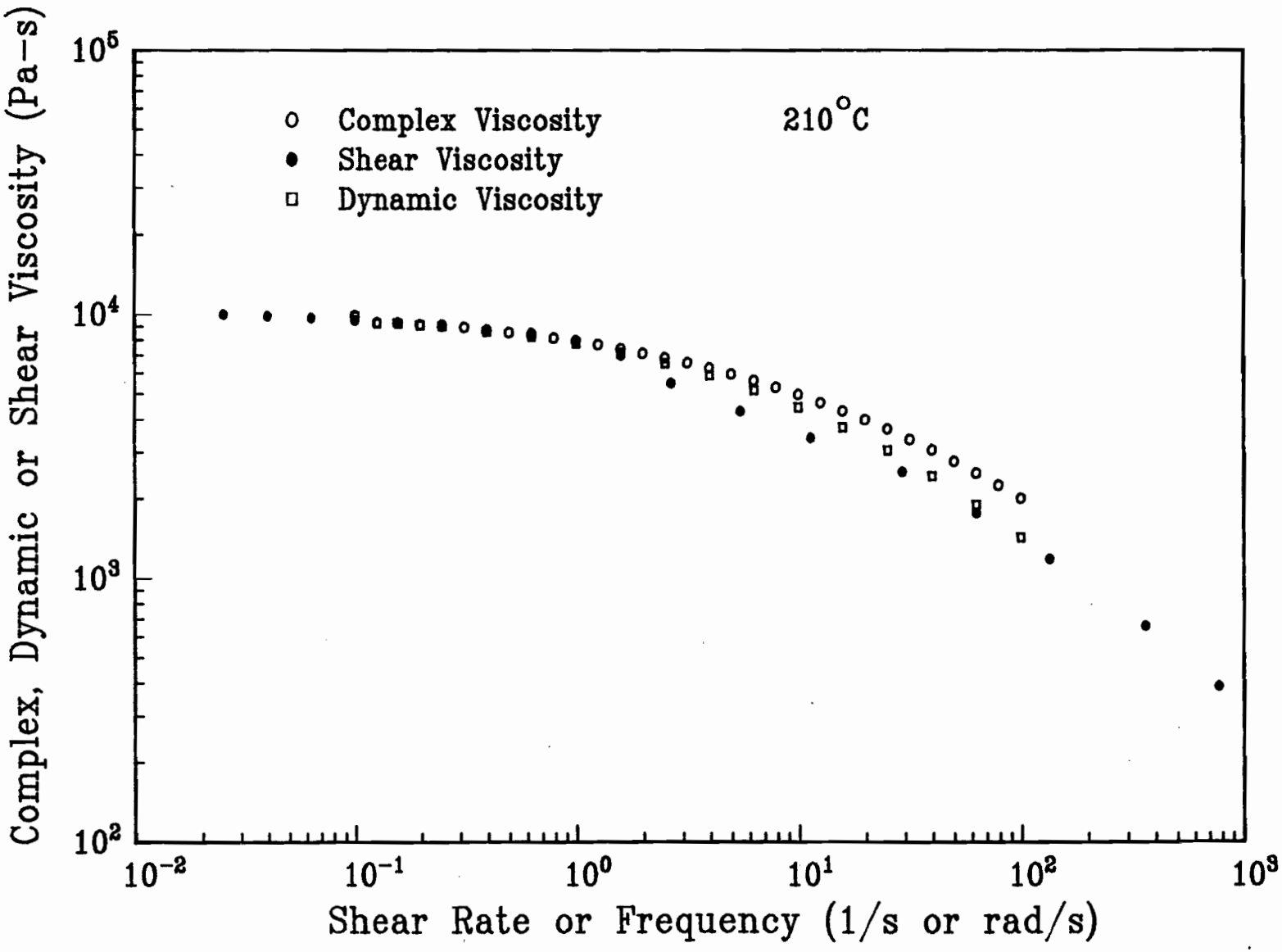

Figure 49: Comparison of shear, dynamic and complex viscosities for resin 31 at 210°C.

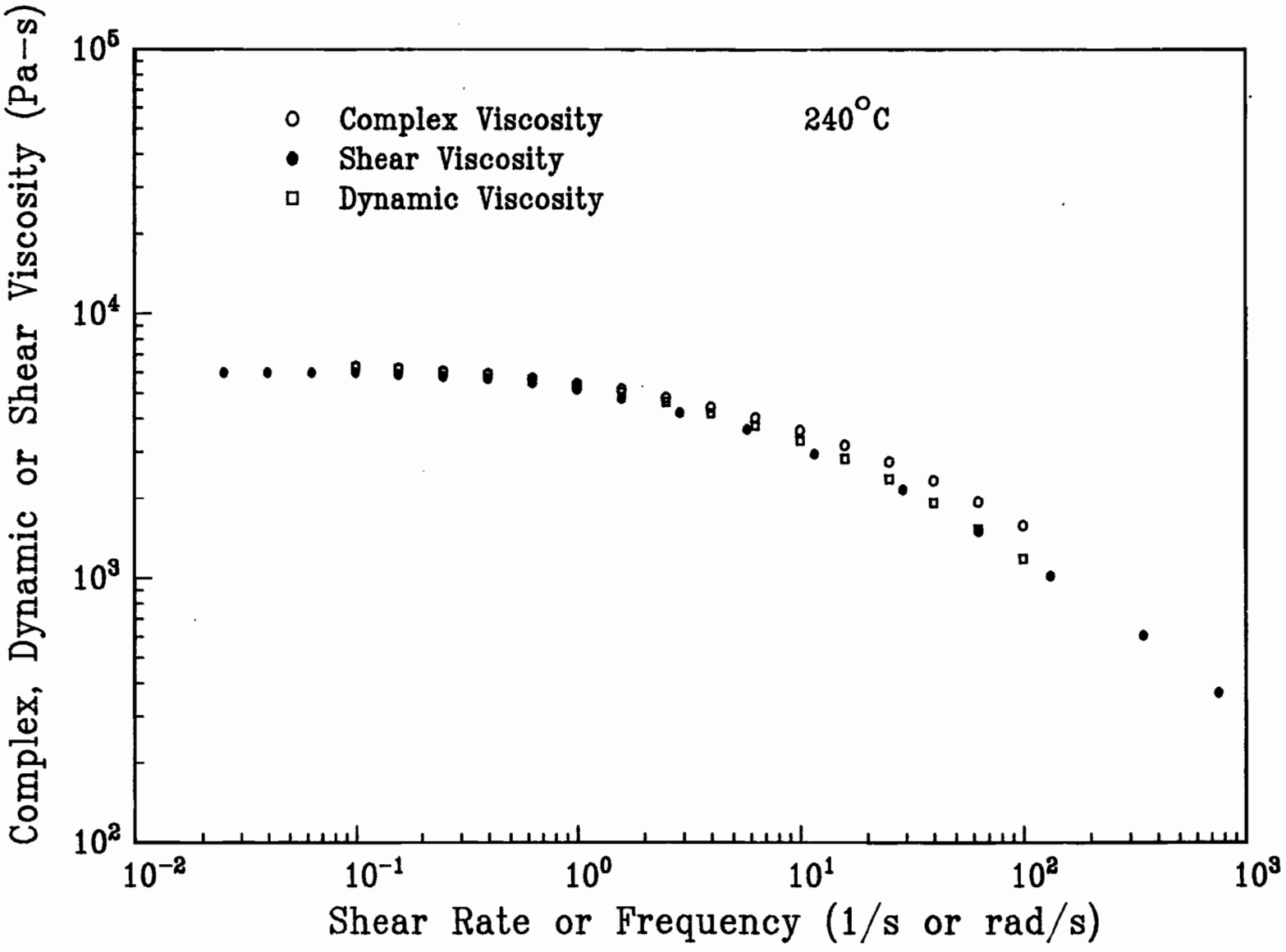

Figure 50: Comparison of shear, dynamic and complex viscosities for resin 31 at 240°C.

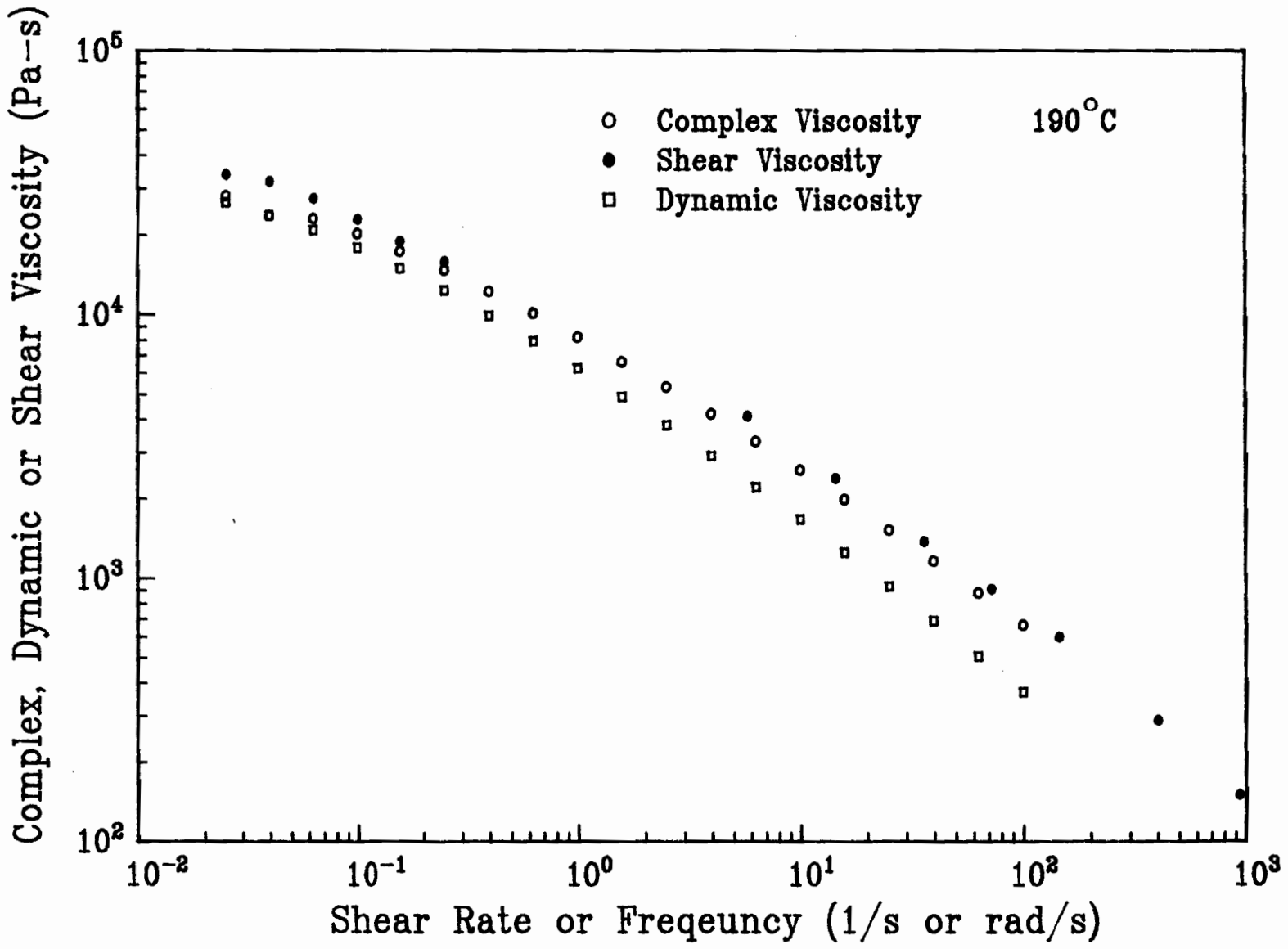

Figure 51: Comparison of shear, dynamic and complex viscosities for resin 32 at 190°C.

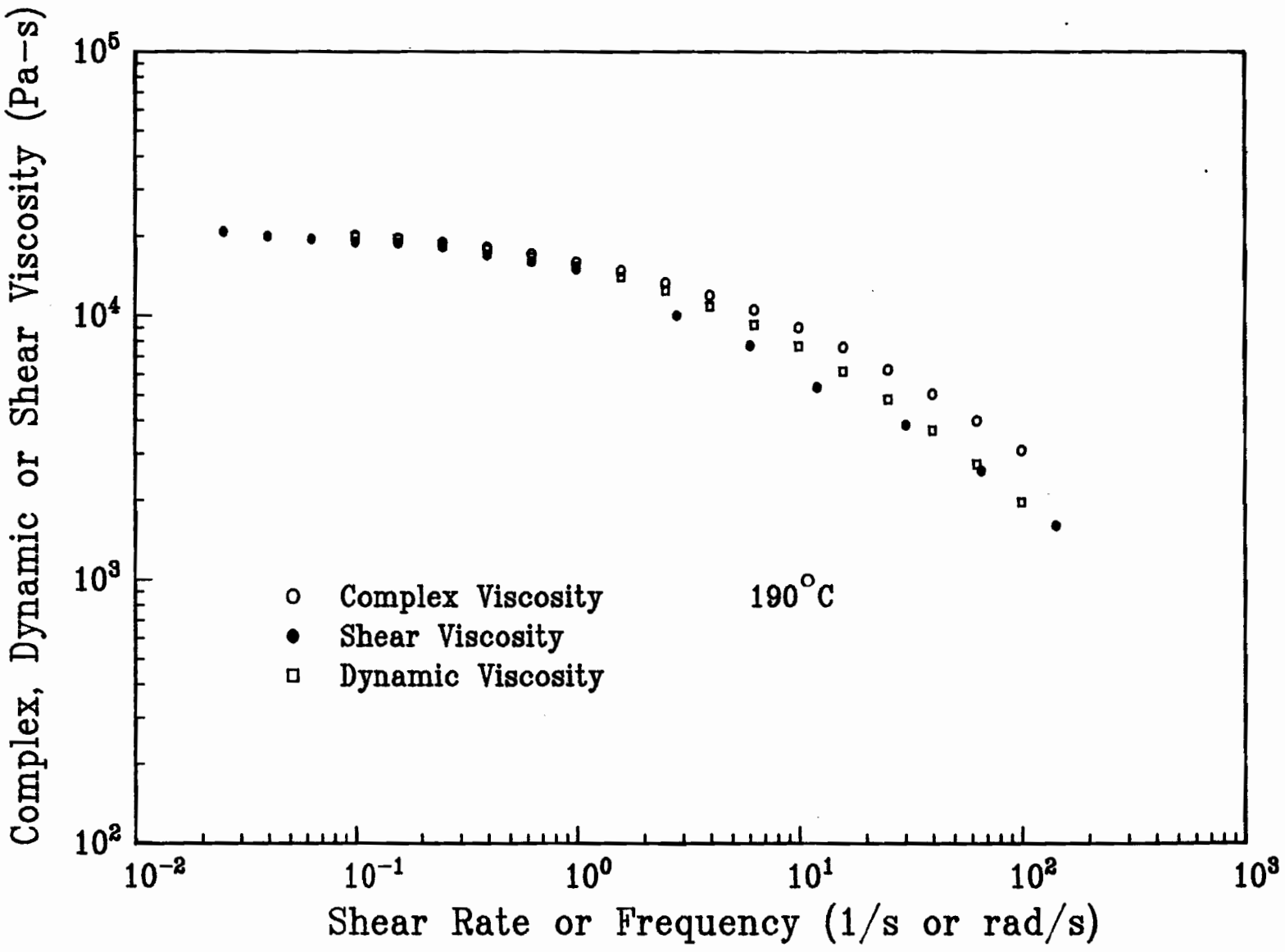

Figure 52: Comparison of shear, dynamic and complex viscosities for resin 33 at 190°C.

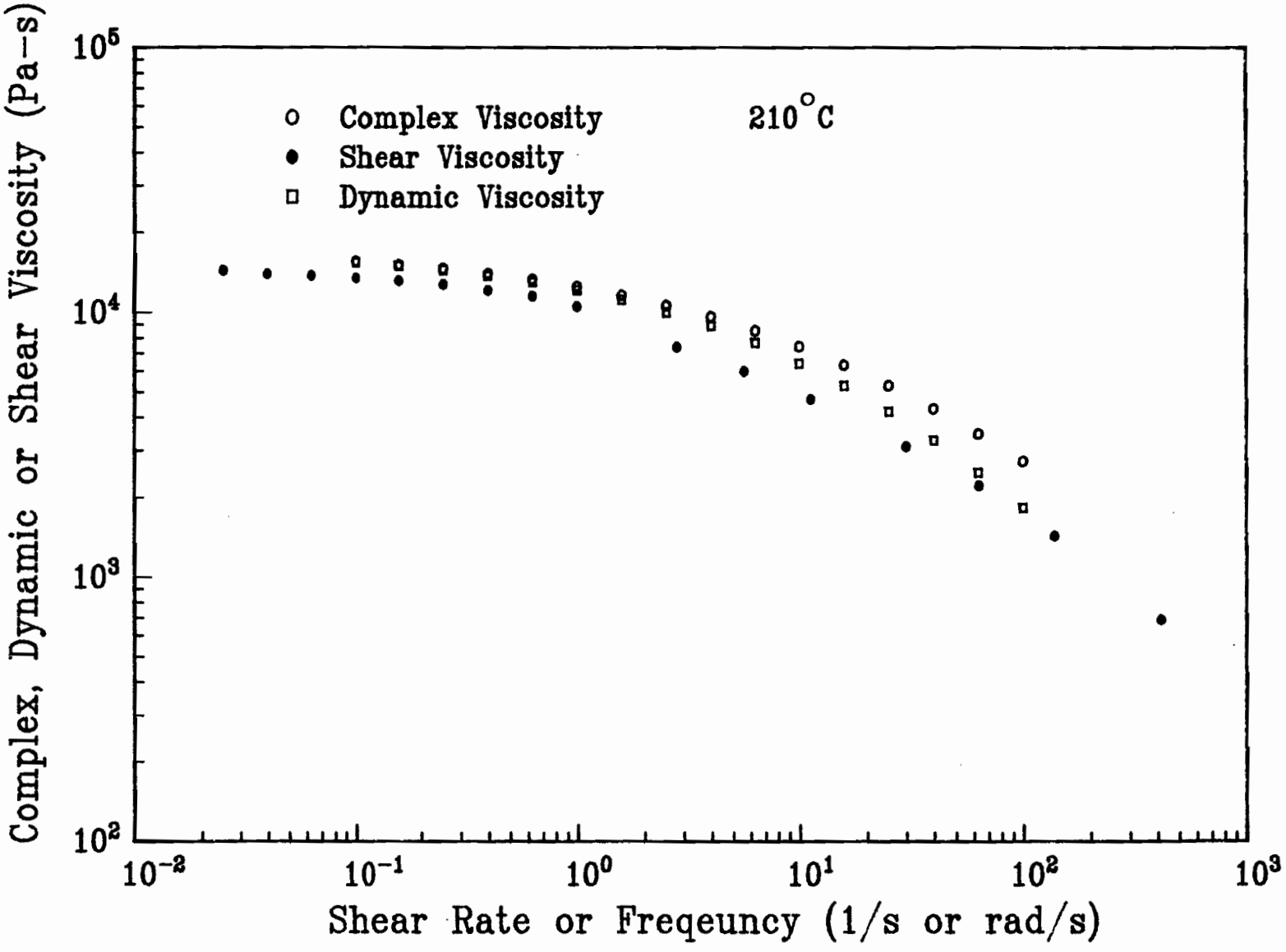

Figure 53: Comparison of shear, dynamic and complex viscosities for resin 33 at 210°C.

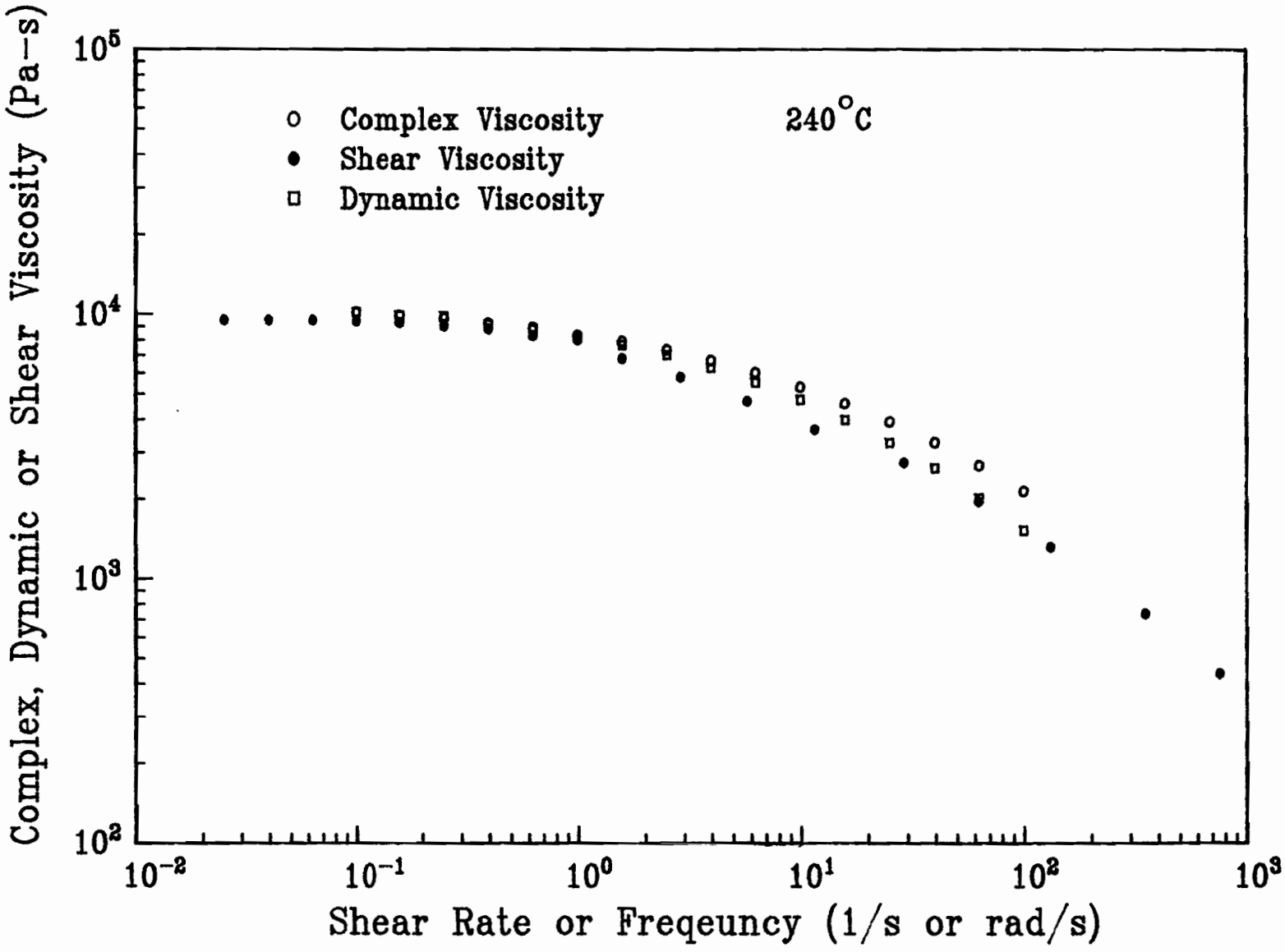

Figure 54: Comparison of shear, dynamic and complex viscosities for resin 33 at 240°C.

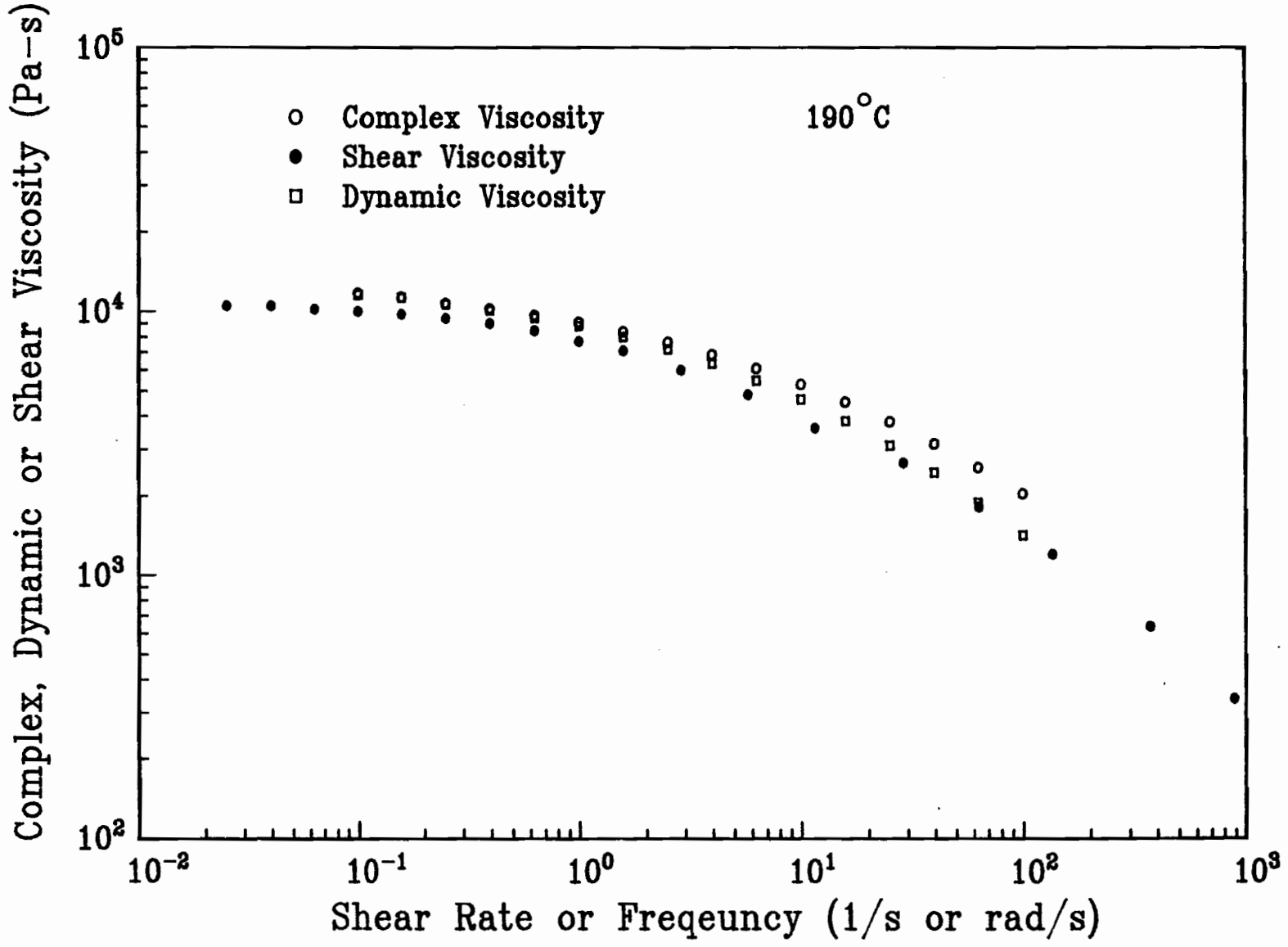

Figure 55: Comparison of shear, dynamic and complex viscosities for resin 30 at 190°C.

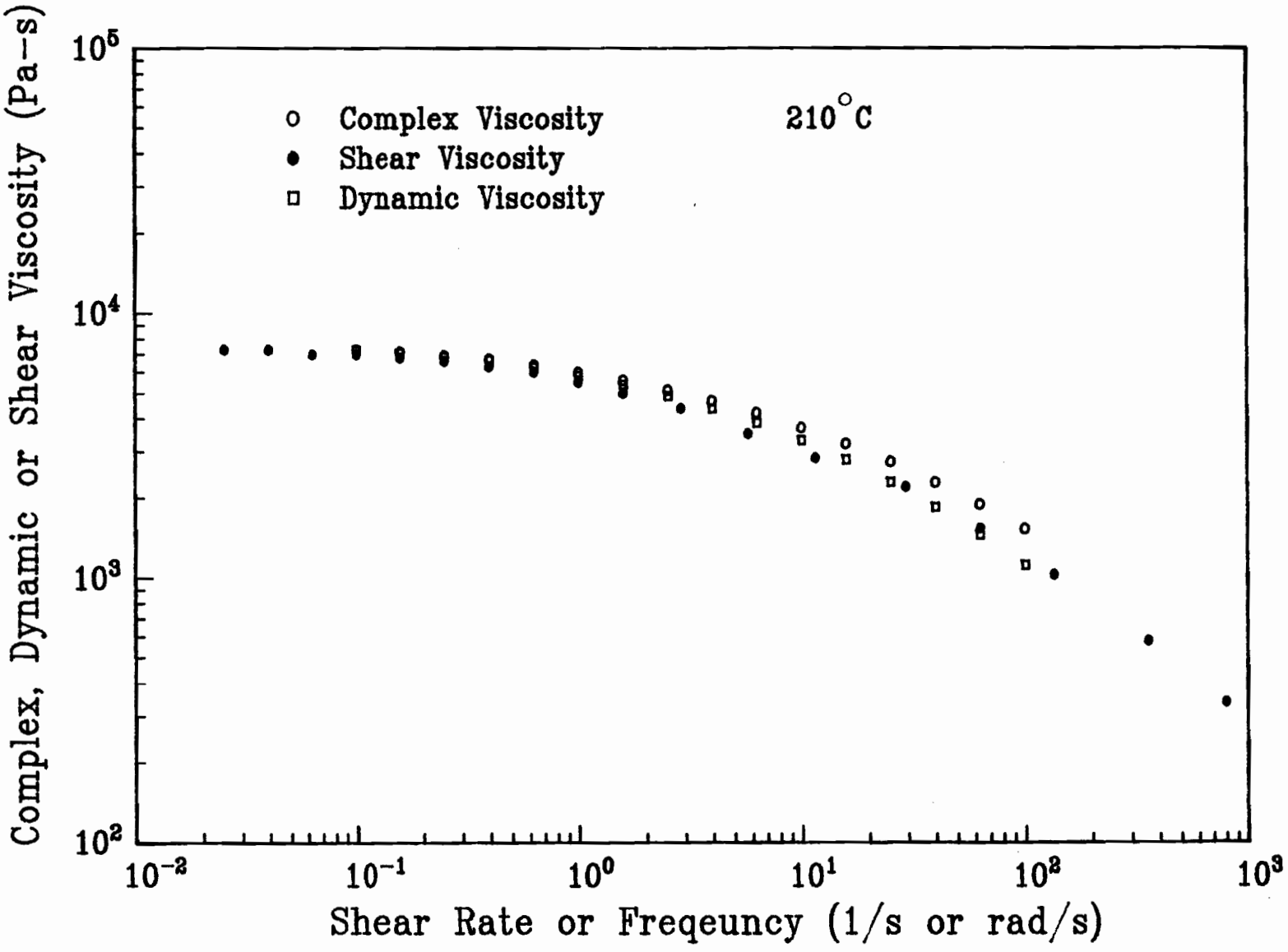

Figure 56: Comparison of shear, dynamic and complex viscosities for resin 30 at 210°C.

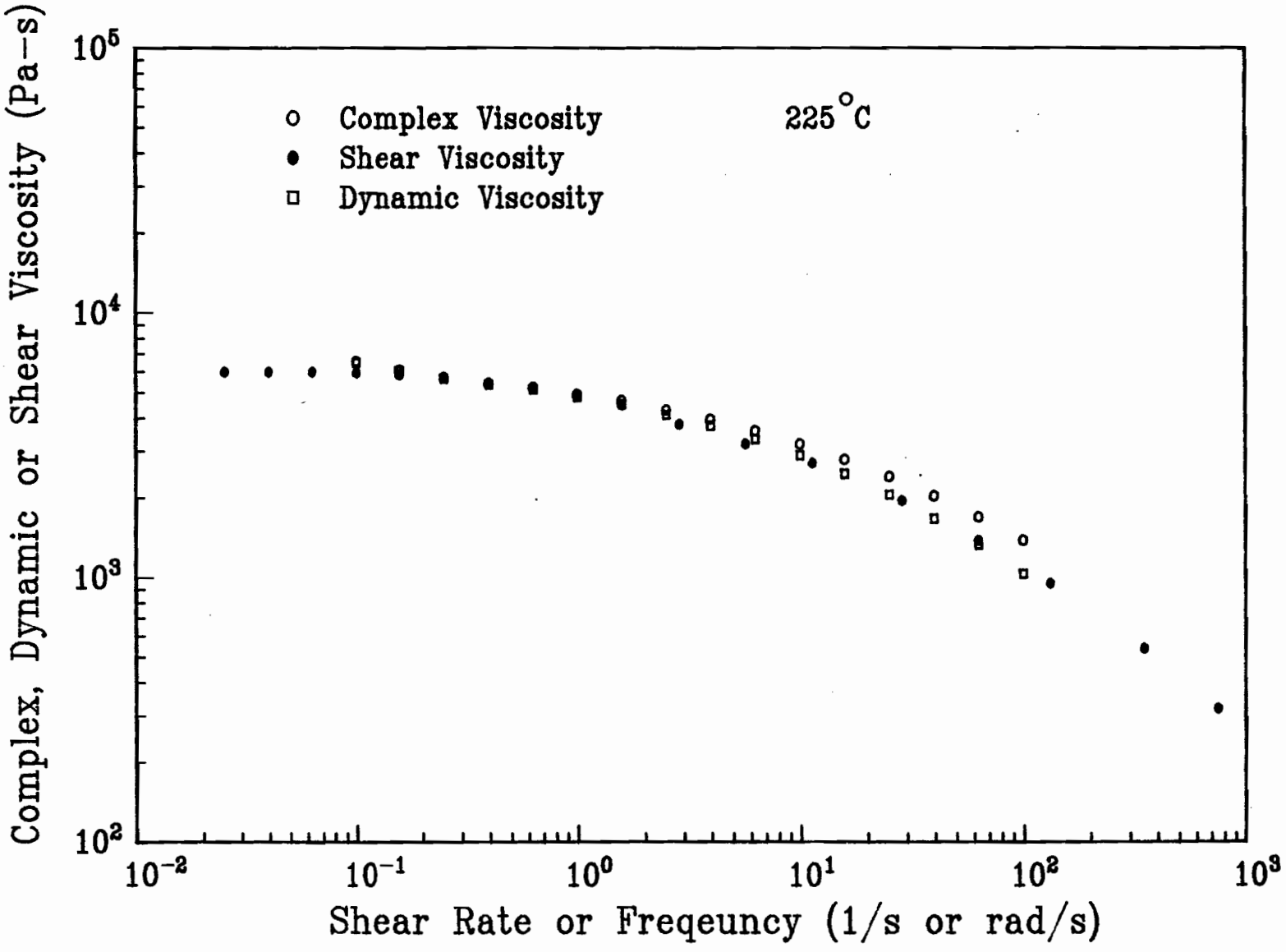

Figure 57: Comparison of shear, dynamic and complex viscosities for resin 30 at 225°C.

$$\tau + \lambda_i \frac{\partial \tau}{\partial t} = -\mu_i \dot{\gamma} \qquad (66)$$

The relaxation modulus of such an element is as follows,

$$G_i(s) = \frac{\mu_i}{\lambda_i} e^{-s/\lambda_i} \qquad (67)$$

For an infinite number of Maxwell elements placed in parallel, the relaxation spectrum is defined in terms of these relaxation moduli.

$$G(s) = \sum_{i=1}^{\infty} G_i(s) = \int_{-\infty}^{+\infty} H(\lambda) e^{-s/\lambda} d(\ln \lambda) \qquad (68)$$

The term H(λ) is referred to as the spectrum strength and λ as the relaxation time. The spectrum strength can be viewed as a measure of the relative contribution of each relaxation time to the material's viscoelastic response. The advantage offered by using the relaxation spectrum is that all other linear viscoelastic properties can, in principle, be derived from it.

In this work the relaxation spectra were derived from the loss and storage modulus data. Because of their accuracy [39] the second order approximation methods developed by Tschoegl [149] were used. These expressions are presented below.

$$H(\lambda) = G'\left\{\frac{d\log G'}{d\log\omega} - \frac{1}{2}\left(\frac{d\log G'}{d\log\omega}\right)^2 - \frac{1}{4.61}\frac{d^2\log G'}{d(\log\omega)^2}\right\}\Bigg|_{\lambda=\frac{\sqrt{2}}{\omega}} \quad (69)$$

$$H(\lambda) = \frac{2}{\pi}\left\{G'' + \frac{4}{3}\frac{dG''}{d\ln\omega} + \frac{1}{3}\frac{d^2G''}{d(\ln\omega)^2}\right\}\Bigg|_{\lambda=\frac{\sqrt{5}}{\omega}} \quad (70)$$

Both the loss and storage modulus data were fitted to a polynomial function of the following form.

$$y = a_0 + a_1x + a_2x^2 + \ldots + a_nx^n \quad (71)$$

In most cases a fourth order polynomial fit the data adequately. This function was then manipulated as required by the approximation formulas. The relaxation spectra of the four resins are presented in Figures 58-67. The agreement between the predictions from the loss and storage modulus are very good for the LLDPE resins but is quite poor for resin 32 (Figure 67). Considering the similar shapes of the data from which these spectra were derived, the similarity between the spectra of resins 30, 31 and 33 is expected. Again, at all temperatures, the spectrum strengths of resin 33 were highest followed by resin 31 and 30. Characteristic of these resins were low values of the spectrum strength at relaxation times greater than about 8 seconds. For resin 32 the spectrum strengths are lower than the LLDPE resins for short relaxation times, but are substantially higher at the longer relaxation times (λ>8 s).

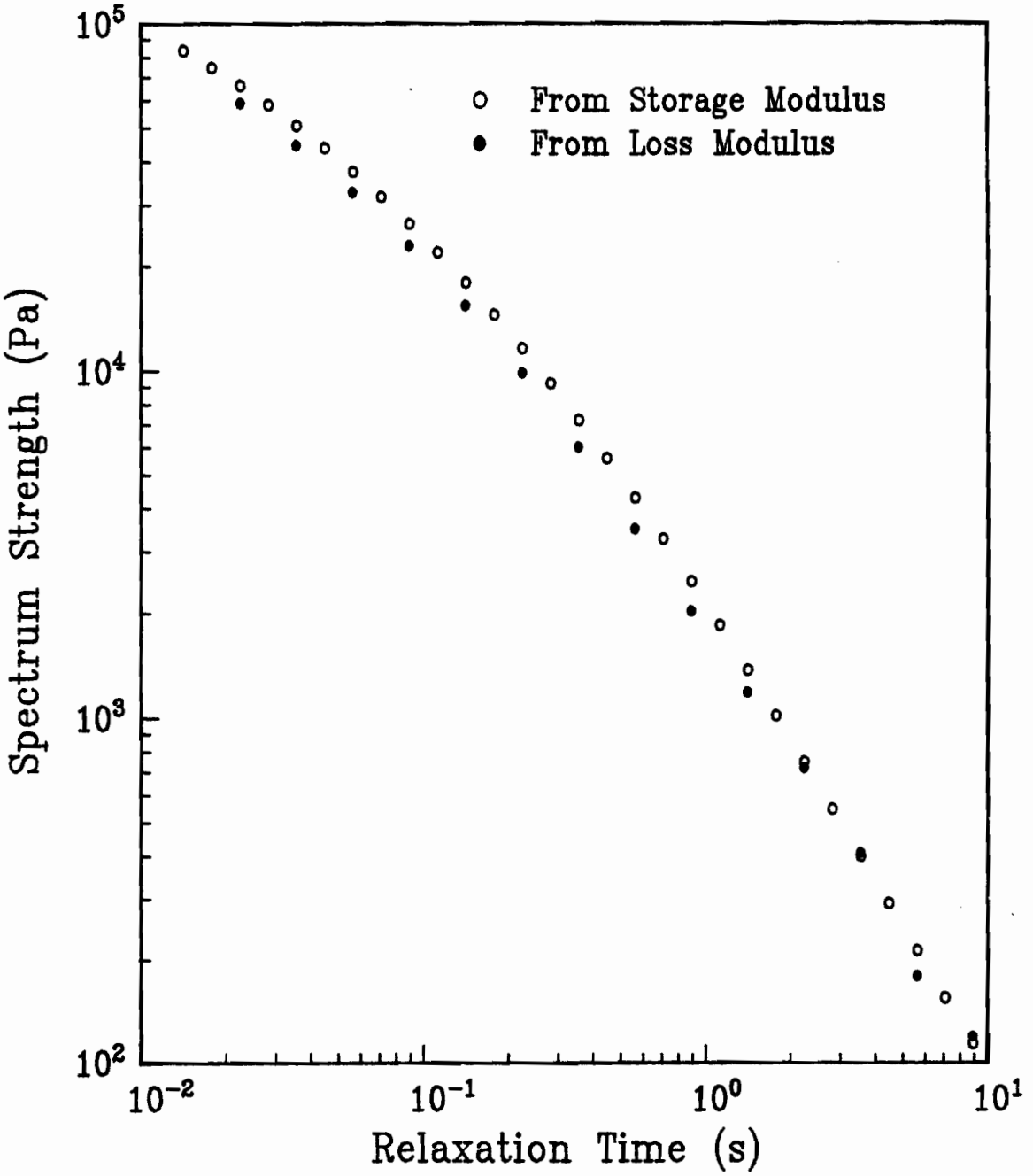

Figure 58: Relaxation spectra of resin 31 at 190°C. Calculated from storage and loss moduli data.

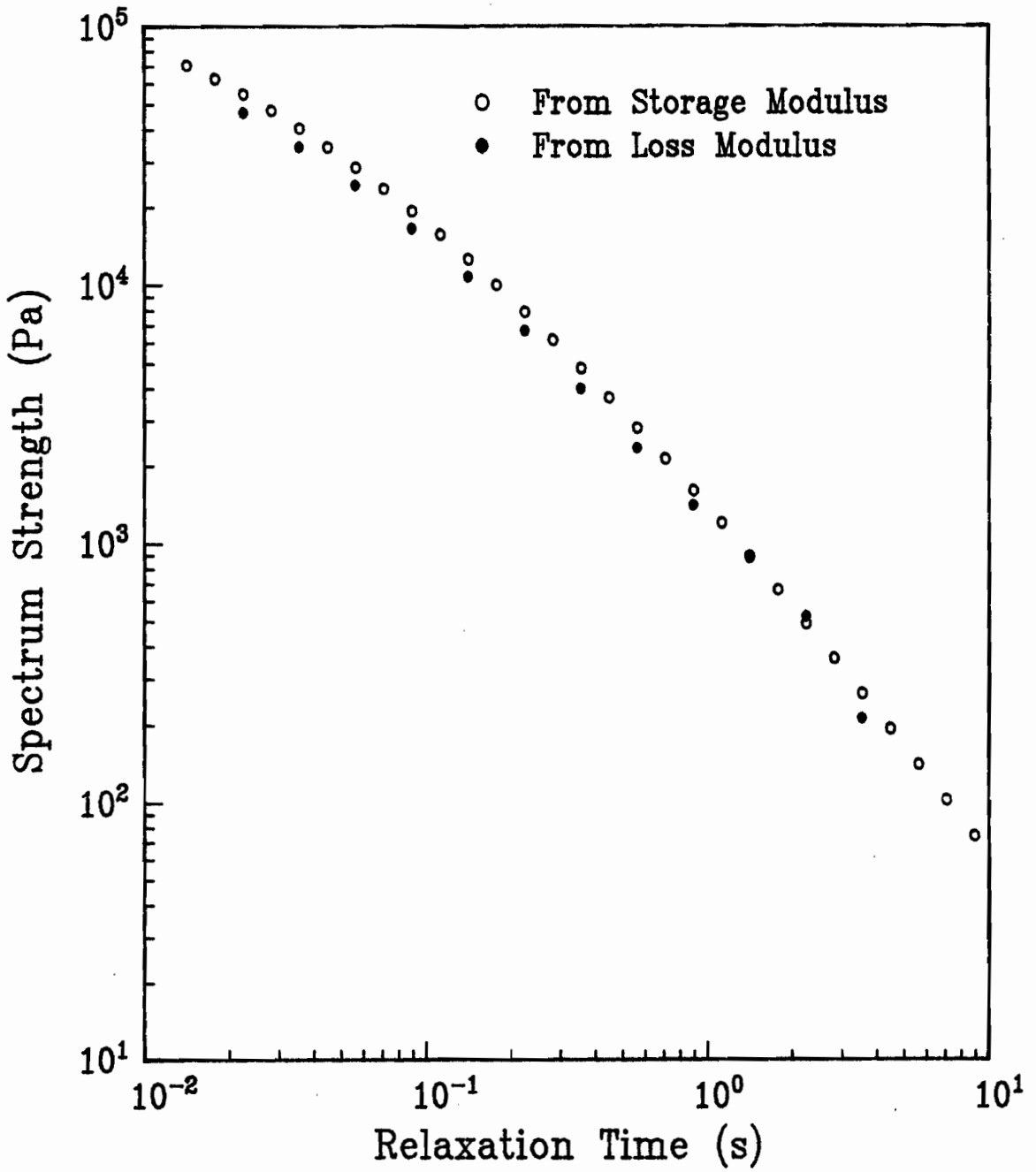

Figure 59: Relaxation spectra of resin 31 at 210°C. Calculated from storage and loss modulus data.

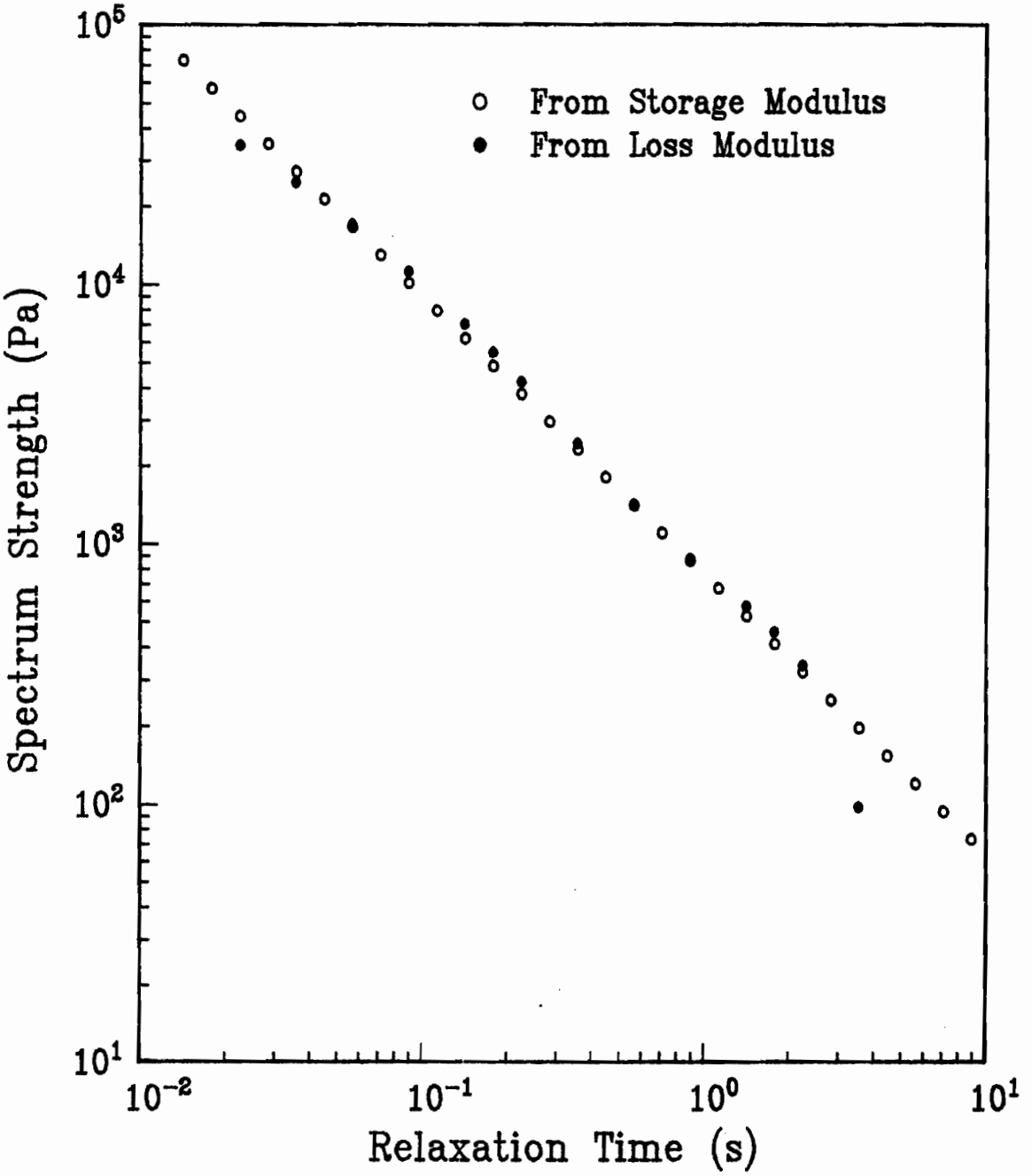

Figure 60: Relaxation spectra of resin 31 at 240°C. Calculated from storage and loss modulus data.

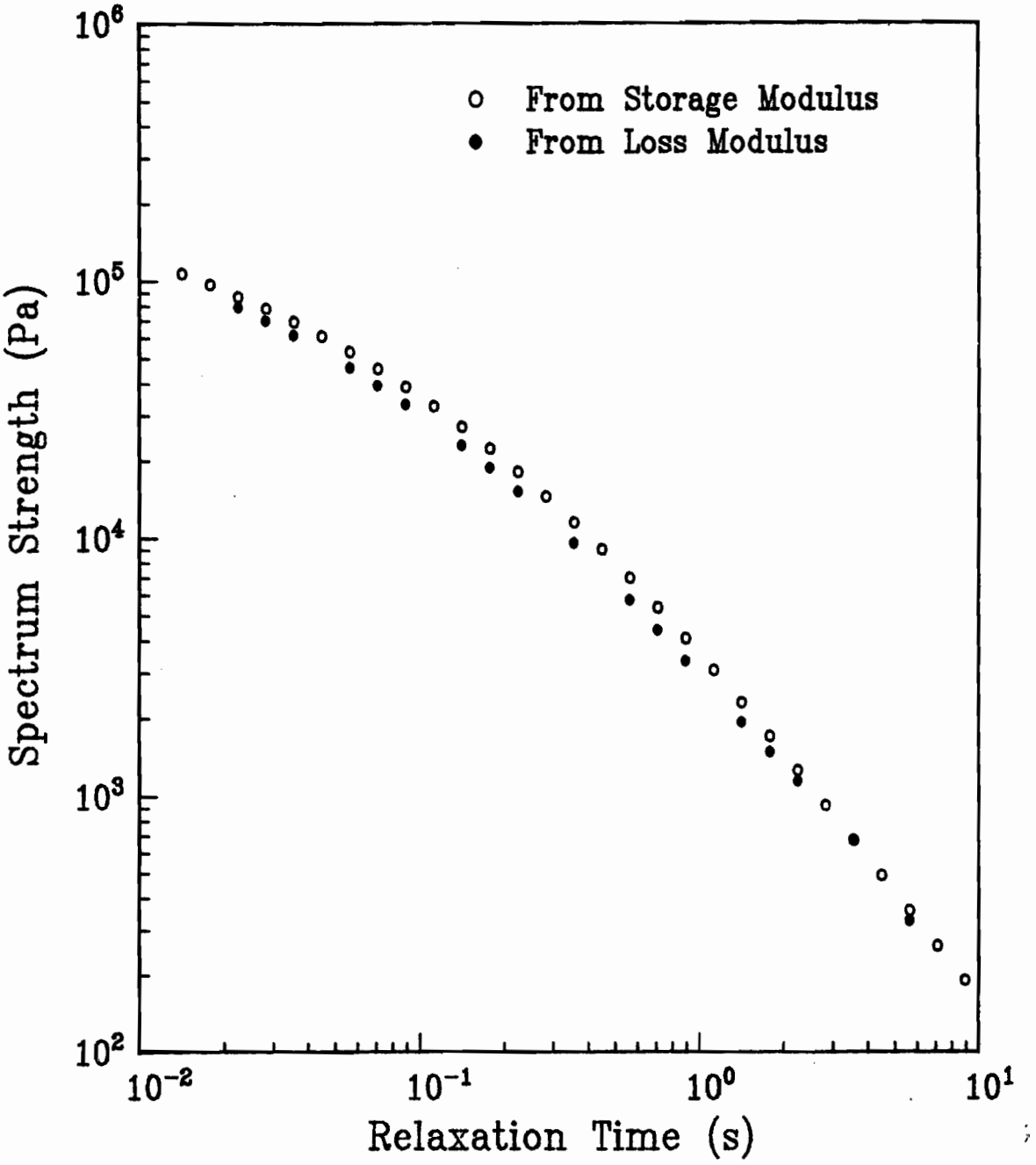

Figure 61: Relaxation spectra of resin 33 at 190°C. Calculated from storage and loss moduli data.

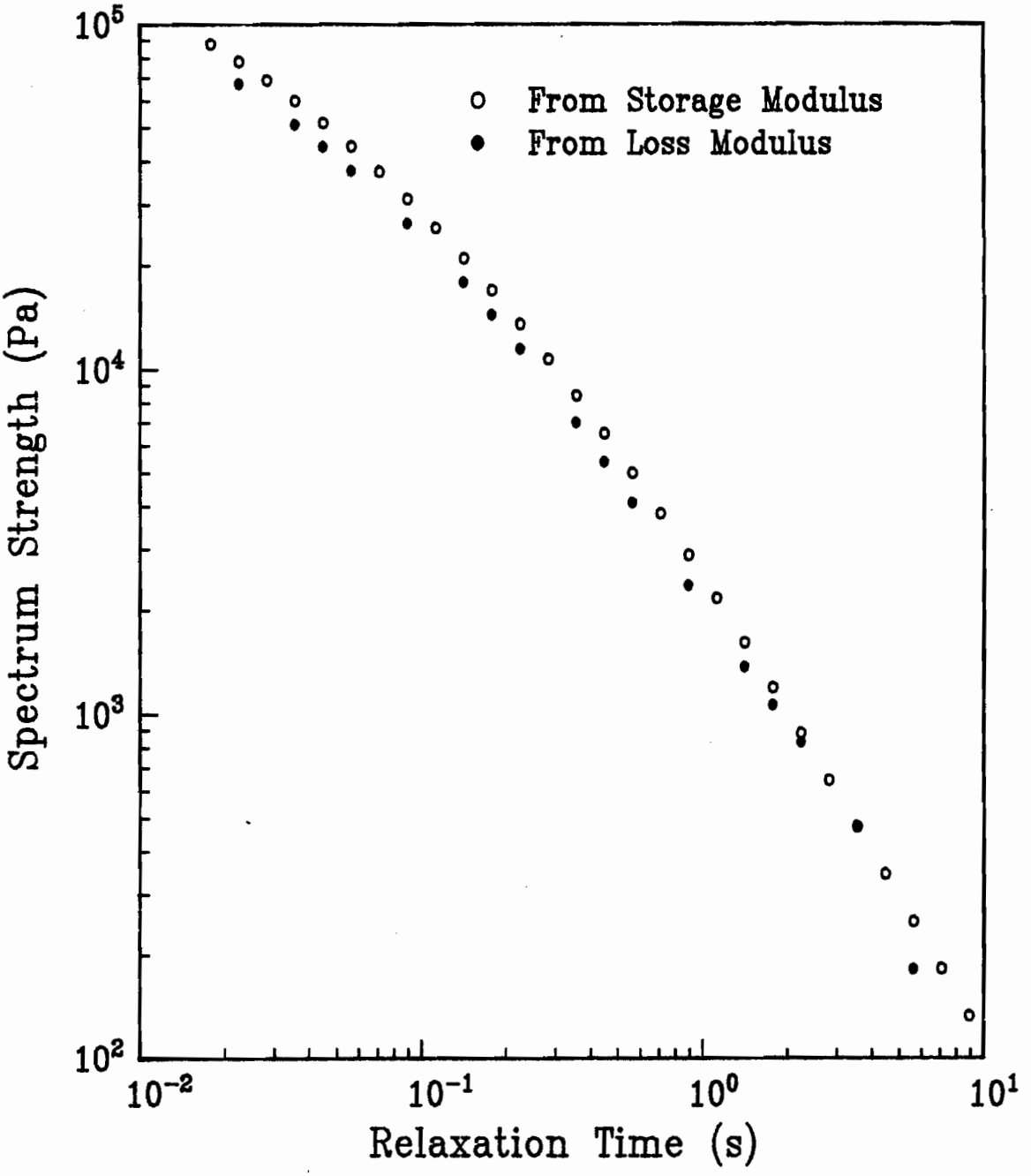

Figure 62: Relaxation spectra of resin 33 at 210°C. Calculated from storage and loss modulus data.

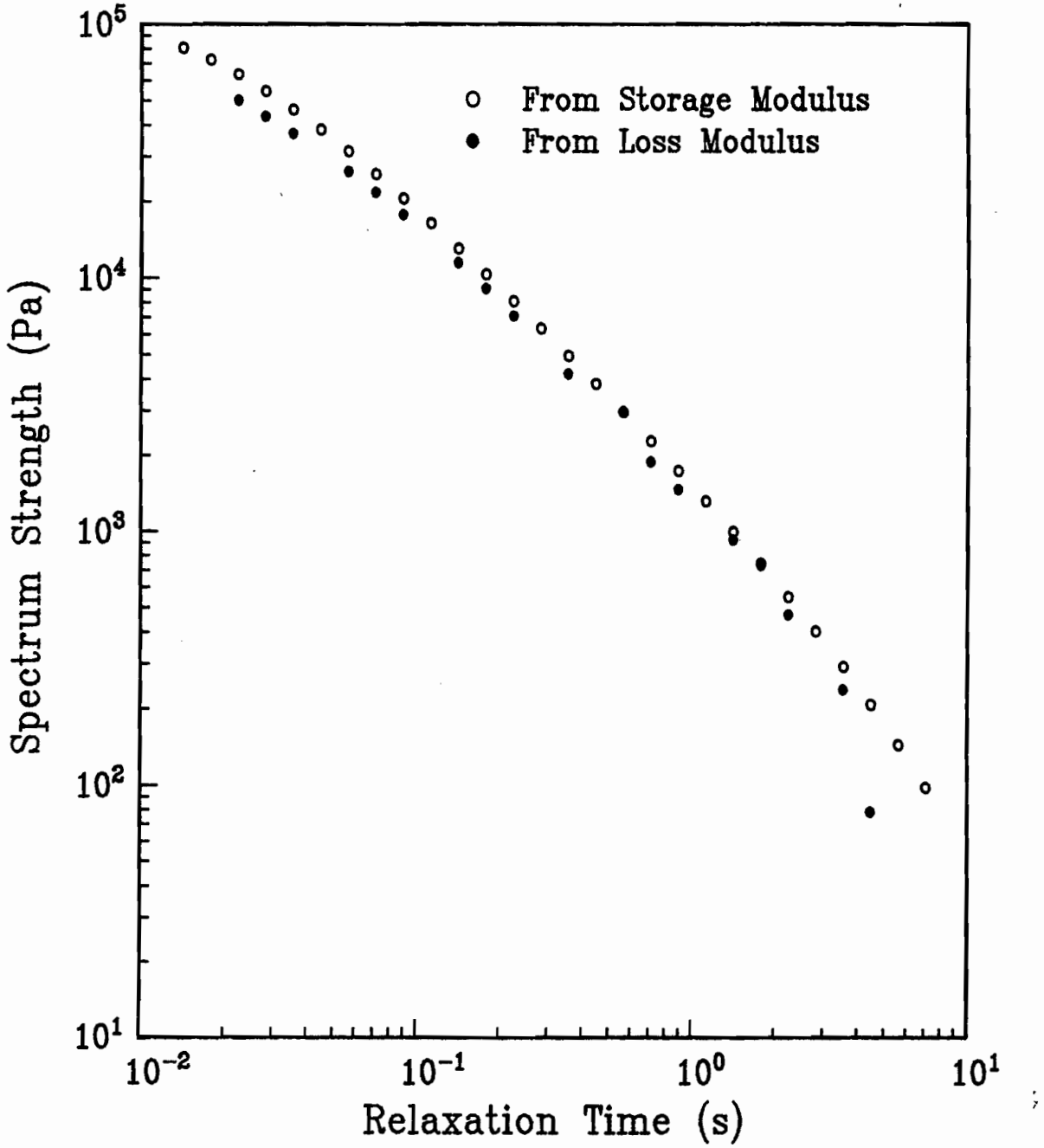

Figure 63: Relaxation spectra of resin 33 at 240°C. Calculated from storage and modulus loss data.

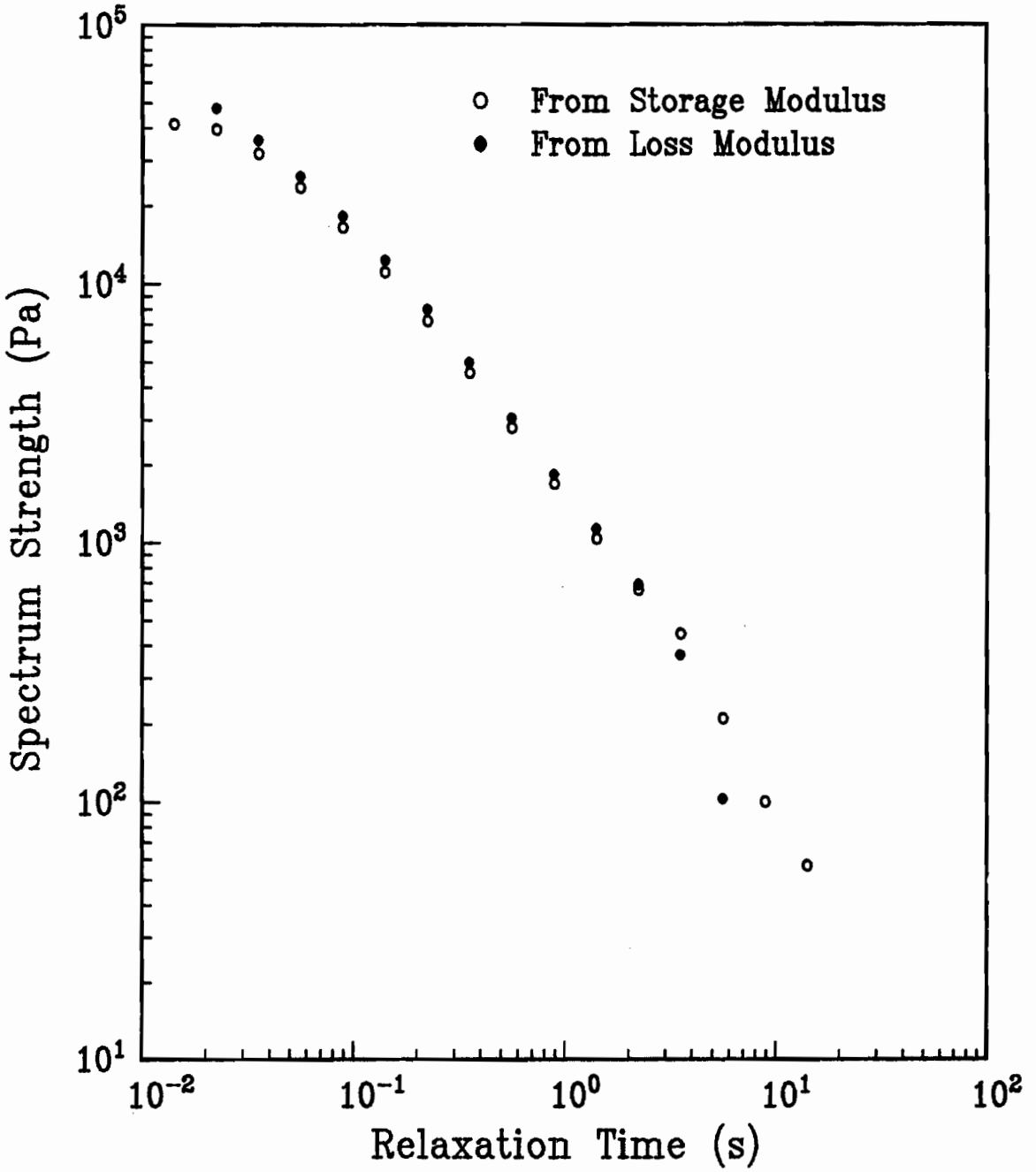

Figure 64: Relaxation spectra of resin 30 at 190°C. Calculated from storage and loss modulus data.

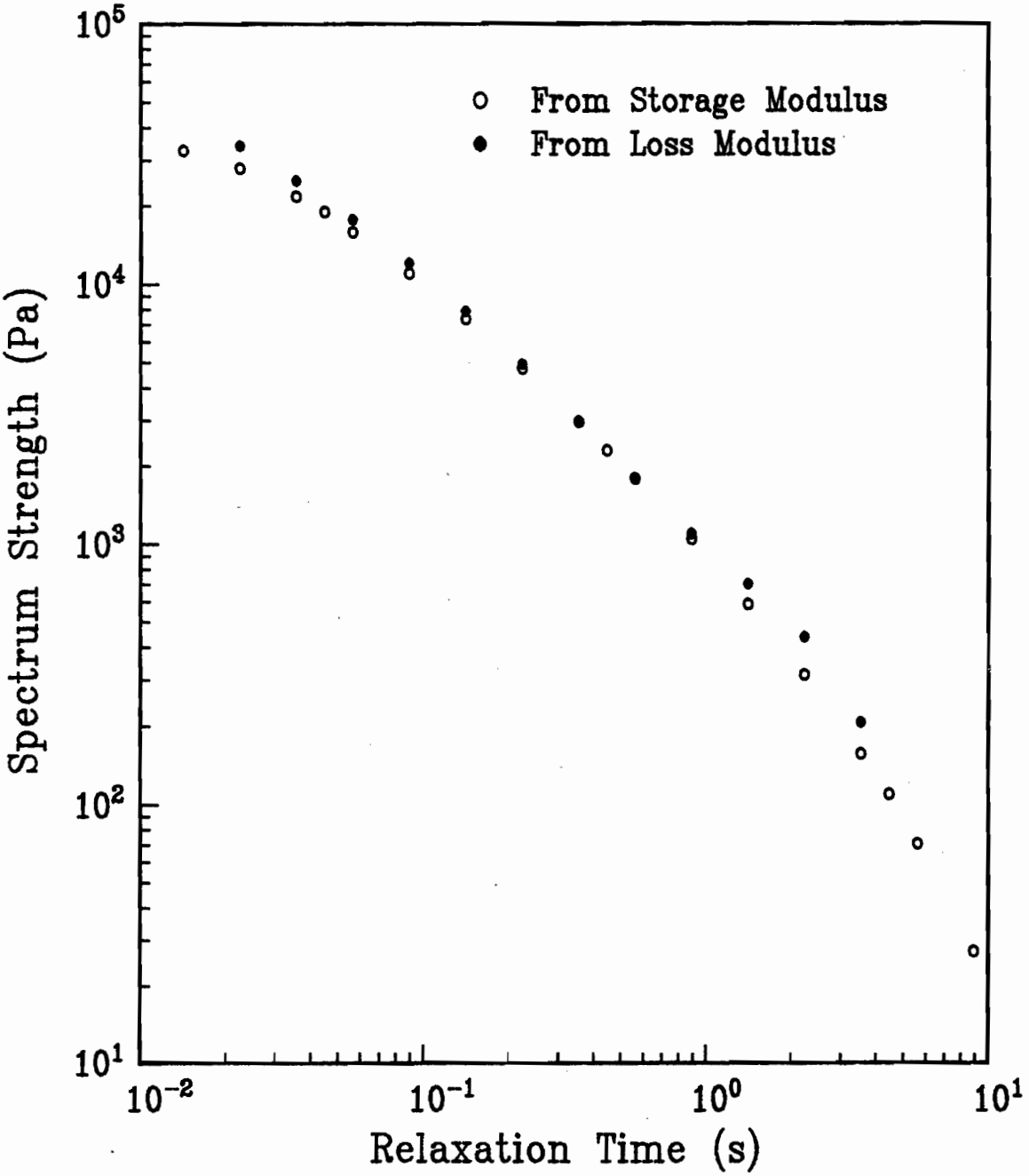

Figure 65: Relaxation spectra of resin 30 at 210°C. Calculated from storage and loss modulus data.

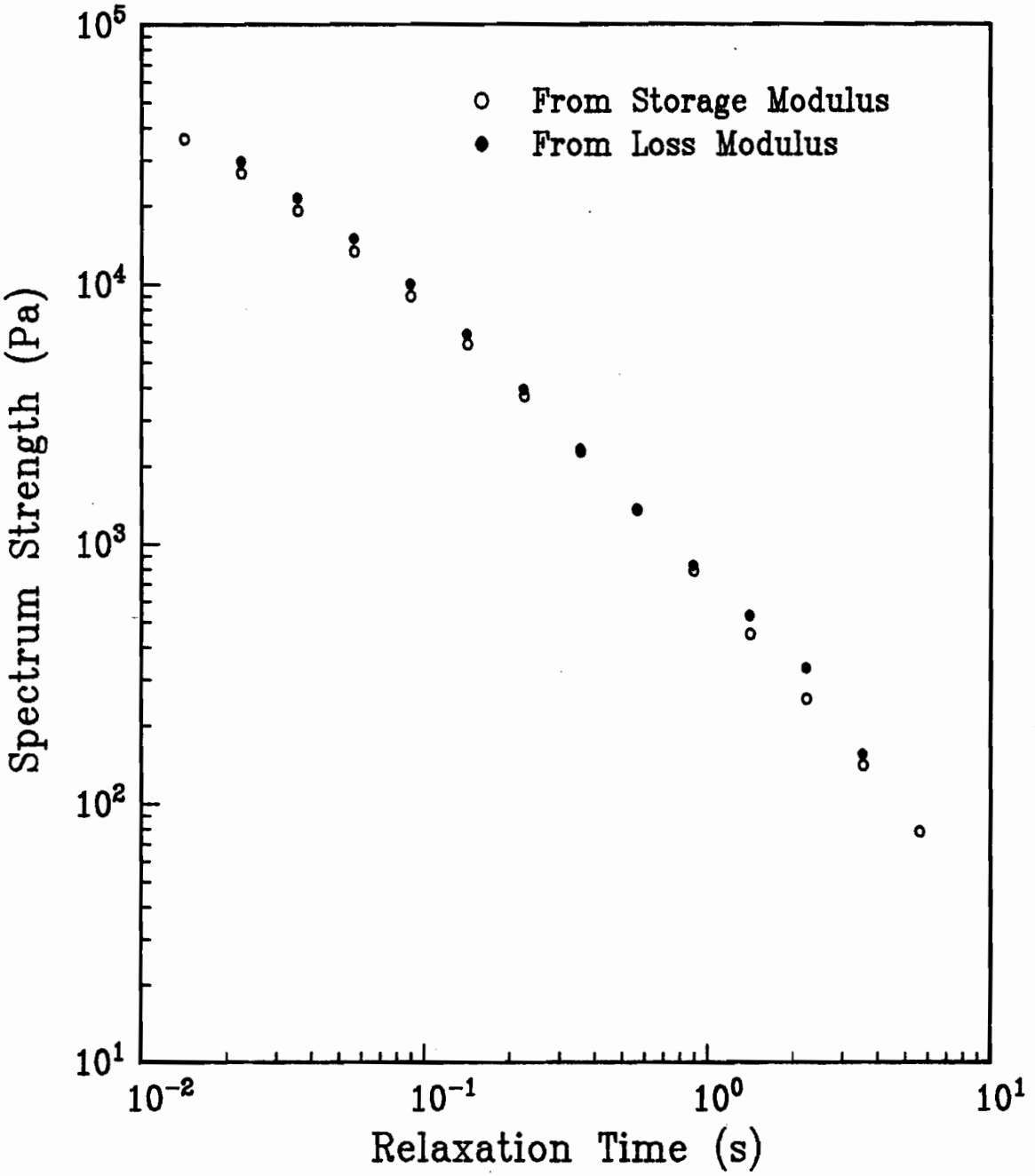

Figure 66: Relaxation spectra of resin 30 at 225°C. Calculated from storage and loss modulus data.

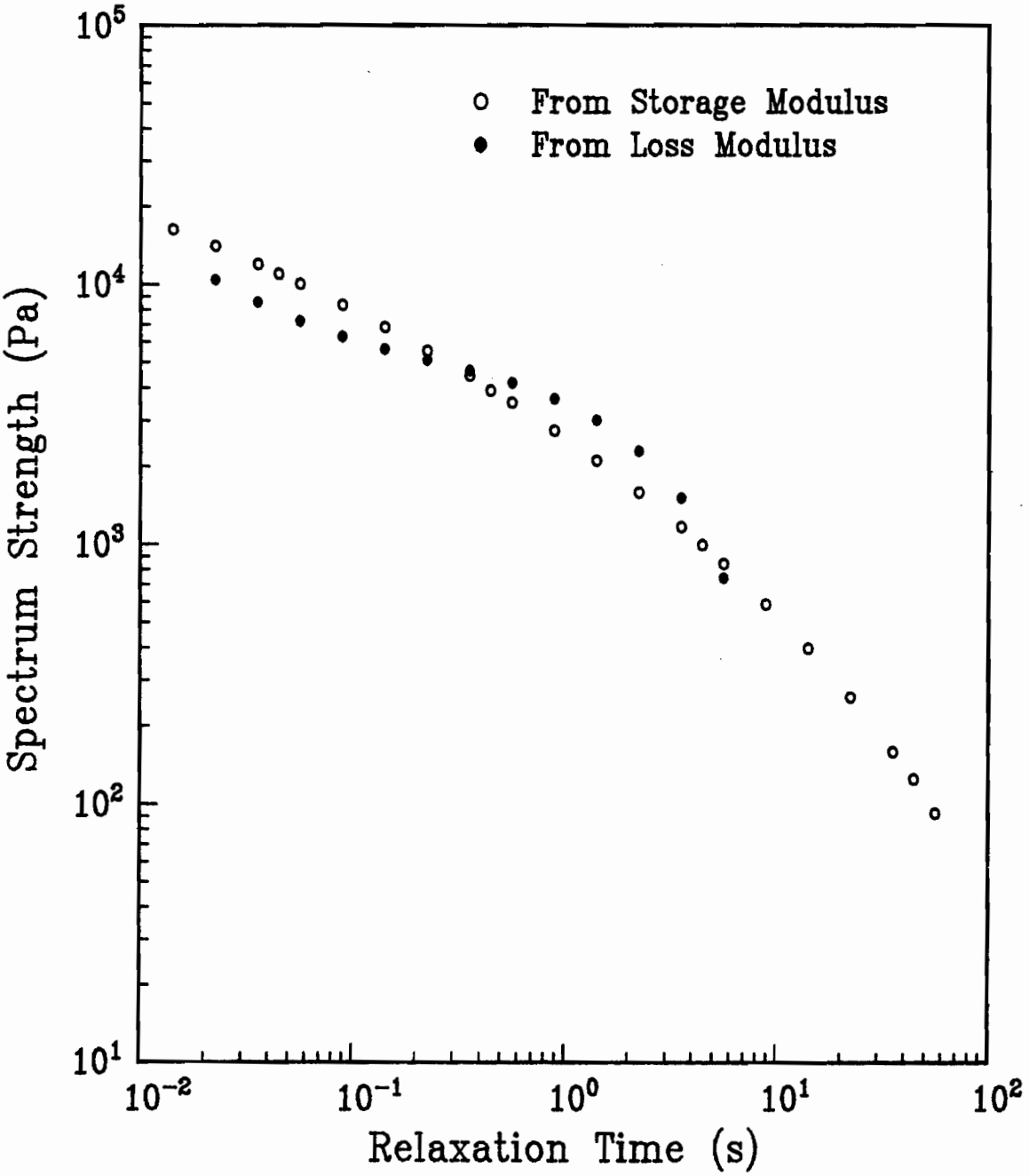

Figure 67: Relaxation spectra of resin 32 at 190°C. Calculated from storage and loss modulus data.

5.4 Acierno Model Predictions

5.4.1 Procedure For Model Usage

The model proposed by Acierno et al. [3], hereafter referred to as "Acierno's model", was used to predict the steady shear behavior of the resins studied. Before this could be done, a decision had to be made as to which version of the relaxation spectrum should be used in the computations; that predicted from the storage or from the loss modulus data. It was decided to use the spectrum that gave a value of the zero-shear viscosity closest to the experimentally determined value using the linear viscoelasticity expression below.

$$\eta_0 = \int_{-\infty}^{+\infty} H\lambda \, d(\ln\lambda) \qquad (72)$$

It was thought that since the task at hand was to predict steady shear data, it would be advisable to ensure that such a key component of the model as the relaxation spectrum be able to predict this linear viscoelastic shear function. The experimental values of the zero-shear viscosities (only for the LLDPE resins since a zero-shear viscosity was not observed for resin 32) as well as the predictions from both

PREDICTION OF ZERO-SHEAR VISCOSITY FROM RELAXATION SPECTRA

190 °C

	Resin 30	Resin 31	Resin 33
Measured Value (Pa-s)	1.05E+04	1.40E+04	2.15E+04
From G′ Spectrum (Pa-s)	1.06E+04	1.26E+04	2.09E+04
Fron G′′ Spectrum (Pa-s)	0.80E+04	1.14E+04	1.79E+04

210 °C

	Resin 30	Resin 31	Resin 33
Measured Value (Pa-s)	0.725E+04	1.00E+04	1.45E+04
From G′ Spectrum (Pa-s)	0.719E+04	0.888E+04	1.49E+04
From G′′ Spectrum (Pa-s)	0.645E+04	0.845E+04	1.29E+04

240 °C

	Resin 30	Resin 31	Resin 33
Measured Value (Pa-s)	0.600E+04★	0.600E+04	0.950E+04
From G′ Spectrum (Pa-s)	0.593E+04	0.540E+04	0.945E+04
From G′′ Spectrum (Pa-s)	0.564E+04	0.534E+04	0.928E+04

★225 °C

Table 7

relaxation spectra are presented in Table 7. Notable is the particularly good agreement between the zero-shear viscosity calculated from the G′ derived spectrum and the measured value for resins 33 and 30. One would suspect this to be fortuitous were it not for its consistancy. For resin 31 the agreement is not as good, but still better than that obtained with the G′′-derived spectrum. Thus in all of the following work the spectra derived from the storage modulus data were used.

The equations comprising Acierno's model reduce to the following for the case of steady simple shear.

$$\eta_i = G_{oi}\,\lambda_{oi}\,x_i^{2.4} \tag{73}$$

$$(\tau_{11}-\tau_{22})_i = 2\,G_{oi}\,\lambda_{oi}^2\,x_i^{3.8}\,\dot{\gamma}^2 \tag{74}$$

$$\frac{1-x_i}{x_i^{2.4}} = \alpha_i\,\lambda_{oi}\,\dot{\gamma} \tag{75}$$

$$\eta = \sum_i \eta_i \quad ; \quad (\tau_{11}-\tau_{22}) = \sum_i (\tau_{11}-\tau_{22})_i \tag{76}$$

The time dependant moduli, G_{oi}, are derived from the relaxation times, λ_{oi}, and their corresponding spectrum strengths, $H(\lambda_{oi})$, using the following expression.

$$G_{oi} = H(\lambda)\,\Delta(\ln \lambda_{oi}) \tag{77}$$

The relaxation times and moduli for each resin and temperature are tabulated in Appendix D. To fit the model to the data, the adjustable parameter, a, must be estimated for each material and temperature to give the best fit. The procedure used is one suggested by Garcia-Rejon [113], and is summarized below.

(1) For a particular shear rate, $\dot{\gamma}$, a value of the adjustable parameter, a, is guessed (usually around 0.5). For each relaxation time, λ_{oi}, a value of x_i is computed from equation (75).

(2) The values of the x_i, G_{oi} and λ_{oi} are used to calculate the viscosity and normal stress difference components from equations (73) and (74).

(3) The viscosity and normal stress difference terms are then summed as in equation (76).

(4) The model predictions are then compared to the data; if the agreement is unsatisfactory a new estimate of a is made and the procedure repeated.

A simple program was written to perform these computations and is listed in Appendix E.

5.4.2 Model Predictions

The model predictions of the shear viscosity and first normal stress difference are presented in Figures 68-87. These are principally plots of the best fits to the data. The values of a that gave the best fit to both the first normal stress difference and shear viscosity data are presented in Appendix F. The value of a required to fit the viscosity data was dependant on the resin and, to a lesser extent, the experimental temperature. The model was able to fit the viscosity curve quite well with a single value of the adjustable parameter in the case of resins 33 and 31. For resins 30 and 32, however, poor agreement was observed at very low shear rates while the agreement was quite good at the higher shear rates. For the case of resin 30, the model underestimated the value of the zero shear viscosity no matter how low a value of a was used. Both Garcia-Rejon [113] and Tsang [106] also observed such behavior with some of their resins. In most cases the normal stress difference data and the viscosity data could not be fitted with the same value of the adjustable parameter.

5.4.3 Prediction of Linear Viscoelastic Behavior

In the limit of linear viscoelastic deformations all models yield the following expression for the storage modulus, G′,

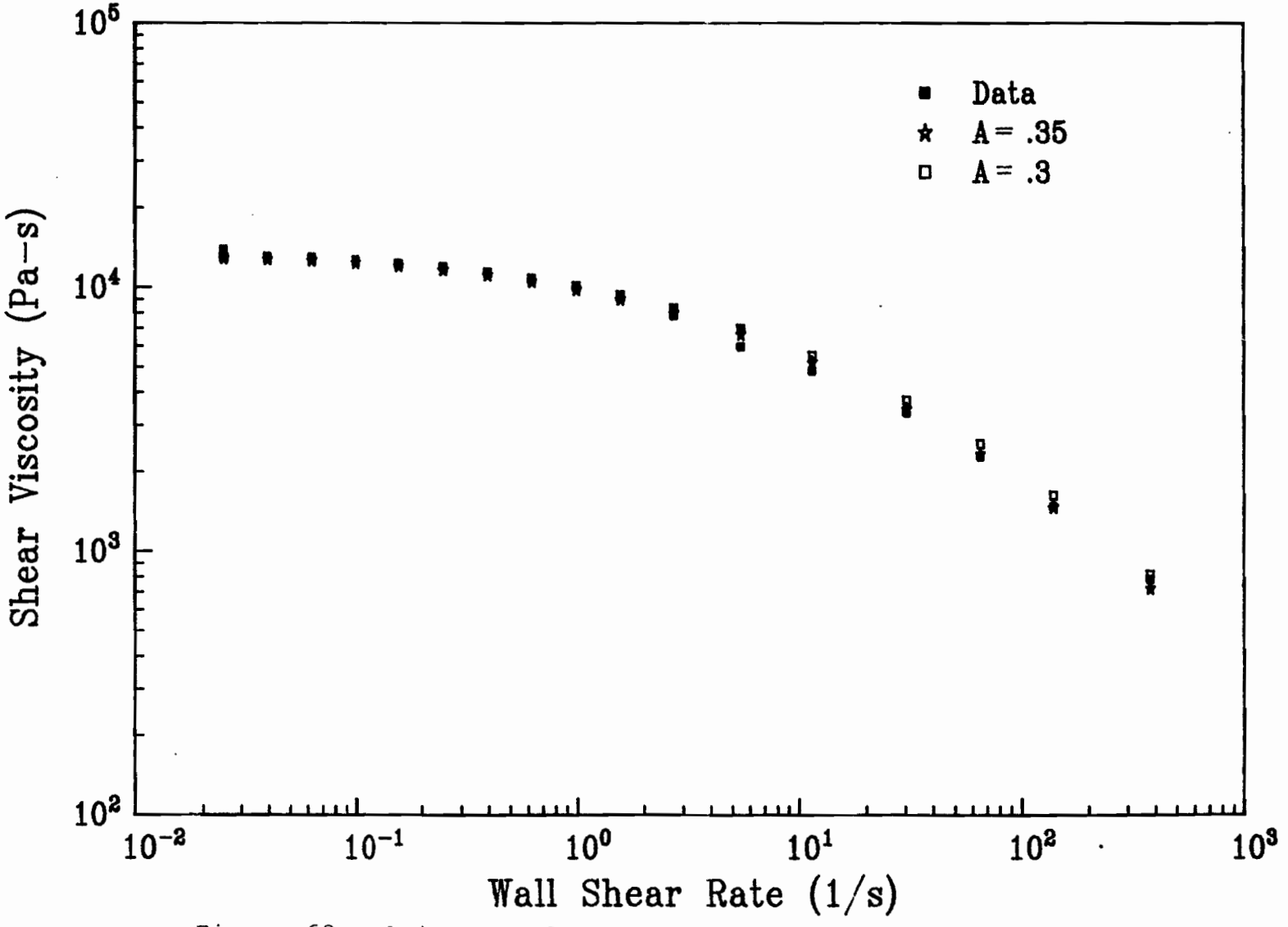

Figure 68: Acierno model predictions of shear viscosity for resin 31 at 190°C.

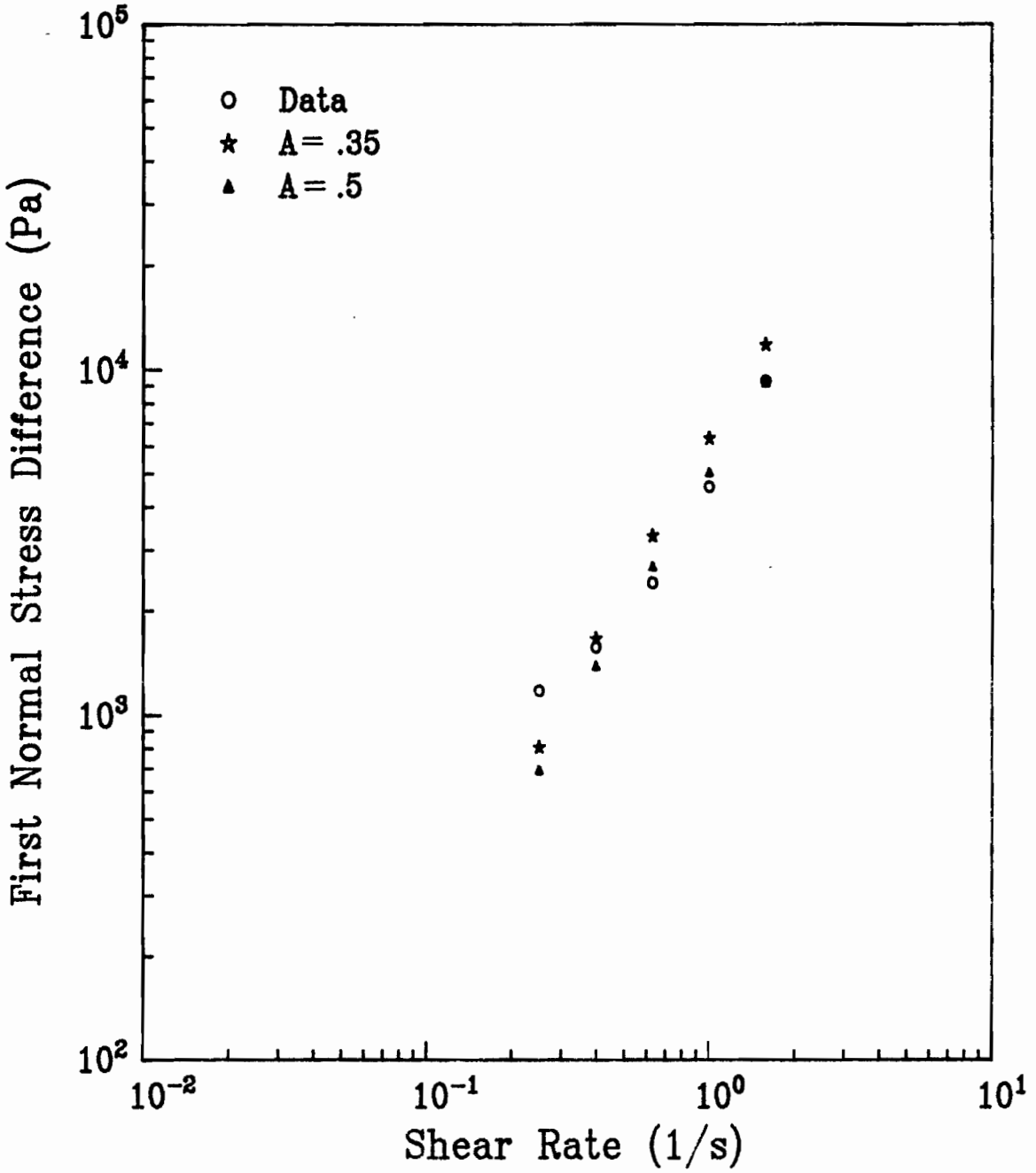

Figure 69: Acierno model predictions of normal stress difference data for resin 31 at 190°C.

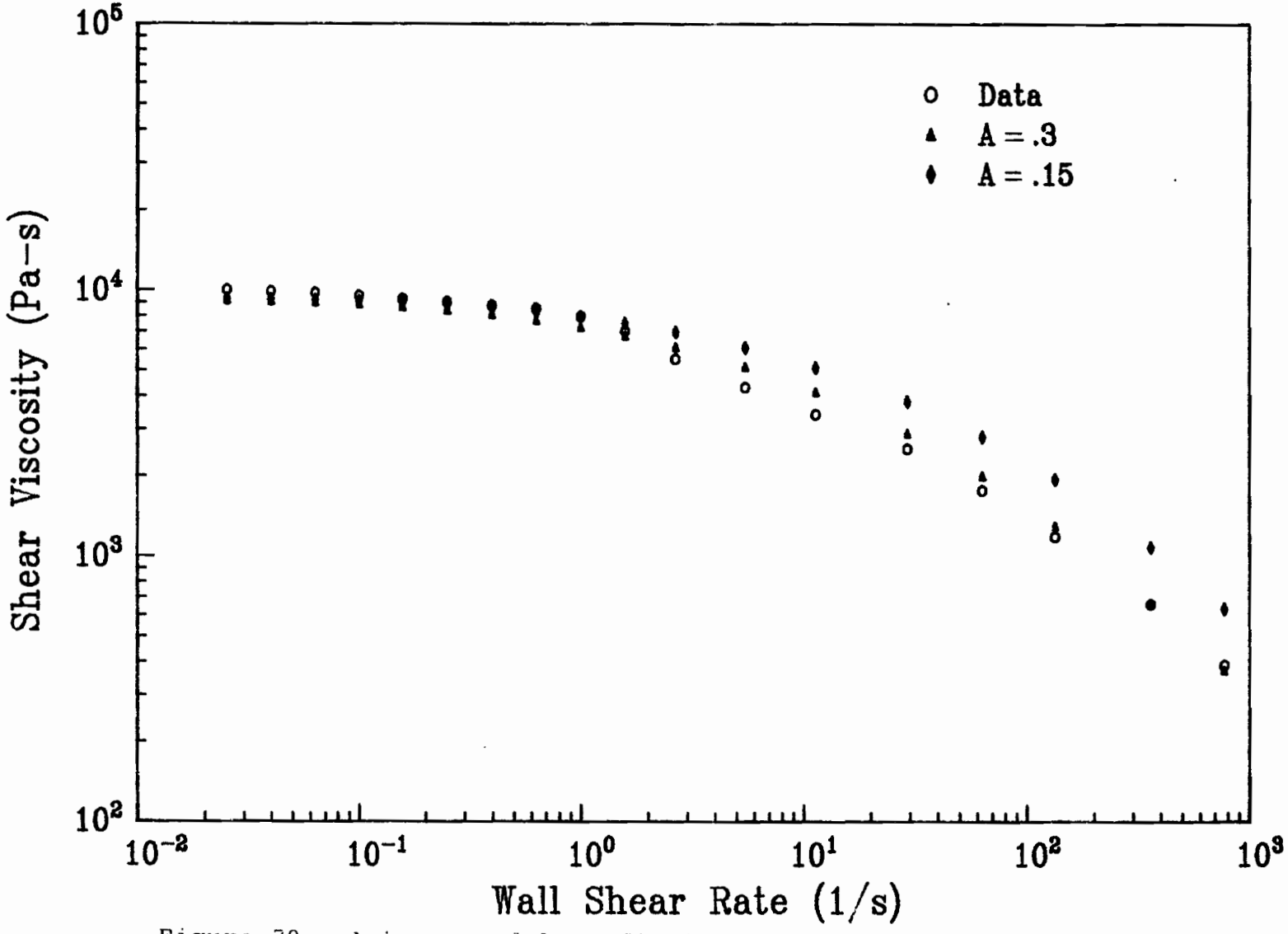

Figure 70: Acierno model predictions of shear viscosity data for resin 31 at 210°C.

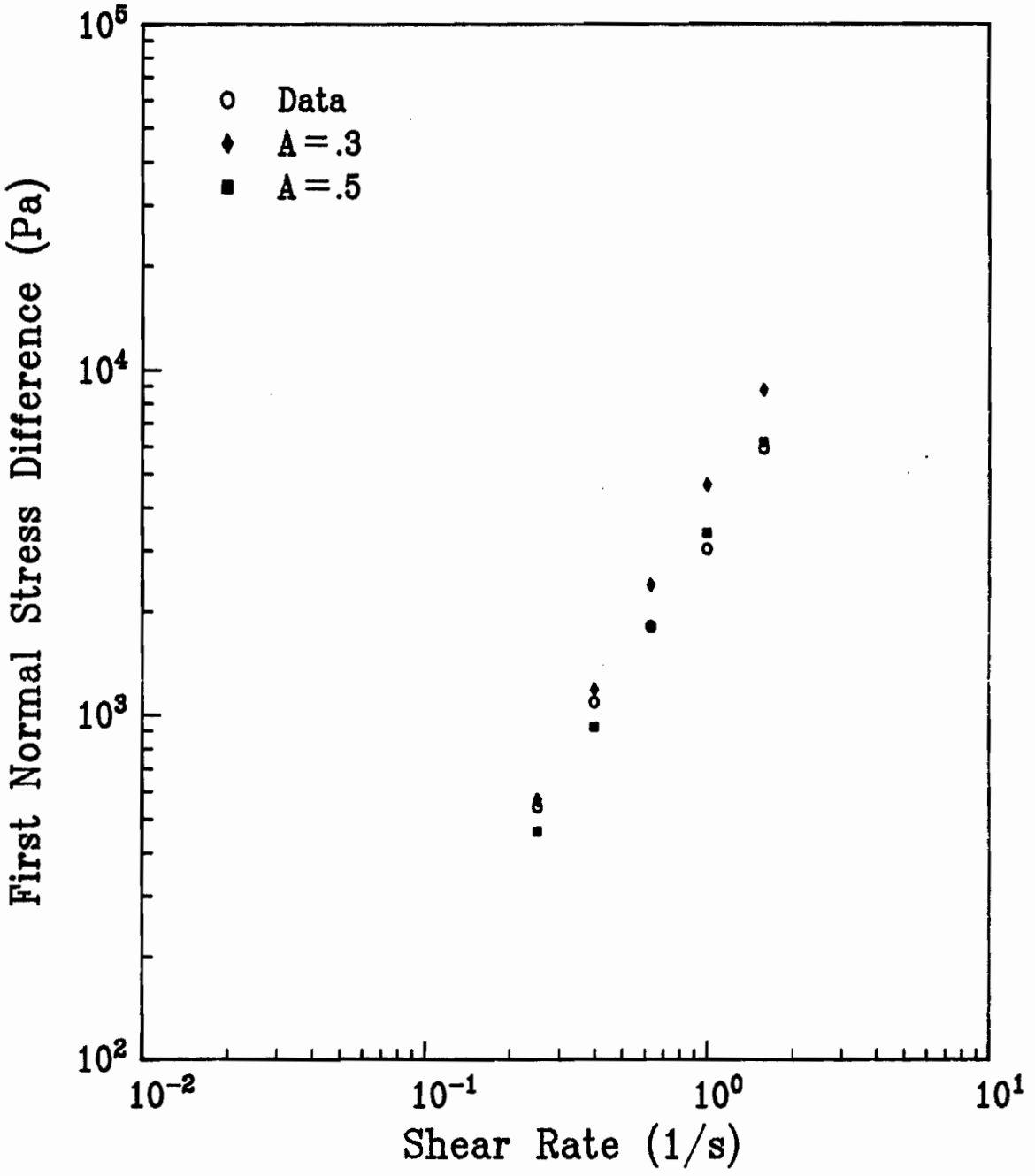

Figure 71: Acierno model predictions of normal stress difference data for resin 31 at 210°C.

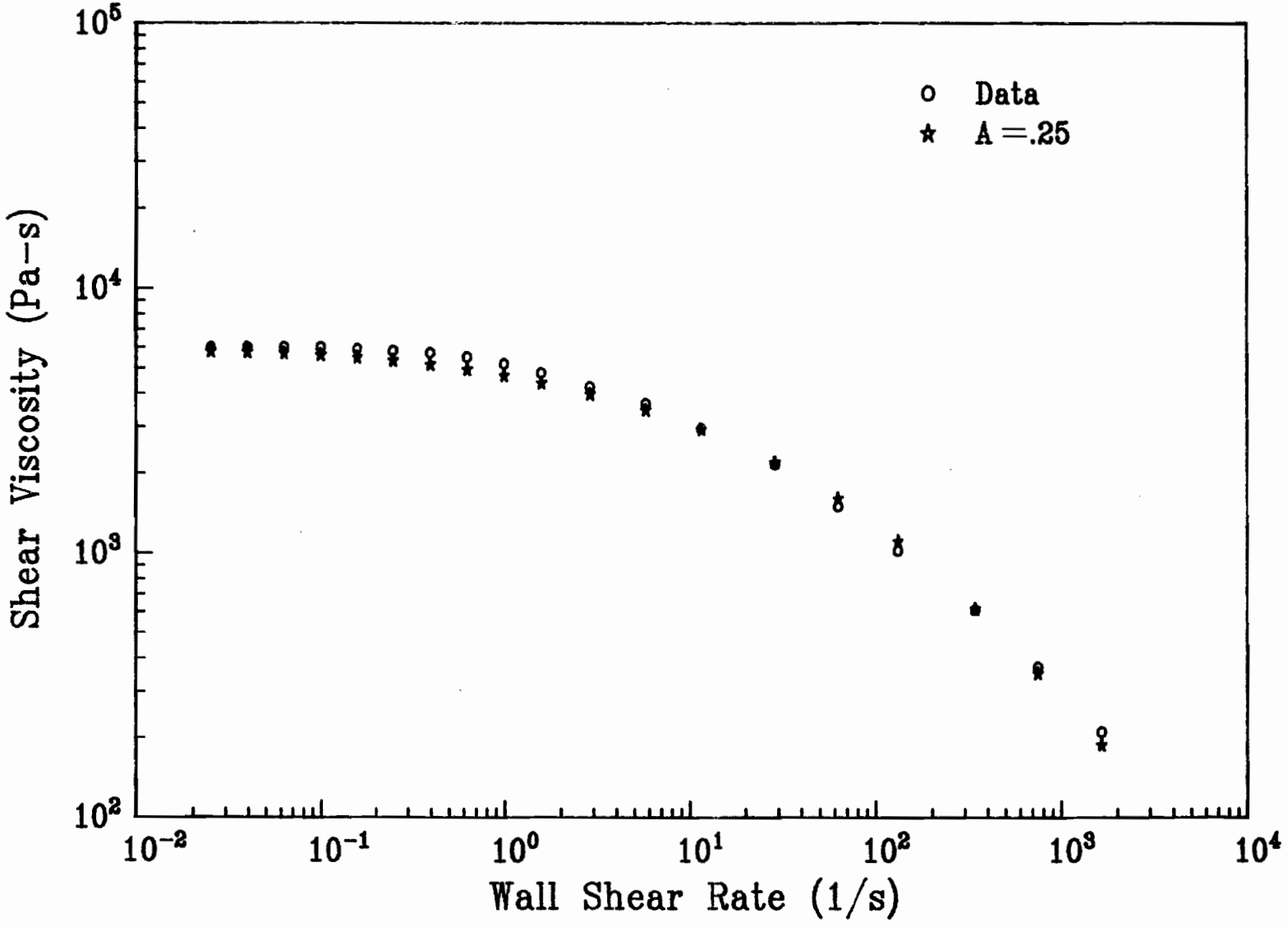

Figure 72: Acierno model predictions of shear viscosity for resin 31 at 240°C.

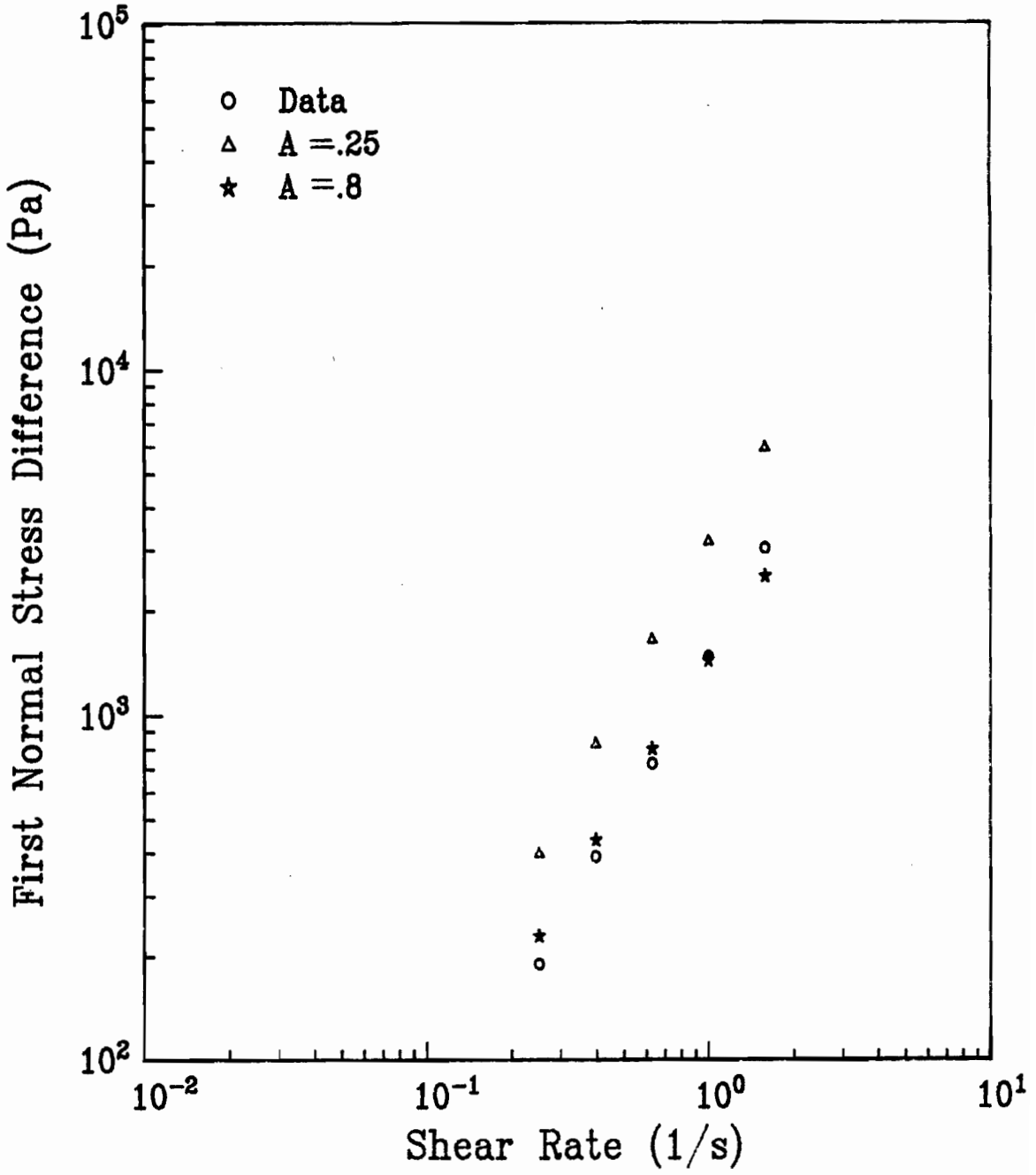

Figure 73: Acierno model predictions of normal stress difference for resin 31 at 240°C.

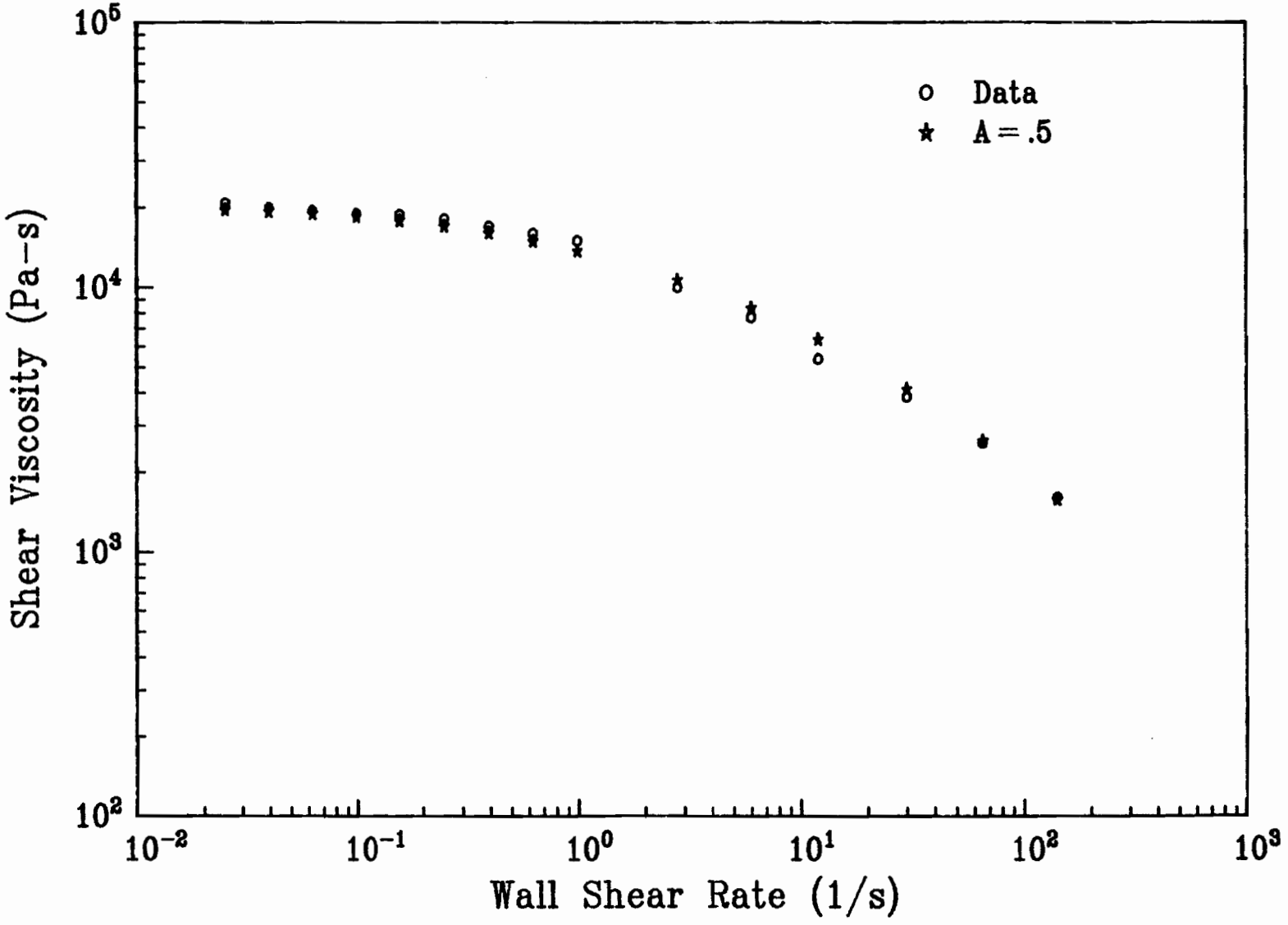

Figure 74: Acierno model predictions of shear viscosity for resin 33 at 190°C.

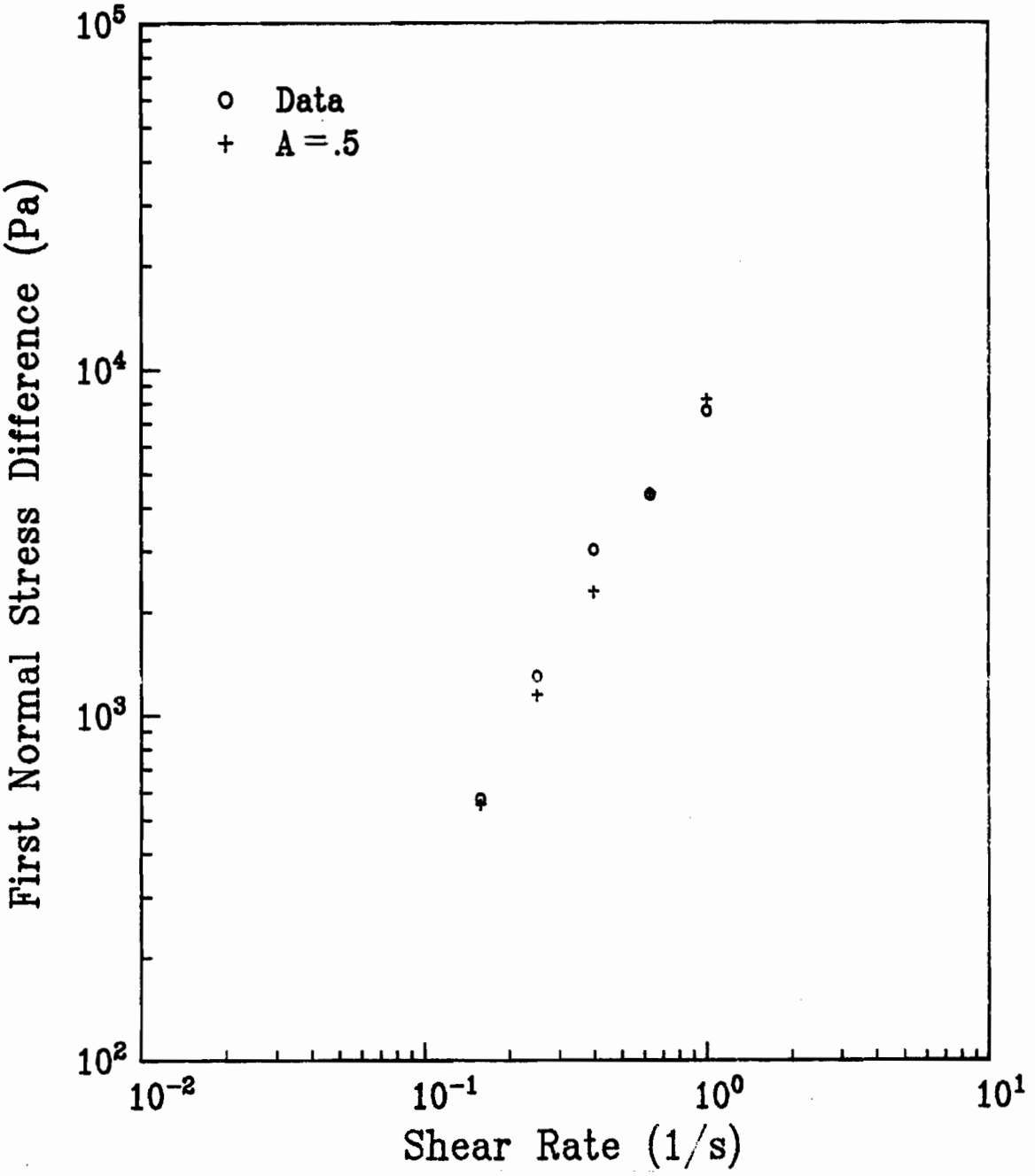

Figure 75: Acierno model predictions of normal stress difference for resin 33 at 190°C.

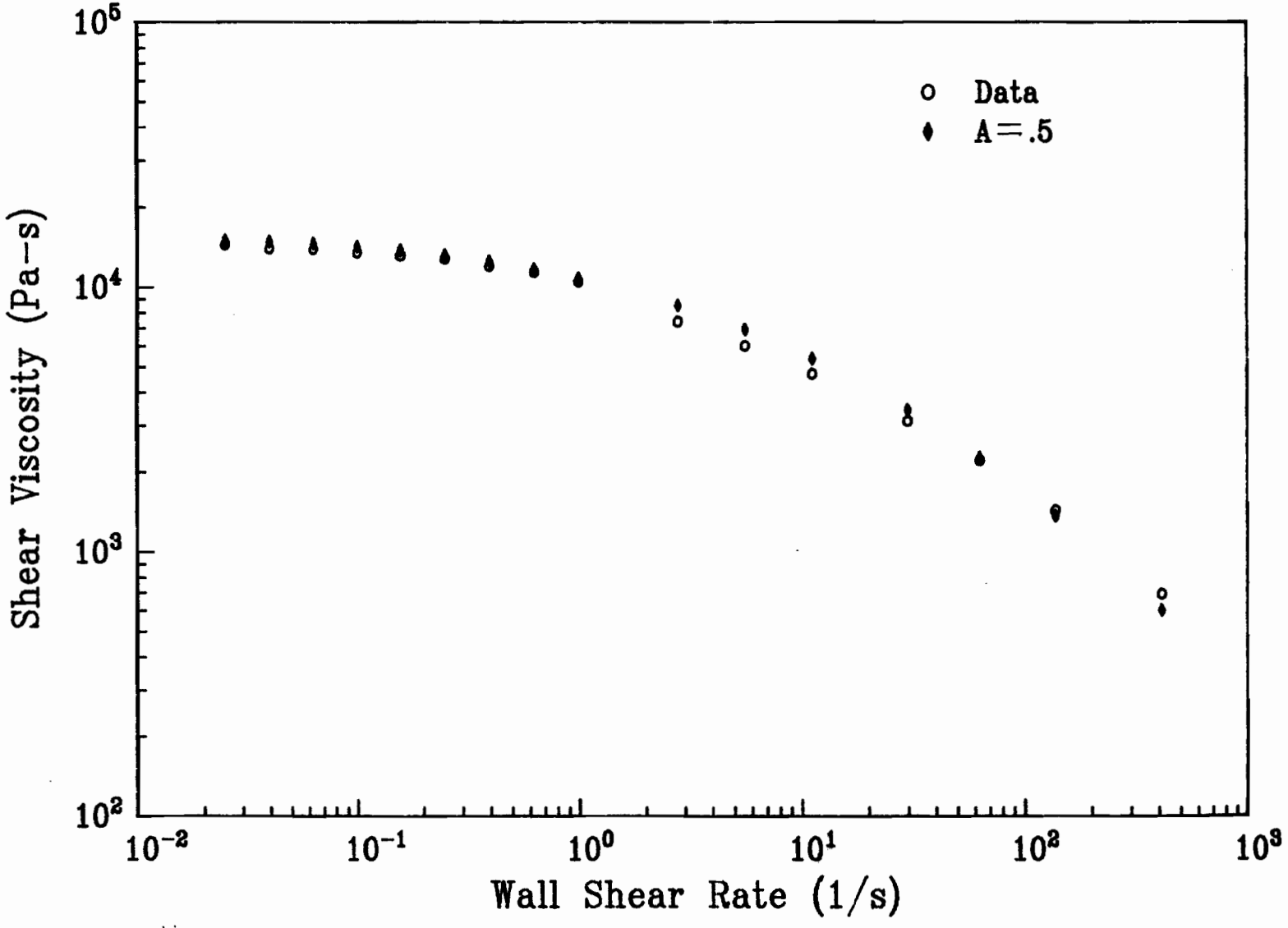

Figure 76: Acierno model predictions of shear viscosity for resin 33 at 210°C.

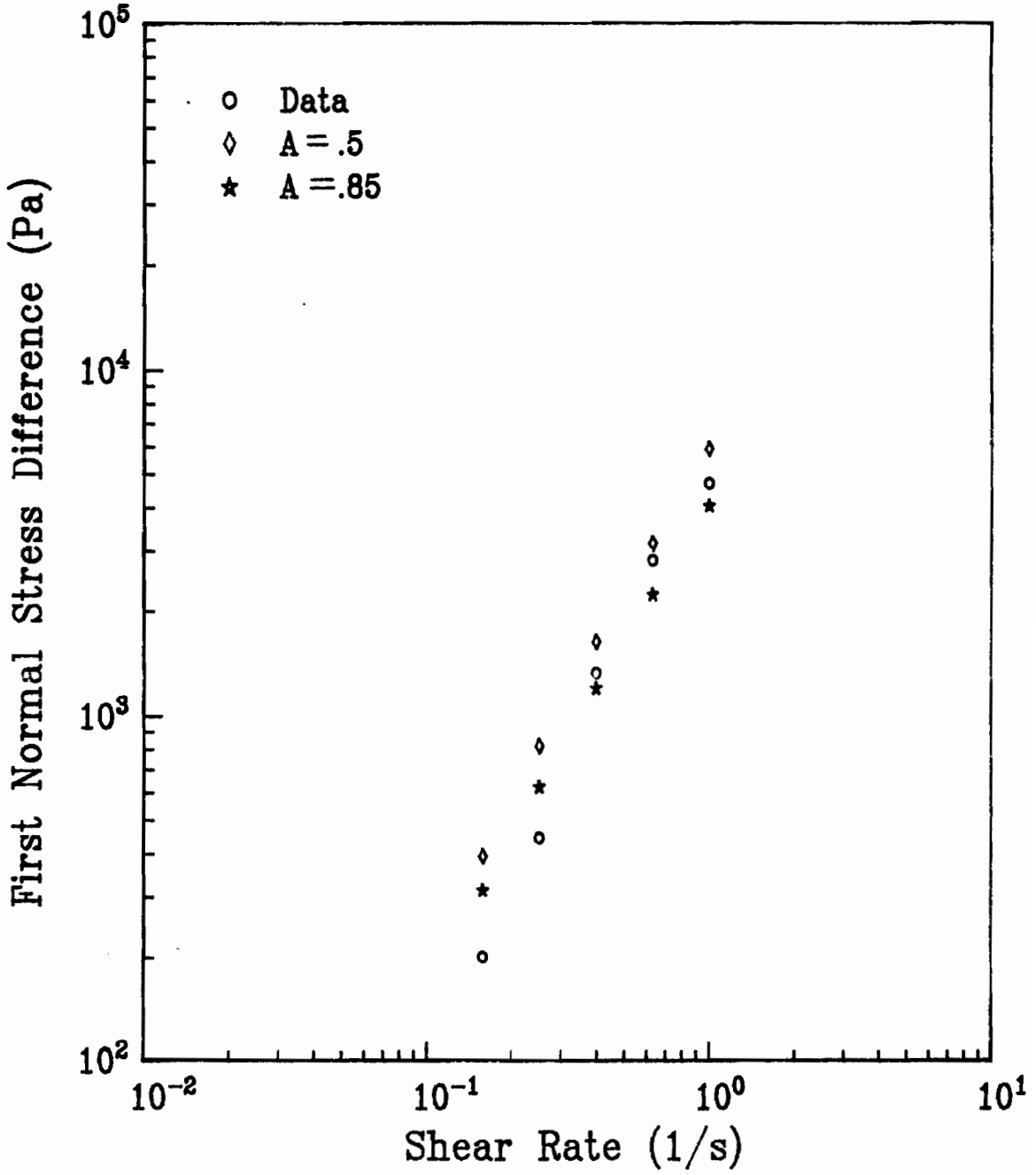

Figure 77: Acierno model predictions of normal stress difference for resin 33 at 210°C.

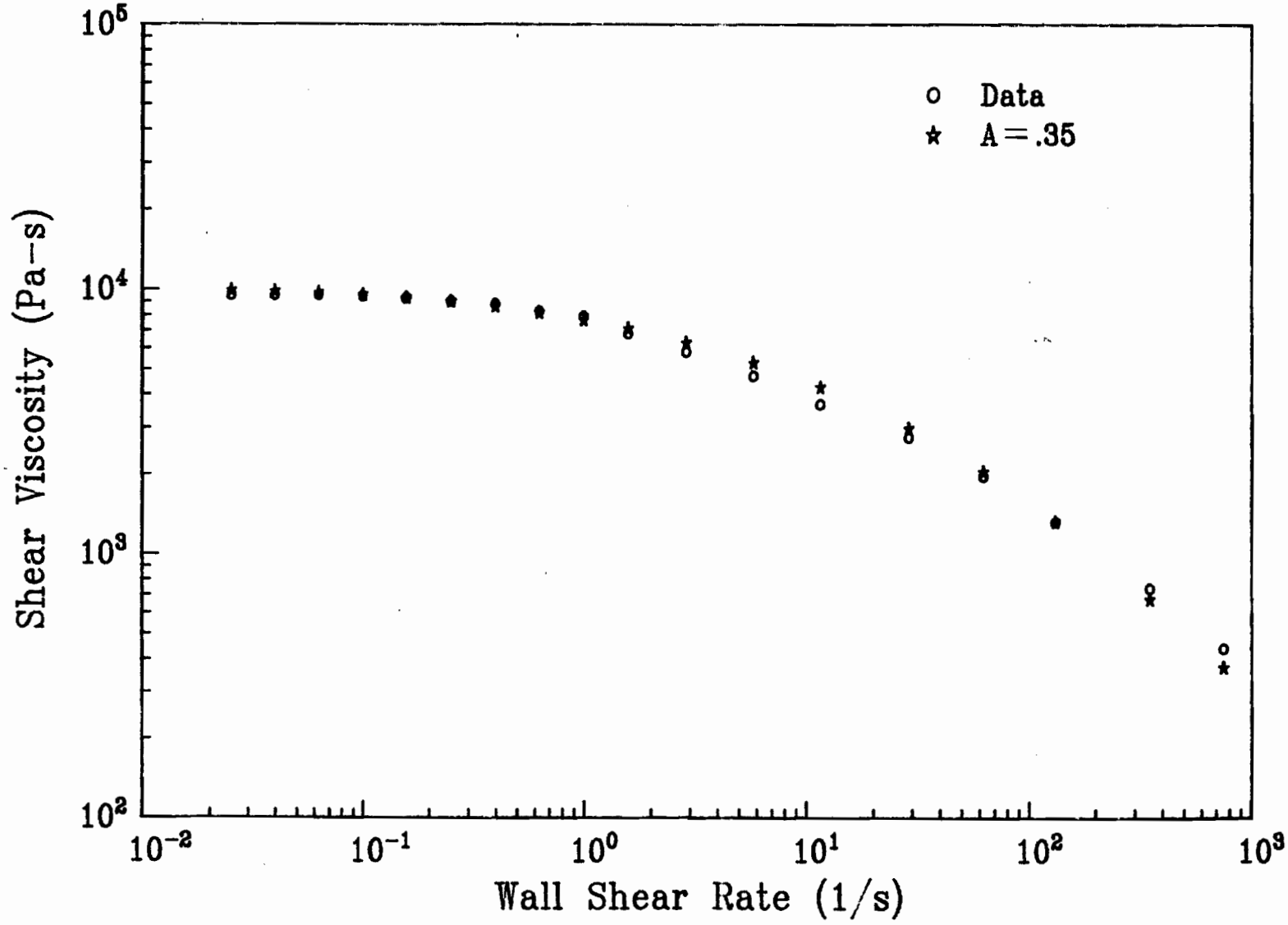

Figure 78: Acierno model predictions of shear viscosity for resin 33 at 240°C.

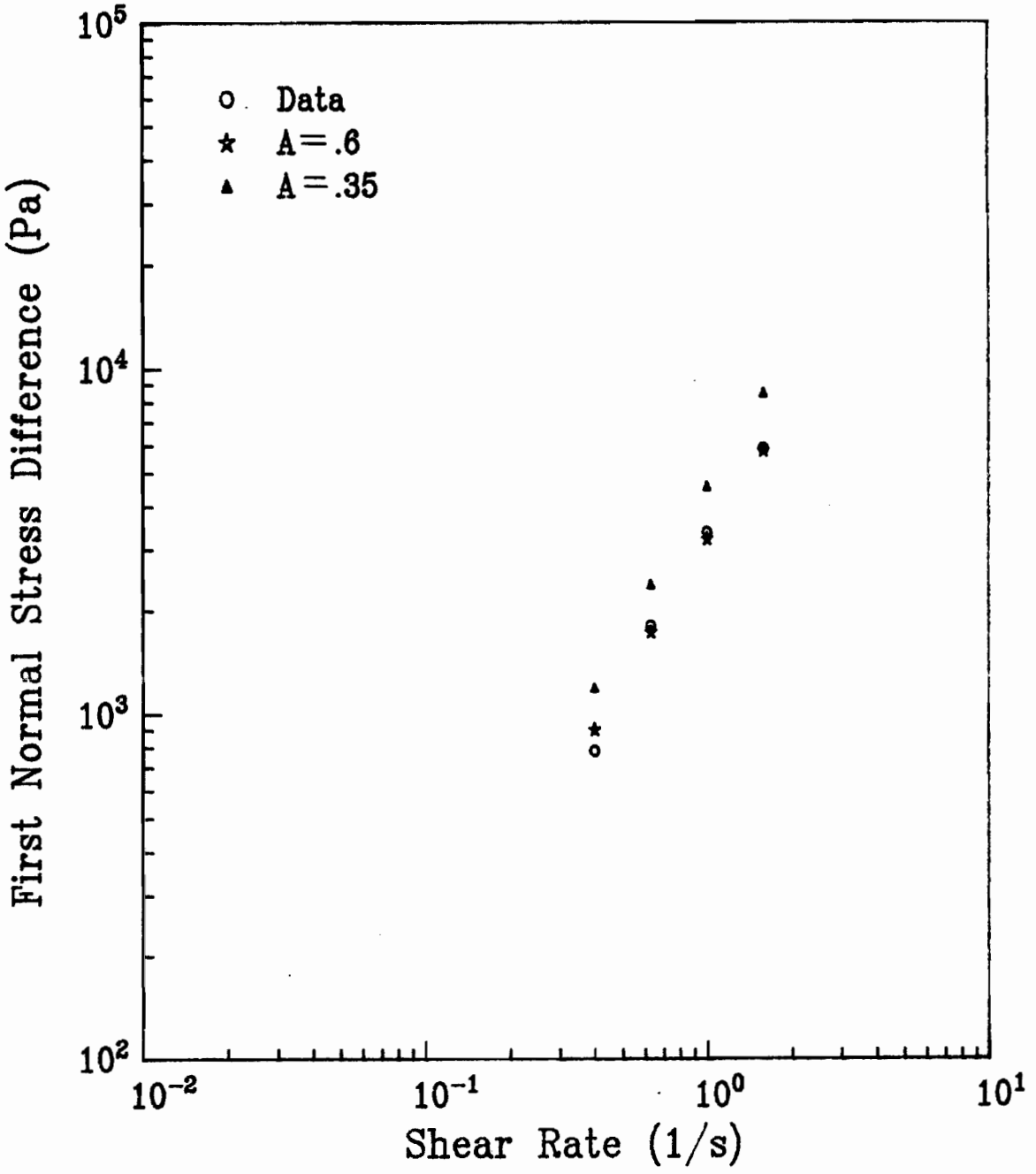

Figure 79: Acierno model predictions of normal stress difference for resin 33 at 240°C.

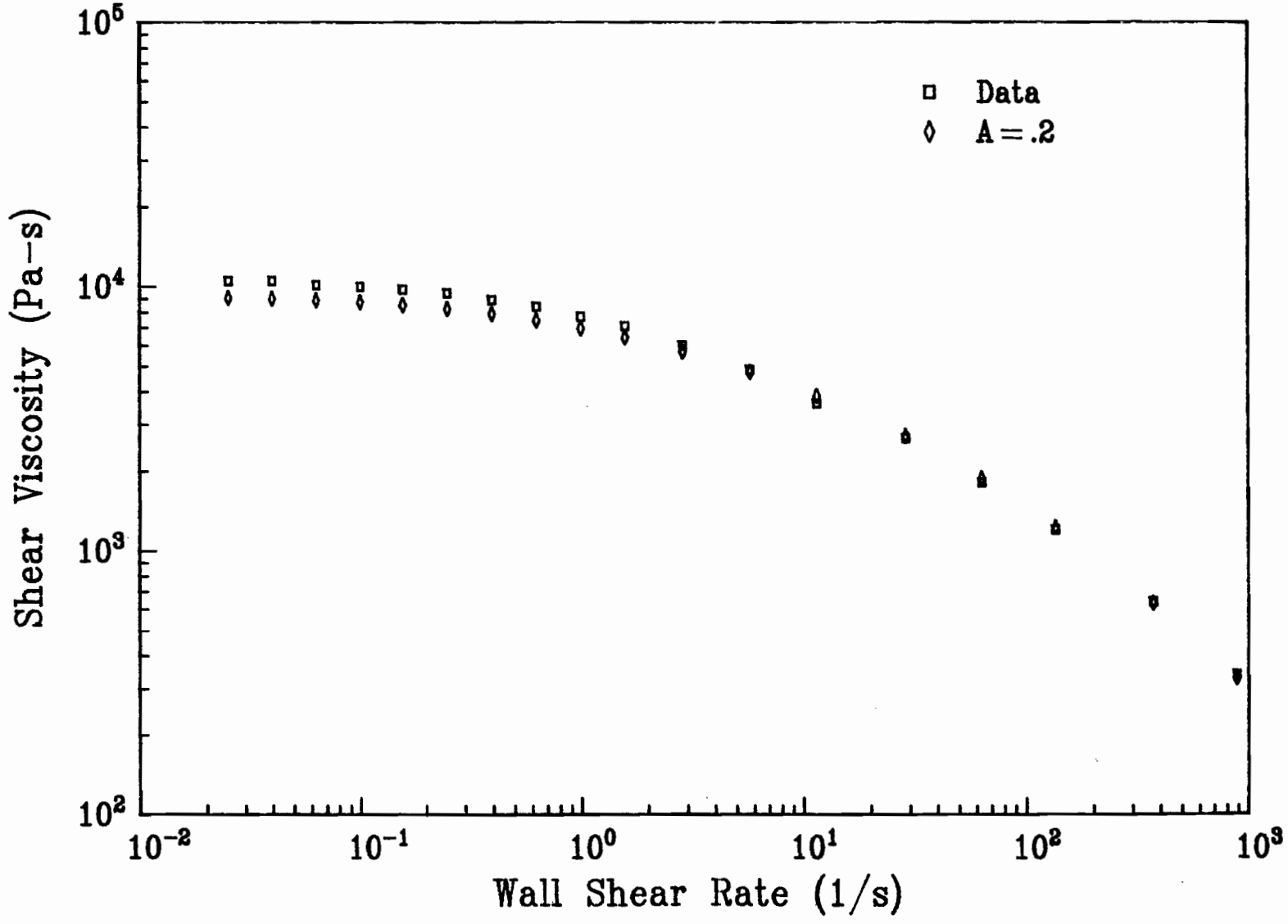

Figure 80: Acierno model predictions of shear viscosity for resin 30 at 190°C.

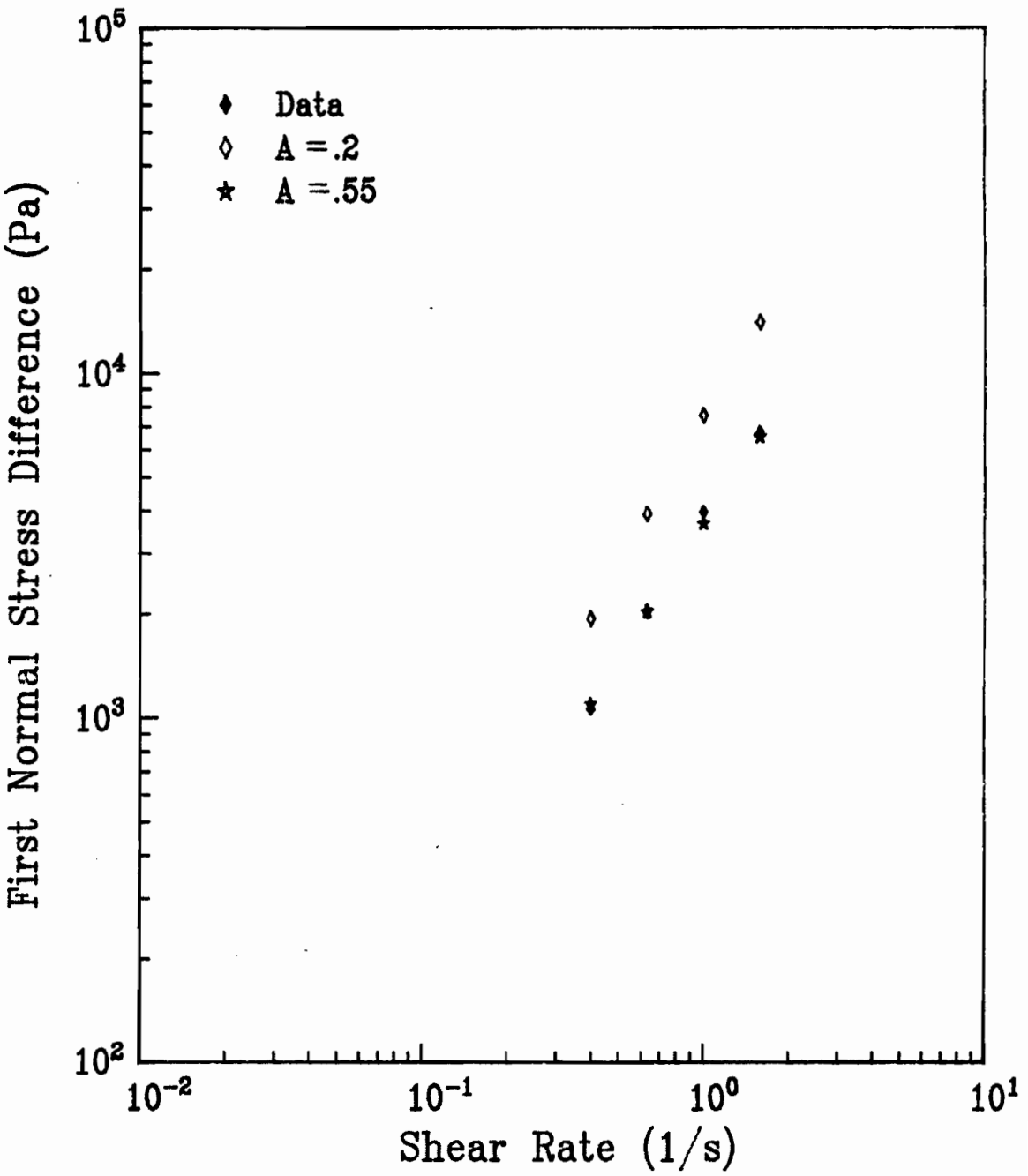

Figure 81: Acierno model predictions of normal stress difference for resin 30 at 190°C.

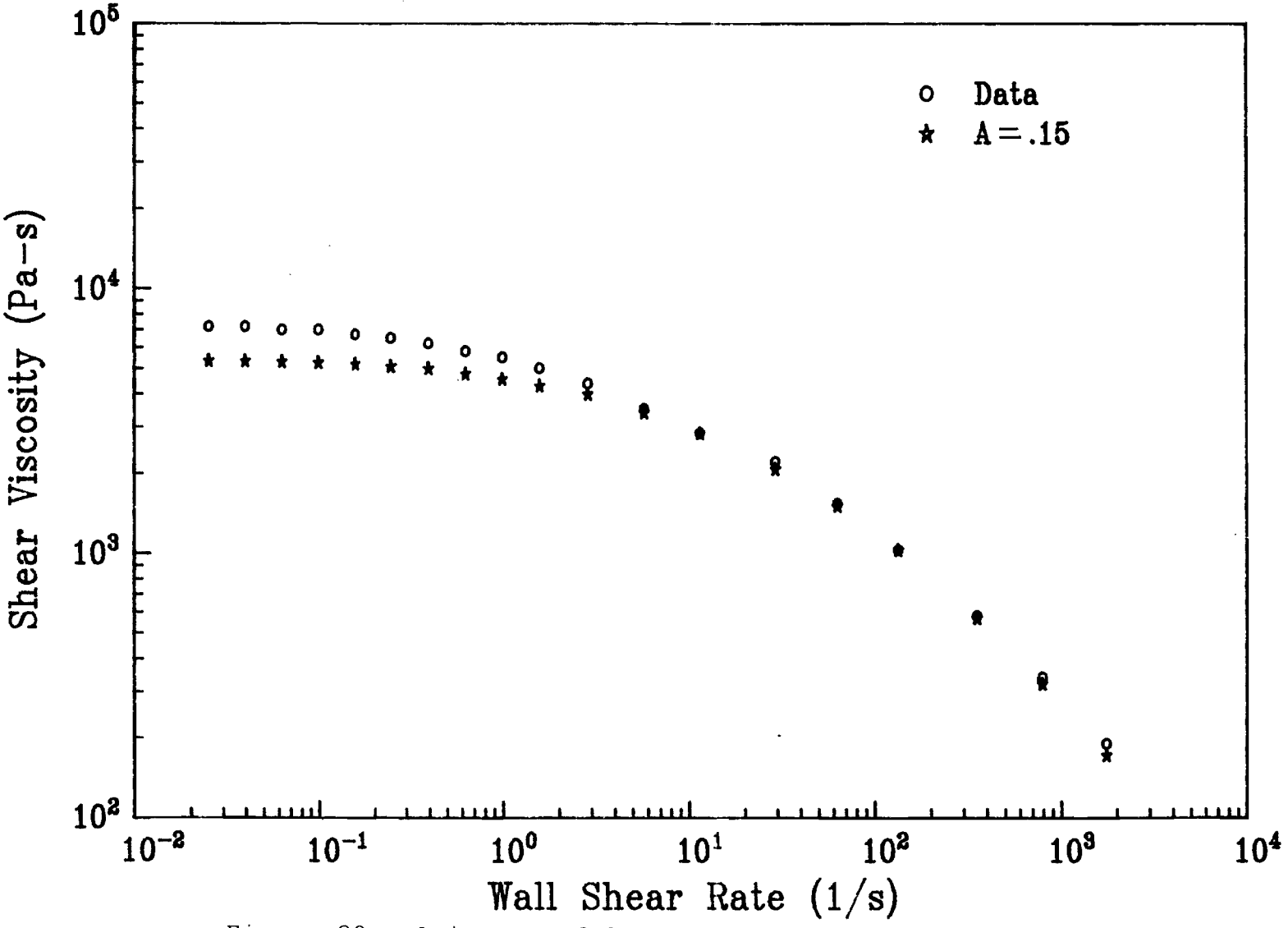

Figure 82: Acierno model predictions of shear viscosity for resin 30 at 210°C.

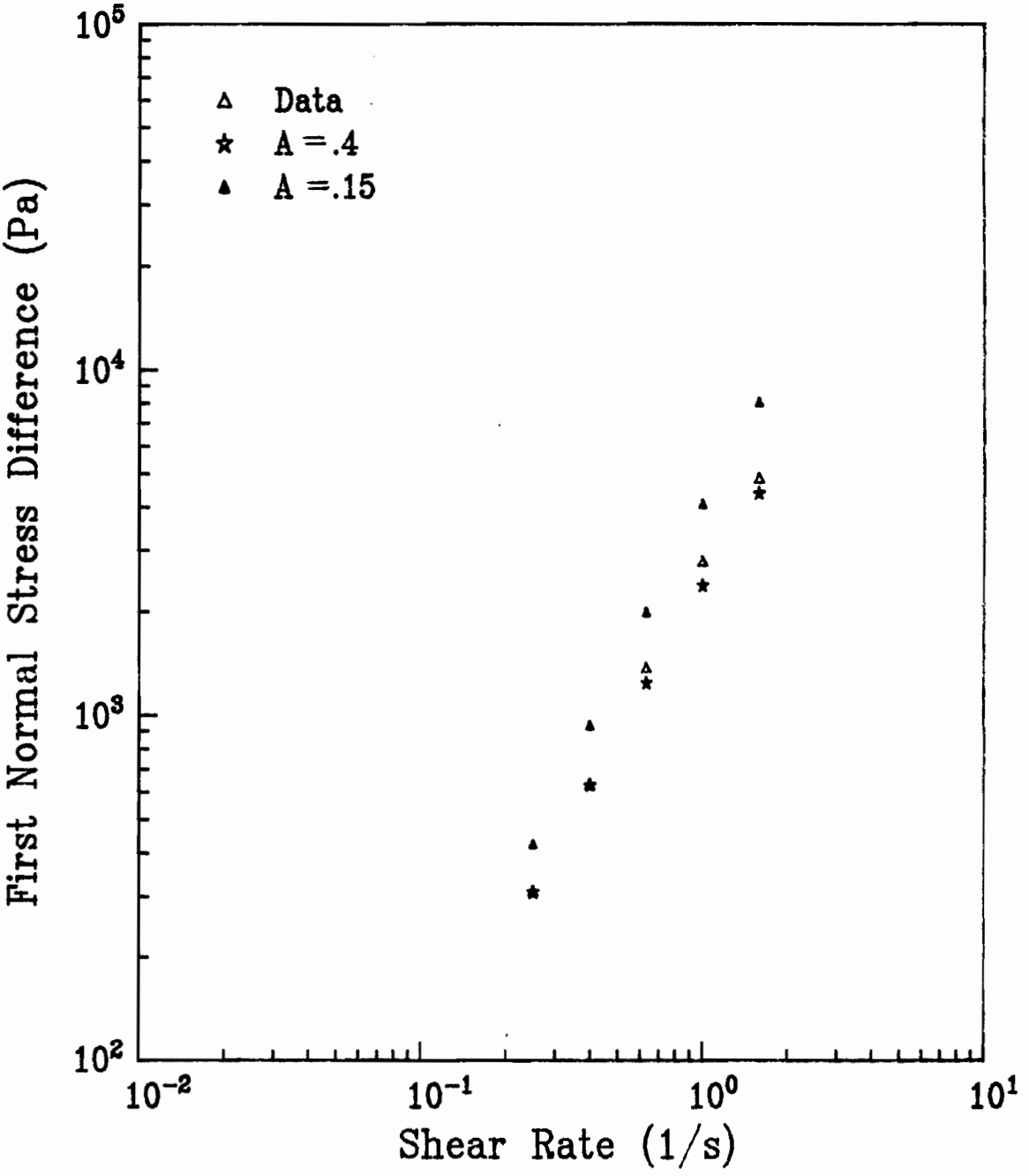

Figure 83: Acierno model predictions of normal stress difference for resin 30 at 210°C.

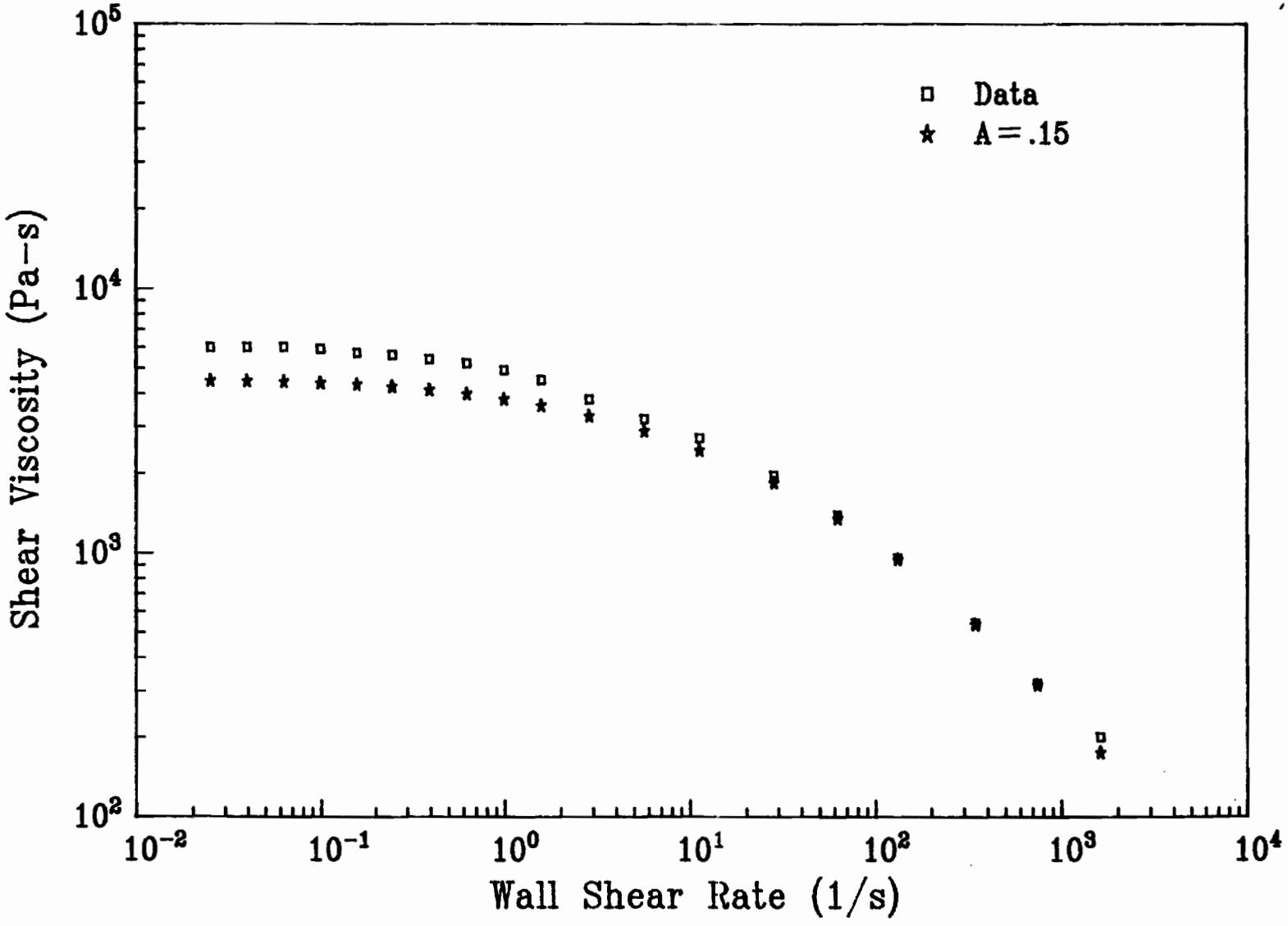

Figure 84: Acierno model predictions of shear viscosity for resin 30 at 225°C.

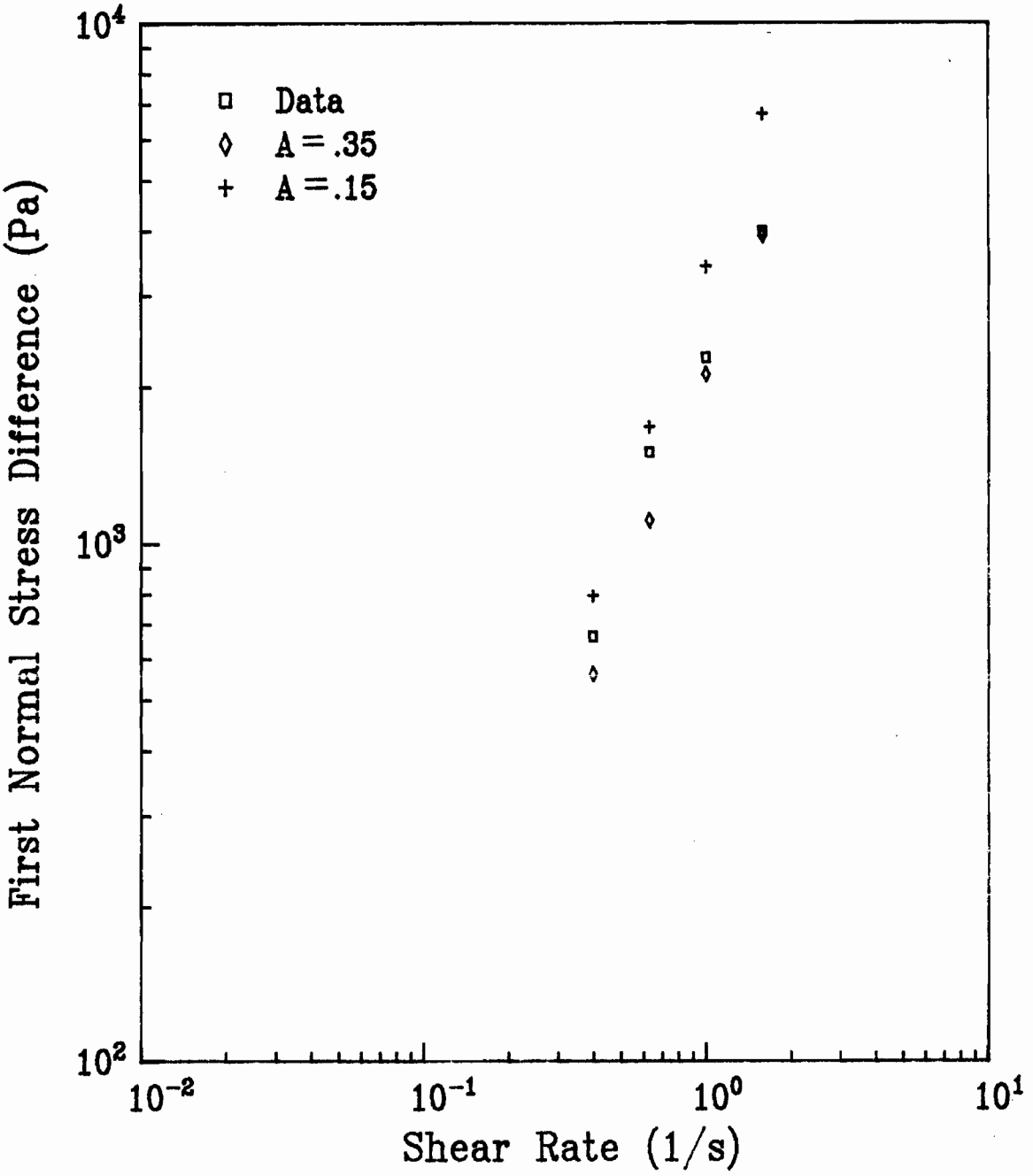

Figure 85: Acierno model predictions of normal stress difference for resin 30 at 225°C.

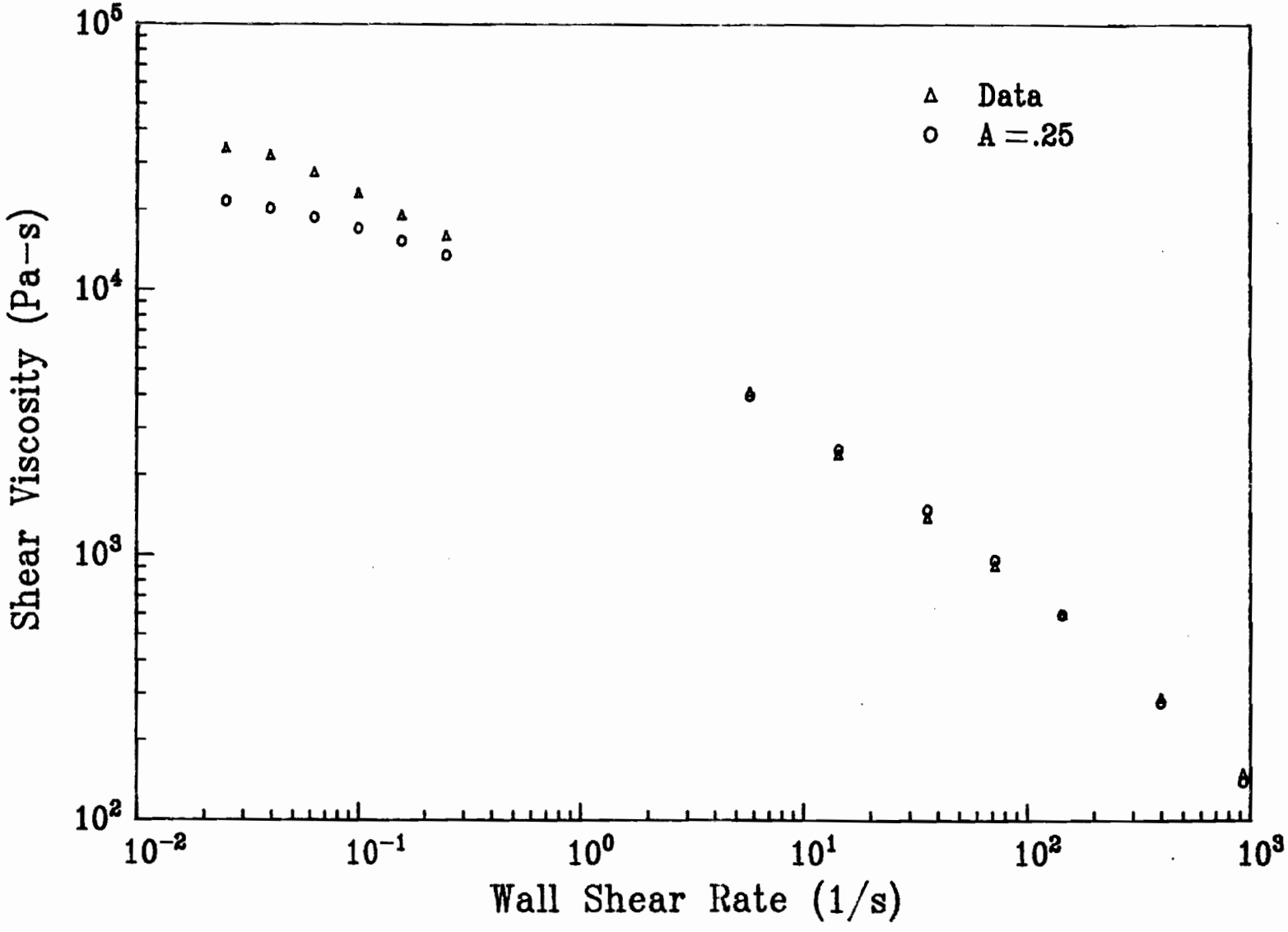

Figure 86: Acierno model predictions of shear viscosity for resin 32 at 190°C.

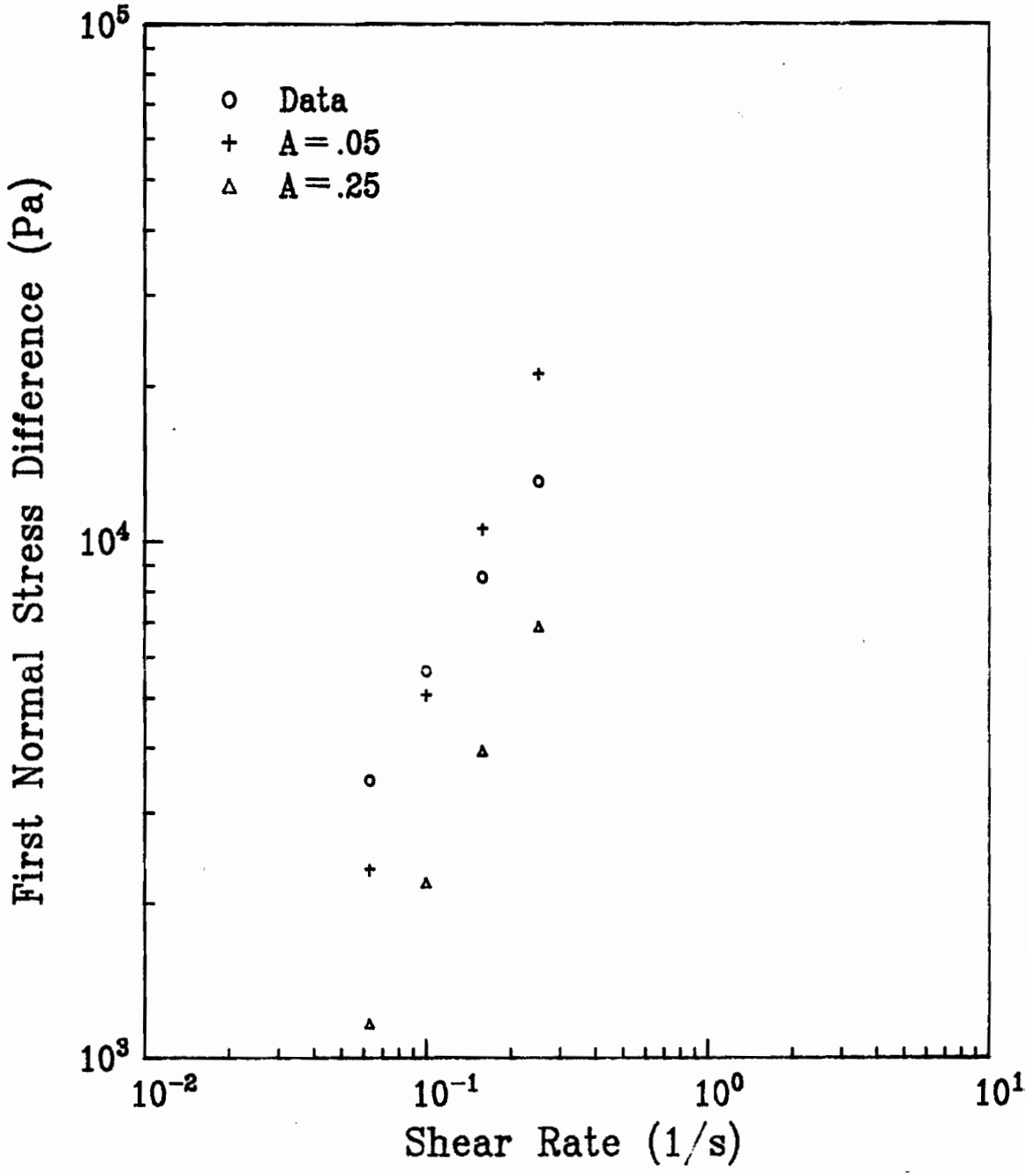

Figure 87: Acierno model predictions of normal stress difference for resin 32 at 190°C.

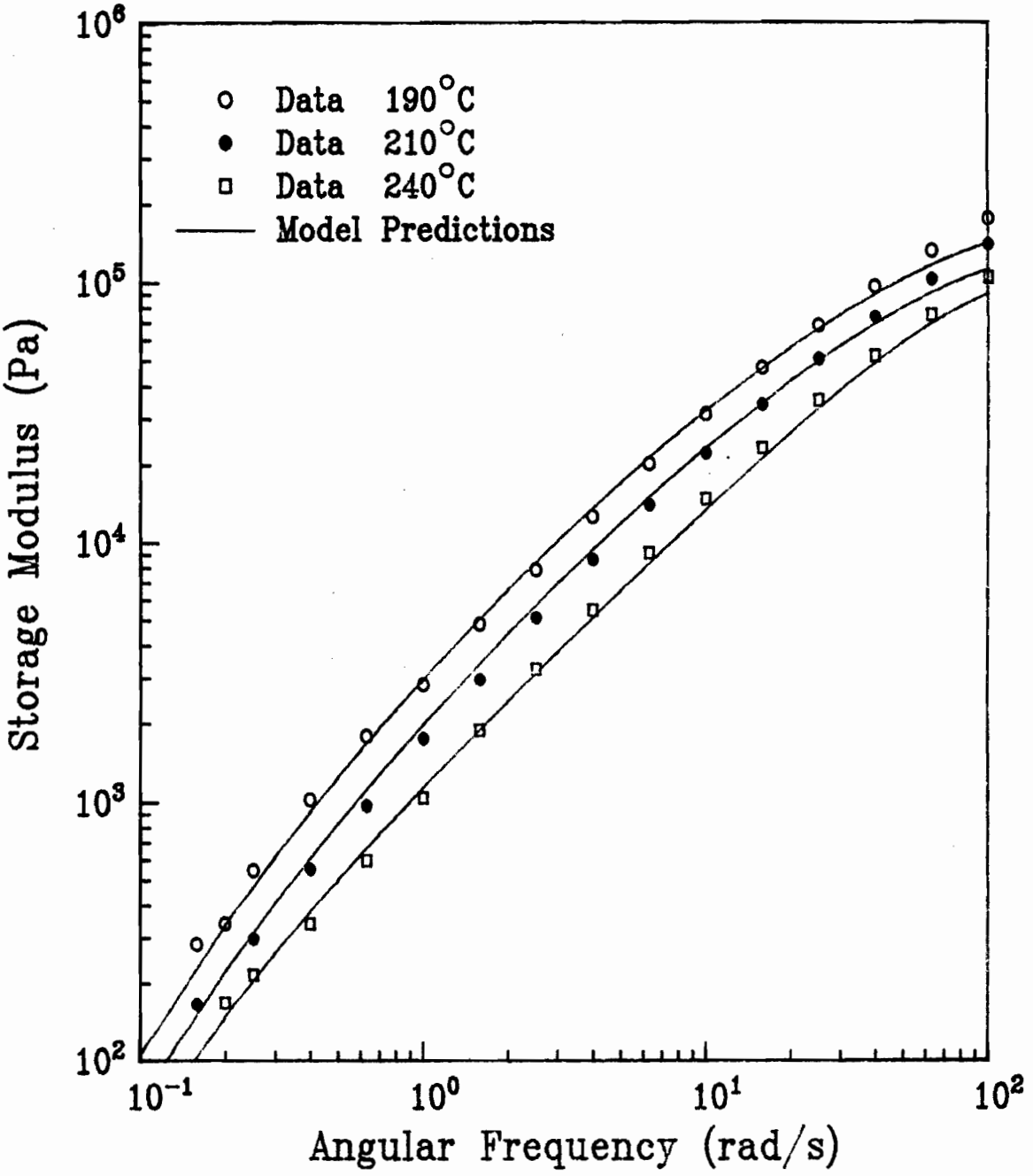

Figure 88: Linear viscoelastic theory prediction of storage modulus for resin 31.

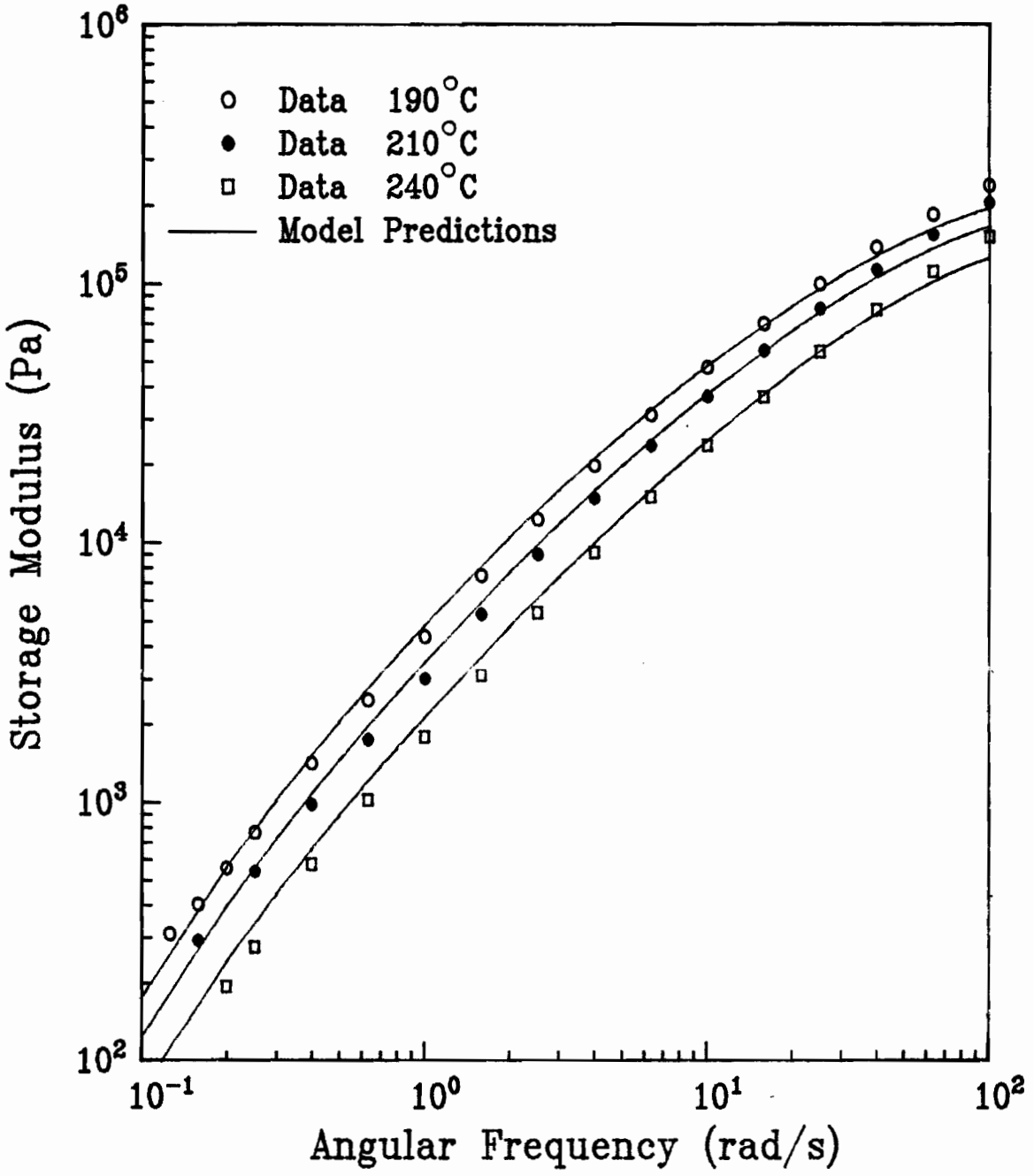

Figure 89: Linear viscoelastic theory prediction of storage modulus for resin 33.

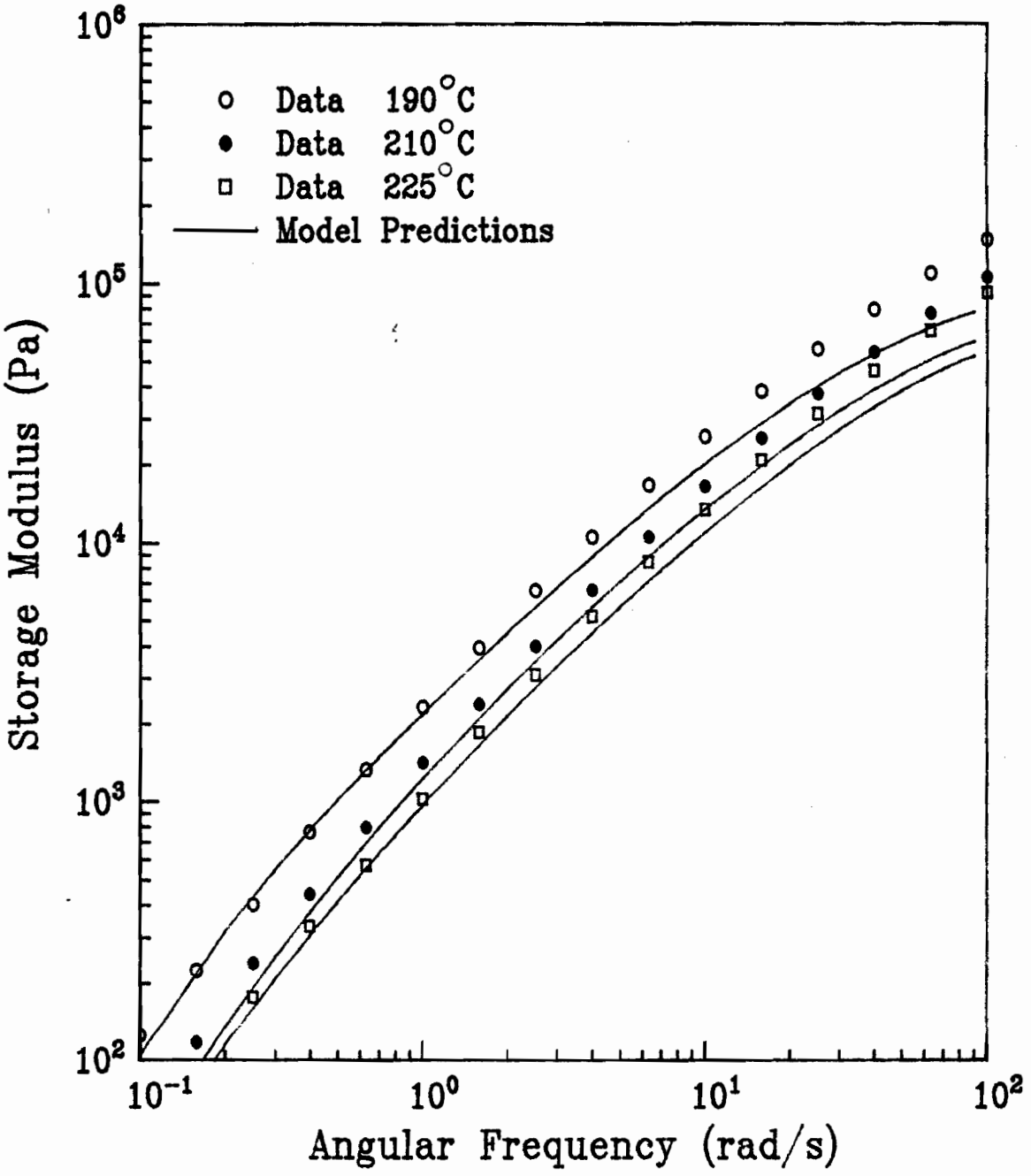

Figure 90: Linear viscoelastic theory prediction of storage modulus for resin 30.

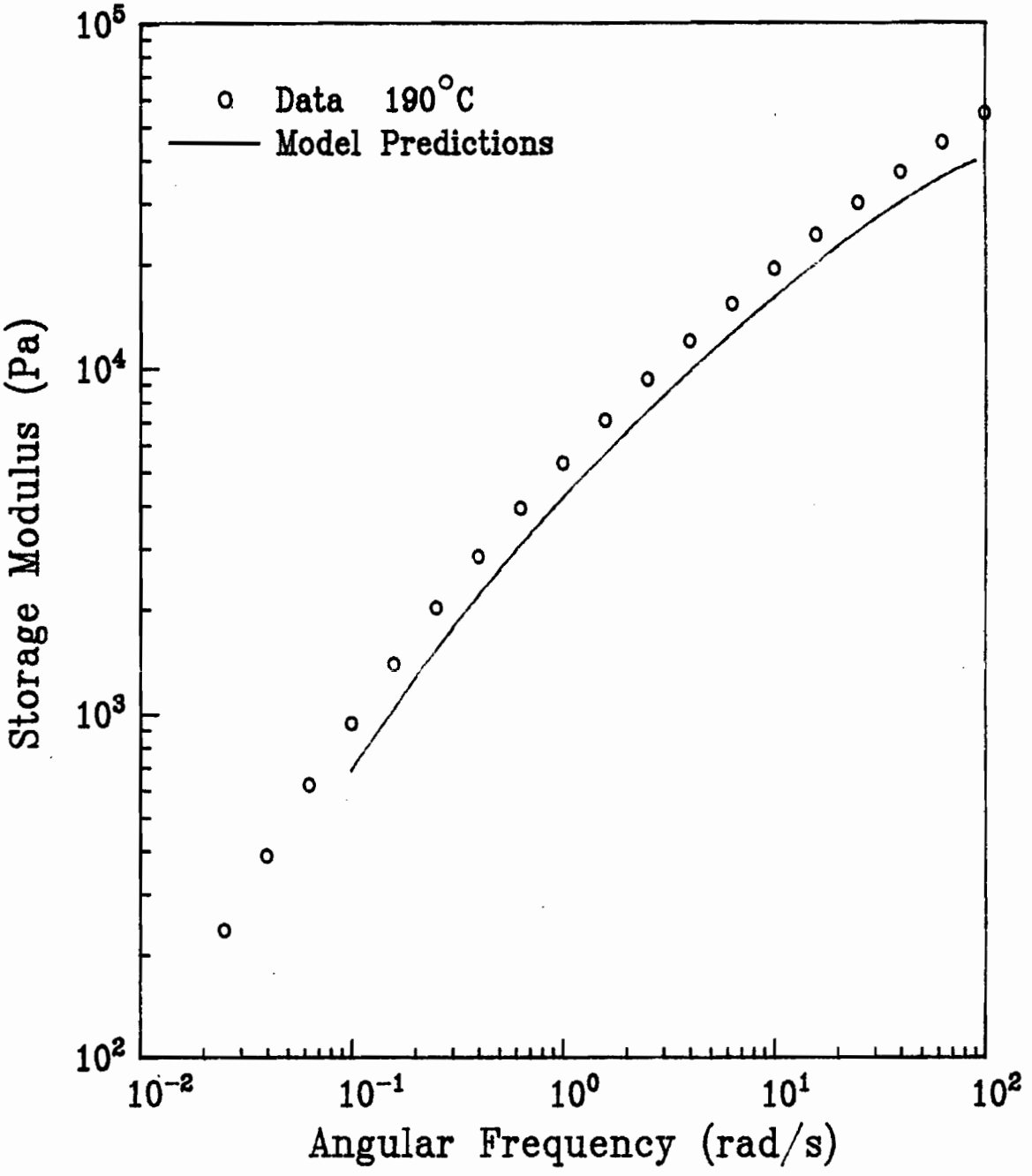

Figure 91: Linear viscoelastic theory prediction of storage modulus for resin 32.

$$G' = \sum_{i=1}^{\infty} \frac{H_i \lambda_i \omega^2}{1 + \omega^2 \lambda_i^2} \qquad (78)$$

This expression utilizes the same values of the relaxation times and moduli used in the prediction of steady shear behavior. The data and model predictions are compared in Figures 88-91. The qualitative agreement is generally good between the two, although in the case of resin 30 the model substantially underestimates the elasticity at high frequencies. The fact that the theoretical predictions tend to "flatten out" prematurely at high frequencies suggests that perhaps the longer relaxation times are overemphasized in the prediction.

5.5 Extrudate Swell Results

The density corrected extrudate swell ratios of the four resins are presented in Figures 92-94. Estimates of the melt density were made according to a method developed by Olabisi et al. [150] and recommended by Utracki et al. [100]. The lowest shear rate at which measurements of the swell ratio were obtained was about 6 s^{-1}. At shear rates lower than this the extrudate exiting from the capillary moved so slowly that it solidified before entering the heated oil bath. The upper

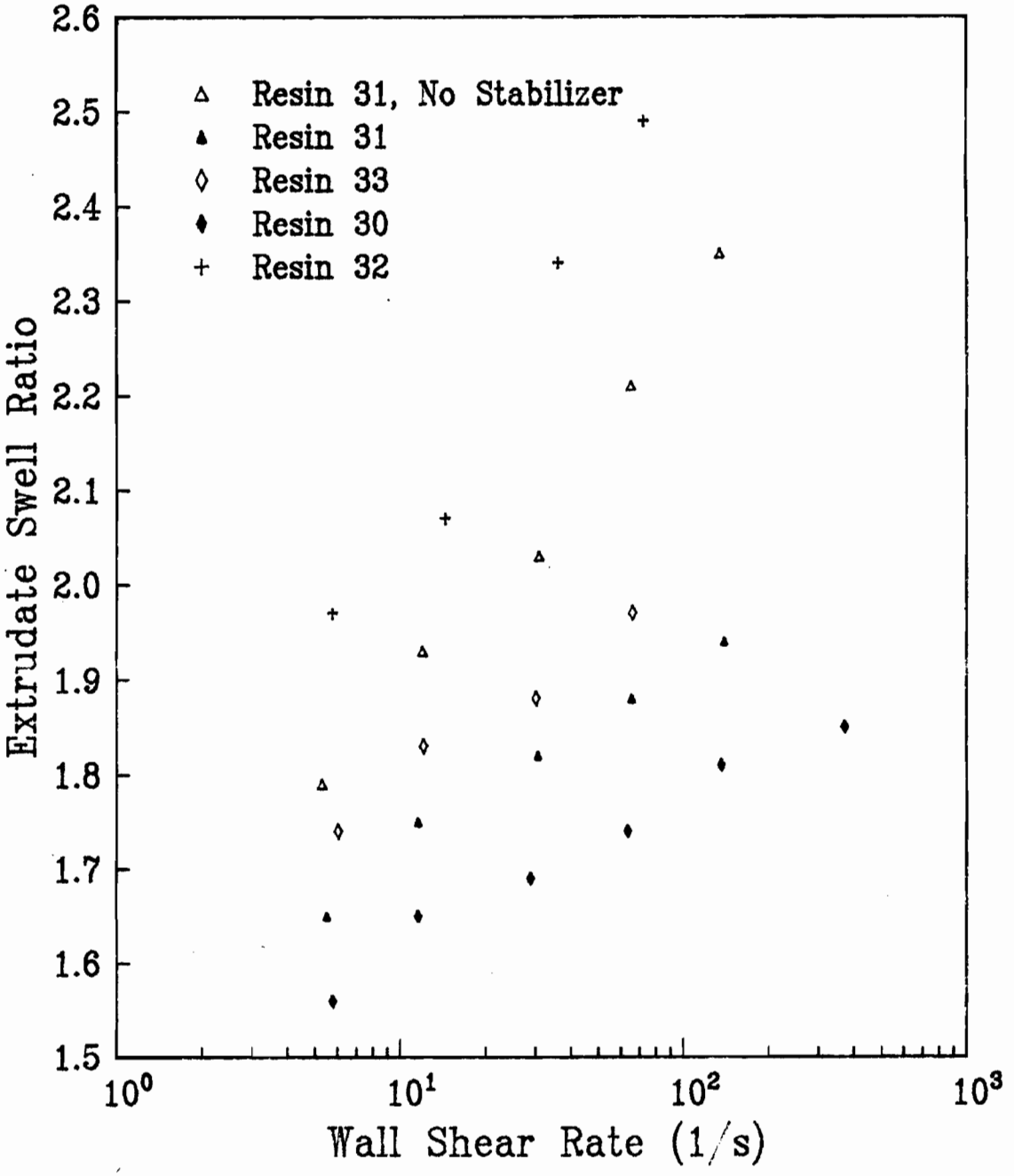

Figure 92: Extrudate swell as a function of wall shear rate at 190°C.

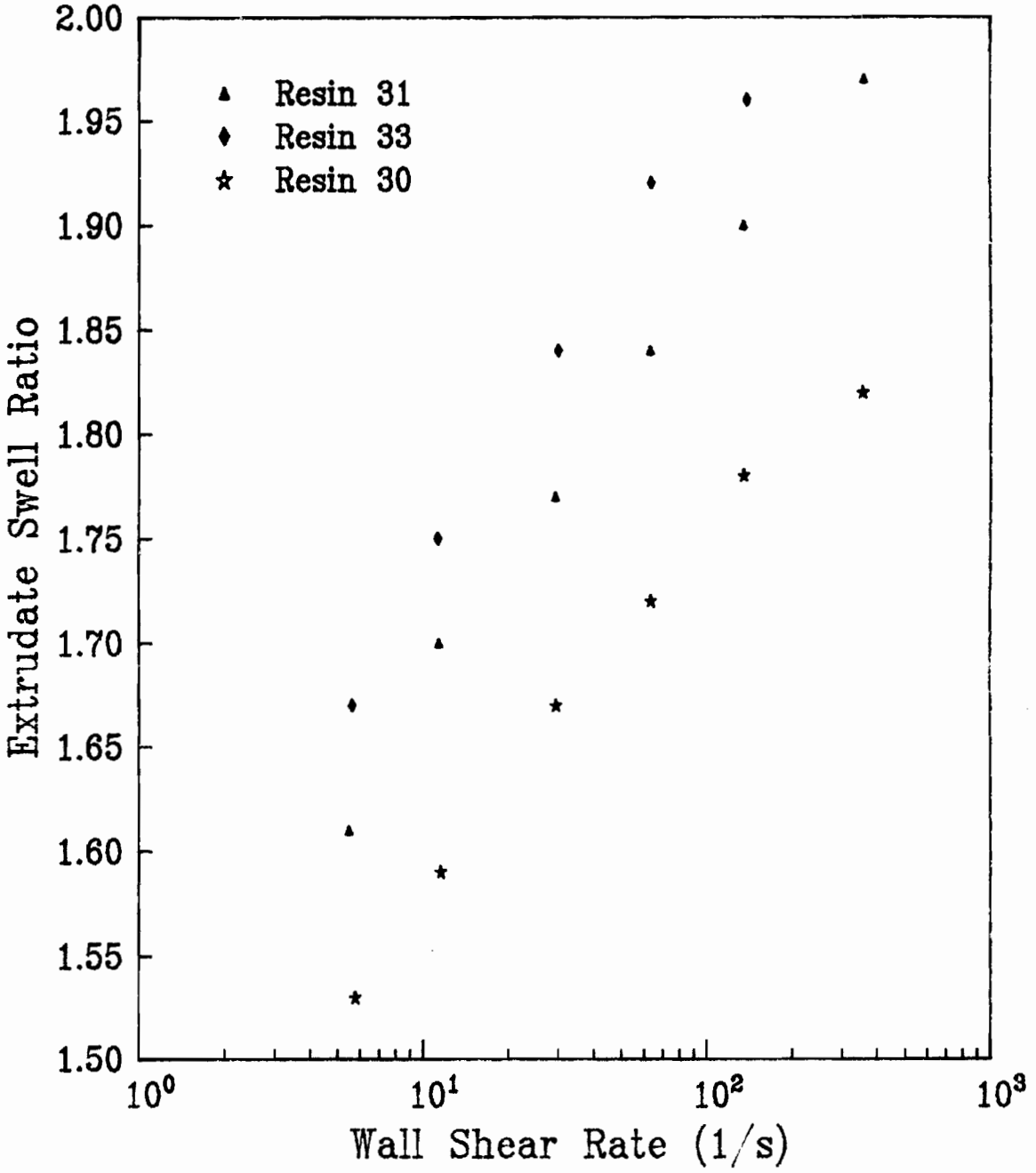

Figure 93: Extrudate swell as a function of wall shear rate at 210°C.

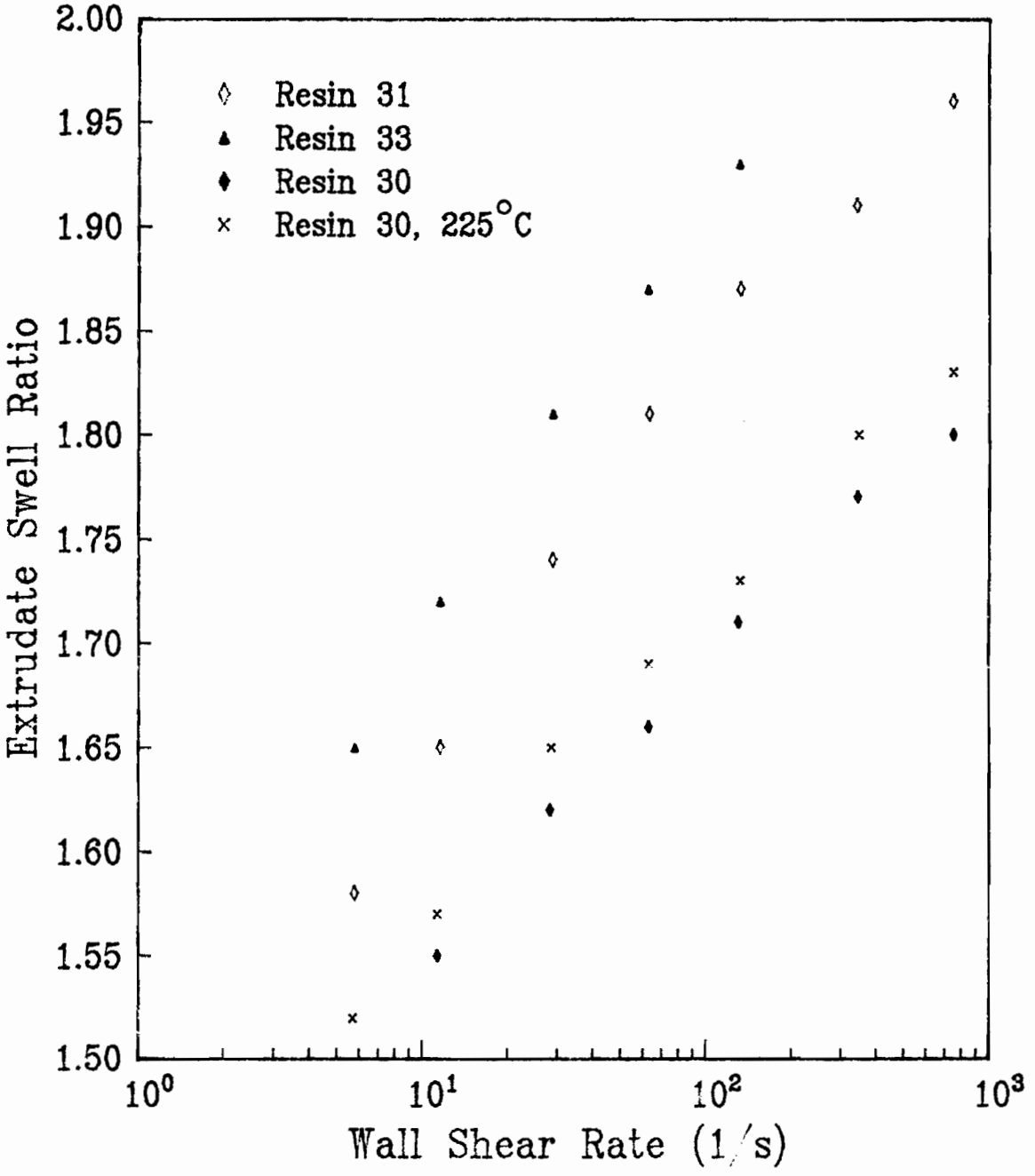

Figure 94: Extrudate swell as a function of wall shear rate at 240°C.

limit at which measurements could be made was dictated by the onset of flow instabilities. Thus, the highest shear rates at which swell data are reported are those at which extrudate distortion were first observed. These results are discussed in further detail in the next sections.

The resins exhibited increased degrees of swell in the following order: 30, 31, 33, and 32. Apparent in Figure 92 is the strong dependance the swell ratio of resin 32 had on shear rate in comparison to the LLDPE resins. The higher values of the swell ratio of the LDPE resin as compared to LLDPE resins have been observed by other workers [33,118] and are attributed to the presence of long chain branching and the wider molecular weight distributions of LDPE resins [30,58]. These results are in qualitative agreement with the first normal stress difference data in that they both suggest that resin 33 is the most elastic of the LLDPE 's followed by resins 31 and 30.

Based on the observation that as these LLDPE resins degrade, the value of the storage modulus, G', increased, it was concluded that the resins tended to become more elastic. This is nicely confirmed at high shear rates in Figure 92 where the swell data for an unstabilized sample of resin 31 are presented. The increase in elasticity due to degradation is manifested in swell ratios substantially higher (by 10 to

60%) than for the stabilized resin. Not only are the swell values higher, but the swell ratio seems to have a much stronger shear rate dependance as well (although this may also be a result of the different thermal histories of polymer samples). In all of the swell experiments, roughly 10 minutes elapsed between the time the polymer sample was inserted into the Instron Capillary Rheometer (ICR) barrel and the first swell sample was taken. Subsequently, samples could be taken every couple of minutes. Thus a series of measurements at different shear rates would typically subject the polymer samples to the extrusion temperature for between 20 and 25 minutes.

It had been mentioned earlier (see section on degradation experiments) that although it was not possible to adequately stabilize resin 30 at 240 ^{o}C using the Irganox B561 stabilizer, it had been observed that shear viscosity data taken at this temperature using the ICR did not seem to be affected by the degradation. To test this further, swell measurements on resin 30 were made at 240 ^{o}C using the same stabilizer levels as used at 225 ^{o}C. These results are plotted in Figure 94 and, judging from them, it is not at all obvious that the degradation known to be occuring has a significant effect on the swell behavior. Presumably, the extent to which degradation is occurring does not have a strong effect on the swell behavior.

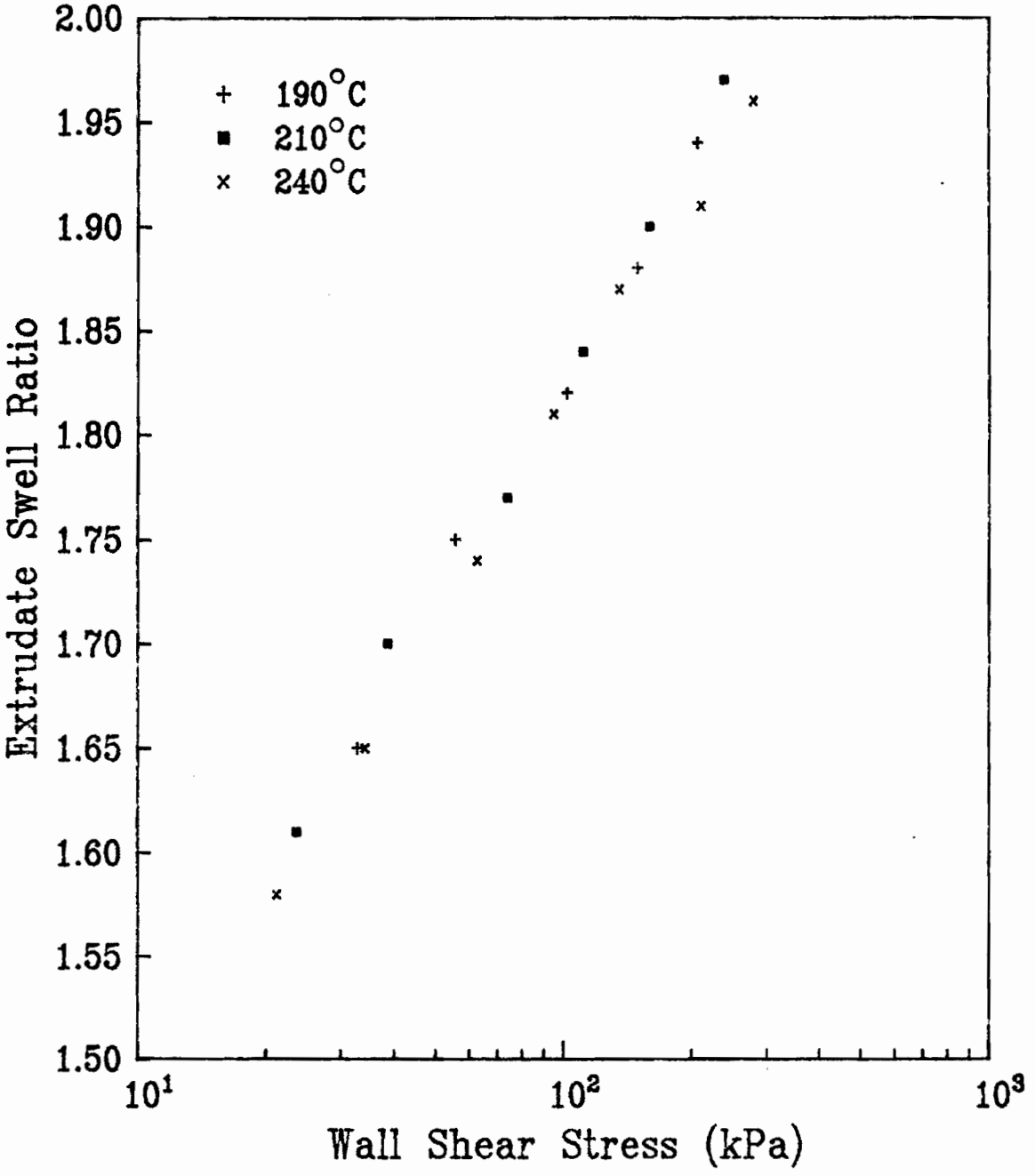

Figure 95: Extrudate swell as a function of wall shear stress for resin 31.

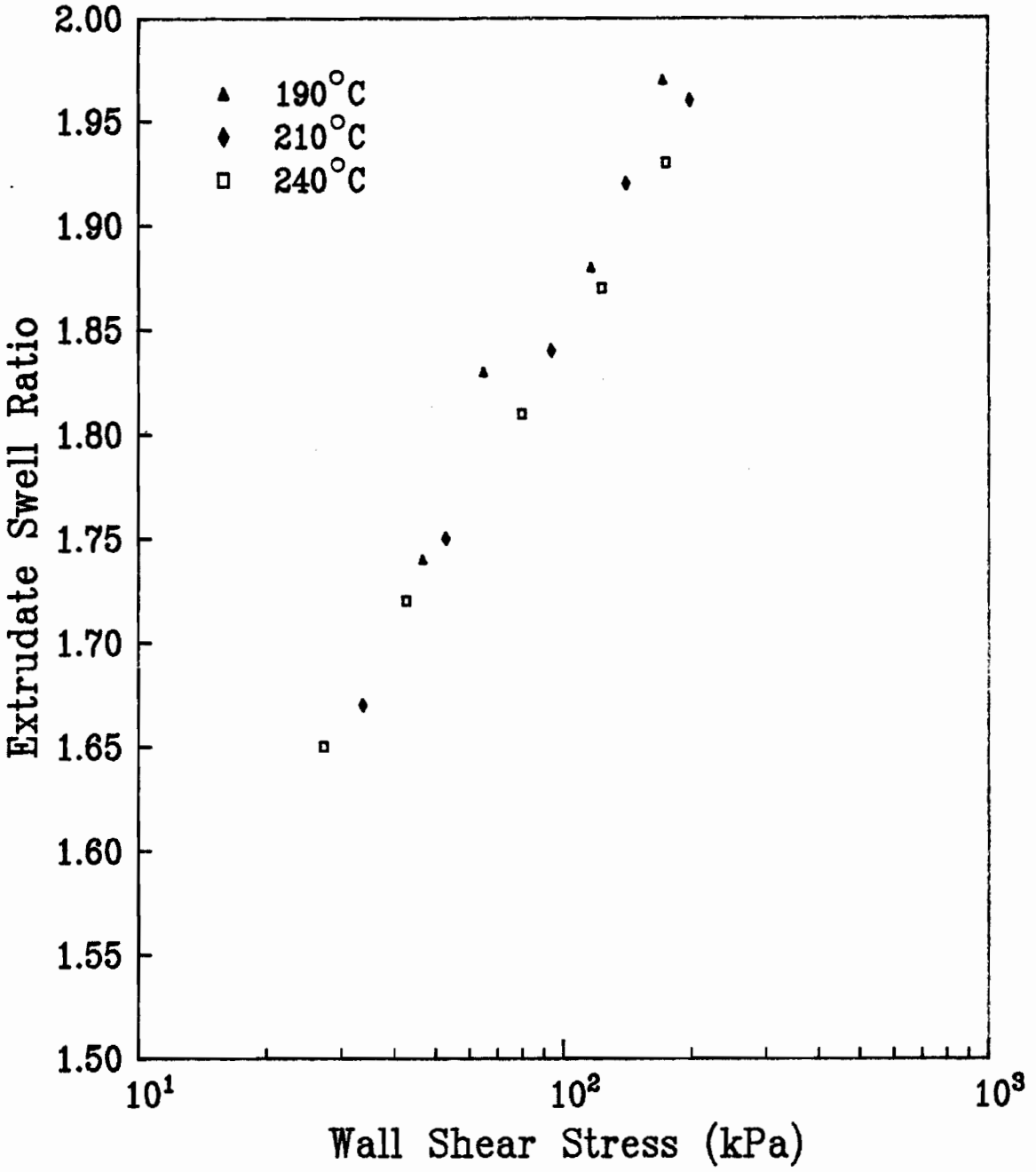

Figure 96: Extrudate swell as a function of wall shear stress for resin 33.

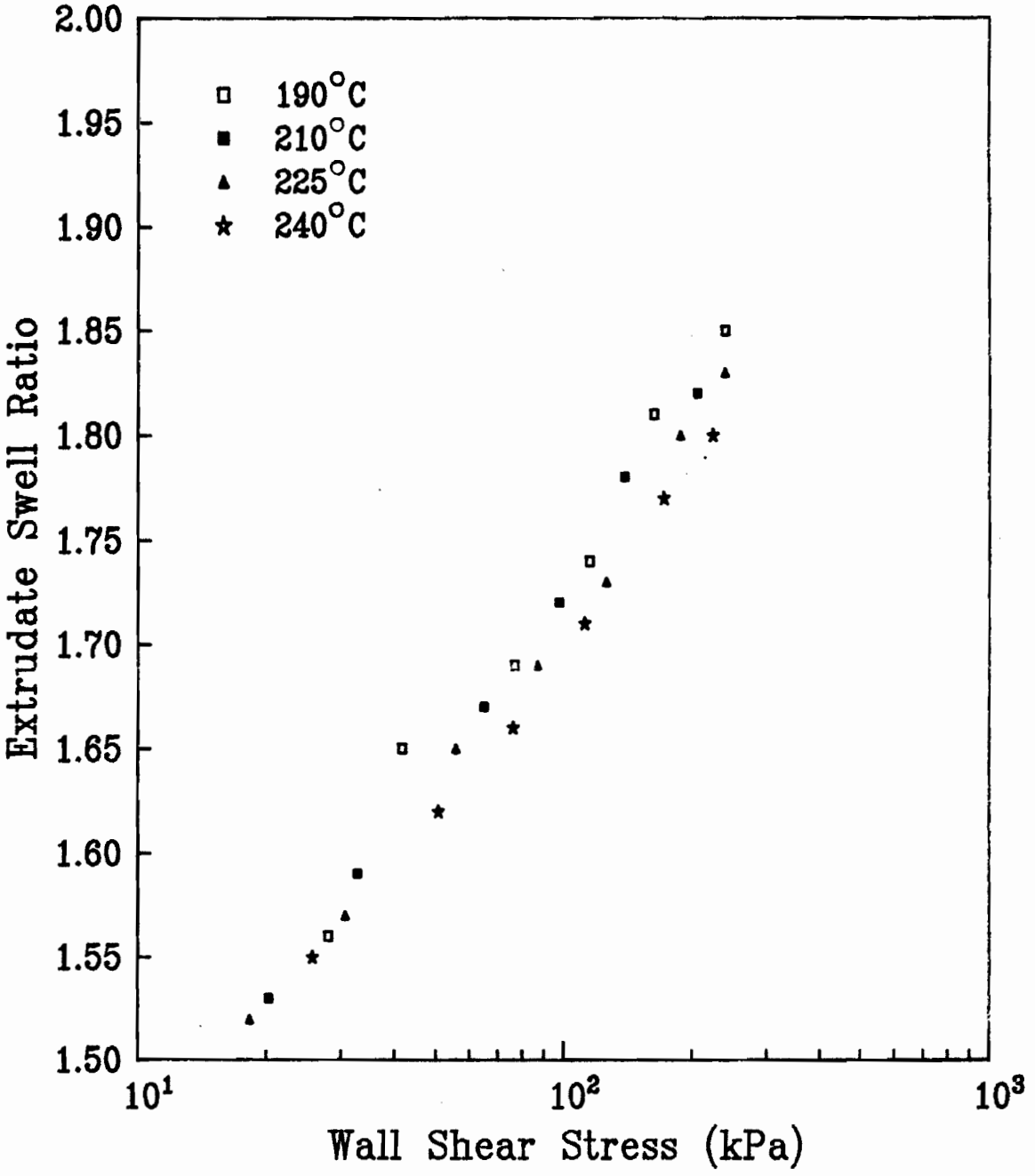

Figure 97: Extrudate swell as a function of wall shear stress for resin 30.

It has been suggested [30] that the swell data for a resin at different temperatures may be collapsed onto one curve if they are plotted against the wall shear stress rather that the shear rate. This is an inherently more useful way to present the data since only one curve is needed to describe data at several temperatures (in principle, at least). The data are compiled in this manner in Figures 95-97. As can be seen, the temperature parameter is quite effectively eliminated.

5.6 Extrudate Distortion Observations

5.6.1 Qualitative Observations

At certain values of the wall shear rate, all four resins exhibited various types of extrudate distortion. The distortions commence at higher shear rates as the extrusion temperature is increased. Unless otherwise noted, all samples and measurements were obtained with a 0.132 cm diameter capillary with an L/D ratio of 20 having a 90° entrance angle and fabricated from type 420 stainless steel.

In Figures 98-110 photographs of samples of extrudates taken at various wall shear rates and temperatures are presented. At 190 °C, the differences in behavior of the four

resins are evident. The very fine surface roughness known as "sharkskin" is present in LLDPE extrudates at shear rates starting as low as 66 s^{-1} with resin 33, while starting at about 140 and 370 s^{-1} for resins 31 and 30 respectively. In Figure 102 a photograph at 70X magnification of extrudates of resin 31 at 190 ^{o}C and 140 s^{-1} shows what this incipient sharkskin looks like. With the LLDPE resins, the sharkskin fracture becomes more evident at higher shear rates. An example of this higher shear rate roughness is shown in Figure 103; conditions are the same as for Figure 102 but the shear rate is higher. Note that the frequency of the surface roughness is less but the surface ridges are much larger than at lower shear rates. The regular surface roughness of LLDPE is in striking contrast to the gnarled distortion exhibited by resin 32 in Figure 100. These differences in behavior between branched and linear polyethylenes are well known [30,84,90]. Attalla et al. [123] and Utracki et al. [129] have also reported these differences in behavior between LDPE and LLDPE. Particularly interesting is the periodic transition from a smooth to rough extrudate surface for the LLDPE resins as the shear rate is increased. The shear rate at which this phenomenon first occurs increases as the extrusion temperature is increased. It was not observed with resin 30 in the shear rate range covered but was very evident in resins 31 and 33. This phenomenon is referred to as

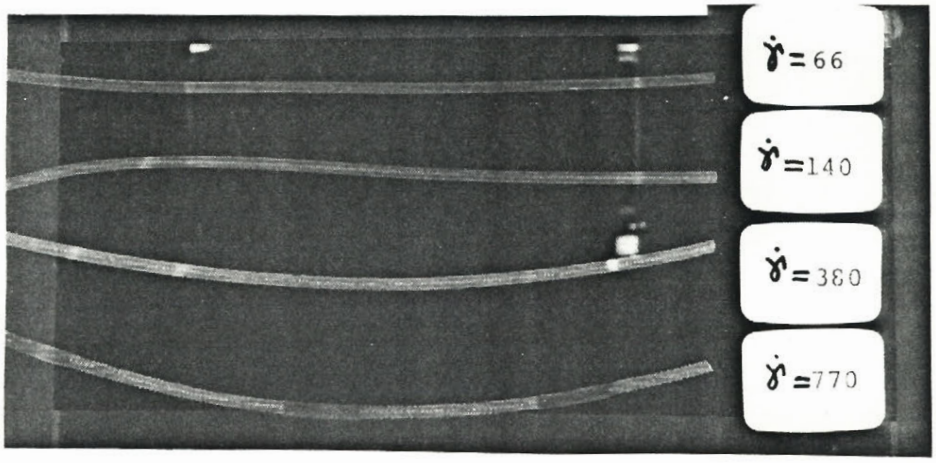

Figure 98: Extrudate distortion of resin 31 at 190°C.

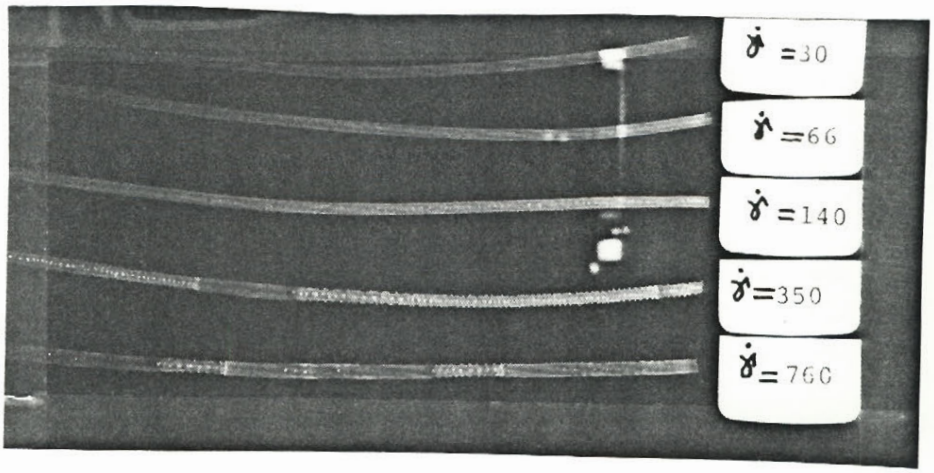

Figure 99: Extrudate distortion of resin 33 at 190°C.

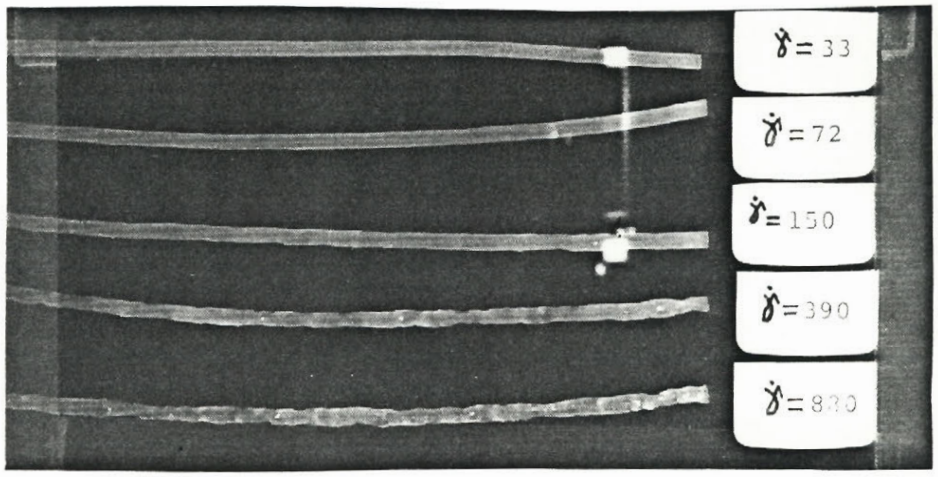

Figure 100: Extrudate distortion of resin 32 at 190°C.

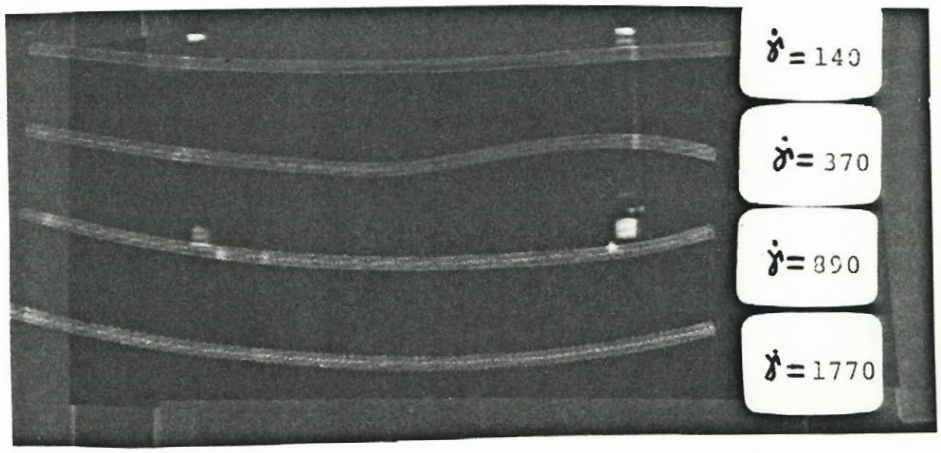

Figure 101: Extrudate distortion of resin 30 at 190°C.

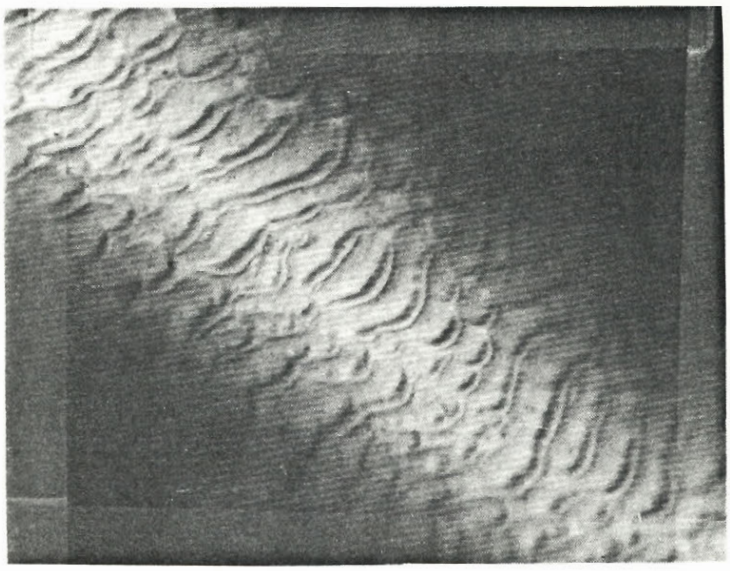

Figure 102: Incipient distortion of resin 31 at $\dot{\gamma}$=140 s^{-1} 190°C, 70X magnification.

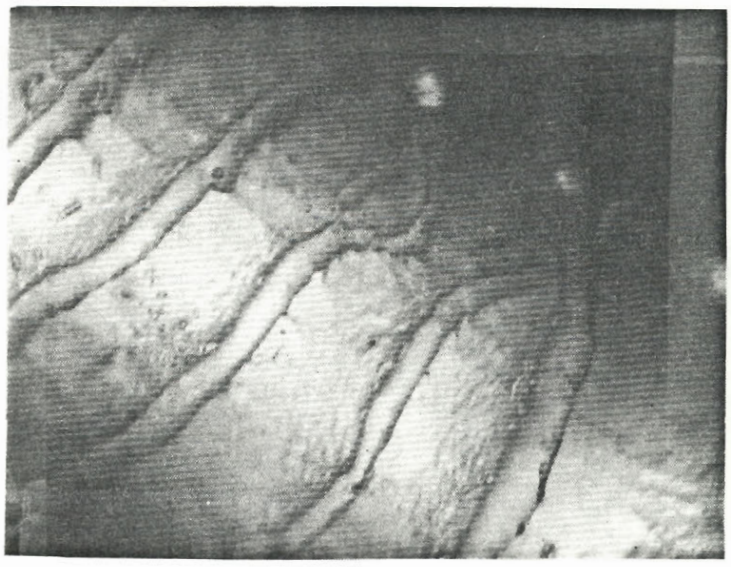

Figure 103: Distortion of resin 31 at $\dot{\gamma}$=380 s^{-1} 190°C, 70X magnification.

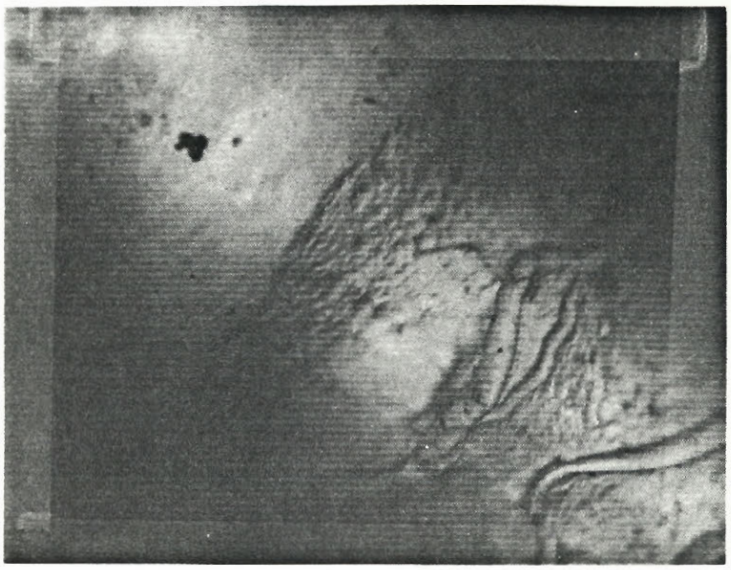

Figure 104: Stick-slip distortion of resin 31 at $\dot{\gamma}$ =770 s^{-1} 190°C, 70X magnification.

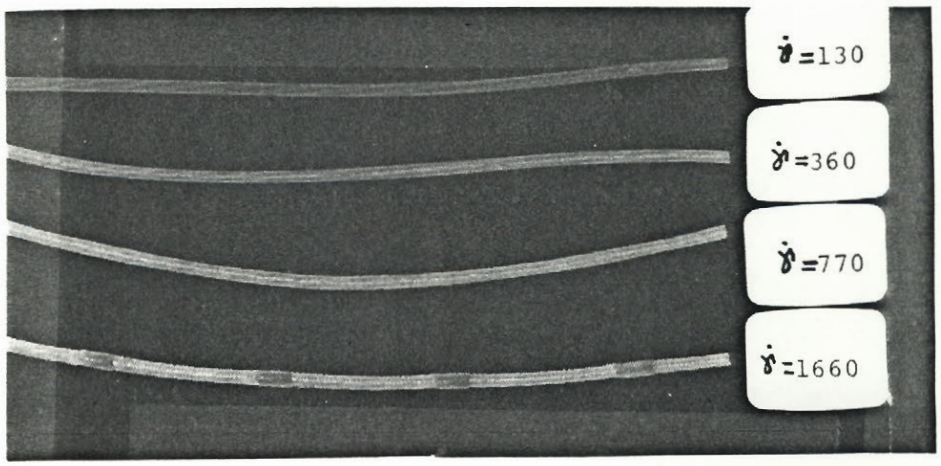

Figure 105: Extrudate distortion of resin 31 at 210°C.

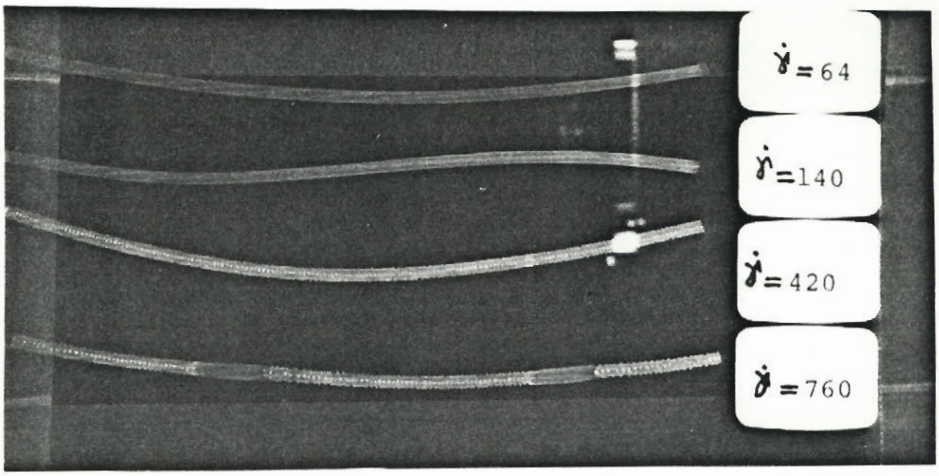

Figure 106: Extrudate distortion of resin 33 at 210°C.

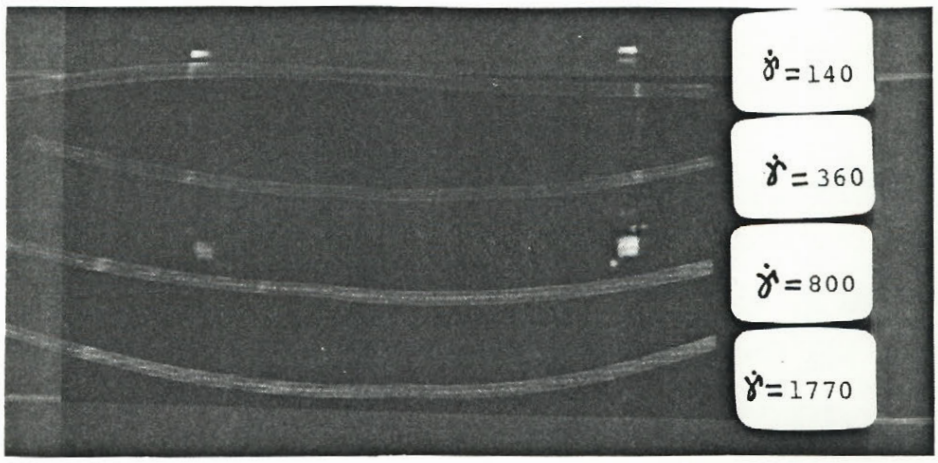

Figure 107: Extrudate distortion of resin 30 at 210°C.

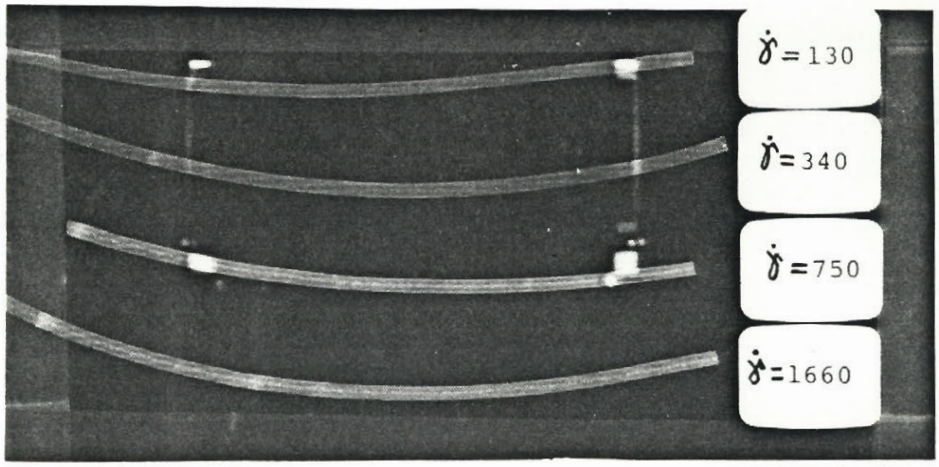

Figure 108: Extrudate distortion of resin 31 at 240°C.

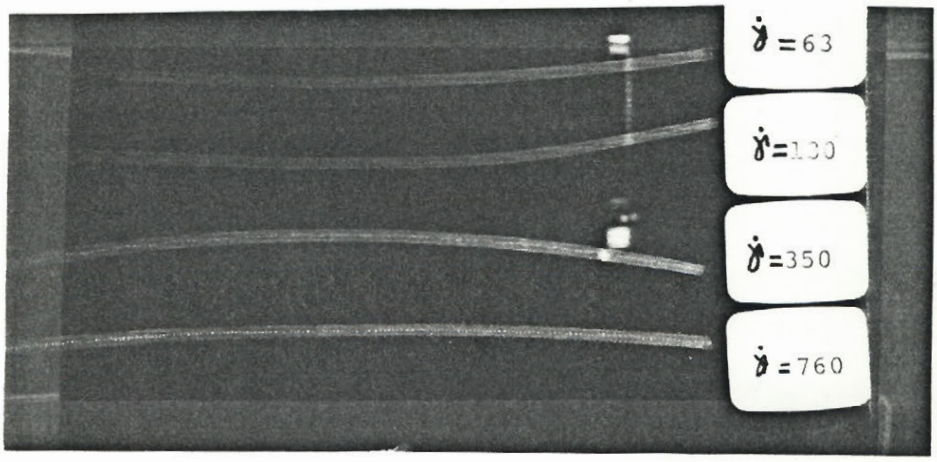

Figure 109: Extrudate distortion of resin 33 at 240°C.

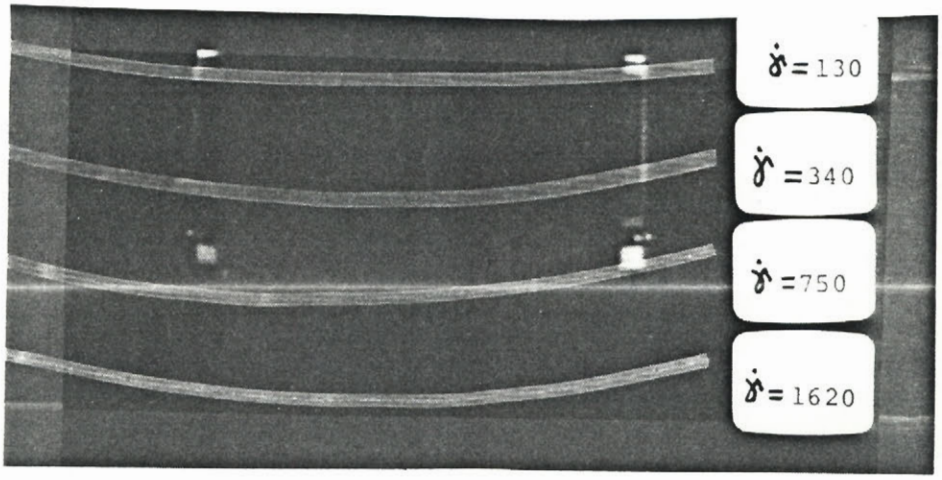

Figure 110: Extrudate distortion of resin 30 at 240°C.

stick-slip flow [25] or "land fracture" [151]. This phenomenon is accompanied by periodic oscillations in the pressure drop through the capillary. The pressure decreases as the polymer slips (smooth section), and then increases as adhesion (or cohesion) is regained. A close up view of the boundary region between stick and slip is shown in Figure 104. Note how smooth the slip region appears to be in comparison to the region of adhesion. It was also observed that the smooth sections of the extrudate tended to have a higher instantaneous flow rate than the rough sections as they left the capillary. Since the plunger that forces the polymer through the capillary travels at a constant speed, this could only occur if fluctuations in the density of the polymer melt also occur. Measurements of such density fluctuations have been made by Rudin et al. [152] and Uhland [90] on HDPE, which has a linear structure similar to that of LLDPE. They found that the smooth, high flow rate sections of the extrudate had lower melt densities than did the rough sections. As the shear rate is increased the slip flow regime begins to predominate (see Figure 99), and although not shown, ultimately continuous slip occurs. This is accompanied by only a minor increase in the wall shear stress. This will be discussed further in the subsequent section.

The shear rates and shear stresses at which flow

CONDITIONS AT WHICH FLOW INSTABILITIES ARE FIRST OBSERVED

Resin	190 °C		210 °C		240 °C	
	τ_w(Pa)	$\dot{\gamma}_w$(sec)	τ_w(Pa)	$\dot{\gamma}_w$(sec)	τ_w(Pa)	$\dot{\gamma}_w$(sec)
32	65700	72.2	----------		----------	
30	239000	372.8	206000	355.7	224000	748.0
31	206000	139.4	238000	360.9	279000	753.4
33	171000	66.2	198000	138.6	260000	351.0

Table 8

instabilities were first observed for all four resins are presented in Table 8. Regardless of the extrusion temperature, the type of fine surface roughness shown in Figure 102 seems to appear at shear stresses ranging from 171 to 279 kPa for the LLDPE resins, although the shear rate at which sharkskin is first observed increases with temperature. In his work with LLDPE, Utracki [129] found that sharkskin first occurred at shear stresses of about 240 kPa. Resin 32 first exhibits distortion at a shear stress of 66 kPa, much lower than the LLDPE's, which corresponds to a shear rate of 72 sec^{-1}. At this shear rate the instability is manifested as minor kinks in the body of the extrudate, with a surface that is still remarkably smooth.

The onset of flow instability is generally dictated by the elasticity of the polymer melt, more elastic materials exhibiting instabilities at lower shear rates [30]. This observation satisfactorily accounts for the relative susceptibility of the LLDPE's to flow instabilities, but does not explain the dramatically different type of instabilities exhibited by LDPE and LLDPE resins.

Bergem [84] suggests that the sharkskin distortion characteristic of linear polymers such as LLDPE has its origin at the exit of the capillary. On emerging from the capillary the velocity distribution across the extrudate

changes quickly resulting in an acceleration of the outer layers. This induces tensile stresses that may exceed the tensile strength of the melt. The melt may then tear, resulting in a relaxation of these stresses. If this occurs around the periphery of the extrudate, the screw thread pattern characteristic of sharkskin results. The wall slippage is thought to occur as a result of the sudden disentanglement of the molecules in the layer of melt directly adjacent to the capillary wall from those in the main flow, at a critical shear stress. As the polymer slips, the shear stress at the slip interface drops until it reaches a certain level at which the entanglements reform leading to stick flow; the cycle then repeats itself. With highly branched materials like LDPE it is hypothesized that the flow instabilities originate at the entrance of the capillary. Ballenger et al. [83] observed that, at sufficiently high shear rates, the large recirculating eddies that are present in the entry region of the capillary tend to periodically rejoin the main flow resulting in the mixing of molten polymer of different thermal and deformation histories. The frequency and duration of the joining of the eddies with the main flow increases with increasing shear rate at a given temperature.

5.6.2 Pressure Fluctuations

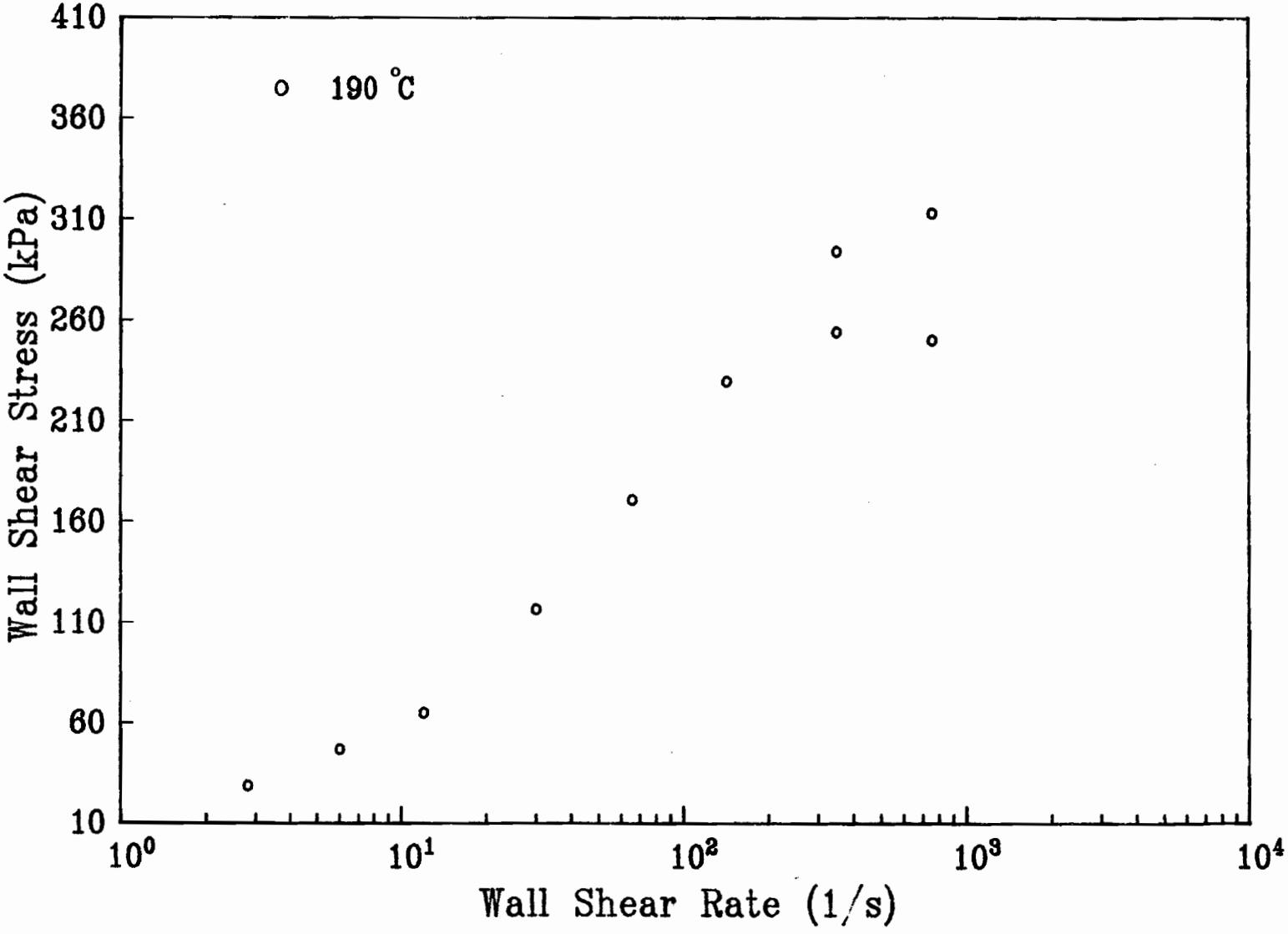

Figure 111: Flow curve for resin 33 at 190°C.

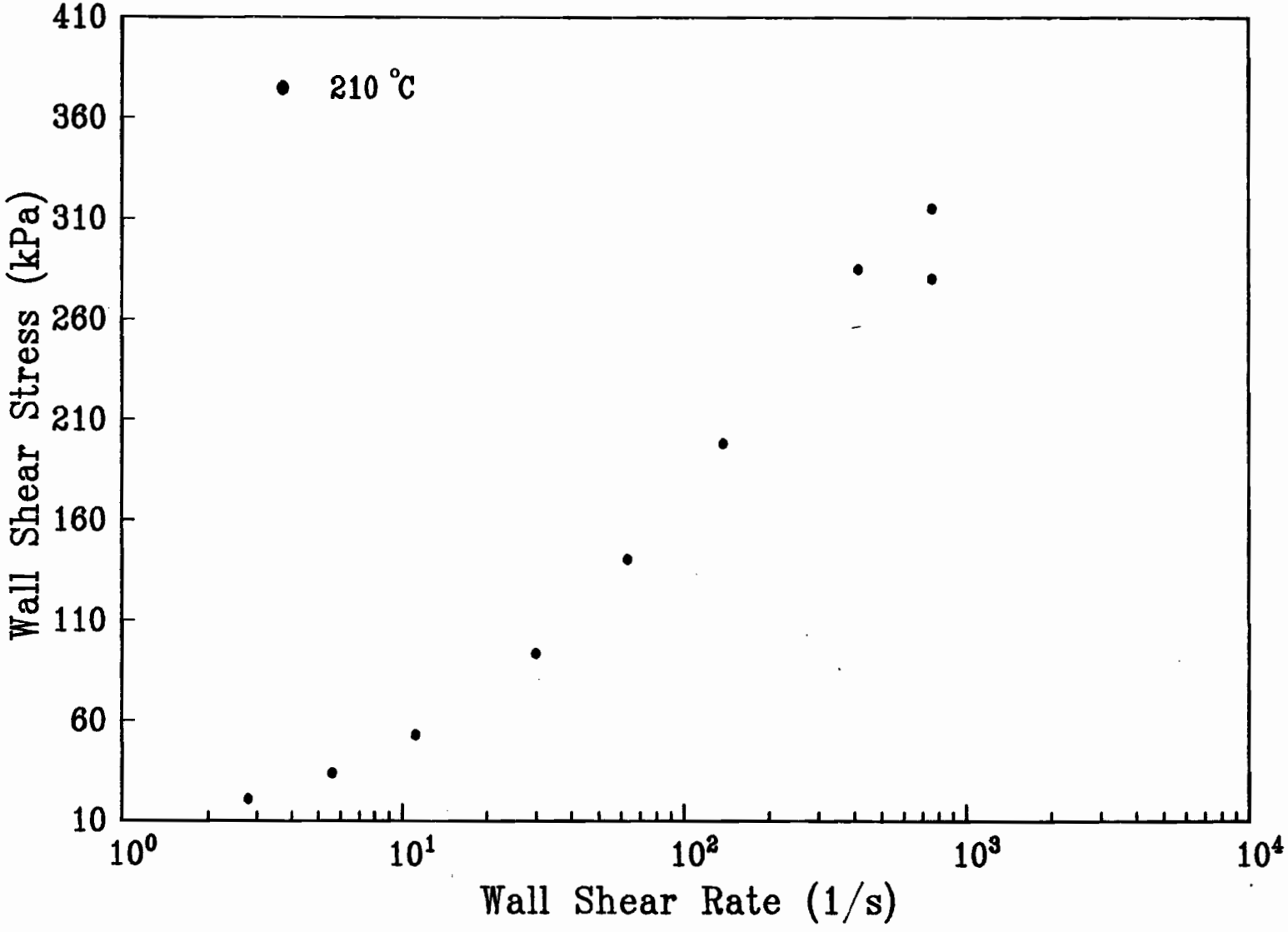

Figure 112: Flow curve for resin 33 at 210°C.

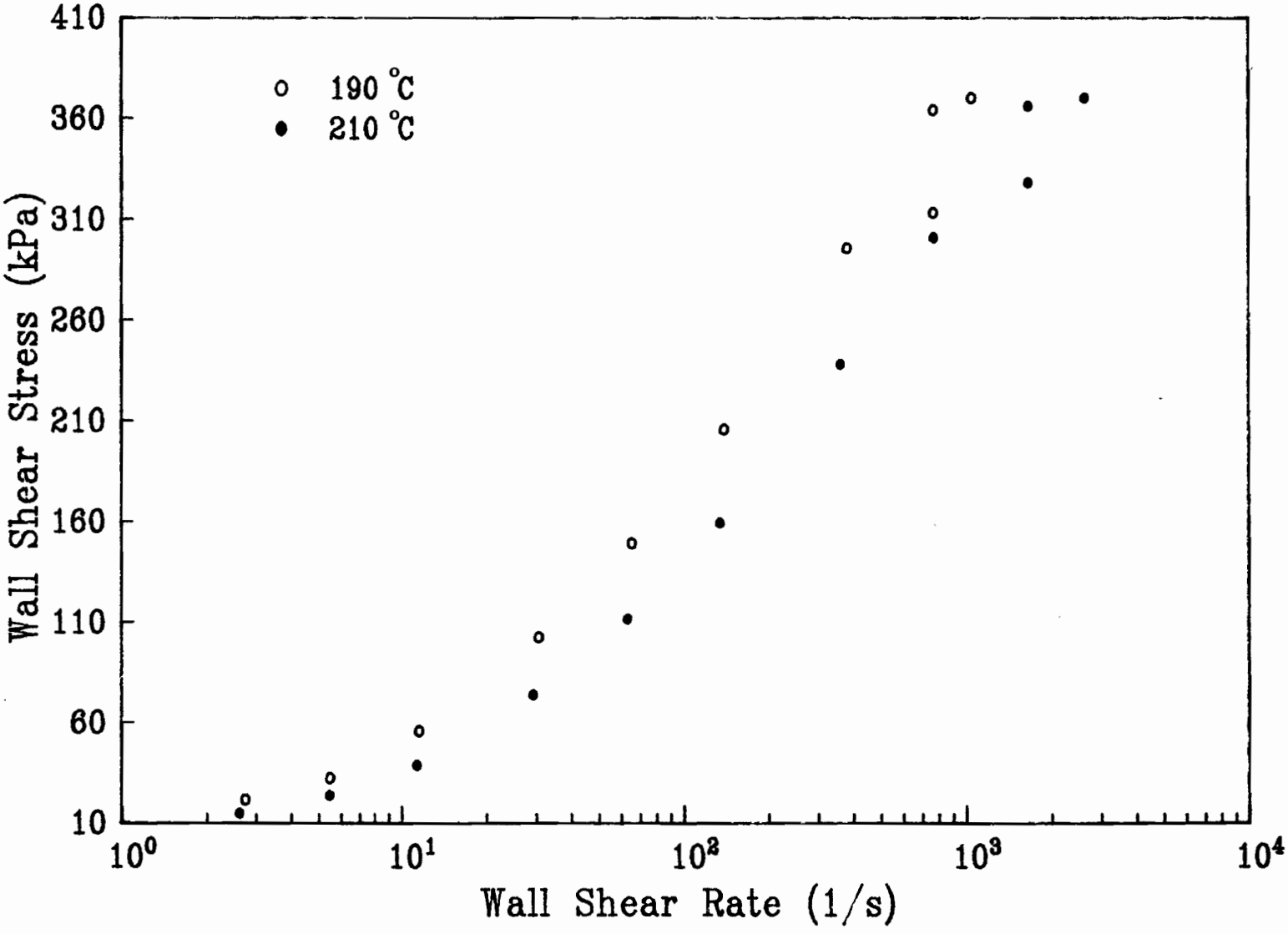

Figure 113: Flow curve for resin 31 at 190°C and 210°C.

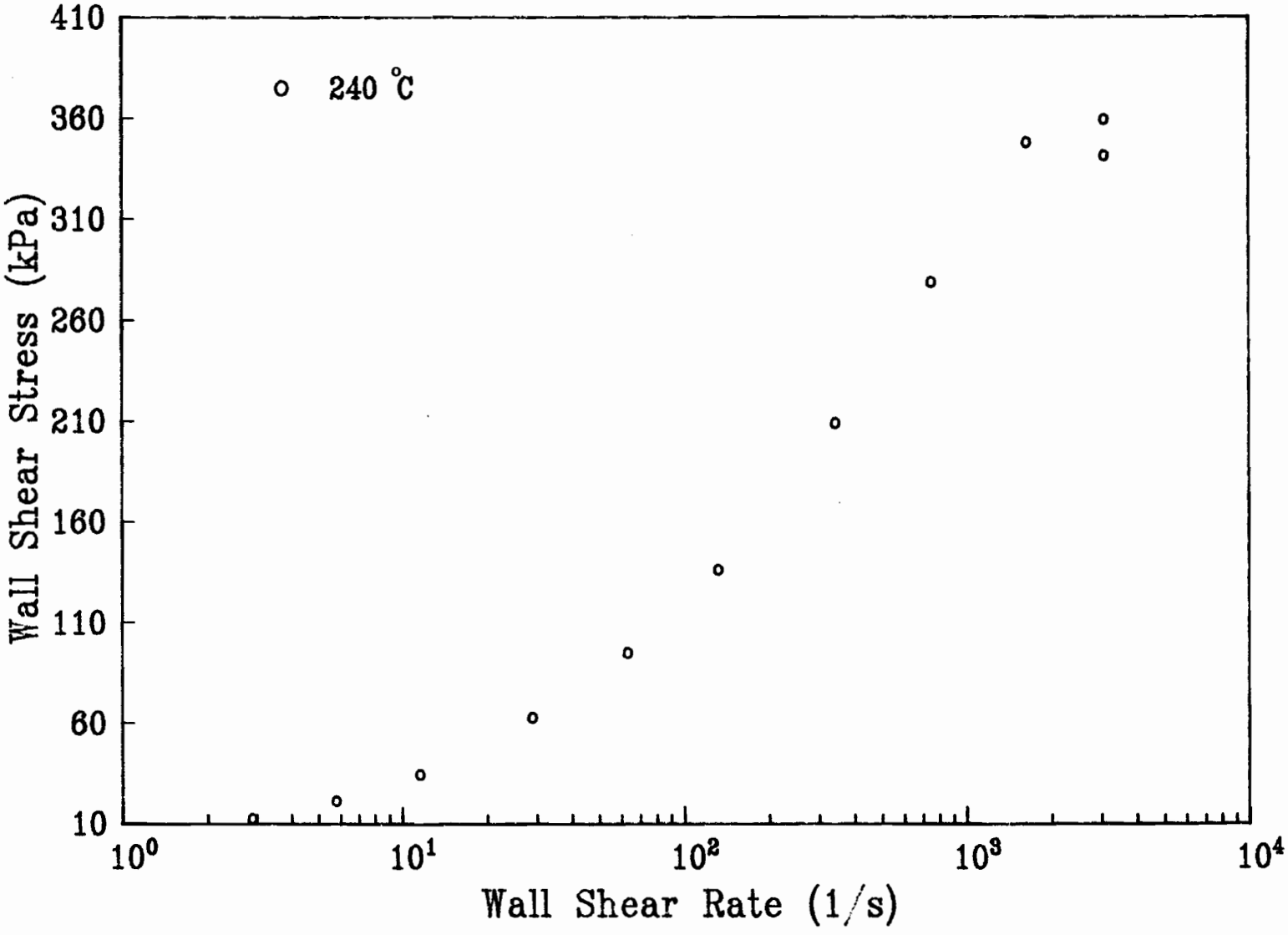

Figure 114: Flow curve for resin 31 at 240°C.

FLUCTUATIONS IN WALL SHEAR STRESS IN CAPILLARY EXTRUSION.

Capillary: D=0.132 cm
L/D=20
Entrance angle= 90°

A. Resin #33

190 °C: $\dot{\gamma}_w$=350 sec^{-1}

τ_w(max)=2.94E+05 Pa
τ_w(min)=2.54E+05 Pa

τ_w(max)/ τ_w(min)=1.16
Frequency= .25 Hz

$\dot{\gamma}_w$=760 sec^{-1}

τ_w(max)=3.13E+05 Pa
τ_w(min)=2.50E+05 Pa

τ_w(max)/ τ_w(min)=1.25
Frequency= .67 Hz

210 °C: $\dot{\gamma}_w$=760 sec^{-1}

τ_w(max)=3.15E+05 Pa
τ_w(min)=2.80E+05 Pa

τ_w(max)/ τ_w(min)=1.13
Frequency= .67 Hz

B. Resin #31

190 °C: $\dot{\gamma}_w$=770 sec^{-1}

τ_w(max)=3.36E+05 Pa
τ_w(min)=3.11E+05 Pa

τ_w(max)/ τ_w(min)=1.08
Frequency= .83 Hz

240 °C: $\dot{\gamma}_w$=2800 sec^{-1}

τ_w(max)=3.59E+05 Pa
τ_w(min)=3.55E+05 Pa

τ_w(max)/ τ_w(min)= 1.01
Frequency= 2.0 Hz

210 °C: $\dot{\gamma}_w$=1660 sec^{-1}

τ_w(max)=3.76E+05 Pa
τ_w(min)=3.34E+05 Pa

τ_w(max)/ τ_w(min)=1.13
Frequency= 1.8 Hz

Table 9

As was mentioned earlier, the stick-slip flow of the LLDPE resins was associated with a fluctuation in the pressure drop through the capillary. The lower pressure drop was associated with the smooth (slip) region and the higher pressure with the higher (stick) region. In Figures 111-114 are presented plots of wall shear stress vs wall shear rate for resins 31 and 33. The onset of slippage is seen to be delayed by increasing the extrusion temperature, and in fact does not occur at all with resin 33 in the shear rate range covered at 240 ^{o}C. In Figure 113 the complete slippage of the extrudate is indicated by the relativley small increase in the wall shear stress as the shear rate is increased. The amplitudes and frequencies of the observed pressure fluctuations for each resin are given in Table 9. The wall shear stress values during slip flow are only approximations since it is difficult to know what value of the Bagley correction should be used when slip is occuring. By making measurements with several capillaries and plotting the values of the slip pressure drops in the form of a Bagley plot, the entrance correction was obtained. Conversely, the higher value of the pressure drop during stick-slip flow was used to estimate the Bagley constant for stick flow.

The frequency with which the stick-slip phenomenon occurs seems to increase with the shear rate, ranging from as low as .25 Hz up to 1.8 Hz, with resin 31 exhibiting

generally higher frequencies. In addition, the ratio of the maximum to minimum shear stress ranged from 1.08 to 1.25, generally having higher values for resin 31 than for resin 33. Utracki et al. [129] found that the LLDPE's he studied exhibited ratios ranging from 1.06 to 1.16.

Chapter 6

CONCLUSIONS AND RECOMMENDATIONS FOR FURTHER WORK

The branched and linear polyethylene film resins studied exhibited significant differences in shear rheology, elasticity and extrudate distortion characteristics. The differences in behavior between the linear and branched resins are, in general, due to the different molecular structures and weight distributions of the two types of resin. In particular, the long chain branches and relatively broad molecular weight distribution of the branched material are responsible for its different rheological properties.

The branched low density polyethylene (LDPE), resin 32, had a lower viscosity at the higher shear rates than did the linear low density polyethylenes (LLDPE), the opposite being true at low shear rates. In addition, resin 32 had a lower value of the power law index than any of the LLDPE resins, which is a reflection of its more rapid shear thinning behavior. Based on measurements of their linear viscoelastic properties, it was determined that the viscoelastic behavior of the LDPE was affected by longer relaxation time molecular

entanglements to a greater extent than was the viscoelastic behavior of the LLDPE resins.

In general resin 32 appeared to be more elastic than the linear copolymers. This is indicated by higher values of the extrudate swell ratio and first normal stress difference, and by a greater tendency to exhibit edge fracture in cone and plate flow than the linear resins. In the linear viscoelastic region, resin 32 had higher values of the storage modulus (a measure of elasticity) than the LLDPE's at low frequencies and lower values at higher frequencies. Surprisingly, resin 32 showed the lowest value of the entrance pressure drop in capillary flow, of the four resins studied. Since the high entrance pressure drops are primarily a result of the elastic nature of molten polymers, the LDPE resin would be expected to have the largest entrance pressure drop. It is thought that the viscous contribution to the entrance pressure drop is less than 5% of the total [141], thus one would not expect the higher viscosities of the LLDPE resins to significantly increase the entrance pressure drops of these materials. The reason for this discrepancy is not then obvious.

Striking differences between the forms of extrudate distortion exhibited by the branched and linear resins were observed. The former exhibiting a waviness of the extrudate

in the incipient stages of distortion, which becomes more pronounced at higher shear rates. The linear resins exhibited similar distortion behavior to that reported for HDPE (a linear homopolymer) [84,90], beginning with a very fine surface roughness at lower shear rates, increasing in severity with shear rate until a regular screw thread pattern known as sharkskin results. At higher shear rates, two of the copolymer resins exhibited a periodic fluctuation in the pressure drop through the die. This was accompanied by a periodic loss of cohesion (or adhesion) with the capillary wall, resulting in smooth sections of extrudate alternating with sharkskin. As the shear rate was increased, the smooth sections predominated, ultimately leading to complete slippage in the case of resin 31. Extrudate distortion occurred at similar shear rates for both types of resins, but at much lower shear stresses for resin 32.

Of the three LLDPE resins, resin 33 was the most viscous and elastic at all temperatures, followed by resin 31 and then 30. The differences in shear viscosity between these three resins were most pronounced at very low shear rates, becoming less pronounced at high shear rates, particularly between resins 31 and 33. Manifestations of the greater elasticity of resin 33 were it's higher first normal stress difference, storage modulus, entrance pressure drop, extrudate swell, greater propensity for edge fracture and

it's greater susceptability to extrudate distortion. All three of these resins first exhibited extrudate distortion at shear stresses ranging from 171 to 279 kPa. The critical shear rate at which extrudate distortion first occurred increased substantially with extrusion temperature, as did the shear rate at which pressure oscillations were first observed.

The differences in rheology between resin 30 and resins 31 and 33 may be attributed, at least in part, to resin 30's lower molecular weight. Acierno et al. [133] found that both the critical shear rate at which extrudate distortion was observed and the zero-shear viscosity were strong functions of weight average molecular weight for LLDPE, although the correlations they fitted to their data did not fit the data obtained in this work. Differences in comonomer type are not thought to affect melt rheology [8], although this is the subject of some debate [119]. What is puzzling is the significant difference in the rheology of resins 33 and 31. These materials have almost identical values of both M_w and M_n, as well as containing the same comonomer (1-butene), however, the quantities of comonomer present are not known to us. What is also of interest, is that the differences in behavior of these copolymers are most evident in their very low shear rate rheology and in their high strain rate elastic properties such as entrance pressure drop and extrudate

swell.

The extensional rheology data of these resins, obtained using the method suggested by Shroff et al. [142], are very approximate and only give a qualitative ranking of the behavior of the LLDPE resins in an extensional flow. This method predicts that the extensional viscosity of resin 32 is less than that of the LLDPE resins. These findings contradict those of other workers [119,120] who, using devices specifically designed for measuring extensional rheology, found that the extensional viscosity of LLDPE resins was always less than that of LDPE resins. Shroff et al. [142] observed the same puzzling behavior with the LDPE resins they studied. These results indicate that approximate methods such as this one are only of use in comparing resins which are relatively similar in molecular structure and should be viewed with some skepticism when used to compare the behavior of resins with dramatically different structures.

The importance of extensional flows in the film-blowing process makes a knowledge of a resins extensional rheology particularly important. Further studies of the resins investigated in this work should attempt to study their extensional rheology at strain rates comparable to those experienced by the melt in processing [153]. The sensitivity

of the high strain rate elastic properties of these resins to subtle differences in molecular structure indicates that further study of such properties may be warranted. Efforts to develop techniques to permit such studies are underway in this laboratory [28]. Any characterization of polymeric materials will be of greatest use when combined with a study of the processing behavior of the materials. Such a study would serve to improve the understanding of how melt rheology affects processing behavior.

REFERENCES

1. Billmeyer, F.W., Jr., Textbook of Polymer Science, 3rd Ed., John Wiley & Sons, NY, 1984.

2. Tadmor, Z., et al, Principles of Polymer Processing, John Wiley & Sons, NY, 1979.

3. Acierno, D., et al, J. Non-Newt. Fl. Mech., Vol.1, p. 125 (1976).

4. Rhi-Sausi, J., Ph.D. Thesis, Dept. Chem. Eng., McGill University, 1979.

5. Yang, M.C., M.Eng. Thesis, Dept. Chem. Eng., McGill University, 1981.

6. Rodriguez, F., Principles of Polymer Systems, 2nd Ed., Hemisphere Pub. Co., 1982.

7. Kurtz, S. J., U.S. Patent, # 4,282,177, Aug. 4, 1981.

8. Shirayama, K., et al, Die Makromolekulare Chemie, Vol. 151, p. 97 (1972).

9. Bork, S., Kunststoffe Vol. 74 (9), p. 474 (1984).

10. Martino, R., Mod. Plast., Vol. 61, p.4 (1984).

11. Chem. Eng., Vol. 88 (8), p. 47 (1981).

12. Martino, R., Mod. Plast., Vol. 60 (4), p. 66 (1983).

13. Sinclair, K.B., Polyolefin Process Technology Update, SRI Report, 1981.

14. Martino, R., Mod. Plast. Int., Vol. 12 (4), p. 44 (1982).

15. Imhausen, K.H., et al, J. Appl. Poly. Sci., Applied Polymer Symp., Vol. 36, p.1 (1981).

16. Chem. Eng., Feb. 21, 1983.

17. Chem. Eng., Feb. 18, 1985.

18. C.T. Elston, U.S. Patent # 3,645,992, Feb. 29, 1972.

19. Bubeck, R.A., et al, Polymer, Vol. 23 (10), p. 1680 (1982).

20. W.A. Anderson, et al, U.S. Patent #4,076,698, 1978.

21. Kurtz, S.J., et al, Plast. Eng., Vol. 6, p. 45 (1892).

22. Miller, J.C., Tappi J., Vol. 67 (6), p. 64 (1984).

23. Strater, K., M. Eng. Thesis, Dept. Chem Eng., McGill University, 1985.

24. Speed, C.S., Plast. Eng., Vol. 7, p. 39 (1982).

25. Dealy, J.M., Rheometers for Molten Plastics, Van Nostrand Reinhold, 1982.

26. Bird, R.B., et al, Dynamics of Polymeric Liquids, Vol. I, John Wiley & Sons, 1977.

27. Soong, S.S., Ph.D. Thesis, Dept. Chem. Eng., McGill University, 1983.

28. Giacomin, A.J., Ph.D. Project Proposal, Dept. Chem. Eng., McGill University, 1984.

29. Boger, D.V., et al, J. Non-Newt. Fl. Mech., Vol. 6, p. 163 (1980).

30. Han, C.D., Rheology in Polymer Processing, Academic Press, 1976.

31. Course notes 302-732, Dept. Chem. Eng., McGill University, 1983.

32. Bird, R.B, et al, Transport Phenomena, John Wiley & Sons, 1960.

33. Garcia-Rejon, A., M.Eng. Thesis, Dept. Chem. Eng., McGill University, 1975.

34. White, J.L., et al, J. Non-Newt. Fl. Mech., Vol. 3, p. 41 (1977).

35. Ballenger, T.F., et al, Chem. Eng. Sci., Vol 25, p. 1191 (1970).

36. Brizitsky, V.I., et al, J. Appl. Poly. Sci., Vol. 22, p. 751 (1978).

37. Han, C.D., Trans. Soc. Rheol., Vol. 18 (1), p. 163 (1974).

38. Bagley, E.B., J. Appl. Phys., Vol. 28, p. 624 (1957).

39. Ferry, J.D., Viscoelastic Properties of Polymers, John Wiley & Sons, 1980.

40. Report of the Nomenclature Committee, Society of Rheology, 1982.

41. Meissner, J., et al., J. Rheology, Vol. 25, p.1 (1981).

42. Dealy, J.M., Personal Communications.

43. Stevenson, J.F. (Gen. Tire, Akron) Personal Communication with J.M. Dealy.

44. Chatraei, S., et al., J. Rheology, Vol. 25, p.433 (1981).

45. Papanastasiou, A.C., Macosko, C.W., Scriven, L.E., paper in preparation.

46. Dealy, J.M., Personal Communications.

47. Treloar, L.R.G., Trans. Inst. Rubber Ind., Vol. 19, p. 201 (1944).

48. Denson, C.D., et al., Poly.Eng. & Sci., Vol. 11, p. 174 (1971).

49. Rhi-Sausi, J., et al., Poly. Eng. & Sci., Vol. 21, p. 227 (1981).

50. Van Aken, J.A., et al., Rheol. Acta, Vol. 20, p. 419 (1981).

51. Dealy, J.M., Plastics Engineering, March 1983, p. 57.

52. Middleman, S., Fundamentals of Polymer Processing, McGraw-Hill, 1977.

53. Vlachopoulos, J., Rev. Def. of Mater., Vol. 3, p. 219 (1981).

54. Graessly, W.W., Trans. Soc. Rheol., Vol. 14 (4), p. 519 (1970).

55. Lodge, A.S., Elastic Liquids, Academic Press, 1964.

56. Racin, R., et al, J. Rheology, Vol. 23, p. 263 (1979).

57. Rokudai, M., J. Appl. Poly. Sci., Vol. 26, p. 1427 (1981).

58. Hamliec, L.A., et al, J. Appl. Poly. Sci., Vol. 28, p. 2389 (1983).

59. Han, C.D., et al, J. Appl. Poly. Sci., Vol. 22, p. 1677 (1978).

60. Garcia-Rejon, A., et al, Poly. Eng. & Sci., Vol. 22, p. 3 (1982).

61. Utracki, L.A., et al, J. Appl. Poly. Sci., Vol. 19, p. 481 (1975).

62. Garcia-Rejon, A., M. Eng. Thesis, Dept. Chem. Eng., McGill University, 1976.

63. Spencer, R.S., et al, J. Colloid Sci., Vol. 3, p. 163 (1948).

64. Bagley, E.B., Trans. Soc. Rheol., Vol. 14, p.545 (1970).

65. Cogswell, F.N., Plast. & Polym., Vol. 12, p. 391 (1970).

66. Tanner, R.J., J. Poly. Sci., Vol. A2 (8), p. 2067 (1970).

67. Vlachopoulos, J., et al, Trans. Soc. Rheol., Vol. 16 (4), p. 669 (1972).

68. Metzner, A.B., et al, Trans. Soc. Rheol., Vol. 5, p. 133 (1961).

69. Tanner, R.J., Computational Analysis of Polymer Processing, J.R.A. Pearson (ed.), Allied Science publishers, 1963.

70. Vlachopoulos, J., et al, J. Appl. Poly. Sci., Vol. 21, p. 1177 (1973).

71. Vinogradov, G.V., et al, Poly. Eng. and Sci., Vol. 5, p. 323 (1972).

72. Petrie, C.J.S., et al, A.I.Ch.E. Journal, Vol. 22, p. 209 (1976).

73. Lupton, J.M., et al, Poly. Eng. & Sci.,Vol. 5, p. 235 (1965).

74. Bagley, E.B., Trans. Soc. Rheol., Vol. 5, p. 355 (1961).

75. Vlachopoulos, J., et al, Poly. Eng. & Sci., Vol. 12, p. 3 (1972).

76. Atwood, B.T., Ph.D. Thesis, Dept. Chem. Eng., Princeton University, 1983.

77. Smith, F.P., Ph.D. Thesis, Dept. Chem. Eng., Texas A&M, 1975.

78. Overdiep, W.S., et al, J. Appl. Poly. Aci., Vol. 9, p. 2779 (1965).

79. Bartos, O., J. Appl. Phys., Vol. 35, p. 2767 (1964).

80. Cogswell, F.N., et al, Bull. Brit. Soc. Rheol., Vol. 15, No. 2,29 (1972).

81. Blyler, L.L., et al, Poly. Eng. & Sci., Vol. 10, p. 193 (1970).

82. Vlachopoulos, J., et al, Poly. Eng. & Sci., Vol. 11, p. 1 (1971).

83. Ballenger, T., et al, Trans. Soc. Rheol., Vol. 15 (2), p. 195 (1971).

84. Bergem, N., VIIth Int. Conf. Rheol., Gothenburg (1976).

85. Benbow, J.J., et al, S.P.E. Trans., Vol. 3, p. 7 (1963).

86. Vinogradov, G.V., et al, J. Poly. Sci., Vol. A2 (10), p. 1061 (1972).

87. Weill, A., Rheol. Acta, Vol. 19, p. 623 (1980).

88. den Otter, J.L., Rheol. Acta, Vol. 10, p. 200 (1971).

89. Vinogradov. G.V., Polymer, Vol. 18, p. 1275 (1977).

90. Uhland, E., Rheol. Acta, Vol. 18, p. 1 (1979).

91. Drott, E. and Mendelson, R., J. Poly. Sci., Vol. 8A-2, p. 1361 (1970).

92. Wild, L., et al, Polymer Preprints, p. 133, (1982).

93. White, J.L., Rheological Behavior of Unvulcanized Rubber, in Science and Technology of Rubber, ed. Eirich, F.R., Academic Press, 1978.

94. La Mantia, F.P., et al, Rheol. Acta, Vol. 22, p. 299 (1983).

95. Graessly, W.W., et al, J. Poly. Sci., Part A2, Vol. 6, p. 1886 (1968).

96. Peticolas, W.L., Rubber Chem. Tech. Rev., Vol. 36, p. 1422 (1963).

97. Muenstedt, H., et al, Rheol. Acta, Vol. 18, p. 492 (1963).

98. Muenstedt, H., et al, Rheol. Acta, Vol. 20, p. 211 (1981).

99. Attala, G., et al, Proc. VIIIth Int. Congress of Rheology, Naples (1980) p. 407.

100. Utracki, L.A., et al, Paper presented at the International Workshop on Extensional Flows, 24-28 January 1983, Mulhouse-Bresse, France.

101. Utracki, L.A., et al, Proc. ANTEC 1984, p. 417 (1984).

102. Laun, H.M., Proc. VIIIth Int. Congress of Rheology, Naples, p. 419 (1980).

103. Bersted, B.H., J. Appl. Poly. Sci., Vol. 24, p. 671 (1979).

104. Muenstedt, H., Proc. VIIIth Int. Congress of Rheology, Naples (1980), p. 413.

105. Muenstedt, H., J. Rheol., Vol. 24, p. 847 (1980).

106. Tsang, W.K.W., Ph.D. Thesis, Dept. Chem. Eng., McGill University, 1980.

107. Bird, R.B., et al, Dynamics of Polymeric Liquids, Vol. 2, 1977.

108. Lodge, A.S., Trans. Faraday Soc., Vol. 52, p. 120 (1956).

109. Carreau, P.J., Trans. Soc. Rheol., Vol. 16 (1), p. 99 (1972).

110. Bernstein, G., et al, Trans. Soc. Rheol., Vol 7, p. 391 (1963).

111. Yen, H.C., et al, Trans. Soc. Rheol., Vol. 18 (4), p. 495 (1974).

112. Marruci, G., et al, Rheol. Acta., Vol. 12, p. 269 (1973).

113. Garcia-Rejon, A., Ph.D. Thesis, Dept. Chem. Eng., McGill University, 1979.

114. Stivala, S.S., Poly. Eng. and Sci., Vol. 20, p. 654 (1980).

115. Mascia, L.,The Role of Additives in Plastics, Edward Arnold Press, London, 1974.

116. David, C., Degradation of Polymers, Elsevier, New York (1975).

117. Arch. F., et al, Proceedings of Tappi Film Extrusion Conference, Atlanta, S.60 (1982).

118. Patterson, W.C., Sclair Blending Resins for Foam Extrusion, DuPont, Canada, 1978.

119. Kalyon, D.M., Moy, F.H., Proc. ANTEC 1985, p. 680 (1985).

120. Al-Bastaki, N.M., M.Eng. Thesis, Dept. Chem. Eng., McGill University, 1982.

121. Saini, D.R., et al, Eur. Poly. J., Vol. 19 (9), p. 811 (1983).

122. Saini, D.R., et al, Poly. Eng. Sci., Vol. 24 (15), p. 1215 (1984).

123. Attala, G., et al, J. Appl. Poly. Sci., Vol. 28, p. 3503 (1983).

124. Tordella, J.P., J. Appl. Poly. Sci., Vol. 7, p. 215 (1963).

125. Cogswell, F.N., Rheol. Acta, Vol. 8, p. 187 (1969).

126. Cogswell, F.N., Trans. Soc. Rheol., Vol. 16, p. 383 (1972).

127. Han, C.D. et al, J. Appl. Poly. Sci., Vol. 28, p. 3399 (1983).

128. Kwack, T.H., et al, J. Appl. Poly. Sci., Vol. 28, p. 3419 (1983).

129. Utracki, L.A. J. Rheol., Vol. 28 p. 601 (1984).

130. Vasudevan, G., et al, Proc. ANTEC 1985, p. 459 (1985).

131. Winter, H.H., et al, Proc. ANTEC 1985, p. 613 (1985).

132. Capolupo, J.D., Proc. ANTEC 1985, p. 982 (1985).

133. Acierno, D., et al, J. Rheol., Vol. 29, p. 323 (1985).

134. Macosko, C., et al,S.P.E.J., Vol. 27, p. 38 (Nov. 1971).

135. Rheometrics Mechanical Spectrometer Operations Manual, Rheometrics Ins., New Jersey.

136. Pangalos, G.C., M.Eng. Thesis, Dept. Chem. Eng., McGill University, 1983.

137. Orbey, N., Ph.D. Thesis, Dept. Chem. Eng., McGill University, 1983.

138. Gordon, N., Summer Research Project, McGill University, 1982.

139. Fraser, W.A., et al, Mod. Plast., Vol. 57, p. 11 (1980).

140. Hutton, J.F., Nature, Vol. 200, p. 646 (1963).

141. Han, C.D., AIChE J., Vol. 17, p. 1480 (1971).

142. Shroff, R.N., et al, Trans. Soc. Rheol., Vol. 21 (3), p. 429 (1977).

143. Meissner, J., Rheol. Acta, Vol. 4, p. 137 (1971).

144. Han, C.D., et al, Trans. Soc. Rheol., Vol. 16, p. 447 (1972).

145. Huang, T.A., et al, Proc. ANTEC 1985, p. 84 (1985).

146. Cox, W.P., et al, J. Poly. Sci., Vol. 28, p. 619 (1958).

147. Coleman, B.D., et al, J. Appl. Phys., Vol. 35, p. 1 (1964).

148. Utracki, L.A., et al, Proc. AIChE 1982, Los Angeles, CA, Nov. 14-19, paper No. 3b (1982).

149. Tschoegl, N.W., The Theory of Linear Viscoelastic Behaviour, Academic Press, NY, 1981.

150. Olabisi, O., et al, Macromolecules, Vol. 8, p. 211 (1975).

151. Tordella, J.P., Rheology, Vol. 5, F.P. Eirich, Ed., Academic Press, NY, 1969.

152. Rudin, A., et al, J. Appl. Poly. Sci., Vol. 22, p. 781 (1978).

153. Farber, R., M.Eng. Thesis, Dept. Chem. Eng., McGill University, 1973.

154. Fusey, I., Additional Information on the Biaxial Extensiometer, McGill University, January 7, 1983.

155. Martino, R., Mod. Plast., Vol. 59 (4) p.58 (1982).

156. Samara, M. K., M.Eng. Thesis, Dept. Chem. Eng., McGill University, 1985.

APPENDIX A

MECHANICAL PROPERTIES OF POLYETHYLENE FILMS

Polymer type	LLDPE	LLDPE	LDPE	HDPE
Commercial name	GRSN-7047	Dowlex 2045	Conventional grade	Conventional grade
Resin properties				
Density, g/cm^3	.918	.919	.920	.950
Melt index, g/10 min	1.0	1.0	0.7	1.0
comonomer	1-butene	1-octene	----	----
Film properties				
Gage, mils	1.5	1.5	1.5	1.25
Dart drop impact, g.	145	190	120	----
Puncture, in.-lb/mil	15	14	8	----
Tensile strength, psi				
MD	5800	6300	2900	6300
TD	4600	5000	2700	4200
Elongation, %				
MD	600	590	250	550
TD	760	720	550	650
Elmendorf tear resistance, g.				
MD	248	440	210	35
TD	548	1000	160	750

Reference [155]

APPENDIX B

MOLECULAR WEIGHT DISTRIBUTIONS OF LLDPE RESINS

	CUMULATIVE WEIGHT %		
Weight Fraction*	Resin 30	Resin 31	Resin 33
1000000	0.078	0.227	0.1
700000	0.618	1.248	1.0
500000	1.904	3.28	2.9
300000	6.194	9.307	8.8
100000	29.626	36.709	36.6
10000	94.057	95.992	96.5
5000	97.46	98.659	98.7
2000	99.21	99.786	99.6

* Fraction of polymer with molecular weight greater than indicated value.

These data were kindly supplied by Dr. D. Axelson of DuPont, Canada (Kingston), and were obtained by the method of size exclusion chromatography (SEC).

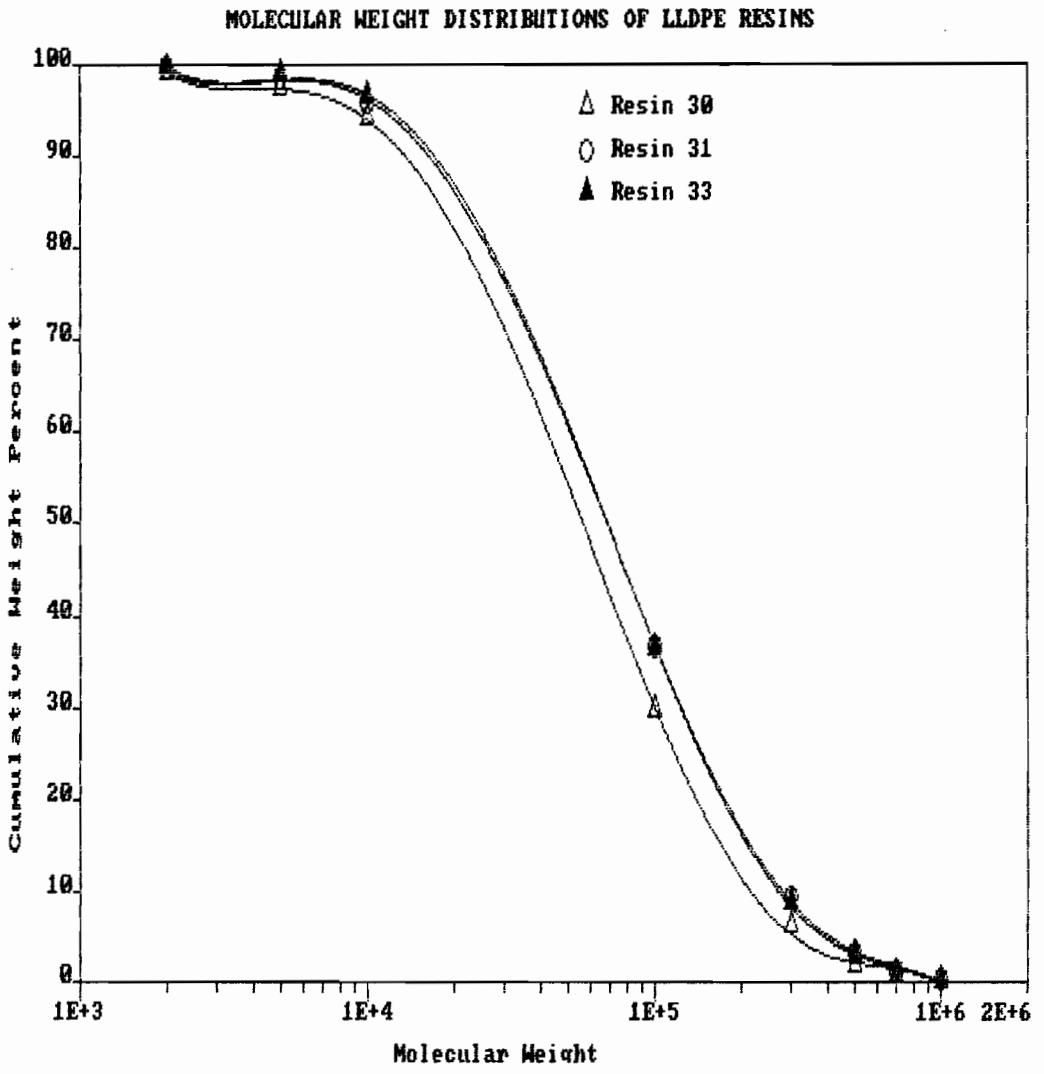
MOLECULAR WEIGHT DISTRIBUTIONS OF LLDPE RESINS
Resin 30
Resin 31
Resin 33
Cumulative Weight Percent
100
90
80
70
60
50
40
30
20
10
0
1E+3
1E+4
1E+5
1E+6
2E+6
Molecular Weight

Figure 115

APPENDIX C

FIRST NORMAL STRESS DIFFERENCE DATA

FIRST NORMAL STRESS DIFFERENCE DATA

Resin 30:

190°C $N_1 * 10^{-2}$ (Pa)

$\dot{\gamma}(s^{-1})$	I	II	III	IV	V	VI	$\bar{N}_1$	95% con. interval
.3981	9.1	11.1	10.3	10.9	10.0	12.8	10.7	±1.31
.6310	18.0	18.9	21.2	19.5	21.3	23.5	20.4	±2.09
1.00	40.1	38.3	36.7	39.2	40.4	44.1	39.8	±2.62
1.585	65.2	64.3	67.5	68.5	66.6	72.9	67.5	±3.20

210°C $N_1 * 10^{-2}$ (Pa)

$\dot{\gamma}(s^{-1})$	I	II	III	IV	V	VI	$\bar{N}_1$	95% con. interval
.2512	2.99	3.04	2.89	2.96	3.29	3.55	3.12	±.264
.3981	6.00	6.28	6.14	6.02	6.65	6.71	6.34	±.330
.6310	12.5	13.7	12.9	13.2	16.2	14.3	13.8	±1.40
1.00	26.7	27.2	26.9	28.5	27.6	31.1	28.0	±1.73
1.585	48.5	48.8	45.8	50.6	46.2	52.3	48.7	±2.62

FIRST NORMAL STRESS DIFFERENCE DATA

Resin 30:

225°C $N_1 * 10^{-2}$ (Pa)

$\dot{\gamma}$ (s^{-1})	I	II	III	IV	V	VI	$\bar{N}_1$	95% con. interval
.3981	4.46	4.73	5.18	5.07	5.36	4.72	4.92	±.355
.6310	9.38	9.64	10.5	10.2	9.75	10.3	9.97	±.466
1.00	21.5	20.9	24.6	24.3	22.4	23.1	22.8	±1.56
1.585	37.4	38.3	42.5	39.7	40.6	40.9	39.9	±1.94

FIRST NORMAL STRESS DIFFERENCE DATA

Resin 31:

190°C $N_1 * 10^{-2}$ (Pa)

$\dot{\gamma}(s^{-1})$	I	II	III	IV	$\bar{N}_1$	95% con. interval
.2512	11.2	11.9	12.4	11.7	11.8	±.79
.3981	17.2	16.0	14.9	14.8	15.7	±1.79
.6310	24.7	22.7	24.9	24.2	24.1	±1.58
1.0	48.8	42.6	46.1	45.7	45.8	±4.03
1.585	103.3	93.7	89.7	84.7	92.6	±12.5

210°C $N_1 * 10^{-2}$ (Pa)

$\dot{\gamma}(s^{-1})$	I	II	III	IV	$\bar{N}_1$	95% con. interval
.2512	5.26	5.39	5.49	5.54	5.42	±.197
.3981	10.6	9.81	11.5	11.7	10.9	±1.39
.6310	18.0	19.1	17.2	18.1	18.1	±1.24
1.00	28.7	28.9	32.4	31.2	30.3	±2.87
1.585	53.4	58.8	59.9	64.7	59.2	±7.40

FIRST NORMAL STRESS DIFFERENCE DATA

Resin 31:

240°C

$\dot{\gamma}(s^{-1})$	N_1*10^{-2} (Pa) I	II	III	IV	V	$\bar{N}_1$	95% con. interval
.2512	1.83	1.90	1.80	2.04	1.98	1.91	±.125
.3981	4.04	3.83	3.75	4.21	3.72	3.91	±.261
.6310	7.23	7.51	6.96	7.49	7.11	7.26	±.297
1.00	14.0	16.9	13.8	15.9	13.4	14.8	±1.89
1.585	29.6	31.3	32.5	28.7	32.1	30.8	±2.11

Resin 32:

190°C

$\dot{\gamma}(s^{-1})$	N_1*10^{-2} (Pa) I	II	III	IV	$\bar{N}_1$	95% con. interval
.0631	35.2	38.7	31.3	33.2	34.6	±5.03
.0995	55.8	58.5	57.2	53.7	56.3	±3.27
.1578	85.5	82.1	84.9	88.3	85.2	±4.04
.2500	132.0	137.0	121.0	132.0	130.5	±10.7

FIRST NORMAL STRESS DIFFERENCE DATA

Resin 33:

190°C

$\dot{\gamma}(s^{-1})$	N_1*10^{-2} (Pa) I	II	III	IV	V	$\bar{N}_1$	95% con. interval
.1585	5.26	5.18	6.11	5.84	6.46	5.77	±.681
.2512	12.4	12.3	12.7	13.8	13.8	13.0	±.925
.3981	31.5	32.1	29.4	28.2	29.8	30.2	±1.97
.6310	43.6	42.2	45.0	43.9	43.3	43.6	±1.53
1.00	78.5	77.1	74.9	76.6	73.0	76.0	±2.64

210°C

$\dot{\gamma}(s^{-1})$	N_1*10^{-2} (Pa) I	II	III	IV	V	$\bar{N}_1$	95% con. interval
.1585	2.11	2.16	1.80	1.95	2.08	2.02	±.180
.2512	4.61	4.55	4.30	4.38	4.46	4.46	±.185
.3981	14.2	14.5	13.5	10.5	13.8	13.3	±2.00
.6310	28.9	29.1	29.0	27.1	27.4	28.3	±1.20
1.00	49.4	48.9	45.2	45.8	46.2	47.1	±2.38

240°C

$\dot{\gamma}(s^{-1})$	N_1*10^{-2} (Pa) I	II	III	IV	V	$\bar{N}_1$	95% con. interval
.3981	7.50	8.26	8.17	7.73	7.49	7.83	±.454
.6310	19.6	17.9	18.3	17.0	17.2	18.0	±1.29
1.00	35.9	31.2	33.1	34.7	32.6	33.5	±2.28
1.585	61.7	54.5	63.0	56.3	58.5	58.8	±4.43

APPENDIX D

RELAXATION TIMES OF RESINS

Relaxation Times, Spectrum Strengths and Moduli of Resins

GRSN-7047, resin 31:

190 °C	λ_{oi}(s)	H_{oi} (Pa)	G_{oi} (Pa)
	.014142	83620	96230
	.044697	43920	50536
	.14142	17970	20679
	.44697	5600	6445
	1.4142	1375	1583
	4.4697	292	336

210 °C	λ_{oi}(s)	H_{oi} (Pa)	G_{oi} (Pa)
	.014142	71025	81731
	.044697	34230	39430
	.14142	12590	14490
	.44697	3681	4239
	1.4142	896	1032
	4.4697	193	222

240 °C	λ_{oi}(s)	H_{oi} (Pa)	G_{oi} (Pa)
	.014142	57000	65593
	.044697	21358	24577
	.14142	6225	7163
	.44697	1815	2089
	1.4142	529	609
	4.4697	154	177

Relaxation Times, Spectrum Strengths and Moduli of Resins

GERS-6937, resin 33:

190°C	λ_{oi} (s)	H_{oi} (Pa)	G_{oi} (Pa)
	.014142	107250	123420
	.044697	60950	70140
	.14142	27195	31290
	.44697	9048	10412
	1.4142	2300	2645
	4.4697	492	567

210°C	λ_{oi} (s)	H_{oi} (Pa)	G_{oi} (Pa)
	.014142	97230	111890
	.044697	51774	59580
	.14142	20993	24158
	.44697	6523	7506
	1.4142	1616	1860
	4.4697	346	398

240°C	λ_{oi} (s)	H_{oi} (Pa)	G_{oi} (Pa)
	.014142	80862	93053
	.044697	38410	44198
	.14142	13089	15062
	.44697	3839	4418
	1.4142	991	1150
	4.4697	208	240

Relaxation Times, Spectrum Strengths and Moduli of Resins

Dowlex 2045, resin 30:

	λ_{oi} (s)	H_{oi} (Pa)	G_{oi} (Pa)
190 °C			
	.014142	41476	47730
	.044697	27000	31070
	.14142	11106	12780
	.44697	3500	4028
	1.4142	1036	1192
	4.4697	360	414
210 °C	λ_{oi} (s)	H_{oi} (Pa)	G_{oi} (Pa)
	.014142	38123	43870
	.044697	19000	21864
	.14142	7347	8455
	.44697	2300	2647
	1.4142	590	679
	4.4697	110	127
225 °C	λ_{oi} (s)	H_{oi} (Pa)	G_{oi} (Pa)
	.014142	36000	41427
	.044697	16000	18412
	.14142	5878	6764
	.44697	1750	2014
	1.4142	450	517
	4.4697	105	121

DYNJ-4, resin 32:

	λ_{oi} (s)	H_{oi} (Pa)	G_{oi} (Pa)
190 °C			
	.014209	16295	18675
	.044697	11000	12606
	.14209	6838	7837
	.44697	3900	4470
	1.4209	2104	2411
	4.4697	1000	1146
	14.209	398	456
	44.697	125	143

APPENDIX E

ACIERNO MODEL PROGRAM LISTING

Calculation of shear viscosity and first normal stress difference using Acierno model.

Input_variables:

GOI- Resin relaxation moduli.

LMOI- Resin relaxation times.

GMD- Shear rates at which viscometric functions will be estimated.

Output_variables:

VISC- Estimates of shear viscosity.

NSD- Estimates of first normal stress difference.

```
1 DIM GOI#(8)
2 DIM LMOI#(8)
5 DIM GMD#(13)
10 DIM ET#(8)
20 DIM NS#(8)
30 DIM VISC#(13)
40 DIM NSD#(13)
50 FOR I=1 TO 8
60 READ LMOI#(I)
70 NEXT I
80 DATA     RELAXATION TIMES
85 DATA 44.697#
90 FOR I=1 TO 8
100 READ GOI#(I)
110 NEXT I
120 DATA     RELAXATION MODULI
130 FOR I=1 TO 13
140 READ GMD#(I)
150 NEXT I
160 DATA    SHEAR RATES
170 DATA
180 LET SUNS#=0#
190 LET SUET#=0#
200 LET A#=.25#
210 FOR J=1 TO 13
220 FOR I=1 TO 8
230 LET C#=A#*LMOI#(I)*GMD#(J)
240 GOSUB 500
250 LET ET#(I)=GOI#(I)*LMOI#(I)*X2#^2.4
260 LET NS#(I)=2*GOI#(I)*(LMOI#(I)^2)*(X2#^3.8)*(GMD#(J)^2)
270 LET SUET#=SUET#+ET#(I)
280 LET SUNS#=SUNS#+NS#(I)
290 NEXT I
300 LET VISC#(J)=SUET#
310 LET NSD#(J)=SUNS#
315 LPRINT GMD#(J), VISC#(J), NSD#(J)
320 LET SUET#=0
330 LET SUNS#=0
340 NEXT J
380 END
500 LET X1=1#
510 LET FX1#=1#-C#*X1#^2.4
520 IF FX1#<0 THEN X1#=X1#/5#: GOTO 510
530 LET X2#=FX1#
540 LET FX2#=1#-C#*X2#^2.4
550 LET X3#=(X1#*FX2#-X2#*FX1#)/(X1#-X2#+FX2#-FX1#)
560 LET FX3#=1#-C#*X3#^2.4
570 LET X1#=X2#
580 LET FX1#=1#-C#*X1#^2.4
590 LET X2#=X3#
600 LET FX2#=1#-C#*X2#^2.4
610 LET Z#=ABS((X2#-X1#)/(X2#+X1#))
620 IF Z#>.00001# GOTO 550
630 RETURN
640 END
```

APPENDIX F

ACIERNO MODEL PARAMETERS USED TO FIT STEADY SHEAR DATA

VALUES OF ADJUSTABLE PARAMETER IN ACIERNO MODEL USED TO FIT VISCOSITY AND FIRST NORMAL STRESS DIFFERENCE DATA

	190°C		210°C		240°C	
Resin	η	N_1	η	N_1	η	N_1
30	0.2	0.55	0.15	0.4	0.15*	0.35*
31	0.35	0.5	0.3	0.5	0.25	0.8
32	0.25	0.05	-----	------	------	------
33	0.5	0.5	0.5	0.85	0.35	0.6

* 225°C

APPENDIX G

EXPERIENCES WITH THE BIAXIAL EXTENSIOMETER

EXPERIENCES WITH THE BIAXIAL EXTENSIOMETER

Work was initiated to confirm the operational readiness of the biaxial extensiometer developed by Rhi-Sausi [4] and subsequently modified by Yang [5]. As mentioned in Chapter 3, this device is based on the bubble inflation method. The instrument consists of two horizontally mounted stainless steel cylindrical chambers. In between the two chambers is a sample holder. Schematics of the two chambers and the sample holder are given in Figures 116-118. The sample is about 7.6 cm in diameter and 0.3 cm thick. During an experiment, these cylinders are clamped together and filled with a silicon oil. This oil serves to conduct heat to the sample, thus melting it, as well as to support the molten polymer; thus, the density of the oil should be close to that of the molten polymer. Within each chamber are immersion heaters which heat the oil. A moveable piston is mounted at the rear of the fixed chamber. In the course of an experiment, this piston travels forward and displaces oil contained in the fixed chamber. In turn this displaced oil causes the molten polymer disk to inflate to form a hemispherical bubble. The velocity of the piston is controlled so that the deformation experienced by the molten polymer at the pole of the bubble closely approximates equal biaxial extension. Photographs of the deforming bubble are taken periodically through the end of the mobile chamber. These photographs are then analyzed

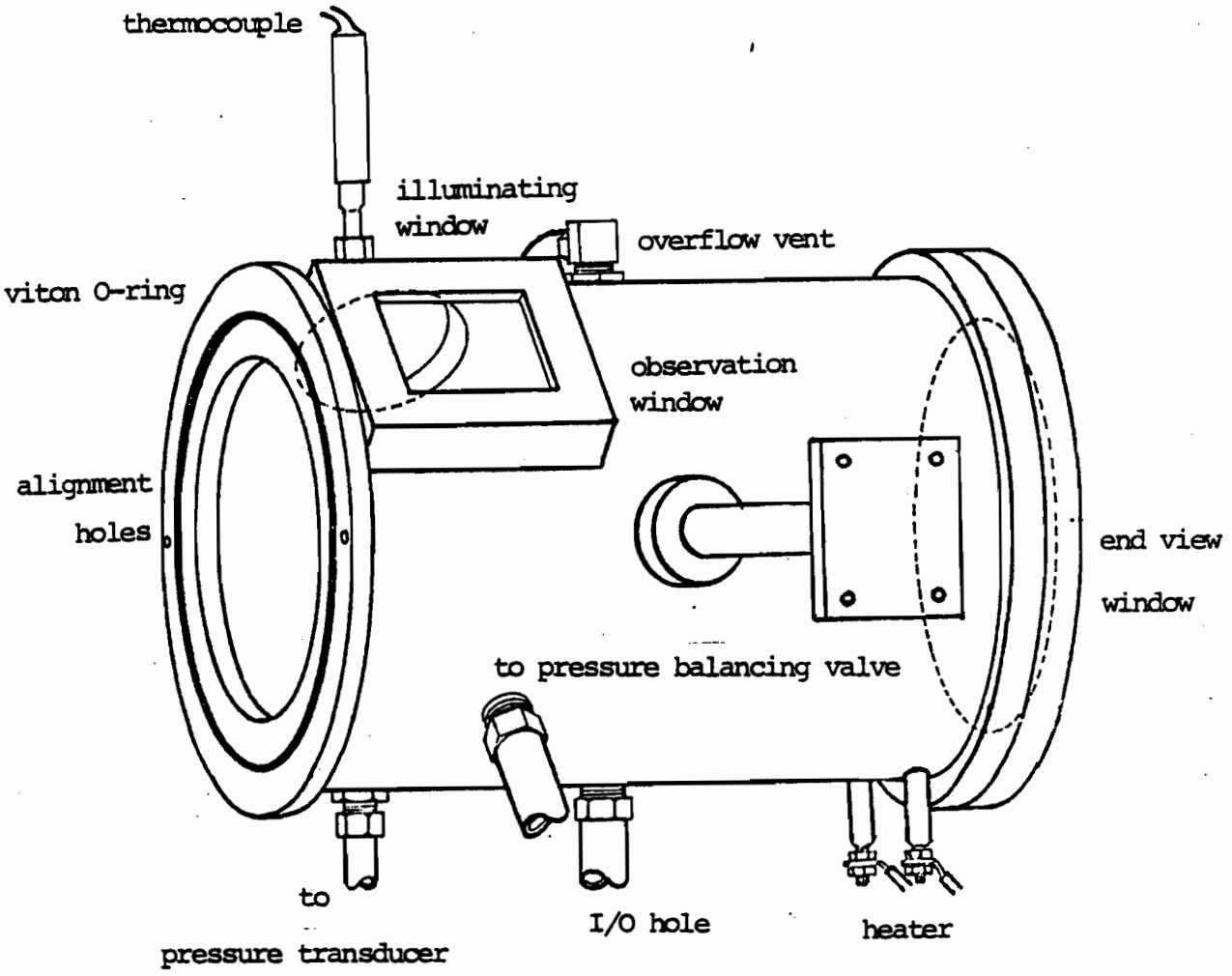

Figure 116: The Mobile Chamber

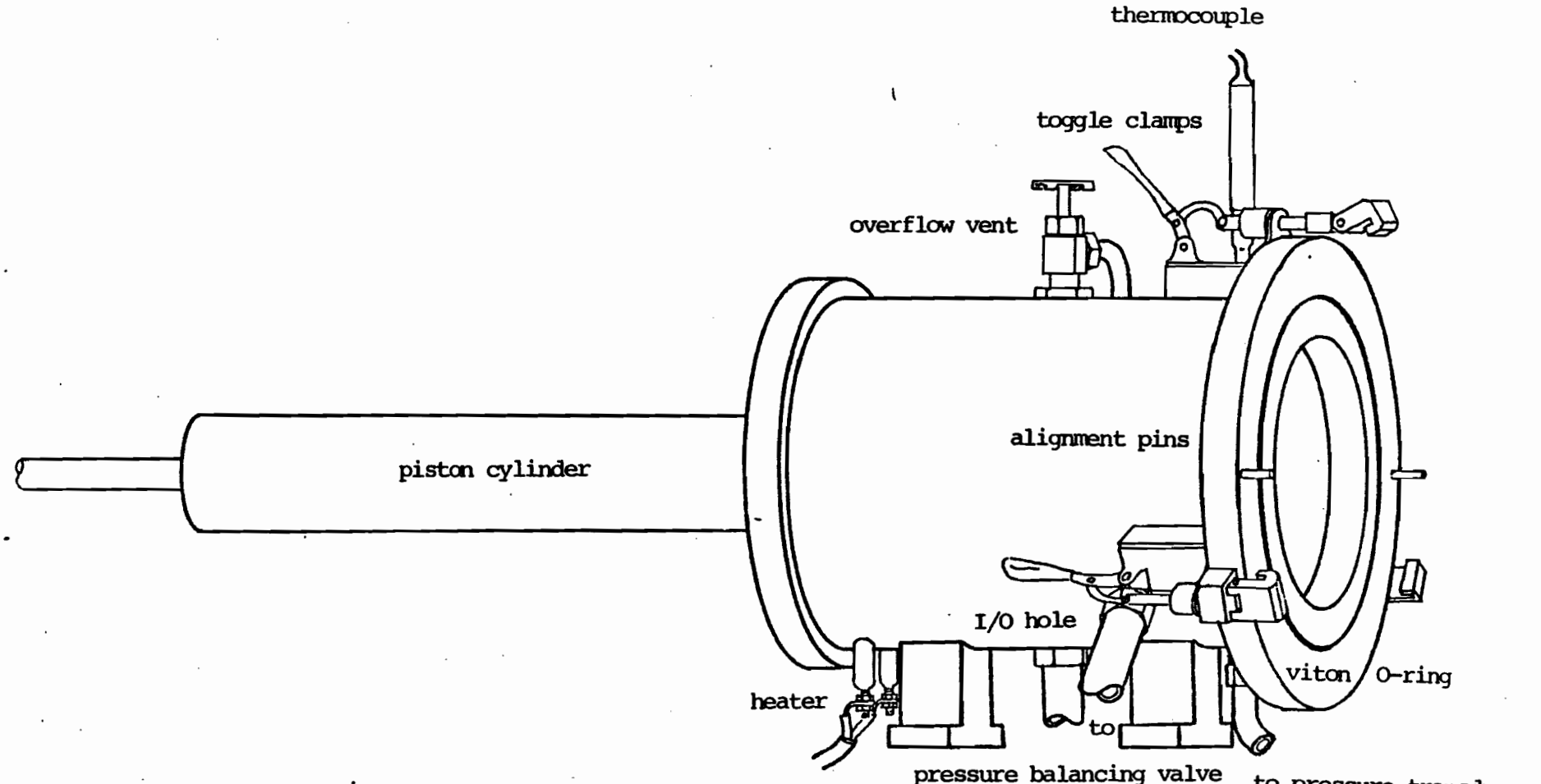

Figure 117: The Fixed Chamber

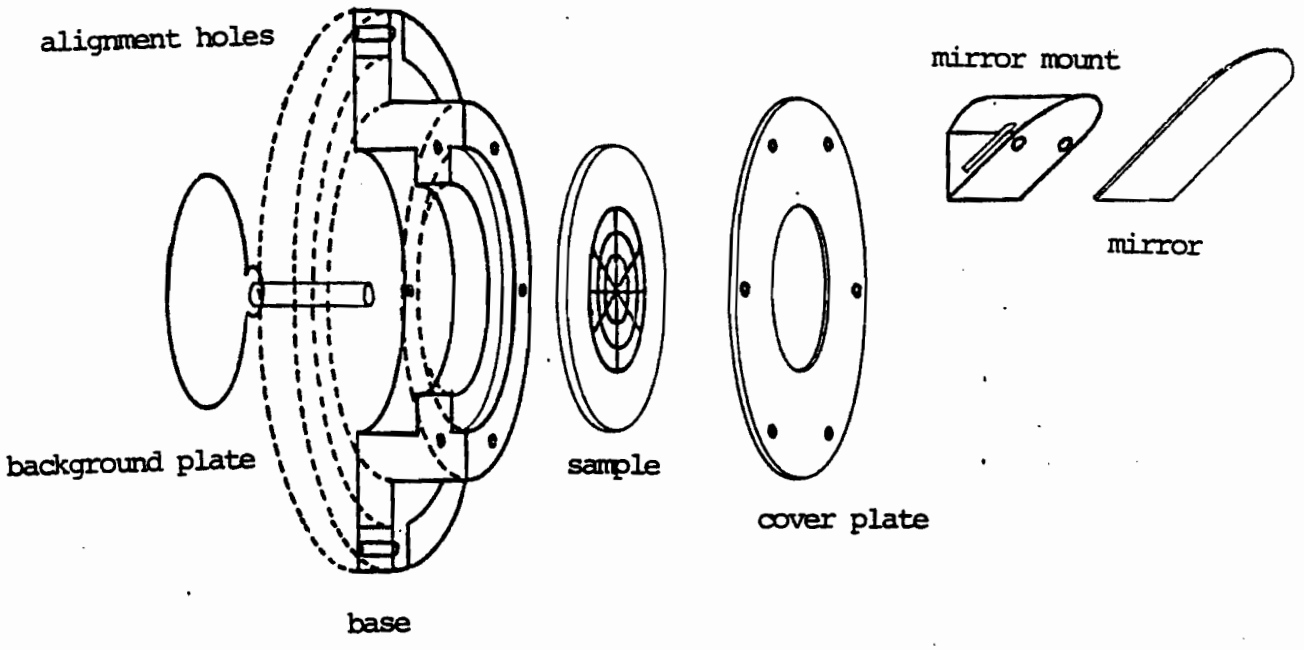

Figure **118** : <u>The Clamping Ring</u>

and the changing diameter of the innermost circle at the bubble's pole is measured. A differential pressure transducer is used to measure the pressure difference, P, between the opposite sides of sample as it is deformed. In Figure 119 a sketch of a sample with the circular pattern on it is shown. Only the innermost circle is used to measure the total Hencky strain experienced by the sample. Referring to Figure 119, the biaxial Hencky strain at time t is defined as follows.

$$\epsilon_b = \ln\left(\frac{x}{x_0}\right) \qquad (G\text{-}1)$$

where x_0 is the original diameter of the innermost circle and x is it's diameter at any later time. The biaxial extensional stress may be approximated by the following expression [5],

$$\tau_b = PR\left(\frac{x}{x_0}\right)^2 \Big/ d_0\left(1 + \left[1 - \left(\frac{x}{2R}\right)^2\right]^{1/2}\right) \qquad (G\text{-}2)$$

where d_0 is the original thickness of the sample and R is the radius of curvature of the molten polymer bubble. When photographing the deformation process, a mirror is mounted at a 45° angle to the plane of the sample, thus the photograph taken contains a side view of the bubble in addition to the head on view. The radius of curvature of the bubble is found by superimposing circles of known radius on the bubble until one is found which "fits" the bubble radius. Once the stress

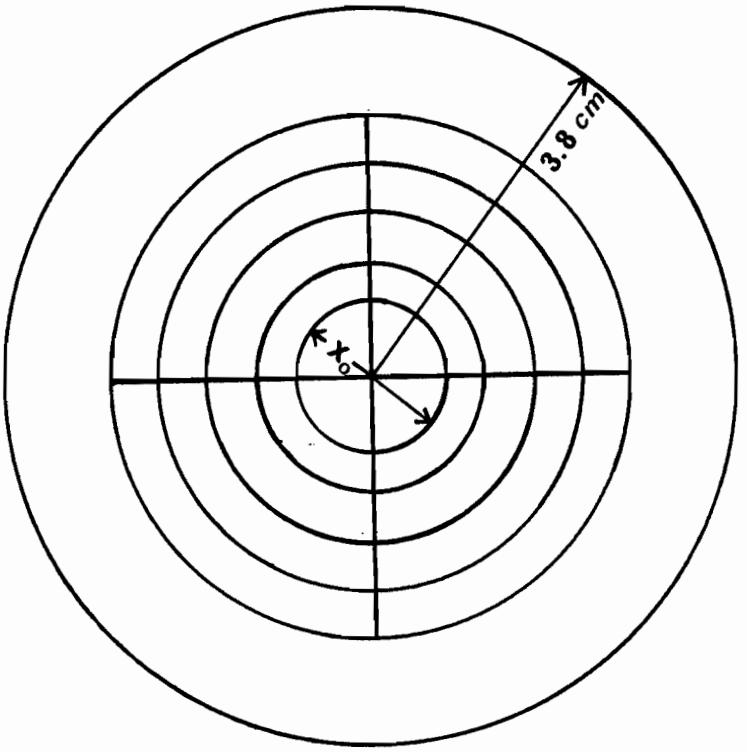

Figure **119**: Schematic of polymer sample
for McGill biaxial extensiometer

is known, the biaxial extensional stress growth function is readily calculated using the following expression.

$$\eta_b^+(\dot{\epsilon}_b, t) = \tau_b / \dot{\epsilon}_b \qquad (G-3)$$

Preliminary work showed that the differential pressure transducer was not working; a new, more sensitive transducer (± 1 psi) was purchased. This device performed quite satisfactorily. Fusey [154] installed additional thermocouples around the circumference of both chambers to determine if isothermal conditions existed. She ultimately installed a stirrer in each chamber to insure that isothermal conditions were attained. The entry points of the thermocouples into the chambers were frequently sources of leaks. After unsuccessfully attempting to seal these entry points using a variety of different sealants, it was decided to remove these extra thermocouples and permanently seal their entry holes. Since isothermal conditions were known to exist at steady state (which typically took about 15 minutes to achieve when an operating temperature of 135 °C was used), they were no longer needed. Various fittings and seals on the chambers were also replaced and the unit was finally made relatively leak free. This is an important point since leaks, in addition to being an inconvenience and a hazard (spurting hot oil), allow oil displaced by the piston to escape, rather than deform the sample.

Of importance in obtaining data is a reliable method for printing the grid pattern on the samples. Yang [5] originally used a rubber stamp to print the pattern. Fusey [154] found that a screenprinting process was more suitable since the lines were finer and did not spread out as much as the disk expanded. The ink used was a mixture of carbon black and polyethylene enamel (PLY, M 710 from Advance Co., Montreal.). This is an extremely viscous material and could not be applied uniformly, so it was diluted with varsol (4 parts ink to 1 part varsol). The printed sample was allowed to dry for about 1 hour at room temperature before use. This method was not satisfactory since the ink lines tended to break off the sample as it deformed, particularly at total strains above .2-.5 . As an alternative, four dots 5 mm from the center of the sample were used, each dot being at a 90 angle from the other. Thus by measuring the changing distance between dots on opposite sides of the sample center, the strain could be determined.

Having solved these problems, the next objective was to determine if this device was capable of generating an equal biaxial extensional flow. The extensiometer's control system is based on a Commodore PET microcomputer. The controlled variable is the velocity of the piston. The input variable to the control system is the position of the piston. At any time the position of the piston is compared to where it

should be; depending on whether it is beyond or before it's prescribed position at that time, the system will speed up or slow down the motor driving the piston. Further details of the control system are given by Yang [5] and Fusey [154]. This system was found to work somewhat erratically. A frequent problem was the sudden loss of control of the piston speed causing the piston to travel at a constant speed-usually the last one signalled to it. It was first thought that this was caused by spikes in the line voltage feeding the interface unit. A voltage "smoother" was installed but had little, if any, affect. While a constant strain rate experiment was in progress the voltages leading out of the amplifiers on the digital to analog (D/A) converter were monitored to see if spurious signals could be discerned, some were but these did not coincide with a loss of control, and the problem persisted. Finally the amplifiers on both the D/A and the analog to digital (A/D) boards were changed. This seemed to help matters at first but this behavior ressumed after several experiments. Some measurements to determine if equal biaxial strain was attained were made. An example of the findings is given in Figure 120. This was the most successful experiment carried out. Although the programmed strain rate was not attained, the resulting strain rate was quite constant. The higher values of the strain are not particularly reliable since the,

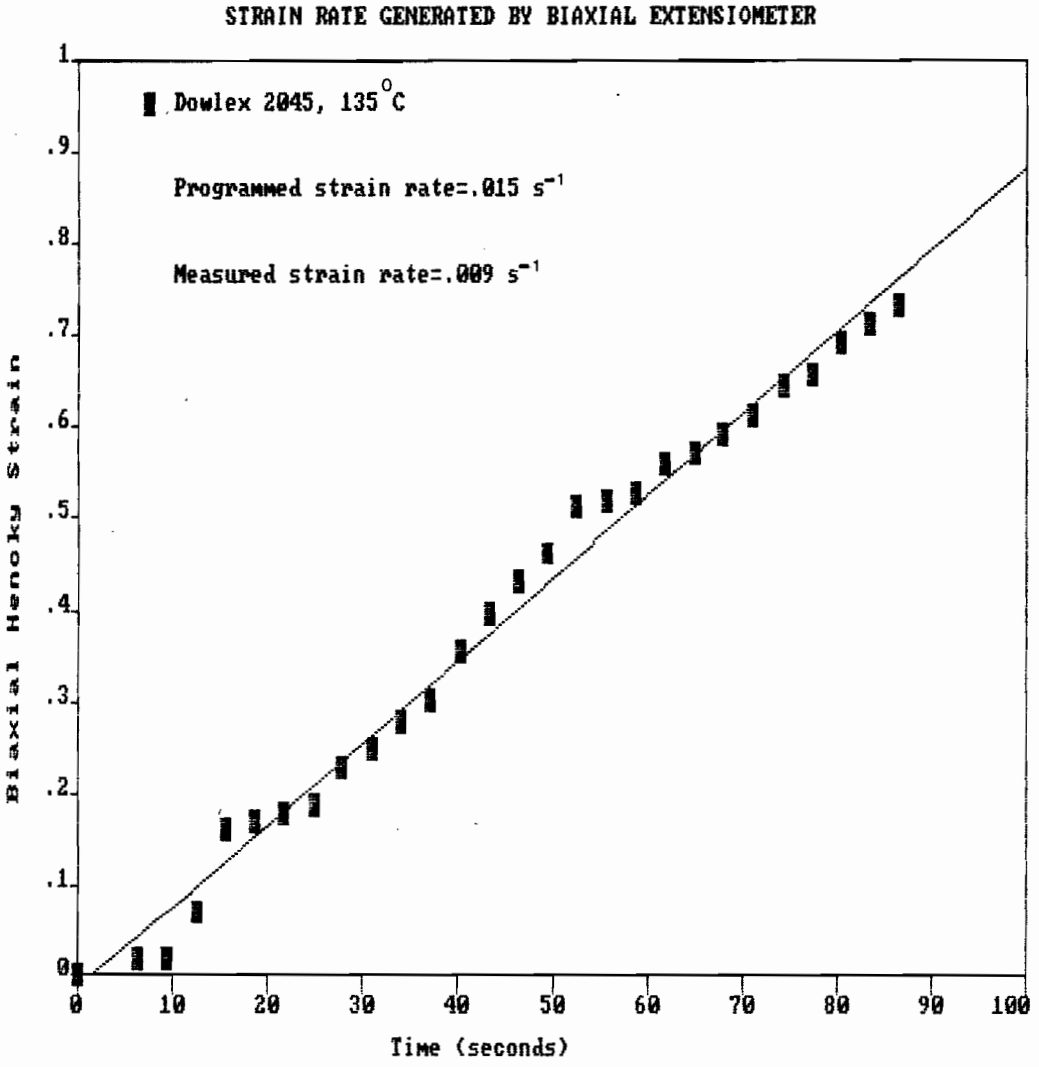
STRAIN RATE GENERATED BY BIAXIAL EXTENSIOMETER
Dowlex 2045, 135°C
Programmed strain rate=.015 s⁻¹
Measured strain rate=.009 s⁻¹
Biaxial Henoky Strain
Time (seconds)
0
.1
.2
.3
.4
.5
.6
.7
.8
.9
1
0
10
20
30
40
50
60
70
80
90
100

Figure 120

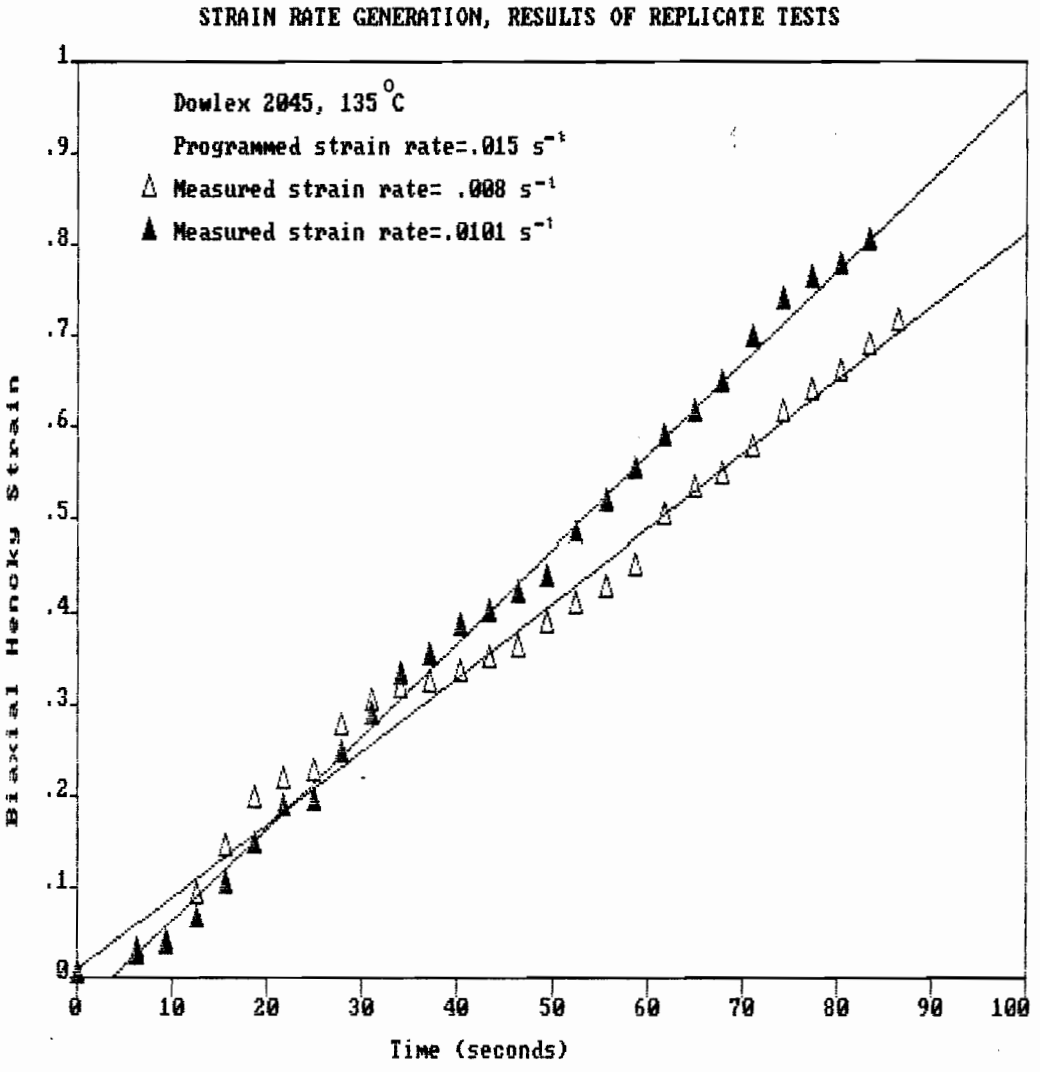
STRAIN RATE GENERATION, RESULTS OF REPLICATE TESTS
Dowlex 2045, 135 °C
Programmed strain rate=.015 s⁻¹
Measured strain rate= .008 s⁻¹
Measured strain rate=.0101 s⁻¹
Biaxial Henoky Strain
Time (seconds)
0
.1
.2
.3
.4
.5
.6
.7
.8
.9
1
0
10
20
30
40
50
60
70
80
90
100

Figure **121**

by now fairly large bubble, tended to deform nonuniformly at high strains. Examples of other results obtained using the same programmed strain rate are shown in Figure 121. These results indicate that although a relatively constant strain rate seems to be generated, it is not the one programmed nor were the results reproducible.

It is apparent that additional work is required to improve the reliability of the control system, and to insure that it is capable of generating constant strain rate flows. It was felt that this was beyond the scope of this work and was not pursued further.

APPENDIX H

STANDARD DEVIATIONS FOR SHEAR VISCOSITY DATA

The percent standard deviations of the shear viscosity reported are defined by the following expression

$$\eta\% = \frac{S_{\bar{\eta}}}{\bar{\eta}} \times 100$$

where $S_{\bar{\eta}}$ is given by

$$S_{\bar{\eta}} = \left\{ \frac{1}{n-1} \sum_{i=1}^{n} (\eta_i - \bar{\eta})^2 \right\}^{1/2}$$

and $\bar{\eta}$ is the mean value of the viscosity at a particular shear rate. Four measurements were made at each shear rate above 2 s^{-1}. Below this shear rate the number of measurements varied between four and six (See Appendix C).

Standard deviations for shear viscosity data obtained with RMS and Instron Capillary Rheometer.

Resin 30, 190°C		Resin 30, 210°C	
$\dot{\gamma}$, s^{-1}	η, %	$\dot{\gamma}$, s^{-1}	η, %
0.02512	1.84	0.02512	1.63
0.03981	2.16	0.03981	1.44
0.0631	1.47	0.0631	1.55
0.100	1.38	0.100	2.02
0.1585	2.20	0.1585	1.88
0.2512	1.73	0.2512	1.99
0.3981	2.49	0.3981	2.34
0.631	2.31	0.631	1.53
1.00	3.08	1.00	2.58
1.585	2.86	1.585	2.71
2.88	3.47	2.88	3.65
5.78	3.16	5.78	4.08
11.55	2.95	11.55	3.23
28.88	3.06	29.4	3.18
63.53	3.83	63.4	3.29
135.9	2.65	134.9	3.80
372.8	4.10	355.7	2.11
887.3	3.89	795.4	4.64
		1767	4.29

Standard deviations for shear viscosity data obtained with RMS and Instron Capillary Rheometer.

Resin 30, 225°C		Resin 30, 240°C	
$\dot{\gamma}$, s^{-1}	η, %	$\dot{\gamma}$, s^{-1}	η, %
2.88	3.14	0.02512	2.38
5.71	3.35	0.03981	2.14
11.34	4.41	0.0631	2.84
28.6	3.82	0.100	1.68
63.0	3.92	0.1585	2.03
132.3	4.07	0.2512	2.74
348.1	4.62	0.3981	2.49
748.2	4.00	0.631	3.00
1625	4.77	1.00	2.89
		1.585	3.65
		2.83	4.08
		5.67	3.67
		11.34	2.61
		28.35	3.02
		62.9	3.13
		130.2	1.56
		348.1	2.93
		748	5.21
		1617	5.03

Standard deviations for shear viscosity data obtained with RMS and Instron Capillary Rheometer.

Resin 31, 190°C		Resin 31, 210°C	
$\dot{\gamma}$, s^{-1}	η, %	$\dot{\gamma}$, s^{-1}	η, %
0.02512	1.24	0.02512	1.83
0.03981	1.35	0.03981	1.77
0.0631	2.11	0.0631	1.92
0.100	1.88	0.100	2.14
0.1585	1.92	0.1585	0.84
0.2512	2.05	0.2512	1.03
0.3981	2.45	0.3981	1.11
0.631	2.55	0.631	1.31
1.00	2.89	1.00	2.29
2.75	3.45	1.585	3.02
5.51	4.23	2.67	3.28
11.55	3.75	5.49	3.44
30.65	4.41	11.34	3.38
65.63	4.00	29.27	2.18
139.9	2.07	63.26	3.57
381.28	2.43	134.4	3.11
		360.9	4.48
		771.8	4.96

Standard deviations for shear viscosity data obtained with RMS and Instron Capillary Rheometer.

Resin 31, 240°C		Resin 33, 190°C	
$\dot{\gamma}$, s^{-1}	η, %	$\dot{\gamma}$, s^{-1}	η, %
0.02512	1.11	0.02512	0.57
0.03981	0.83	0.03981	0.74
0.0631	1.23	0.0631	0.88
0.100	1.42	0.100	1.05
0.1585	1.37	0.1585	0.92
0.2512	1.29	0.2512	1.28
0.3981	1.56	0.3981	1.42
0.631	1.62	0.631	1.97
1.00	1.28	1.00	2.56
2.90	2.68	2.83	2.46
5.80	3.02	6.05	1.56
11.60	3.16	12.1	2.97
29.01	3.56	30.25	3.21
63.26	3.19	66.24	2.83
132.8	2.35	143.1	3.40
344.5	2.86		
753.4	3.71		
1659	4.62		

Standard deviations for shear viscosity data obtained with RMS and Instron Capillary Rheometer.

Resin 33, 210°C		Resin 33, 240°C	
$\dot{\gamma}$, s^{-1}	η, %	$\dot{\gamma}$, s^{-1}	η, %
0.02512	1.16	0.02512	1.34
0.03981	0.97	0.03981	0.66
0.0631	0.46	0.0631	1.00
0.100	1.25	0.100	1.38
0.1585	1.34	0.1585	0.59
0.2512	1.57	0.2512	1.90
0.3981	1.50	0.3981	0.84
0.631	1.89	0.631	1.82
1.00	2.15	1.00	2.29
2.80	2.88	1.585	2.62
5.62	2.17	2.90	3.08
11.24	3.12	5.80	2.44
29.99	2.33	11.6	3.10
63.5	1.24	29.0	2.77
138.6	2.78	62.7	2.51
415.4	3.00	131.8	2.60
		351.0	4.17
		755.2	3.47

Standard deviations for shear viscosity data obtained with RMS and Instron Capillary Rheometer.

Resin 32, 190°C

$\dot{\gamma}$, s^{-1}	η, %
0.02512	0.55
0.03981	0.79
0.0631	0.88
0.100	1.27
0.1585	1.23
0.2512	1.42
5.78	2.88
14.44	2.66
36.1	3.21
72.2	2.83
144.4	3.54
400.3	3.13
931.9	4.29

APPENDIX I

STANDARD DEVIATIONS FOR COMPLEX VISCOSITY DATA

The percent standard deviations of the complex viscosity is defined as follows,

$$\eta^{*}\% = \frac{S_{\bar{\eta}^{*}}}{\bar{\eta}^{*}} \times 100$$

with $S_{\bar{\eta}^{*}}$ being given by

$$S_{\bar{\eta}^{*}} = \left\{ \frac{1}{n-1} \sum_{i=1}^{n} \left(\eta_i^{*} - \bar{\eta}^{*} \right)^2 \right\}^{1/2}$$

and $\bar{\eta}^{*}$ being the mean value of four separate measurements made at particular frequency.

Standard deviations for complex viscosity data.

	Resin 30, η^* %		
ω, rad/s	190°C	210°C	225°C
0.100	1.19	1.84	----
0.1585	2.16	1.72	1.66
0.2512	1.45	1.23	2.14
0.3981	1.24	1.93	2.44
0.631	1.11	2.00	1.69
1.00	1.55	2.62	1.63
1.585	2.01	1.01	2.13
2.512	1.89	1.82	2.25
3.981	1.22	1.95	2.10
6.310	2.58	1.88	2.12
10.0	2.34	1.56	1.54
15.85	1.69	2.44	2.99
25.12	1.09	1.32	2.81
39.81	1.70	1.40	2.38
63.10	1.85	1.45	2.31
100.0	2.09	1.87	1.63

Standard deviations for complex viscosity data.

	Resin 31, 7 * %		
ω ,rad/s	190°C	210°C	240°C
0.100	1.87	----	----
0.1585	1.47	1.99	1.32
0.2512	2.11	1.43	1.65
0.3981	1.22	1.97	1.29
0.631	1.66	1.43	2.01
1.00	1.44	1.20	1.32
1.585	1.86	2.33	2.37
2.512	1.00	1.80	2.06
3.981	1.11	2.30	2.45
6.310	1.25	1.85	1.32
10.0	1.89	2.13	2.36
15.85	1.90	2.00	2.74
25.12	1.57	1.83	2.08
39.81	2.01	2.26	1.73
63.10	1.64	1.44	1.69
100.0	2.64	1.50	1.77

Standard deviations for complex viscosity data.

ω, rad/s	Resin 32, η^*, % 190°C
0.01	1.55
0.01585	1.77
0.02512	2.31
0.03981	0.43
0.0631	1.35
0.100	1.23
0.1585	0.46
0.2512	1.37
0.3981	1.35
0.631	1.68
1.00	1.24
1.585	1.87
2.512	0.87
3.981	1.86
6.310	2.12
10.0	1.64
15.85	1.67
25.12	2.46
39.81	1.34
63.10	1.67
100.0	0.78

Standard deviations for complex viscosity data.

	Resin 33, 7 * %		
ω, rad/s	190°C	210°C	240°C
0.100	1.90	----	----
0.1585	1.34	1.24	1.67
0.2512	1.45	2.18	2.00
0.3981	1.84	1.92	1.84
0.631	1.38	1.83	1.95
1.00	1.55	1.23	2.39
1.585	0.42	0.93	1.57
2.512	1.39	1.06	1.32
3.981	0.25	1.27	1.65
6.310	1.33	1.98	2.46
10.0	1.76	2.23	1.97
15.85	1.74	1.87	2.35
25.12	0.27	1.84	1.56
39.81	1.76	1.49	2.34
63.10	1.67	2.27	2.67
100.0	1.09	1.62	1.84

APPENDIX J

STANDARD DEVIATIONS FOR EXTRUDATE SWELL DATA

The percent standard deviation of the extrudate swell ratio is defined as,

$$B\% = \frac{S_{\bar{B}}}{\bar{B}} \times 100$$

again, with $S_{\bar{B}}$ defined as

$$S_{\bar{B}} = \left\{ \frac{1}{n-1} \sum_{i=1}^{n} (B_i - \bar{B})^2 \right\}^{1/2}$$

with $\bar{B}$ being the mean value of four separate measurements of the swell ratio at a particular wall shear rate.

Standard deviations for extrudate swell data.

Resin 30

190 °C

$\dot{\gamma}$, s^{-1}	B, %
5.78	0.48
11.55	1.00
28.88	0.95
63.53	1.23
135.98	1.38
372.8	1.85

210 °C

$\dot{\gamma}$, s^{-1}	B, %
5.78	0.35
11.55	0.88
29.40	1.11
63.4	1.35
134.91	1.20
355.7	1.97

225 °C

$\dot{\gamma}$, s^{-1}	B, %
5.71	0.66
11.34	1.03
28.6	1.09
63.0	1.20
132.3	1.17
348.1	1.49
748.2	5.66

240 °C

$\dot{\gamma}$, s^{-1}	B, %
5.67	0.86
11.34	0.76
28.35	1.34
62.87	0.97
130.2	1.35
344.5	4.67
748.0	3.54

Standard deviations for extrudate swell data.

Resin 31

190°C		210°C	
$\dot{\gamma}$, s^{-1}	B, %	$\dot{\gamma}$, s^{-1}	B, %
5.51	1.59	5.49	1.73
11.55	1.87	11.34	0.69
30.65	1.95	29.27	1.23
65.63	1.34	63.26	1.45
139.41	3.85	134.4	4.28
		360.9	3.88

240°C	
$\dot{\gamma}$, s^{-1}	B, %
5.80	1.25
11.60	1.75
29.01	2.35
63.30	2.89
132.8	1.46
344.5	2.99
753.4	7.85

Standard deviations for extrudate swell data.

Resin 33

190°C		210°C	
$\dot{\gamma}$, s^{-1}	B, %	$\dot{\gamma}$, s^{-1}	B, %
6.05	1.23	5.62	1.40
12.1	1.85	11.24	0.49
30.25	1.63	30.00	1.30
66.20	2.56	63.50	1.96
		138.6	3.68

240°C		Resin 32, 190°C	
$\dot{\gamma}$, s^{-1}	B, %	$\dot{\gamma}$, s^{-1}	B, %
5.80	1.89	5.78	2.45
11.60	2.45	14.44	2.15
29.0	2.78	36.10	3.15
62.7	3.97	72.2	3.85
131.8	2.19		
351.0	2.43		
755.0	4.89		